# BRAIN MORPHOLOGY OF THE EARLY TRIASSIC CYNODONT *THRINAXODON LIORHINUS* AND THE IMPACT OF VARIATION IN DIGITAL ENDOCRANIAL RECONSTRUCTIONS ON UNDERSTANDING MAMMALIAN BRAIN EVOLUTION

by

CHARLOTTE MELANIE BIRD

A thesis submitted to the University of Birmingham for the degree of

DOCTOR OF PHILOSOPHY

School of Geography, Earth and Environmental Sciences

College of Life and Environmental Sciences

University of Birmingham

February 2024

# ABSTRACT

The mammalian brain has an evolutionary history which can be traced back to the late Permian, when basal cynodonts show the first glimmers of mammal-like characteristics. One such early cynodont, *Thrinaxodon liorhinus*, has been widely studied with regards to cranial and postcranial anatomy, yet the morphology of its brain has remained elusive. Given *Thrinaxodon* can provide insights into the baseline brain shape from which mammalian features developed, it is important to peer inside digitally-rendered ('digitised') skulls to reconstruct the soft tissues that may have once been present. Presented here are the first digital reconstructions of *Thrinaxodon liorhinus*' endocranial anatomy for both juvenile and adult specimens, with the main mammalian brain features present (olfactory bulbs, cerebral hemispheres and cerebellum). Yet, between the growth stages there is variation in brain size and shape which has shed light on the possible ontogenetic growth trajectory the brain may have experienced. Comparisons with contemporary cynodonts and the extant opossum, *Monodelphis domestica*, allowed conclusions to be drawn about the cognitive, sensory and behavioural capabilities that may have been influenced by the changing size and shape of the brain. Studies have suggested that basal cynodonts may have been nocturnal, fossorial and could have cared for young. Reconstructed morphological changes to specific brain regions appear to support these statements, particularly when considering the environmental stressors persisting during cynodont diversification following the Permian-Triassic mass extinction. However, shifting endocranial morphology was also considered in the context of variation and the impact the model maker has on endocranial reconstructions. Through experiment, it was found that nineteen modellers produced noticeably different endocasts for a single skull and that neither education level nor segmentation experience significantly improved the consistency of outputs. As such, improvements to the segmentation workflow

have been proposed to help minimise inter-modeller variation. Digital reconstructions of *Thrinaxodon*'s brain have provided a piece of the evolutionary puzzle for mammalian brain development and shown that cynodonts were important stepping stones within the advancement of the mammalian lineage.

*For my grandparents, who never saw me grow up*

*but who I hope to have made proud.*

# ACKNOWLEDGEMENTS

I have always loved learning, but completing a PhD was never a path I had envisaged for myself. With academic and creative free rein, how do you begin to decide where to dedicate four years of your life to study? Well, I would not have completed a PhD at all if it wasn't for the best supervisor you could wish for – Dr Stephan Lautenschlager. With kindness and patience, Stephan has tutored and supported me throughout my education at the University of Birmingham and I am certain that my time as a doctoral researcher would not have run so smoothly if it wasn't for your support. So, to Stephan, I say thank you! Thank you for answering all my questions – the complicated, the silly and especially the SOS emails about calculations! Thank you for your brilliant ideas that have helped to shape my research, your inspirational graphic design skills that I can only hope to emulate and your inquisitive questions that have made my thesis all the better. It has been my pleasure to learn from you during my PhD and now that I have so much free time, I promise to learn more about dinosaurs!

I must also extend my deepest thanks to Professor Paul Barrett from the Natural History Museum, London, who had such a valuable input into the early days of my PhD. I appreciate you letting me rummage in the amazing mammal collections to find fossils that Vincent Fernandez and Brett Clark kindly µCT-scanned. The Covid-19 years prevented me from visiting the cynodont collections at the University of Witwatersrand, South Africa, but I still remember the "once was lost, but now is found" email which unlocked a major part of my research – accessing some of the largest and smallest *Thrinaxodon* fossils yet found. So, it is with much gratitude that I thank Sifelani Jirah, Bernhard Zipfel, Bruce Rubidge and Julien Benoit for sharing your CT scans with me. I would also like to thank Fernando Abdala for providing specimen photographs for fossils that I was not able to see in person during lockdown.

With much gratitude, I thank the first year palaeontology undergraduates (class of 2019) for contributing their endocasts to my research. I also extend my deepest appreciation to Dr Daniel Cox, Dr Luke Meade, Dr Fion Ma, Hannah Bird, Josh Dixon and Adam Manning for offering their valuable time to produce additional endocasts. Your contributions were key to my research, so thank you!

It is only right to acknowledge that most of the cynodont specimens that I studied originated in Africa. While several were collected long ago in South Africa and transported to the UK, I am pleased to see that others have remained in the country where they were discovered for local researchers to work on the collections. I hope that the Karoo Basin continues to deliver pre-mammalian treasures for you. I am also pleased that virtual palaeontology opens up specimens to more researchers around the world, with the CT scans generated for this research being made available through the Natural History Museum, London, so that other researchers can study South African cynodonts.

Over the millions of years of mammal evolution, the brain has changed enormously, a fact I was able to study thanks to the generosity of Thomas Macrini, who provided access to the opossum growth series of brain endocasts, without which, determining ontogenetic characteristics in *Thrinaxodon* would have been much more difficult. And finally, my PhD would not have been possible without the funding of the Natural Environment Research Council (NERC CENTA2 NE/S007350/1) – thank you very much for supporting my research!

The biggest thanks of all must go to my family. I am lucky enough to have the most supportive parents I could wish for. Mom and Dad, you have dedicated decades to making me the best person I could hope to be, teaching me the importance of hard work and determination to

achieve everything I want to. Taking me around the world to support my educational development and opening my eyes to new possibilities. I am proud to be your daughter and I must say the biggest thanks especially for your help during the last months of thesis write up. And to my sister, Hannah… not long and you will have submitted too! Thank you for being my sounding board when you really had no idea what I was talking about! Thank you for all of the proofreading and opening so many Avizo files. I'll repay the favour as you near the end of your PhD and then we can get back to all of our hobbies that have been gathering dust for the last four years!

To Auntie Carol and Uncle Bill – well, I'm finally leaving 'school'! Thank you for all of the reminders that I should not be working on holiday and that I need to take time to relax.

And my final thanks go to Dan. Thank you for your support, your words of encourage, for nodding along when you really had no idea what all of those palaeo words meant and for always telling me "I can do it". Now we can finally start enjoying life – let the adventures commence!

# PAPERS

The following papers were published during the course of my doctoral studies at the University of Birmingham.

Lautenschlager, S., Fagan, M. J., Luo, Z-X., **Bird, C. M.**, Gill, P. and Rayfield, E. J. (2023) Functional reorganisation of the cranial skeleton during the cynodont–mammaliaform transition. *Communications Biology*, 6: 367.

Lautenschlager, S., Aston, R. F., Baron, J. L., Boyd, J. R., Brdiger, H. W. L., Carmona, V. E. T., Ducrey, T., Eccles, O., Gall, M., Jones, S. A., Laker-McHugh, H., Lawrenson, D. J., Mascarenhas, K. J., McSchnutz, E., Quinn, J. D., Robson, T. E., Stöhr, P. W., Strahl, E. J., Tokeley, R. R., Weston, F., Wallace, K. J., Whitehouse, T., **Bird, C. M.** and Dunne, E. M. (2024) Orbit size and estimated eye size in dinosaurs and other archosaurs and their implications for the evolution of visual capabilities. *Journal of Vertebrate Paleontology*, e2295518.

# TABLE OF CONTENTS

# LIST OF FIGURES

# LIST OF TABLES

# CONTRIBUTION STATEMENTS

## CHAPTER ONE

I conducted the literature review and prepared the text and phylogenetic tree figure for this chapter.

## CHAPTER TWO

I decided on the full methodological design of the thesis, writing all text and creating all figures within this chapter.

## CHAPTER THREE

My contribution to this chapter was full research design, including specimen selection, data collection, analysis, interpretation of the results and production of all text, figures and tables. Paul Barrett assisted with specimen selection and feedback on the results was provided by Stephan Lautenschlager.

## CHAPTER FOUR

This chapter was designed in collaboration with Stephan Lautenschlager. Paul Barrett assisted with specimen selection. I solely undertook data collection, analysis, interpretation of the results and production of all text, figures and tables. Feedback was provided by Stephan Lautenschlager.

## CHAPTER FIVE

This chapter was collaboratively designed with Stephan Lautenschlager for an undergraduate palaeontology module. Data collection was conducted by eleven palaeontology undergraduates, two master's students, five PhD researchers (four current and one completed) and one palaeobiology lecturer. I solely undertook data analysis, results

interpretation and produced the text, figures and tables within the chapter. Feedback on the results and discussion were provided by Stephan Lautenschlager.

## CHAPTER SIX

My contribution was to research conception, literature and data analysis, plus figure and text compilation. Stephan Lautenschlager provided feedback on this chapter.

## CHAPTER SEVEN

I developed and wrote the conclusions following earlier discussion of each of the thesis chapters with Stephan Lautenschlager.

# CHAPTER ONE

# The history of cynodont brain evolution and how to investigate it using virtual palaeontological techniques

## 1.1. Evolutionary history of cynodonts to mammals

The complexity of the mammalian brain is the culmination of biological experimentation over millions of years (Kemp 2009; Northcutt 2011; Rowe *et al*., 2011). Two stages of morphological changes are proposed to have contributed to mammalian brain development - first, the enlargement of the olfactory bulbs and cerebral hemispheres in mammalian ancestors, followed by the evolution of the neocortex in mammals from one to six layers of cortex (Kaas 1989; Kemp 2009; Kaas 2011; Kaas 2013; Molnár *et al*., 2014; Karten 2015). The first pulse of brain development is associated with more refined neuromuscular coordination of limbs, while the evolution of the neocortex correlates with sensory enhancements, including the growth of the olfactory bulbs, more acute auditory capabilities at higher frequencies and enlargement of the endocranial cavity as jaw musculature reduced in mass and skull anatomy simplified (Kemp 2009; Northcutt 2011; Rowe *et al.,* 2011; Benoit *et al*., 2016b; Lautenschlager *et al*., 2023). Alongside enhanced tactile sensitivity from the evolution of body hair (Rowe *et al.,* 2011), this combination of features likely supported mammal ancestors during foraging (particularly some early species that were nocturnal; Benoit *et al*., 2023), improving their sensory capabilities in an ecological niche carved out in the shadow of dinosaurs.

Non-mammaliaform cynodonts (hereafter referred to as cynodonts) are ancestral to transitional mammaliaform taxa and extant mammals (Kemp 2005; Botha *et al*., 2007; Benoit *et al*., 2017). The earliest cynodonts are known from the late Permian of South Africa (Botha

and Chinsamy, 2005; Kemp 2005; Botha *et al*., 2007; Kammerer 2016). Approximately 260 million years of anatomical and cognitive changes have shaped the brain and its subsequent coordination of bodily functions in modern mammals including thoughts and emotions (Panksepp 2011), memory (Poldrack and Packard, 2003), motion (Rokszin *et al*., 2010; Poirier *et al*., 2017), thermoregulation (Mota-Rojas *et al*., 2021) and social behaviour (Seebacker and Krause, 2017; Prounis and Ophir, 2020). To better understand the evolutionary origins of these biological and behavioural developments in modern mammals, researchers have collected and studied cynodont cranial and postcranial fossils from around the world, including South Africa (Botha *et al.,* 2007; Kammerer 2016; Benoit *et al.,* 2017), Zambia (Wynd *et al*., 2017; Huttenlocker and Sidor, 2020), Brazil (Bonaparte *et al*., 2003; Rodrigues *et al*., 2014; Martinelli *et al*., 2017; Guignard *et al*., 2018; Pavanatto *et al*., 2019; Rodrigues *et al*., 2019), Argentina (Wallace *et al*., 2019), India (Ray 2015) and Japan (Matsuoka *et al*., 2016). These globally and temporally distributed specimens help to piece together the evolutionary history of cynodont and mammal brains.

### 1.1.1. Evolution of the mammalian lineage

The mammalian evolutionary journey begins in the late Carboniferous (approximately 315 to 330 million years ago (Ma)) when amniotes (a clade of tetrapod vertebrates) split into Synapsida and Sauropsida (dos Reis *et al*., 2015; Ford and Benson, 2020; Brocklehurst *et al.*, 2021), with birds and reptiles belonging to the latter group. In the early Permian, therapsids emerged from Synapsida and diverged into numerous clades, including Cynodontia which would give rise to mammals and their ancestors (figure 1.1; Kemp 2005; Botha-Brink *et al.,* 2018; Ford and Benson, 2020). Although cynodonts appeared in the late Permian (~260 Ma), the group radiated following the Permian-Triassic mass extinction (~252 Ma) as the dramatic reduction in global biodiversity restructured ecosystems (Kemp 2005*;* Botha-Brink *et al.,* 2016;

Botha-Brink *et al.,* 2018). The Early Triassic saw the emergence of well-known taxa such as the epicynodont *Thrinaxodon* (~ 250 Ma), before diverging into two groups of eucynodonts - Cynognathia and Probainognathia (Ruta *et al*., 2013; Botha-Brink *et al*., 2018). Within Cynognathia, Gomphodontia appeared in the Middle Triassic, with subsequent emergence of three families - Diademodontidae, Trirachodontidae and Traversodontidae (Ruta *et al*., 2013; Botha-Brink *et al*., 2018). None of these groups survive today.

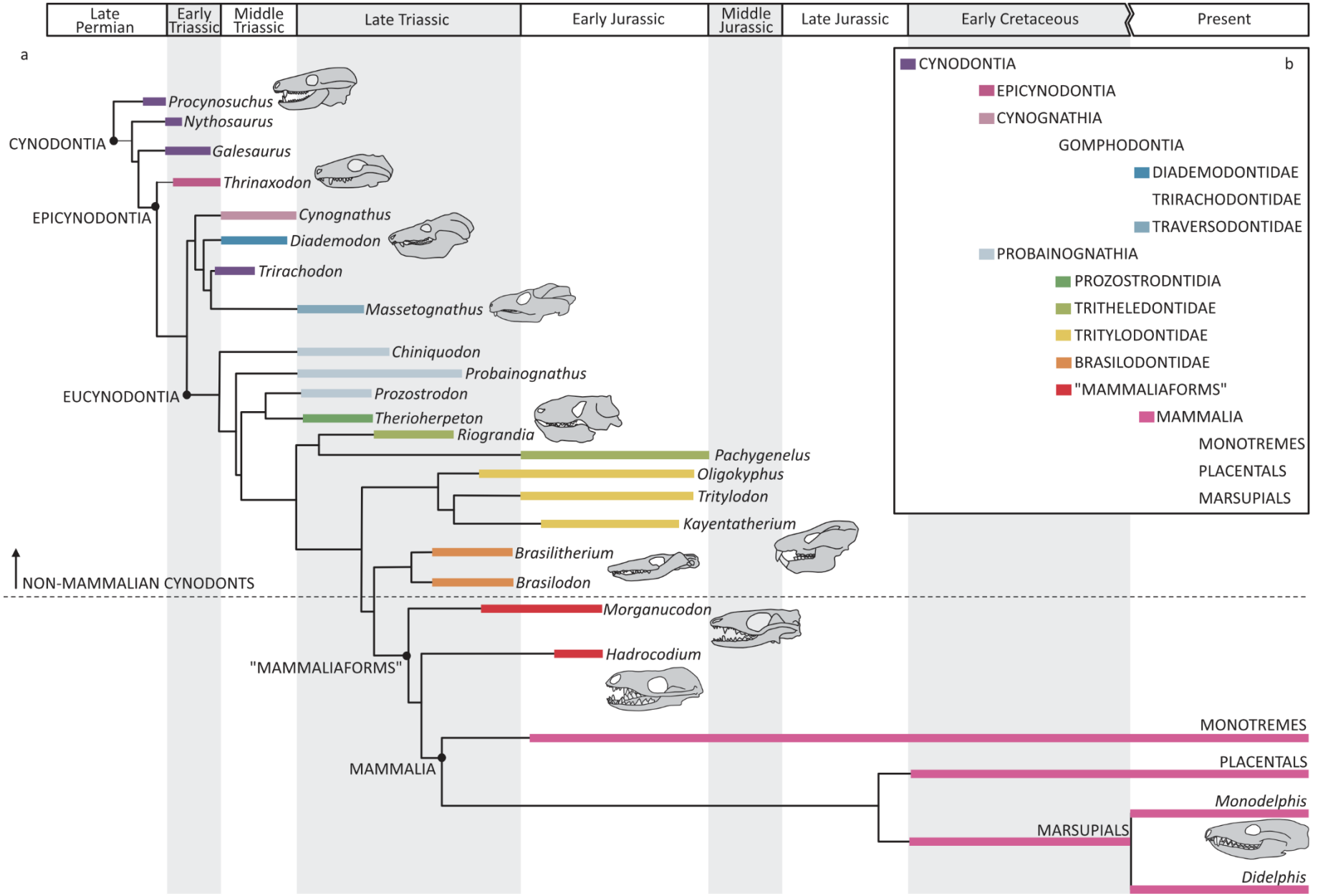
Late Permian
Early Triassic
Middle Triassic
Late Triassic
Early Jurassic
Middle Jurassic
Late Jurassic
Early Cretaceous
Present
a
b
CYNODONTIA
EPICYNODONTIA
CYNOGNATHIA
GOMPHODONTIA
DIADEMODONTIDAE
TRIRACHODONTIDAE
TRAVERSODONTIDAE
PROBAINOGNATHIA
PROZOSTRODNTIDIA
TRITHELEDONTIDAE
TRITYLODONTIDAE
BRASILODONTIDAE
"MAMMALIAFORMS"
MAMMALIA
MONOTREMES
PLACENTALS
MARSUPIALS
Procynosuchus
Nythosaurus
Galesaurus
Thrinaxodon
Cynognathus
Diademodon
Trirachodon
Massetognathus
Chiniquodon
Probainognathus
Prozostrodon
Therioherpeton
Riograndia
Pachygenelus
Oligokyphus
Tritylodon
Kayentatherium
Brasilitherium
Brasilodon
Morganucodon
Hadrocodium
Monodelphis
Didelphis
NON-MAMMALIAN CYNODONTS

**Figure 1.1 (previous page). (a)** Cynodont, mammaliaform and mammalian phylogenetic and stratigraphic relationships for studied specimens and key species of interest. Non-mammalian cynodonts are species shown above the horizontal dashed line. **(b)** Simplified outline of the key evolutionary groups along the cynodont-mammal transition (based on Lautenschlager *et al*., 2017; Botha-Brink *et al*., 2018; Lukic-Walther *et al*., 2019; Lautenschlager *et al.*, 2023 and Pusch *et al.,* 2022).

The mammalian lineage arises from the Early Triassic Probainognathia (figure 1.1) from which Prozostrodontia evolved, followed by Tritheledontidae (Middle Triassic) and Tritylodontidae, Brasilodontidae and mammaliaforms (all in the Late Triassic; Ruta *et al*., 2013; Botha-Brink *et al*., 2018; Lukic-Walther *et al*., 2019). Mammaliaforms represent the crown group from which mammals originated, and the diversity in cynodont, mammaliaform and mammalian cranial anatomy and skull size is evident in figure 1.2. The Mesozoic radiation of mammalian taxa saw subsequent diversification into monotremes in the Early Jurassic (Luo 2007; Zhou *et al*., 2021), then placentals and marsupials in the Early Cretaceous (Luo 2007). Today, mammals are the only living members of Synapsida and have remained the dominant terrestrial vertebrates since the extinction of non-avian dinosaurs.

Deciphering cynodont palaeobiology is challenging due to the lack of modern representatives and the fragmentary nature of the fossil record. However, Didelphidae (opossums) are presently found across the Americas and are often considered a contemporary analogue for extinct cynodonts, despite these basal mammals being phylogenetically far removed from cynodonts and Mesozoic mammals (Luo 2007; Ruta *et al*., 2013; Rodrigues *et al*., 2014; Lukic-Walther *et al*., 2019; Rodrigues *et al*., 2019). This assumption is largely based on cynodont and mammal middle ear bones still being attached to the jaw in embryos, but detaching during

ontogeny, as observed during the evolution of Mesozoic taxa (Rowe 1996; Luo 2007; Benoit *et al*., 2023). It is now convention within scientific literature to use didelphids such as *Monodelphis domestica* and *Didelphis virginiana* as modern comparisons for cynodonts (Kaas 2013; Rodrigues *et al*., 2014; Lautenschlager *et al*., 2017; Guignard *et al*., 2018) with alternative candidates being scarce due to the temporal distance between cynodonts and more derived mammalian taxa.

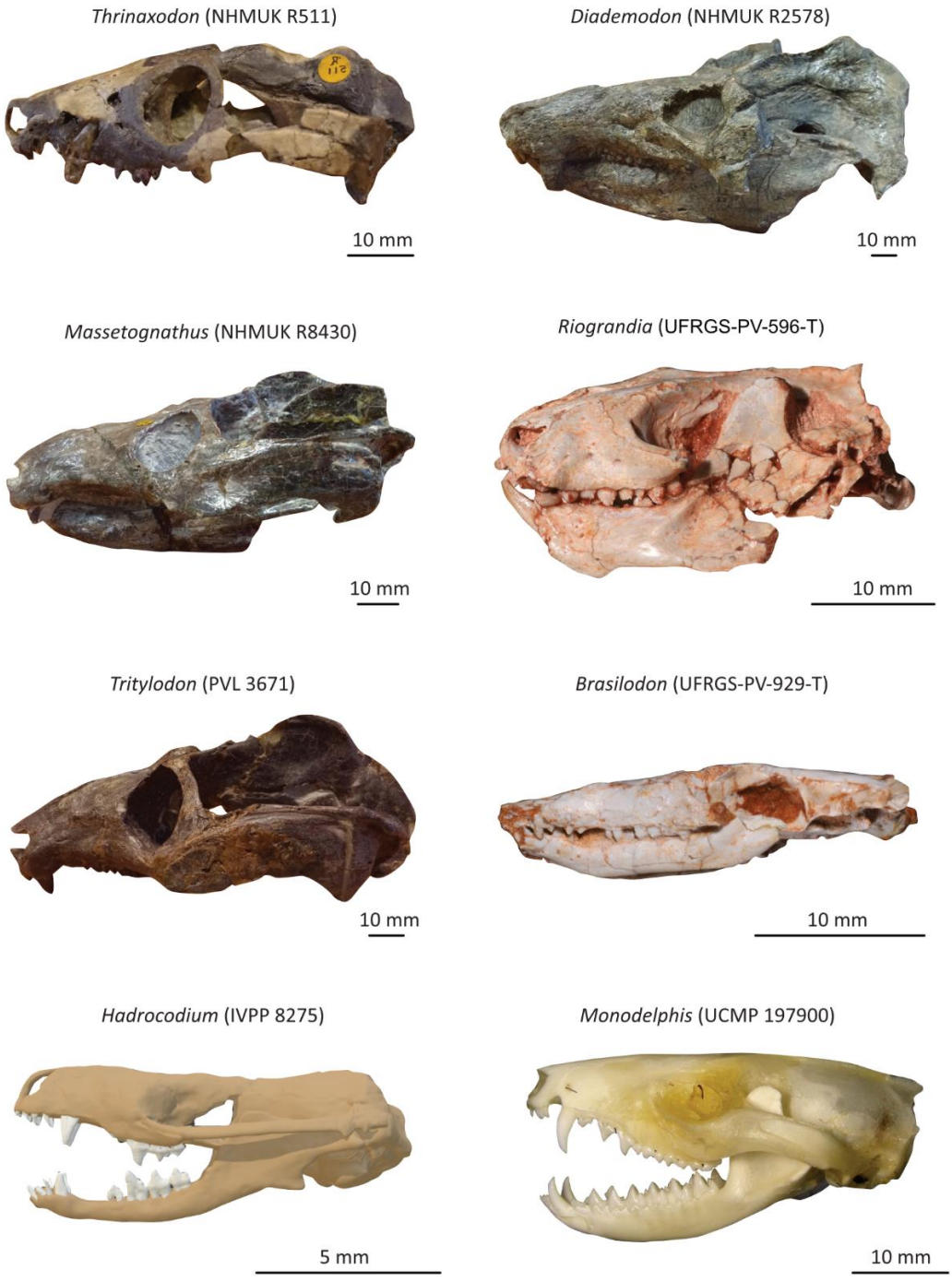

**Figure 1.2. (previous page).** Cynodont, mammaliaform and mammalian cranial anatomy, highlighting the diversity in skull size and shape across the mammalian evolutionary lineage. *Thrinaxodon*, *Diademodon*, *Massetognathus* and *Tritylodon* skull images taken by the study author at the Natural History Museum, London, in 2020. Other specimen images sourced as follows: *Riograndia* (Rodrigues *et al*., 2019), *Brasilodon* (Abdala *et al*., 2020), *Hadrocodium* (Lautenschlager *et al*., 2017) and *Monodelphis* (Moustakas *et al*., 2011).

### 1.1.2. Defining mammalian characteristics

Didelphids, like most mammals, possess a distinct set of characteristics that broadly define organisms as mammals, including the growth of body hair (Vullo *et al*., 2010; Martin *et al*., 2015), the ability to give birth to live young (viviparous; Funston *et al*., 2022), the capacity to produce milk (or an equivalent substance; Curley and Keverne, 2005; Power and Schulkin, 2013), being endothermic (Legendre and Davesne, 2020) and possessing complex brains capable of advanced cognitive and behavioural functions (Curley and Keverne, 2005; Lieberwirth and Wang, 2012). As these characteristics developed over time, they are not all present in all non-mammalian ancestors.

Definitive evidence of fur among cynodonts is contentious as these soft tissues are not preserved in the fossil record. Previous studies have, however, suggested the possible presence of hair-like structures within a late Permian coprolite potentially produced by a therapsid (Bajdek *et al*., 2015; although this is very unlikely), and the potential for whisker-like structures to have grown from pitted foramina on the snout of the basal cynodont, *Thrinaxodon liorhinus* (Damiani *et al*., 2003); although the purpose of the pits is disputed as being linked to the maxillary canal instead (Benoit *et al*., 2023). Conversely, fur was well developed in mammaliaforms (Ji *et al*., 2006; Vullo *et al*., 2010; Zhou *et al*., 2013).

Cynodonts are suggested to have been viviparous, seemingly evidenced by the discovery of 38 perinates (recently born individuals) alongside an Early Jurassic, adult tritylodontid cynodont, *Kayentatherium wellesi* (Hoffman and Rowe, 2018). No eggshells were discovered with the fossil material, though it should be noted that if these juveniles had been born inside leathery, soft tissue eggs (like those produced by monotremes), then the eggs would likely not have been preserved (Sues 2018). Mammaliaforms retained (or developed) the ability to give birth to live young, a trait now observed in extant marsupial and placental mammals (Ferner *et al*., 2017). Some researchers have even suggested the potential of baby carrying among mammaliaforms, where juveniles held on to the back of their parent (Kuznetsov and Panyutina, 2018). Such a behavioural characteristic is suggested by a continuously lopsided gait preserved within a fossil trackway produced by a Middle Jurassic mammaliaform, potentially caused by uneven loading of the parent's body by juveniles on its back (Kuznetsov and Panyutina, 2018). However, despite such behaviours being seen in modern mammals, it is difficult to know whether this behaviour occurred in extinct taxa or whether other factors, such as injury, are more likely causes of a lopsided trackway.

The production of milk (or an equivalent, nutrient-rich substance) from glands likely predates the origin of mammals and is a reproductive trait of synapsids more generally (Oftedal 2002). DNA sequencing of monotreme milk cells confirms ancient origins of lactation, identifying genes coding for milk and whey proteins were present in mammalian ancestors between 166 and 240 Ma (Lefèvre *et al*., 2010). Therefore, milk production is a characteristic that has likely been retained across the numerous evolutionary transitions towards extant mammals.

The origins of mammalian endothermy (maintaining a body temperature between 31°C and 45°C, predominantly through metabolic activity; Araújo *et al*., 2022) are highly contentious,

with numerous anatomical approaches having been considered to define when this mammalian feature evolved. Araújo *et al*. (2022) proposed that the viscosity of fluid within the semi-circular canals of the inner ear is influenced by body temperature and, therefore, understanding more about endolymph (fluid) development could help to define when endothermy originated. From analysing the inner ear morphology of 56 extinct synapsid species, the study suggests that endothermy developed in Late Triassic mammaliamorphs, when increased metabolic and behavioural activities raised body temperatures between 5°C and 9°C. These factors combined thus supported more refined balance, motor control, spatial awareness and navigation controlled by the semi-circular canals and fluidity of the endolymph (fluid) within.

Conversely, Benton (2021) suggested that endothermy originated in the late Permian but became more prolific in the Early Triassic following the Permian-Triassic mass extinction (~252 Ma), based on phylogenetic mapping of macroevolutionary characteristics including changes to bone histology and the development of body hair. Furthermore, oxygen isotope analysis of apatite in Permo-Triassic therapsid bones and teeth may also corroborate a Permian origination for endothermy (Rey *et al.,* 2017). The isotopic ratio of oxygen-16 ($^{16}O$) and oxygen-18 ($^{18}O$), recorded in apatite as isotope fractionation between body fluids and apatite minerals, is dependent on body temperature (Rey *et al*., 2017). By analysing the chemistry of apatite in more than 100 therapsid and non-therapsid fossils, Rey *et al*. (2017) found that the $\delta^{18}O$ ratio for therapsids such as *Kannemeyeria, Cynognathus* and *Diademodon* were noticeably different from temnospondyl amphibians such as *Xenotosuchus* and *Microposaurus* (−1.5 ±1.1‰ to +0.9 ±1.5‰), falling within the range considered to be endothermic and, therefore, this characteristic seemingly developed prior to the emergence of these Middle Triassic taxa. It appears that numerous lines of evidence suggest that

endothermy developed in the mammalian lineage in the Permo-Triassic, possibly as early as the end of the Permian, which may have been an evolutionary advantage to help cynodonts survive the climatic fluctuations at this time.

The final characteristic synonymous with mammals is possessing a complex brain (although many birds have also developed relatively large and complex brains; Smaers *et al*., 2021). In extant birds and mammals, brains can be up to ten times larger (relative to body mass) than in their ancestors, controlling metabolic and behavioural characteristics including endothermy, learning and parental care (Northcutt 2011; Benton 2021). Many studies use the relative brain size of cynodonts compared to mammals to derive potential cognitive capabilities, as relative brain size is a balance between energetic requirements and the need to respond to changing environmental stimuli (Smaers *et al*., 2021). The most noticeable modifications to the mammal brain have been to the size of the olfactory bulbs, cerebral hemispheres and cerebellum; particularly the development of the neocortex in the cerebral cortex (Northcutt 2011). The neocortex is responsible for higher order brain functions such as cognition, sensory perception, language and spatial awareness, and constitutes 80% of the human brain volume (Kaas 2013). However, early mammals had much smaller brains compared to body size (Benton 2021) and possessed little to no neocortex; emphasis was instead placed on larger olfactory bulbs for sensory processing (Kaas 2013). Brain complexity is also influenced by the density of neurons within different brain regions, but it is not possible to reconstruct neural densities for extinct taxa.

### 1.1.3. The archetypical cynodont: *Thrinaxodon liorhinus*

While modern mammals can provide information about the palaeobiology of extinct ancestors, understanding more about cynodont and mammaliaform life histories relies upon

analysing suitably preserved fossil material, which is generally very scarce. One exception is the Early Triassic (~250Ma) basal cynodont *Thrinaxodon liorhinus*, which is one of the most frequently preserved cynodonts from the Karoo Basin, South Africa (Abdala and Ribeiro, 2010; Abdala *et al*., 2013). Studying this species provides insights into the origin of the earliest cynodonts. *Thrinaxodon* was first described by Harry Seeley in 1894 (Seeley 1889; Seeley 1894a; Parrington 1933), although Richard Owen had previously misidentified the type specimen NHMUK R511 (housed at the Natural History Museum, London) as *Galesaurus planiceps* in 1887 (Owen 1887). *Thrinaxodon* has since been well studied with regards to cranial (Broom 1938; Abdala *et al*., 2013; Jasinoski *et al*., 2015; Benoit *et al*., 2017) and postcranial anatomy (Damiani *et al*., 2003; Botha and Chinsamy, 2005; Botha *et al*., 2007; Fernandez *et al*., 2013; Jasinoski and Abdala, 2017), although research into the endocranial anatomy is lacking.

Jasinoski *et al*. (2015) analysed *Thrinaxodon*'s cranial anatomy to identify whether ontogenetic changes (that is, changes occurring during the life cycle of an individual) are apparent within fossilised skulls. Sixty-eight specimens were studied, representing ontogenetic stages from juveniles through to adults, revealing compartmentalisation of skull development. Growth rates were slower for the orbit and posterior region of the palate, but faster for the rest of the palate, snout and temporal bones. There may also have been instances of sexual dimorphism, with males assumed to have wider skulls (particularly associated with the zygomatic arches) to accommodate larger musculature, as observed in several opossum species (Bubadué *et al*., 2021). The research by Jasinoski *et al.* (2015) is the largest accumulation of *Thrinaxodon* skulls studied together and highlights that there are a large number of well-preserved specimens available, yet study of *Thrinaxodon*'s brain anatomy has so far been neglected.

*Thrinaxodon*'s dentition suggests that it was omnivorous (Jasinoski *et al*., 2015) and had post canine morphology resembling that of *Morganucodon*, a basal mammaliaform (Abdala *et al*., 2013). Pitted foramina preserved on the surface of fossilised snouts have erroneously been attributed to the presence of whisker-like structures to enhance sensory capabilities during the pursuit of prey (Damiani *et al*., 2003), but were more likely associated with the maxillary canal (Benoit *et al*., 2023). It has also been suggested that *Thrinaxodon* lived in burrows. A compelling case for a fossorial (burrowing) lifestyle was presented by Fernandez *et al*. (2013) following synchrotron imaging of a fossilised burrow from South Africa. The curled posture of *Thrinaxodon* is inferred as a position adopted during a state of aestivation (dormancy) during summer months or the dry season (Damiani *et al*., 2003; Fernandez *et al*., 2013). Further evidence of a potential burrowing lifestyle comes from a 251-million-year-old burrow cast containing an articulated *Thrinaxodon* skeleton (Damiani *et al*., 2003). Whether *Thrinaxodon* dug burrows itself or made use of those created by other taxa is still debated as *Thrinaxodon* does not exhibit any obvious osteological features to indicate a fossorial lifestyle (Damiani *et al*., 2003; Butler *et al.,* 2019). Living (or partially living) underground may have been a behavioural adaptation employed in light of changing environmental conditions at the Permo-Triassic boundary. It is likely that *Thrinaxodon* exhibited a semi-sprawling posture, with knees and hindlimbs orientated forwards to allow movement within burrows (a precursor to the upright posture of mammals), and possibly causing the sloping shafts preserved in fossilised burrows, if indeed *Thrinaxodon* did excavate its own burrows (Damiani *et al*., 2003; Kemp 2005).

Regarding life history, osteological data suggests that within the first year of life, *Thrinaxodon* grew rapidly and continuously until reaching skeletal (and possibly reproductive) maturity, when growth then slowed (Botha and Chinsamy, 2005; Butler *et al.*, 2019). Jasinoski and

Abdala (2017) proposed that *Thrinaxodon* may have lived in family groups, following the discovery of numerous, mixed-aged assemblages of *Thrinaxodon* fossils from the Early Triassic of the Karoo Basin. Juveniles were found to be less than 40% of the adult size (indicating the presence of different ontogenetic stages), with the juveniles all being similar in size. This suggests that the individuals were part of the same clutch and raises the question of whether *Thrinaxodon* was capable of parental care (Jasinoski and Abdala, 2017).

### 1.1.4. Evolution of the mammalian brain

Although the skeletal anatomy of *Thrinaxodon* has been well studied, few attempts have been made to reconstruct its endocranial anatomy (that is, the brain, inner ear, nerves and blood vessels), despite an abundance of well-preserved skulls. The numerous available specimens provide an opportunity to study the morphology of an ancestral mammal-like brain (which sheds light on the timing of when some characteristically mammalian features emerged) and permits investigation into instances of endocranial variability (which may have impacted cognitive and sensory capabilities). Ultimately, understanding more about the endocranial anatomy of one of the earliest cynodonts provides insights into the evolution of the mammalian brain and the less complex structure it has evolved from.

Traditionally, the cynodont brain is considered to have been small, with reduced olfactory bulbs, narrow cerebral hemispheres and minimal cortex over the midbrain leading to low-resolution sensory capabilities when compared to modern mammals (Rowe *et al*., 2011; Kaas 2013). Numerous endocranial transitions occurred along the evolutionary lineage towards extant mammals, leading to larger brains with expanded olfactory bulbs, neocortex and cerebellum. Rowe *et al*. (2011) proposed that these evolutionary changes occurred in three pulses; first driven by improved olfactory acuity, neuromuscular coordination and tactile

sensitivity from body hair, and subsequently followed by a second phase of brain enlargement to mammalian proportions, again suggested to have been driven by olfactory improvements. As crown Mammalia emerged, a third pulse of evolution was driven by the ossification of nasal turbinals and expansion of olfactory epithelium, matching an increase in the number of odorant receptor genes and leading to the acute olfactory capabilities of modern mammals. The first pulse of brain development was identified in the mammaliaform *Morganucodon* (Late Triassic to Middle Jurassic), with brain volume increasing almost 50% compared to basal cynodonts; the greatest enlargement being concentrated within the olfactory bulbs and cortex (although the cerebellum is also noticeably larger; Rowe *et al*., 2011). By the time *Hadrocodium* (an extinct relative of crown Mammalia) emerged in the Early Jurassic, a second phase of brain development was suggested by further growth of the olfactory bulbs and cerebral hemispheres so that relative brain size approached that of extant mammals (Northcutt 2011; Rowe *et al*., 2011). At this time, the middle ear bones had also detached from the mandible, a condition still observed in modern mammals such as *Monodelphis domestica*.

However, the timing of the three-pulse view of mammalian brain development has been debated by several more recent computed tomography (CT)-based studies of fossil taxa. Ruf *et al*. (2014) examined *Brasilitherium riograndensis*, a derived cynodont in the sister group to mammaliaforms, finding that this cynodont already had olfactory bulbs of comparable size to mammaliaforms. Similarly, the cynodonts *Therioherpeton* and *Riograndia* both possessed enlarged olfactory bulbs (Rodrigues *et al*., 2019; Kerber *et al*., 2021), plus probainognathian cynodont *Chiniquodon* (Rodrigues *et al*., 2019) displayed a mammal-like midline sulcus between the olfactory bulbs, indicating that evolutionary modifications to the size and complexity of the olfactory region had already begun prior to the emergence of

mammaliaforms (Benoit *et al*., 2023). Additionally, the Late Triassic cynodont *Probainognathus* shows expanded cerebral hemispheres, with some midline separation at the posterior implying possible cerebral expansion prior to the origination of mammaliaforms (Rodrigues *et al*., 2019).

Regarding *Thrinaxodon*, previous investigations into its brain morphology have been presented as simplified illustrations (Kielan-Jaworowska *et al.,* 2004), but these have not been updated in light of new, digital palaeontological techniques. To understand the evolution of the cynodont brain towards modern mammals, the morphology of the brain needs to be explored. However, achieving this is a significant challenge due to the rarity of soft tissue preservation in the fossil record and in particular, the scarcity of endocranial fossils. Rare examples of fossilised brains have been discovered within the fossil record of ray-finned fish (Figueroa *et al*., 2023), camel ancestors (Jerison 1991) and birds (Kurochkin *et al*., 2007), among others. Yet there are no known published accounts of preserved cynodont brain tissue, although a natural endocast of Early Triassic cynodont, *Nythosaurus larvatus*, has been discovered (Pusch *et al*., 2022), providing an indication of surface morphology. As such, studies of cynodont brains principally rely on serial segmentation of the endocranial cavity using destructive or digital tomographic techniques (Sutton *et al*., 2014).

## 1.2. Virtual palaeontology: a brief history

Virtual palaeontology is the three-dimensional digital rendering and analysis of fossil material and can include the visualisation of CT or laser scans, segmentation of digital models, mechanical finite element analysis, and many other techniques used to non-destructively study fossils. Virtual palaeontology originated in the early 1980s when medical x-ray CT was first applied to vertebrate fossils (Sutton *et al*., 2014). However, prior to this, physically

destructive sectioning techniques were used to generate internal views of fossils. William Sollas developed the first sectioning technique, with specimens cut at 25µm intervals using a custom-built machine (Sollas 1904). The resulting sections were photographed and traced on to beeswax plates before being gently heated to fuse the sections into a cohesive 3D model (Sollas 1904; Sutton *et al*., 2014). Others used latex moulding to obtain models of internal and external fossil features, but this process relied on the endocranial cavity not being filled with matrix (Radinsky 1968).

With the advancement of technology, and for the long-term preservation of specimens (particularly those of rare or historical significance), digital segmentation techniques have become the preference. Computed tomography scanning was first applied to vertebrate fossils in 1982 (Tate and Cann, 1982; Conroy and Vannier, 1984; Wu and Schepartz, 2009) and has since become commonplace within palaeontological studies due to the ease with which large fossils can be scanned within medical CT scanners. Further advances in imaging technology include the development of magnetic resonance imagery (MRI), X-ray microtomography (for microfossils) and synchrotron scanners which provide the highest definition images currently available (Sutton *et al*., 2014). These scanning methods produce image stacks that can be converted into 3D fossil models using visualisation software (for example, Serial Palaeontological Image Editing and Rendering System (SPIERS), Avizo and 3D Slicer). The 3D models are then digitally segmented, allowing for the isolation of specific regions of interest without causing specimen damage. The models also permit the application of subsequent mathematical or mechanical analyses (such as finite element analysis; Rayfield 2007; Bright 2014; Cunningham *et al*., 2014; Lautenschlager 2022) to provide additional information about biomechanical characteristics of extinct organisms and how these may have impacted mode of life. Furthermore, the production of digital models (from both the

initial scanning technique and subsequent segmentation) greatly increases accessibility to 'digital fossils', enhancing the educational value of palaeontological specimens and promoting collaboration between researchers (Bates *et al*., 2010; Rahman *et al*., 2012; Lautenschlager and Rücklin, 2014; Davies *et al*., 2017; Cunningham 2021).

### 1.2.1. Reconstructing cynodont brains

To reconstruct endocranial anatomy from fossils, researchers have used many different software including Amira, Avizo, Materialise Interactive Medical Image Control System (MIMICS), VGStudio, SPIERS, 3D Slicer, Blender, Maya, Landmark and Meshlab (Macrini *et al*., 2007b; Macrini 2012; Lautenschlager and Hübner, 2013; Cunningham *et al*., 2014; Henderson and Challands, 2018; Pavanatto *et al.*, 2019; Watanabe *et al*., 2019). It is worth noting that these software permit the production of an endocranial reconstruction; a model of the internal anatomy of the brain cavity (plus inner ear, vascular and nerve structures if desired) based upon the skeletal boundary of the braincase (where present). However, such a model may not be a true representation of the original brain anatomy as intracranial fluid, nerves, blood vessels and meninges (protective tissues) may have existed between the brain and braincase of cynodonts (Watanabe *et al*., 2019) which, if present, would almost certainly not have been preserved in the fossil record. Such features are seen in modern mammals, but their brains still largely fill the braincase, therefore a similar state has been suggested for mammal ancestors too (Rowe 1996). The presence of these soft tissues in cynodonts is debated due to the millions of years of evolution between the earliest cynodonts and extant mammals.

Due to the uncertainties associated with which endocranial tissues were present, there may be discrepancies between the volume of the brain cavity and the brain of the living organism.

This can be problematic when making inferences about cognitive capabilities of extinct organisms where no preserved brain material is available. For example, the encephalisation quotient (EQ) is often calculated to provide an approximation of cognitive capabilities among extinct species (Jerison 1973). EQ values are calculated from the ratio between an organism's actual brain size compared to the predicted brain size (based on the individual's body mass). Organisms with an EQ below one, have a brain mass smaller than expected for their body size, whilst organisms with EQ values greater than one have a brain mass exceeding predictions based on body mass. Most cynodonts and mammaliaforms have an EQ between 0.02 and 0.5 (Benoit *et al.,* 2023). The absence of information about intracranial fluids and tissues from fossilised skulls may, therefore, lead to overestimation of the EQ where the entire brain cavity is used. Furthermore, where no postcranial skeleton is preserved, the body mass has to be estimated from skull length, adding another layer of uncertainty in predictions of intelligence (Luo *et al*., 2001; Rodrigues *et al*., 2019). However, where there is no soft tissue evidence, the volume of the brain cavity provides the best approximation for the original brain volume, helping to provide insights about the relative changes to brain volume (and possibly cognitive capabilities) along evolutionary lineages (Rodrigues *et al*., 2019).

Additionally, it is only in rare circumstances that impressions of the brain are left on the inside of the braincase, most prominently in fossil hominins as gyri and sulci (ridges and troughs that increase the surface area of the cerebral cortex; de Sousa *et al*., 2023). Therefore, complex surface ornamentation cannot often be reconstructed, if indeed such surface folds were present in extinct taxa at all. It is considered that most cynodonts had lissencephalic (smooth) brains, which is suggested to be the plesiomorphic (ancestral) condition for pre-mammalian species (Kielan-Jaworowska *et al*., 2004; Macrini *et al*., 2007b). In the same way, it is not possible to reconstruct neural connections within the brain (Karten 2015), hence endocast

morphology only provides an approximation of an organism's cognitive capabilities based on relative proportions of brain regions and subsequent comparison of calculated encephalisation quotients (Rodrigues *et al*., 2019). The paucity of soft tissue preservation to confirm the true morphology of cynodont brains means that endocranial reconstructions (hereafter endocasts) produced through the digital segmentation of scanned fossil skulls represent the best approximation currently available of cynodont brain morphology.

## 1.3. Aims and hypotheses

This research harnesses virtual palaeontological techniques to assess cynodont endocranial anatomy and the impact current reconstruction techniques may have on outputs. Research methods are outlined in **chapter two**, with additional project specific details provided in individual chapters.

The cranial and postcranial anatomy of *Thrinaxodon liorhinus* has been well studied, but following an evaluation of available literature, no known attempt has been made to digitally reconstruct the brain of *Thrinaxodon*. Therefore, the current knowledge of *Thrinaxodon*'s brain morphology is based on simplified (and somewhat outdated) illustrations presented by Kielan-Jaworowska *et al.* (2004) and Rowe *et al*. (2011). **Chapter three** aims to provide new insights into *Thrinaxodon*'s brain morphology using computer-based reconstruction techniques to generate a digital model of the cynodont's endocranial anatomy. Here, the reconstructed brain is presented and described, with interpretations of functional and cognitive capabilities offered.

**Chapter four** addresses whether ontogenetic variation is identifiable within digital endocranial reconstructions of *Thrinaxodon liorhinus*. It is hypothesised that changes to both

brain shape and size will be visible in endocranial reconstructions associated with ontogeny based on known morphological changes observed in *Thrinaxodon*'s skull during development (Jasinoski *et al*., 2015). To test this, endocasts were generated for a juvenile and adult *Thrinaxodon liorhinus* skull and compared with a growth series of opossum (*Monodelphis domestica*) brain models from Macrini *et al*. (2007b). Endocasts were quantitatively analysed to identify size and shape changes between juvenile and adult forms of both the cynodont and opossum, and allometric growth of different brain regions was identified. Comparisons between *Thrinaxodon* and *Monodelphis* endocasts permits projections to be made about the likely developmental trajectory of *Thrinaxodon* during the life cycle of a single individual.

**Chapter five** aims to identify and quantify the influence that modeller subjectivity (arising from, for example, segmenting skill level or prior knowledge of the taxa) imparts upon the reconstructions produced through segmentation software. It is expected that modellers will show some variation in their reconstructions, particularly if braincase boundaries are not well defined, but whether prior segmentation experience (with non-cynodont taxa) influences models is not currently known. The chapter presents procedural protocols that should be implemented to reduce modeller-induced variation in digital reconstruction processes, essential given that endocranial reconstructions are the basis for interpretations about anatomical, behavioural and ecological characteristics of extinct organisms.

As a basal cynodont, *Thrinaxodon* represents the start of the evolutionary lineage towards modern mammals. Since the Early Triassic, a vast array of cynodonts, mammaliaforms and, eventually, mammals have appeared and adapted to a wide range of ecological niches. Over this time, changes have occurred to the body plan of these organisms, including modifications to the brain. The new endocasts presented for *Thrinaxodon* provide an evolutionary starting

point for the mammalian lineage, and the changes to brain morphology that have occurred between cynodonts and modern mammals are presented in **chapter six**. What impact did these changes have on cognitive and sensory capabilities as environments changed? Did wider changes occurring to Earth at this time have any impact on brain development? These themes are explored further in this chapter.

**Chapter seven** outlines the overall conclusions of the research presented here and shines a light on one of the most well studied, basal cynodonts who's brain anatomy has remained largely elusive until now.

# CHAPTER TWO

# Specimens and methods

## 2.1. Studied specimens and skull digitisation

**Museum abbreviations:** Natural History Museum, London (**NHMUK**); University of California Museum of Palaeontology, Berkeley, USA (**UCMP**); Bernard Price Institute for Palaeontological Research, University of the Witwatersrand, South Africa (**BP**); University Museum of Zoology, Cambridge, UK (**UMZC**); Texas Science and Natural History Museum, The University of Texas, Austin, USA (**TMM**); Universidade Federal do Rio Grande do Sul, Brazil (**UFRGS**).

### 2.1.1. *Thrinaxodon liorhinus*

The Early Triassic cynodont, *Thrinaxodon liorhinus*, was chosen as the main study taxon due to its evolutionary position among the earliest mammalian ancestors, the availability of fossils with well-preserved braincases and the small skull size to facilitate CT scanning. To study the endocranial anatomy of *Thrinaxodon liorhinus*, eight skulls were selected for digitisation, comprising seven adult specimens and one juvenile. Throughout this research, the term 'digitisation' (and derivatives of that) refers to the production of a 3D model from an X-ray or CT scan to produce a digital rendering of the skull or brain endocast, as appropriate. The adult specimens are NHMUK PV R511, NHMUK R3731, NHMUK R5480, UCMP 40466, BP/1/5905, BP/1/7199 and UMZC T815, with the single juvenile specimen being BP/1/5372. Individual specimen details are provided below (with further information about the fossils provided in figures 2.1a and 2.1b, plus table 2.1).

The adult and juvenile classifications were derived from Jasinoski *et al*. (2015)'s study of *Thrinaxodon*'s cranial morphology, where cranial features (including suture morphology, sagittal crest development, foramen shape, dental replacement stage and basal skull length (BSL)) were used to determine four ontogenetic (life) stages: early juvenile (BSL ≤37 mm), late juvenile (BSL 39 to 42 mm), subadult (BSL 56 to 68 mm) and adult (BSL ≥69 mm). As such, all except one of the studied *Thrinaxodon* specimens are deemed to be well developed adults. However, as there are no postcranial fossils associated with the studied skulls, no information is available about whether the specimens are male or female, if indeed it is even possible to determine sex within cynodont fossils as there are no known studies on the subject.

Fossils were chosen based on their availability (whether as physical fossils in museums or pre-scanned data sets made available from other studies). For specimens that were scanned specifically for this research, fossils were selected because of their level of preservation, including the completeness of the braincase, amount of plastic and brittle deformation of the skull and volume of sediment infill, which impacts contrast between the endocranial cavity and bones in the CT scans.

Specimen NHMUK R511 (BSL 84 mm) was collected in Orange Free State, South Africa and is housed at the Natural History Museum, London. The fossil was scanned for Lautenschlager *et al*. (2016) at the Natural History Museum, London, using a Nikon Metrology HMX ST 225 CT scanner set at 190 kV and 135 µA, with 3142 projections. The scan was processed into 1763 slices using CT-Pro (Nikon Metrology) reconstruction software, producing a final image stack with a voxel size of 50.2 µm (Lautenschlager *et al*., 2016). The specimen is well-preserved, with only minor fractures and displacements of the braincase bones. The lower jaw is not included within the scan. There is some post-mortem sediment infill of the braincase, but

digital thresholding of greyscale values assigned to the bone and sediment fill creates enough contrast for the brain cavity to be visible, hence sediment fill does not hinder digital reconstruction of the brain for NHMUK PV R511.

Specimen NHMUK R3731 (BSL 71 mm) was collected in Orange Free State, South Africa, and purchased in 1909 by the Natural History Museum, London. The fossil was scanned in 2020 by Vincent Fernandez for this project, using a Nikon Metrology XT H 225 ST CT scanner with a HE5 filter. The scanner was set at 160 kV and 63 µA, with an exposure time of 135000 seconds and 1601 projections. The scan produced 4262 slices with a pixel size of 18.8 µm. This specimen of *Thrinaxodon* shows some fracturing and displacement of the cranium and the jugals, and lower jaw are not preserved, although the braincase is intact. There is some sediment fill within the braincase, but it is of a low density and therefore contrasts well with the surrounding ossified regions, creating a clear boundary between the braincase and brain cavity for digital reconstruction.

Specimen NHMUK R5480 (BSL 78 mm) was also collected in the Orange Free State, South Africa, and was purchased in 1926 by the Natural History Museum, London. This specimen was scanned for this research by Vincent Fernandez in 2020 using a Nikon Metrology XT H 225 ST CT scanner with a HE5 filter. The scanner was set at 160 kV and 63 µA, with an exposure time of 140000 seconds and 1601 projections. An image stack of 3778 slices was produced, with a pixel size of 24.6 µm. NHMUK R5480 has been subjected to moderate plastic and brittle deformation, with some lateral shearing of the braincase and dissociation of bones (including parts of the parietal, epipterygoid, pterygoid and basisphenoid). Deformation of the braincase is more pronounced in the anterior portion; hence the posterior part of the brain cavity is more useful and the specimen also benefits from the brain cavity being largely sediment free.

Despite some deformation being present, this specimen was one of the few *Thrinaxodon* skulls available at the Natural History Museum, London, where the braincase was preserved. Unfortunately, it is more common for the posterior part of the skull to be absent or completely crushed, hence despite deformation being present, the specimen was still included within the studies presented here.

Specimen UCMP 40466 (BSL 74 mm) was collected from the Orange Free State, South Africa, in 1948 for the University of California Museum of Palaeontology, USA. The fossil was X-ray CT scanned for Rowe *et al*. (1993) at the Texas High-Resolution X-ray CT Facility, Austin, with the scan subsequently stored and retrieved from the Digital Morphology Online Catalogue (http://www.digimorph.org/specimens/Thrinaxodon_liorhinus/). The scan produced a data set comprised of 153 slices (each 0.2 mm thick) with an interslice spacing of 0.2 mm. However, such a small number of slices would create a very coarse, angular model, thus the dataset was resampled in Avizo 9.3.0 (www.thermofisher.com/uk/en/home/electron-microscopy/products/software-em-3d-vis/avizo-software.html) by Stephan Lautenschlager to increase the number of slices to 1200. This process subdivided the original scan into more slices, hence the resolution of the scan itself was not altered. UCMP 40466 has a generally well persevered braincase, with negligible post-mortem deformation, although some of the lateral walls in the anterior half of the braincase are absent. The scan resolution is noticeably coarser than in the other specimens used within this study due to the age of the scan and poor resolution technology used to prepare it. However, there is still good contrast between the brain cavity and surrounding skeletal elements due to the lack of sediment fill.

Specimen BP/1/5905 (BSL 87 mm) was collected in South Africa and is housed at the Bernard Price Institute for Palaeontological Research, University of the Witwatersrand, South Africa. The fossil was synchrotron scanned at the European Synchrotron Radiation Facility for Abdala *et al*. (2013). The scan was conducted at 96 kV, with 5000 projections of 0.5 seconds each. The resulting visualisation is comprised of 964 slices, with 45.5 µm pixels and a voxel size of 0.0455 mm. This fossil has a largely intact braincase, with some dislocation of skeletal elements and a slight lateral skew. However, the original scan for Abdala *et al*. (2013) was noisy and contained a gradient which was heavily filtered out by Vincent Fernandez in post-scan processing. As such, the bone texture has been removed and the foramen magnum has been erroneously over-enlarged, but the rest of the brain cavity is relatively complete. Permission of use was granted by Bruce Rubidge, Fernando Abdala and Sifalani Jirah.

Specimen BP/1/7199 (BSL 75 mm) was collected in KwaZulu Natal Province, South Africa in 1975 and is now stored at the Bernard Price Institute for Palaeontological Research, University of the Witwatersrand, South Africa. The synchrotron scan was conducted for Fernandez *et al*. (2013) at the European Synchrotron Radiation Facility at 96 kV, with a white beam filter (containing 12 mm aluminium, 8 mm copper and 0.25 mm tungsten) and 5000 projections. The scan is comprised of 1101 slices with a voxel size of 0.030 mm. The fossil is very well preserved with negligible sediment fill and only minor fracturing and dislocation of cranial bones in the anterior portion of the braincase. Permission to use the scan in this research was granted by Bruce Rubidge, Fernando Abdala and Sifalani Jirah.

Specimen UMZC T815 (BSL 69 mm) was collected in Orange Free State, South Africa, and scanned in 2013 for Stephan Lautenschlager at the University Museum of Zoology, Cambridge, where the specimen is now housed. The scan was conducted using a Nikon Metrology XT H

225 ST High Resolution CT scanner at 190kV, producing an image stack of 1904 slices with a voxel size of 37.7 µm. The fossil has a very well-preserved braincase, with minimal displacement of basicranial elements. There is very good contrast between the brain cavity and cranium, facilitating clear endocranial reconstruction.

Specimen BP/1/5372 (BSL 37 mm) was collected in South Africa and scanned for Abdala *et al*. (2013), with the fossil stored within the collections of the Bernard Price Institute for Palaeontological Research, University of the Witwatersrand, South Africa. The specimen was synchrotron scanned at the European Synchrotron Radiation Facility at 60 kV and 172 µA, with 1800 projections. The subsequent image stack is comprised of 839 slices, with a voxel size of 0.02024 mm. With BP/1/5372 being a juvenile specimen, there is reduced fusion of bones throughout the skull resulting in notable lateral transformation of skeletal elements associated with the braincase. The specimen also appears to have been subjected to some dorsoventral compression, resulting in overlapping bones (particularly the dentary and jugal). However, as juvenile *Thrinaxodon* specimens are very rare, the specimen still provides an insight into early *Thrinaxodon* brain morphology. Permission for scan use was granted by Bruce Rubidge, Fernando Abdala and Sifalani Jirah.

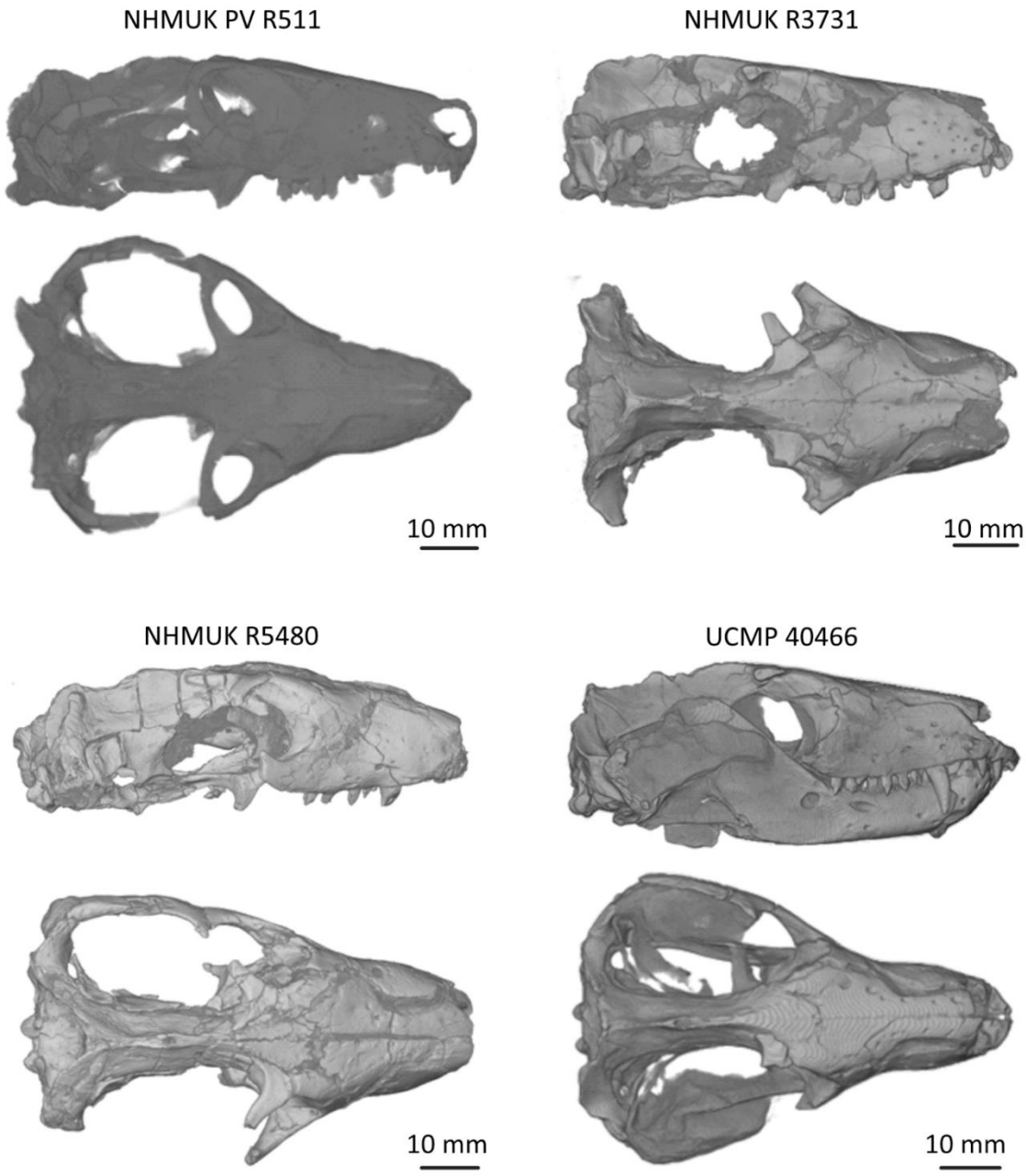


**Figure 2.1a.** Digitised skulls of the adult *Thrinaxodon liorhinus* specimens studied within this research, and for which endocranial reconstructions were produced. For each specimen, the skull is shown in right lateral (top image) and dorsal (bottom image) view.

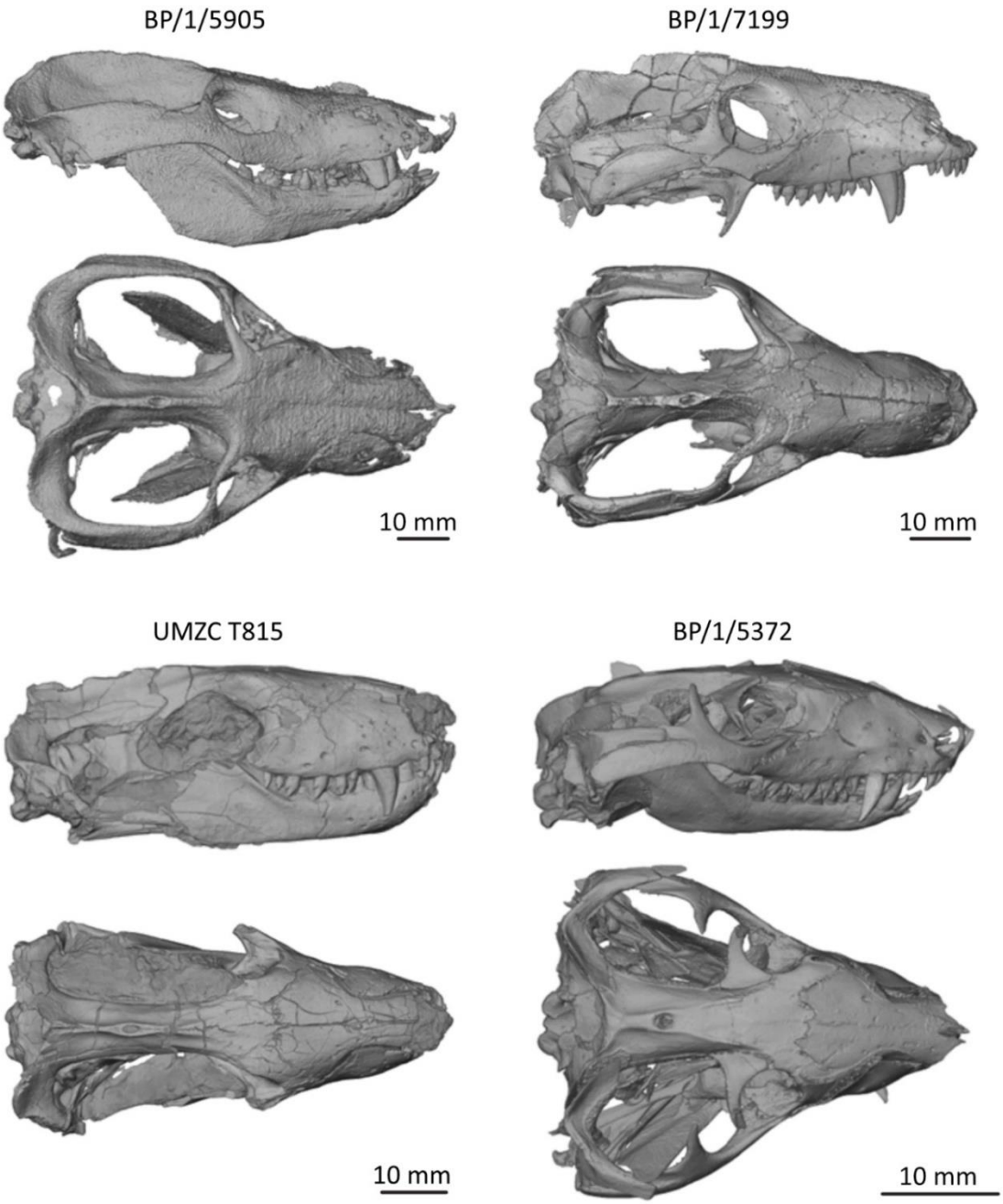


**Figure 2.1b.** Digitised skulls of the *Thrinaxodon liorhinus* specimens studied. Specimens BP/1/5905, BP/1/7199 and UMZC T815 are adults, while BP/1/5372 is a juvenile. For each specimen, the skull is shown in right lateral (top image) and dorsal (bottom image) view.

### 2.1.2. Modern analogues: *Monodelphis domestica* and *Didelphis virginiana*

*Monodelphis domestica* is an extant marsupial from the Didelphidae family, known from South America. This species has a small body size and well-known biology as it is often studied as a laboratory species (Macrini *et al*., 2007b). *Monodelphis domestica* (and its larger, North American relative *Didelphis virginiana*) are frequently included within cynodont studies as a modern analogue (Luo 2007; Rodrigues *et al*., 2014; Jasinoski *et al*., 2015; Rodrigues *et al*., 2019), although the evolutionary and temporal distance between cynodonts and opossums should be considered when drawing conclusions. Nevertheless, for consistency with previous cynodont studies, *Monodelphis domestica* and *Didelphis virginiana* are used here as modern analogues for basal cynodonts such as *Thrinaxodon*.

Six *Monodelphis domestica* endocasts were provided by Thomas Macrini, derived from endocranial reconstructions of the associated skulls (figure 2.2, table 2.1), as presented in Macrini *et al.* (2007b). The studied skulls represent an ontogenetic growth series and include the following specimens from the Southwest Foundation for Biomedical Research in San Antonio, Texas (which were subsequently accessioned to the Texas Science and Natural History Museum, Austin, USA): TMM M-7595 (27 days old; BSL 18.5 mm), TMM M-7536 (day 48; BSL 23.25 mm), TMM M-7539 (day 57; BSL 25.8 mm), TMM M-7542 (day 75; BSL 29.2 mm), TMM M-7545 (day 90; BSL 30.65 mm), and TMM M-7599 (adult; BSL 40 mm).

All *Monodelphis* skulls were X-ray CT scanned in the coronal plane at the University of Texas High-Resolution X-ray CT Facility, Texas, resulting in data sets with the following parameters: TMM M-7595: 495 slices, 0.0371 mm thick, with a 0.0371 mm interslice spacing. TMM M-7536: 381 slices, 0.0625 mm thick, with a 0.0625 mm interslice spacing. TMM M-7539: 381 slices, 0.0625 mm thick, with a 0.0625 mm interslice spacing. TMM M-7542: 481 slices, 0.0608

mm thick, with a 0.0608 mm interslice spacing. TMM M-7545: 455 slices, each 0.0682 mm thick, with a 0.0682 mm interslice spacing. TMM M-7599: 449 slices, 0.095 mm thick, with a 0.09 mm interslice spacing. Endocasts were segmented using VGStudioMax (version 1.2) and made available by Thomas Macrini for the studies presented here. Videos of the CT scans associated with this growth series can be viewed on DigiMorph, although the CT scans themselves are not available to download (http://digimorph.org/specimens/Monodelphis_domestica/day27/index.phtml).

*Didelphis virginiana* is represented by specimen TMM M-2517 (BSL 124 mm) which was retrieved from the Texas Science and Natural History Museum, Austin, USA. The specimen was CT scanned for Macrini *et al*. (2007b) along the coronal axis (859 slices, each 0.132 mm thick) with a 0.132 mm interslice spacing. The skull is very well preserved, with the braincase almost entirely ossified, facilitating clear identification of the brain cavity. The CT scan is freely available to view and download from DigiMorph (http://digimorph.org/specimens/Didelphis_virginiana/). *Didelphis* was not quantitatively analysed for this research, but an endocranial reconstruction was generated purely for evolutionary comparisons (chapter six).

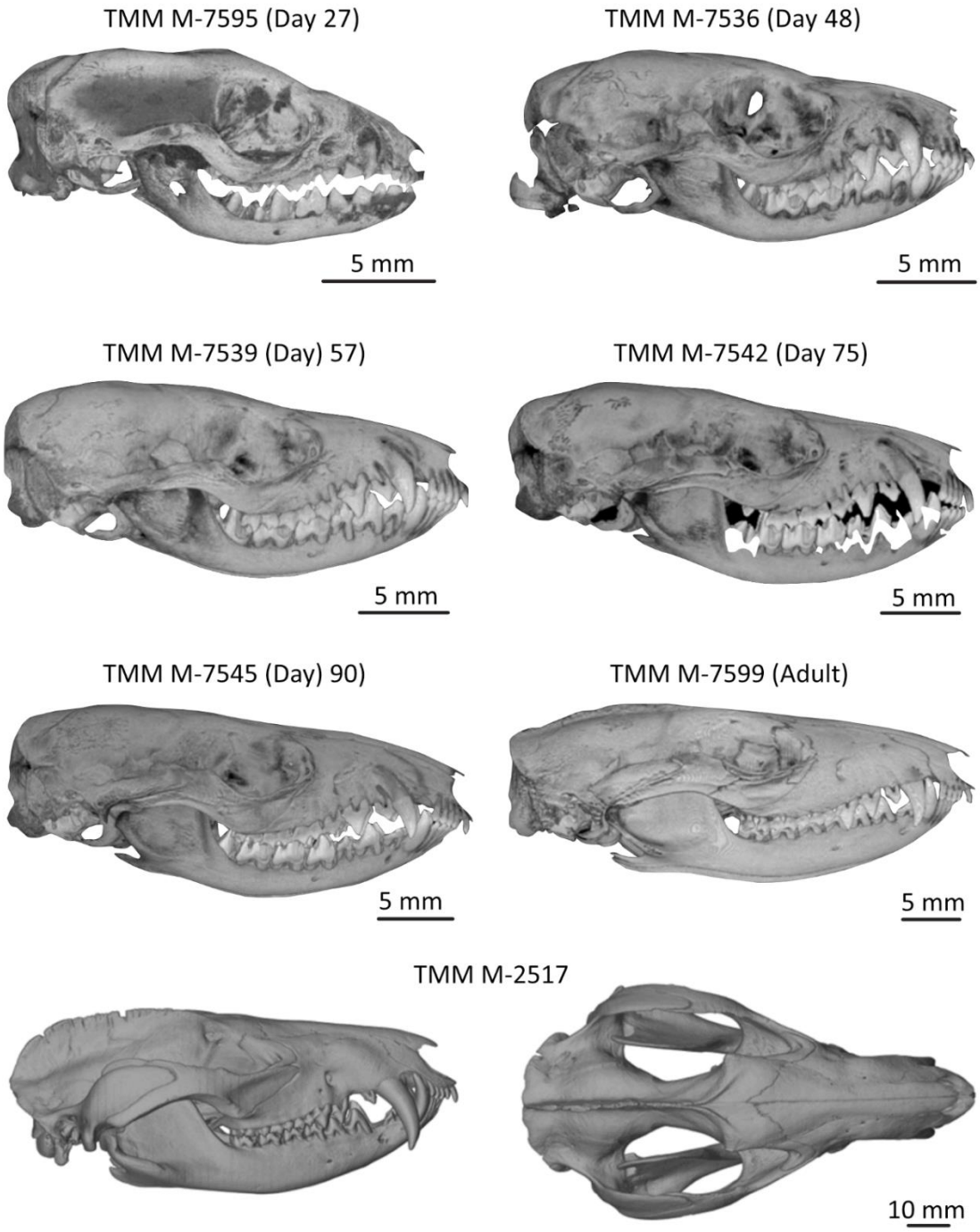


**Figure 2.2.** Digitised skulls of the opossums studied within this research. All specimens are of *Monodelphis domestica,* except for TMM M-2517, which is *Didelphis virginiana*. Only lateral views are provided for *Monodelphis* as the CT scan data is not available on DigiMorph.

### 2.1.3. Brain evolution: considering later cynodonts

To assess the evolutionary changes to cynodont brain morphology towards modern mammals, additional cynodont taxa were also studied (figure 2.3, table 2.1), before the evolutionary transition into mammals. *Diademodon sp.* is a more derived non-mammalian cynodont than *Thrinaxodon*, that lived during the Middle Triassic. The genus has not been extensively studied since it was first described in 1894 (Seeley, 1894b), with no known attempt made to determine its endocranial anatomy using digital reconstruction techniques. Here, specimen UCMP 42446 (BSL 328 mm) was selected for endocranial segmentation. The skull was found in South Africa in 1948 and is now housed at University of California Museum of Palaeontology, USA. The scan was conducted in the coronal plane using an X-ray CT scanner at the University of Texas High-Resolution X-ray CT Facility in 2003. The scanner was set at 420kV and produced an image stack of 410 slices, each 1 mm thick, with an interslice spacing of 0.8 mm. A video of the CT scan can be viewed on DigiMorph (http://digimorph.org/specimens/Diademodon_sp/), but the scan data was provided by Stephan Lautenschlager. The skull and braincase are intact, but the scan resolution is quite poor.

Closer to mammaliaforms is the Late Triassic cynodont *Brasilitherium riograndensis*. Specimen UFRGS-PV-1043-T (BSL 38 mm) was collected in Brazil and is housed within the collections of the Universidade Federal do Rio Grande do Sul, Brazil. The fossil was scanned for Rodrigues *et al*. (2014) in the coronal plane with the Wälischmiller RayScan 200 lCT scanner at Steinbeis-Transferzentrum Gießerei Technologie Aalen, Germany. The resulting scan is comprised of 884 slices, with a voxel size of 0.04634 mm. The scan data was provided by Stephan Lautenschlager for this study. The skull and braincase are reasonably well preserved, although the fossil exhibits a lateral skew. Additionally, a portion from the middle part of the skull scanned for Rodrigues *et al*. (2014) is absent in the scan studied here. However, it is possible to follow

transverse features within the braincase when viewed in the sagittal plane to generate an endocranial reconstruction. Note that endocasts generated for *Brasilitherium* and *Diademodon* are only presented here for evolutionary comparison with *Thrinaxodon* and *Monodelphis* (chapter six) and are not quantitatively analysed in detail within this research.

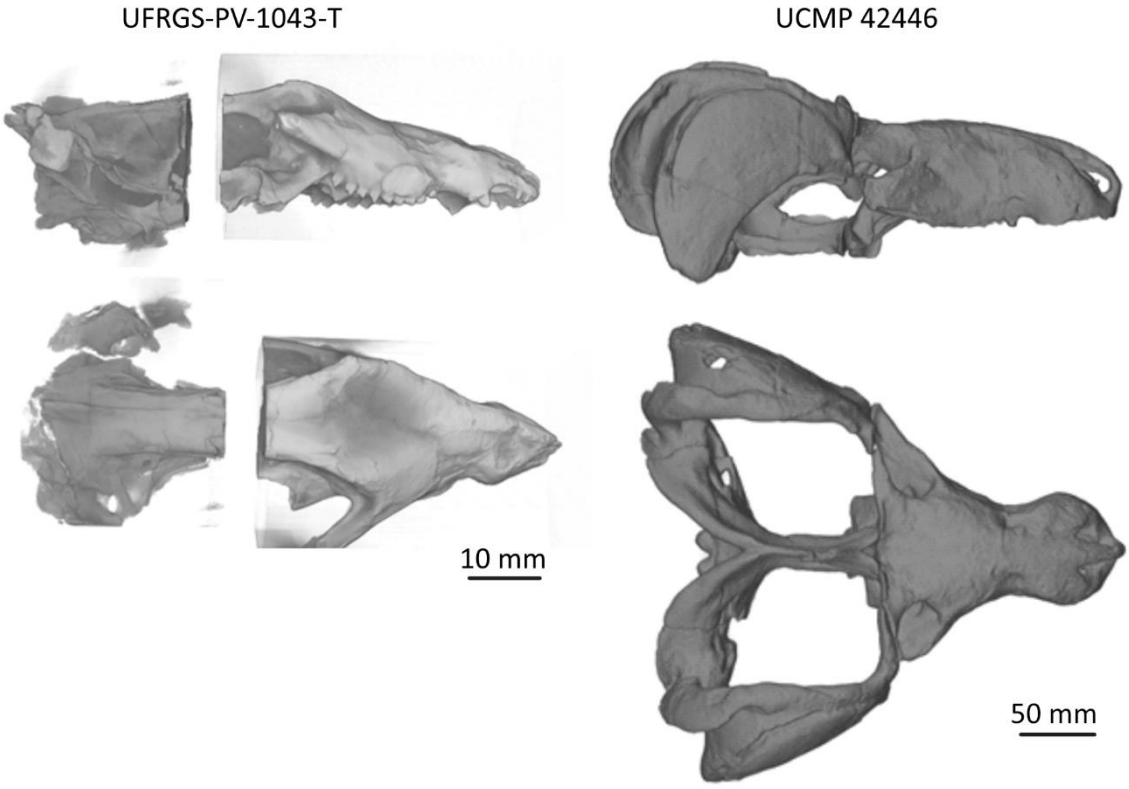


**Figure 2.3.** Digitised skulls of Triassic cynodonts *Brasilitherium riograndensis* (UFRGS-PV-1043-T) and *Diademodon sp.* (UCMP 42446). For both specimen, the skull is shown in right lateral (top image) and dorsal (bottom image) view.

**Table 2.1.** Cynodont and mammalian specimens scanned or retrieved for endocranial reconstruction and included within the research presented.

| Species | Specimen number | Basal skull length (mm) | Age | Reference |
|---|---|---|---|---|
| *Thrinaxodon liorhinus* | NHMUK PV R511 | 84 | Early Triassic | Lautenschlager *et al*., 2016 |
| *Thrinaxodon liorhinus* | NHMUK R3731 | 71 | Early Triassic | Scanned for this research |
| *Thrinaxodon liorhinus* | NHMUK R5480 | 78 | Early Triassic | Scanned for this research |
| *Thrinaxodon liorhinus* | UCMP 40466 | 74 | Early Triassic | DigiMorph |
| *Thrinaxodon liorhinus* | BP/1/5905 | 87 | Early Triassic | Abdala *et al*., 2013 |
| *Thrinaxodon liorhinus* | BP/1/7199 | 75 | Early Triassic | Fernandez *et al*., 2013 |
| *Thrinaxodon liorhinus* | UMZC T815 | 69 | Early Triassic | Scanned for Stephan Lautenschlager in 2013 |
| *Thrinaxodon liorhinus* | BP/1/5372 | 37 | Early Triassic | Abdala *et al*., 2013 |
| *Monodelphis domestica* | TMM M-7595 | 18.50 | Extant – day 27 | Macrini *et al*., 2007b |
| *Monodelphis domestica* | TMM M-7536 | 23.25 | Extant – day 48 | Macrini *et al*., 2007b |
| *Monodelphis domestica* | TMM M-7539 | 25.80 | Extant – day 57 | Macrini *et al*., 2007b |
| *Monodelphis domestica* | TMM M-7542 | 29.20 | Extant – day 75 | Macrini *et al*., 2007b |
| *Monodelphis domestica* | TMM M-7545 | 30.65 | Extant – day 90 | Macrini *et al*., 2007b |
| *Monodelphis domestica* | TMM M-7599 | 40.00 | Extant – adult | Macrini *et al*., 2007b |
| *Didelphis virginiana* | TMM M-2517 | 109.60 | Extant – adult | Macrini *et al*., 2007b |
| *Diademodon sp.* | UCMP 42446 | 328 | Middle Triassic | DigiMorph |
| *Brasilitherium riograndensis* | UFRGS-PV-1043-T | 38 | Late Triassic | Rodrigues *et al*., 2014 |

## 2.2. Segmentation and endocranial reconstruction

Brain reconstructions were generated by importing scan data (TIFF or BMP image stacks or RAW files) into Avizo 9.3.0 segmentation software. When importing the data, the appropriate voxel or pixel size generated by the scan was inputted to ensure that the subsequent skull model was rendered in accurate dimensions. Each scan was digitally rendered by selecting the imported data file and using the volume rendering tool to generate a 3D, digital model of the skull. The skull model provided a visual reference from which sediment and artefacts from the scan could be removed using the thresholding tool. Thresholding assigns greyscale values to the scan data and by using greyscale sliders, certain unwanted values (and therefore areas of the scan data) can be removed (figure 2.4). This function permitted the removal of sediment from inside and outside of the skull, improving the clarity of the brain cavity by increasing the contrast between skeletal elements and the endocranial (brain) space.

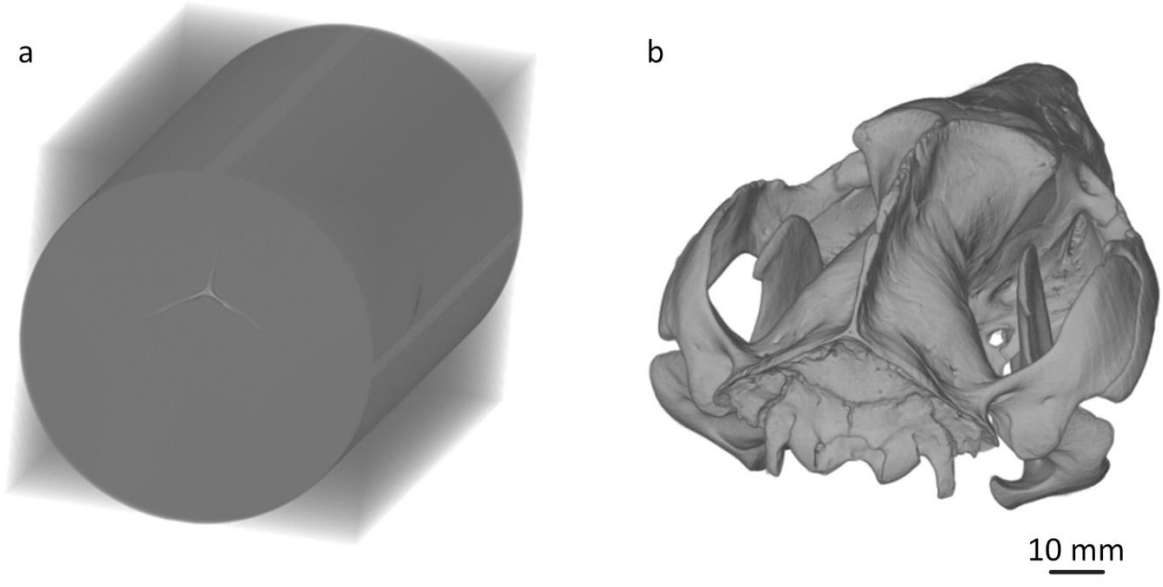


**Figure 2.4.** Specimen TMM M-2517 shown before **(a)** and after **(b)** thresholding was applied. The lower limit of the thresholding greyscale values was set at 30, removing all of the darker pixels below this value (and therefore the darker grey colours concealing the skull in **a**).

After thresholding, digital endocasts were generated through the application of a coloured mask to each image in the data stack, principally in the coronal plane (which is perpendicular to skull length). As such, masks were applied from the posterior to the anterior of each skull, between the foramen magnum at the back of the skull, and where the depression in the frontal bone disappeared in the nasal region. Masks are coloured overlays applied to the scan data which denote that certain pixels belong to a specific object (here, the brain endocast). Masks were generated using the paintbrush tool in Avizo's segmentation editor and interpolated between every five slices for time efficiency, with manual editing of the interpolated slices (where necessary) to ensure the entire brain cavity was filled by the mask. The inner surface of the braincase was used as the outermost edge of the brain model, with this assumption based on the fact that the brain predominantly fills the brain cavity in extant mammals (Macrini *et al.,* 2007a) and it is not possible to know whether additional tissues or intracranial fluid surrounded the brains of the cynodont specimens studied here. Endocasts were generated with the assumption that the brain had symmetrical left and right hemispheres, with attempts made to model similar dorsal and ventral contours for the olfactory bulbs where they are not ventrally constrained by bones.

Editing of the outermost edge of the masks was then performed manually with the paintbrush tool so that the mask was bounded by the braincase (primarily the frontal, parietal, postparietal, epipterygoid, pterygoid, basisphenoid, prootic, supraoccipital, basioccipital and exoccipital bones). After editing in the coronal plane (back to front), Avizo offers the functionality of applying masks in horizontal (dorsal to ventral) and sagittal (left to right) planes. Therefore, each brain model produced in Avizo was segmented in coronal view, with additional edits made first in sagittal, then horizontal view to follow transverse features within the braincase and fine tune the brain model. Once completed the brain model was exported

without smoothing as an STL file for subsequent analysis, as outlined in the individual research chapters. This segmentation process was used for the studies outlined in chapters three, four and six.

However, a variation on the segmentation process was used in chapter five for the investigation into modeller influences on endocranial reconstructions. Here, the CT scan for UCMP 40466 was imported into SPIERSedit (version 3.0.1; https://spiers-software.org/; Sutton *et al*., 2012), with thresholding applied to produce a black and white overlay on the CT scan. A brain mask was then manually applied to this overlay in the coronal plane using the brush tool in mask mode. Spiers does not offer users the ability to view scans or apply masks in horizontal or sagittal planes. Once mask application was completed, the brain mask was exported as an output object and rendered in SPIERSview. From here, the model was exported without smoothing as an STL file for analysis by the study author. Additional methods and analysis associated with SPIERS segmentation are outlined for the specific research project discussed in chapter five.

Avizo was principally used for segmenting endocranial cavities throughout this research as the software can handle large, high-resolution datasets and renders brain models in real time. Additionally, the ability to apply masks in coronal, sagittal and horizontal planes allowed for clearer editing of the brain models than the single plane offered in SPIERS. Furthermore, all linear and volumetric measurements collected for each endocast were gathered using the 2D measurement and surface area volume tools in Avizo as SPIERS does not offer user-friendly measurement functions. However, SPIERS was valuable software to use for chapter five's modeller study as it allowed modellers to generate endocasts on non-specialist computers and overcame the accessibility issue posed by the high license fee associated with Avizo.

Irrespective of the segmentation software used, the final brain models for all scanned specimens were analysed through a variety of methods, including collecting linear and volumetric measurements of the endocasts; assessing relative cognition levels through calculating encephalisation quotients; visually mapping shape changes through point cloud analysis and quantifying shape changes through the application of 3D landmarking and principal component analysis. These techniques are outlined further in the methods sections of each study for ease of reference.

# CHAPTER THREE

# The first digital endocranial reconstruction of *Thrinaxodon liorhinus*

## 3.1. Cynodont brain morphology: current understanding

Endocranial reconstructions are an increasingly common tool employed by palaeontologists to gain insights into the brain morphology of extinct organisms, offering digitally reconstructed evidence of soft tissues lost to the fossil record. A wealth of studies have investigated brain anatomy for cynodonts (using digital and non-digital techniques) including *Brasilitherium riograndensis* (Rodrigues *et al.,* 2014), *Chiniquodon theotenicus* (Kemp 2009), *Exaeretodon riograndensis* (Pavanatto *et al*., 2019), *Galesaurus planiceps* (Pusch *et al*., 2019), *Massetognathus ochagaviae* (Hoffman *et al*., 2019), *Nshimbodon muchingaensis* (Huttenlocker and Sidor, 2020), *Probelesodon kitchingi* (Hoffman *et al*., 2019), *Prozostrodon brasiliensis* (Kerber *et al*., 2023), *Riograndia guaibensis* (Rodrigues *et al*., 2019), *Siriusgnathus niemeyerorum* (Pavanatto *et al*., 2019) and *Therioherpeton cargnini* (Kerber *et al*., 2023). There is also one known example of a natural endocranial cast for the Early Triassic cynodont, *Nythosaurus larvatus*, housed at the Natural History Museum, London (Pusch *et al*., 2022), although no known examples of preserved cynodont brain tissue have been discovered to date. These studies of endocranial morphology are important for identifying and contextualising developmental changes to brain morphology along the evolutionary lineage from cynodonts to extant mammals.

Endocranial studies of cynodont, mammaliaform and mammal brains have thus far recognised some similarities in overarching morphology, with most studies identifying three brain regions: the forebrain, midbrain and hindbrain (Kaas 2009; Kemp 2009; Rowe *et al*., 2011;

Karten 2015; Hoffman *et al*., 2019; Kerber *et al*., 2023). However, the clarity of the boundaries between these regions are not always easily discerned, particularly in cynodonts where the compartmentalisation exhibited by extant mammal brains, such as *Monodelphis domestica* (Macrini *et al*., 2007b; Rowe *et al*., 2011), is not replicated as strongly (Rodrigues *et al*., 2014; Hoffman *et al*., 2019; Rodrigues *et al*., 2019; Kerber *et al.,* 2023). This lack of resolution in brain morphology is in part due to digital reconstructions not detailing enveloping tissues, such as the meninges, if no skeletal impressions are preserved on the inside of the braincase on which to base the reconstruction. However, there is also a true signal that cynodont brains were simpler than mammal brains. Principally, cynodont brains have been found to be narrow with tubular cerebral hemispheres (Rodrigues *et al*., 2014; Hoffman *et al*., 2019; Pavanatto *et al*., 2019; Pusch *et al*., 2019; Rodrigues *et al*., 2019; Huttenlocker and Sidor, 2020; Kerber *et al.,* 2023), although the dorsoventral depth of the cerebral hemispheres may have been much larger than many endocasts depict due to the lack of basicranial bones constraining the ventral boundary of the brain in many early cynodonts (Kemp 2009; Benoit *et al*., 2017; Laaß *et al*., 2017a).

The most pronounced regions of cynodont endocasts are the olfactory bulbs and cerebellum, with the latter usually being the widest part of reconstructions due to the presence of laterally protruding parafloccular lobes (Kemp 2009; Rodrigues *et al*., 2019; Benoit *et al*., 2023; Kerber *et* al., 2023). Other debated structures include the vermis on the dorsal surface of the cerebellum (Kielan-Jaworowska *et al*., 2004; Kerber *et al*., 2023), the pineal body in the centre of the skull roof (Benoit *et al*., 2016a) and exposure of the midbrain (Kaas 2013; Hoffman *et al*., 2019). Macrini *et al*. (2007b) suggest that non-exposure of the midbrain is the plesiomorphic condition for crown-group mammals and in extant mammals, the midbrain is hidden by the cerebral cortex, particularly the six-layered neocortex which is suggested to

have evolved in mammalian ancestors during the Triassic (Rakic 2009; Kaas 2013). Cynodont endocasts narrow posteriorly to a cylindrical cast of the foramen magnum (Pavanatto *et al*., 2019; Rodrigues *et al*., 2019; Kerber *et* al., 2023).

By investigating the size, shape and relative proportions of cynodont brain regions, a greater understanding of the cognitive and sensory capabilities of cynodonts can be gained, with reference to modern analogues. In extant mammals, the olfactory bulbs are responsible for processing scents, with this functionality available from birth, though olfactory acuity enhances during development towards adulthood (Tufo *et al*., 2022). In the epithelium of the nose, olfactory sensory neurons are stimulated by odours, transferring this information via a network of excitatory neurons to the brain (specifically the olfactory cortex; Tufo *et al*., 2022). In extant mammals such as *Monodelphis domestica* and *Didelphis virginiana*, olfactory tracts connect the olfactory bulbs to the telencephalon of the cerebral hemispheres to process olfactory cues (Macrini *et al*., 2007b). However, in cynodonts, it is rarely possible to distinguish the olfactory tracts from the olfactory bulbs due to the lack of full ossification in the nasal region (Pavanatto *et al*., 2019). The appearance of ossified nasal turbinals occurred late in synapsid evolution, although cartilaginous turbinals were present in cynodonts such as *Brasilitherium riograndensis*, providing an evaporative cooling mechanism to counterbalance the high ambient temperatures of the Triassic (Ruf *et al*., 2014; Crompton *et al*., 2017). Additionally, the presence of loosely articulated orbitosphenoids may help to constrain the ventral boundary of the olfactory bulbs in basal cynodonts such as *Galesaurus, Thrinaxodon* and *Cynosaurus*, where preserved (Benoit *et al.*, 2017).

The cerebral hemispheres control higher-order functions such as cognitive thoughts, emotions, language, memory, vision and motor control (Smith 2022), with debate on whether

each hemisphere has specific responsibilities or functions as an interconnected whole (particularly in non-human mammals; Boles 1992; Nicholls 1996; Banich 1998; Kaas 2013). In humans, the left cerebral hemisphere is suggested to regulate language and motor functions while the right hemisphere moderates attention and both spatial and visual perception (Zaidel 2001). The corpus callosum connects the two cerebral hemispheres in placental mammals, creating a shortened pathway along which neuronal information can be transmitted, but this feature is not observed in monotremes or marsupials (Kaas 2013; Suárez *et al*., 2018). Studies of cynodont endocranial cavities have reconstructed long, narrow cerebral hemispheres, but no comments have yet been made on whether the hemispheres functioned separately or together, although Pusch *et al*. (2022) noted that a natural endocast for *Nythosaurus larvatus* displays undifferentiated cerebral hemispheres which may have been common among cynodonts.

In modern mammals, the cerebellum has the greatest density of neurons in the brain and consists of the centralised vermis and two lateral hemispheres which are responsible for muscular control of balance, coordination and movement (Glickstein 2007; Smaers *et al*., 2018). The vermis is not thought to have a separate function to the rest of the cerebellum in cynodonts (Rodrigues *et al*., 2019), but Kielan-Jaworowska *et al*. (2004) did suggest that the presence of a vermis in early cynodonts such as *Thrinaxodon* can be used as a developmental marker along the mammalian lineage. Additionally, the parafloccular lobes are often shown to protrude laterally from the cerebellum (Rodrigues *et al*., 2014; Huttenlocker *et al*., 2018; Pavanatto *et al*., 2019; Rodrigues *et al*., 2019; Kerber *et al*., 2023). The parafloccular lobes fill depressions within the posterior region of the braincase, described by Kemp (2009) as the subarcuate fossa of the supraoccipital and periotic bones in mammals, and assist with coordination and balance (Butler and Hodos, 1996; Rodrigues *et al*., 2019). The majority of the

hindbrain is comprised of the cerebellum, although the posterior limit is denoted by a small cast of the foramen magnum, the skull opening through which the spinal cord and associated neurovascular structures pass (MacLarnon 1996).

Extant mammals also have a pineal gland in the brain, which releases hormones into the blood and controls circadian rhythms (Song 2019). It has been suggested that some early cynodonts also possessed a pineal gland on the dorsal surface of the brain (Rodrigues *et al*., 2019). The presence of the gland is often assumed based on the occurrence of an oval opening in the skull roof (parietal foramen) in cynodonts such as *Thrinaxodon*, where the pineal gland was associated with a parietal eye above it (Jasinoski *et al*., 2015; Rodrigues *et al*., 2019). However, Kielan-Jaworowska *et al*. (2004) proposed that the parietal eye was not present in most eucynodonts (with *Thrinaxodon* being an exception). The parietal eye filled the skull opening and may have acted as a photoreceptor, sending thermoregulatory signals to the pineal gland, as seen in some reptiles (Engbretson and Lent, 1976; Smith *et al*., 2018).

### 3.1.1. The unknown *Thrinaxodon* brain

Despite an abundance of well-preserved specimens of *Thrinaxodon liorhinus* being available (Jasinoski *et al*., 2015), few attempts have been made to determine its brain morphology. To date, any depictions of *Thrinaxodon*'s endocranial anatomy have only been presented as illustrated interpretations based on the skeletal elements preserved (Parrington 1946 (for braincase anatomy); Estes 1961 (the otic region); Kielan-Jaworowska *et al*., 2004 (endocranial reconstruction) and Rowe *et al*., 2011 (schematic depiction of brain morphology)). However, Kielan-Jaworowska *et al*. (2004) is the only study to provide a comprehensive (but still interpretative) illustration of *Thrinaxodon*'s brain morphology to date (figure 3.1).

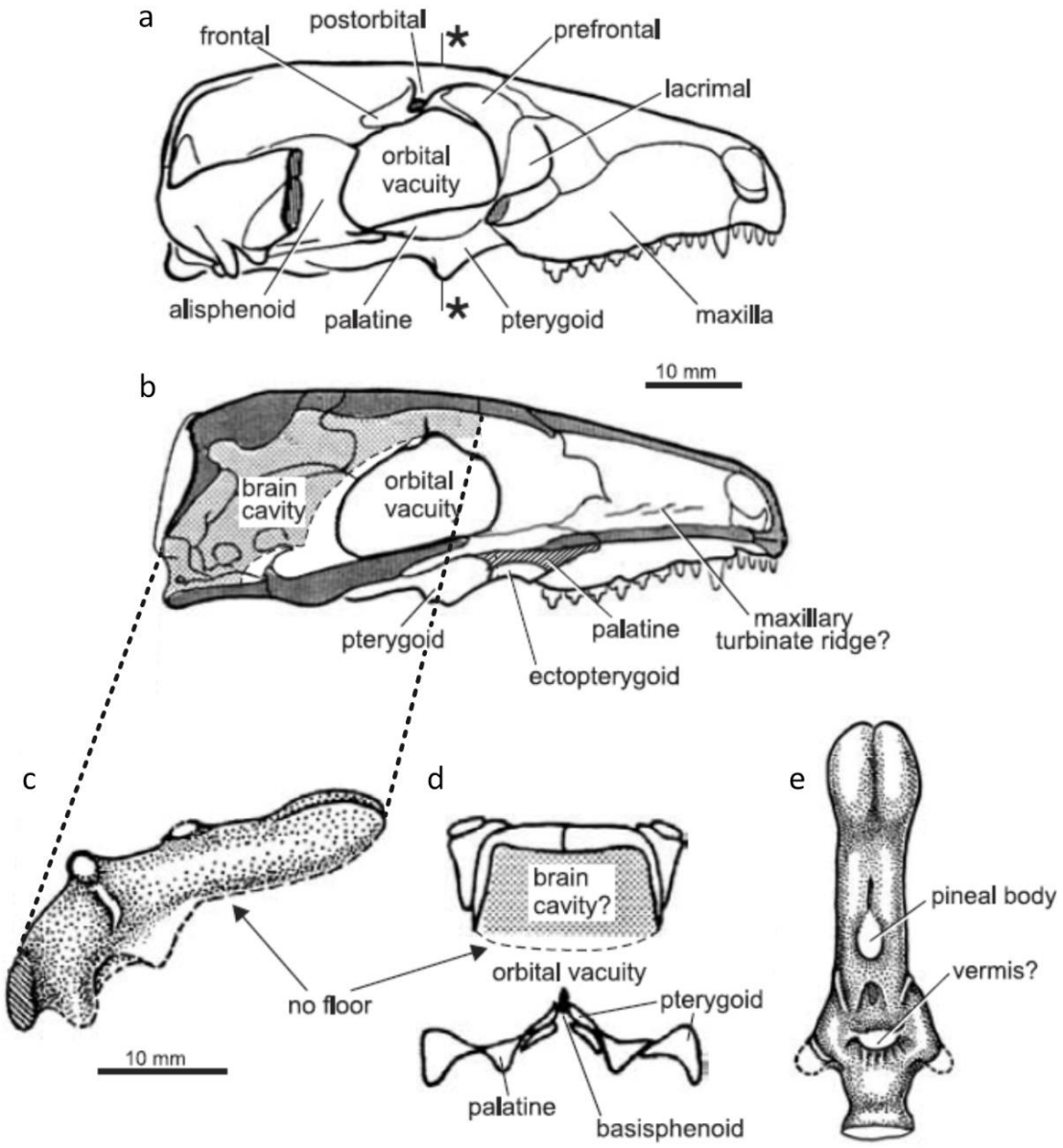


**Figure 3.1.** Hypothesised endocranial anatomy of *Thrinaxodon liorhinus* (reproduced from Kielan-Jaworowska *et al*., 2004). **(a)** Sagittal view of *Thrinaxodon*'s skull. **(b)** The suggested shape and position of the brain within the skull is shown in light grey. Dark grey shading indicates the cross section through cranial bones. **(c)** 3D brain reconstruction in reference to the shaded area in **b**. **(d)** Coronal section of the brain case at the position marked by an asterisk in **a**, with an interpretation of the brain morphology at this point. **(e)** Dorsal view of the brain endocast.

Given that additional interpretations of *Thrinaxodon*'s brain morphology are rare within the literature, generating a digital endocast for *Thrinaxodon* provides a new method to view this cynodont's endocranial anatomy and gain important insights into some of the earliest, mammal-like brain structures to have evolved. Here, seven new models of *Thrinaxodon*'s endocranial anatomy are presented for adult specimens and described to elucidate likely brain morphology. As the brain processes sensory stimuli to enact motor functions (Curley and Keverne, 2005; Rokszin *et al*., 2010; Lieberwirth and Wang, 2012; Poirier *et al*., 2017), the endocasts also provide opportunity to make inferences about *Thrinaxodon*'s sensory capabilities and behavioural characteristics.

## 3.2. Materials and methods

Seven adult specimens of *Thrinaxodon* were chosen for endocranial reconstruction to accommodate variations in preservational state. This represents the largest sample of *Thrinaxodon* skulls yet used for digital endocranial reconstructions (and in fact for any cynodont or mammaliaform species), with numerous brain models offering an opportunity to identify consistently occurring features. Computed tomography (CT) scans were obtained for the following specimens: NHMUK PV R511, NHMUK R3731, NHMUK R5480, UCMP 40466, BP/1/5905, BP/1/7199 and UMZC T815 (see chapter two for detailed specimen information and scanning parameters), with NHMUK PV R 511 being the type specimen of *Thrinaxodon liorhinus*. All specimens have a basal skull length greater than 69 mm, which defines them as adults based on the classification of Jasinoski *et al.* (2015) and Jasinoski and Abdala (2017). The *Thrinaxodon* skulls exhibit varying degrees of preservational completeness associated with the braincase (see chapter two for details of specimen preservation) and therefore these CT scans can be used in conjunction to determine the likely brain morphology of *Thrinaxodon liorhinus*.

CT scans were imported into Avizo 9.3.0 and the brains of each specimen individually reconstructed using the paintbrush tool within the segmentation editor to apply a brain mask. For time efficiency, interpolation was applied between every five slices and manual editing of brain structures was used at the margins of the mask, where necessary (see chapter two, section 2.2 for detailed segmentation methods). The boundaries of mask application were taken as the inner edge of the braincase (when viewing individual slices), with the mask terminating posteriorly where the foramen magnum disappeared and anteriorly where the depression in the frontal bone between the olfactory bulb casts disappeared (figure 3.2). Where basicranial ossification was absent, or where deformation caused misalignment of the braincase, endocasts were reconstructed with gently curved lines across the brain cavity, joining skeletal elements where possible. Reconstructions were assumed to be symmetrical on the left and right sides of the brain and the olfactory bulbs were given similar dorsal and ventral contours where possible as this morphology is observed in other cynodonts (Rodrigues *et al*., 2014; Hoffman *et al*., 2019; Pavanatto *et al*., 2019; Kerber *et al*., 2023) and mammaliaforms (Rowe *et* al., 2011; Huttenlocker *et al*., 2018). While other endocranial features, such as the inner ear or vascular structures, could have been included in the endocasts produced in this study, it was decided to only generate models of the brain. This decision was based on the inner ear and vascular features not being apparent in all CT scans and the inner ear being rarely reconstructed in cynodonts (Rodrigues *et al*., 2013), meaning there are few studies to compare *Thrinaxodon*'s inner ear anatomy to. This is an area for future work.

Rendering of the segmented datasets generated 3D surface models and volumes of *Thrinaxodon*'s endocranial anatomy, which is considered to largely represent the original brain morphology in shape and size, although internal structures, such as neurons, are

impossible to reconstruct. Additionally, protective tissues, vascular structures and intracranial fluids may also have surrounded the brain (as in extant mammals; Macrini *et al.,* 2007a), but to date, no known cynodont fossils have impressions of the brain preserved on the frontal bones. All seven models have been used to provide a morphological description of *Thrinaxodon*'s adult brain and to develop greater understanding about the cognitive and olfactory characteristics of this early cynodont based on linear and volumetric measurements.

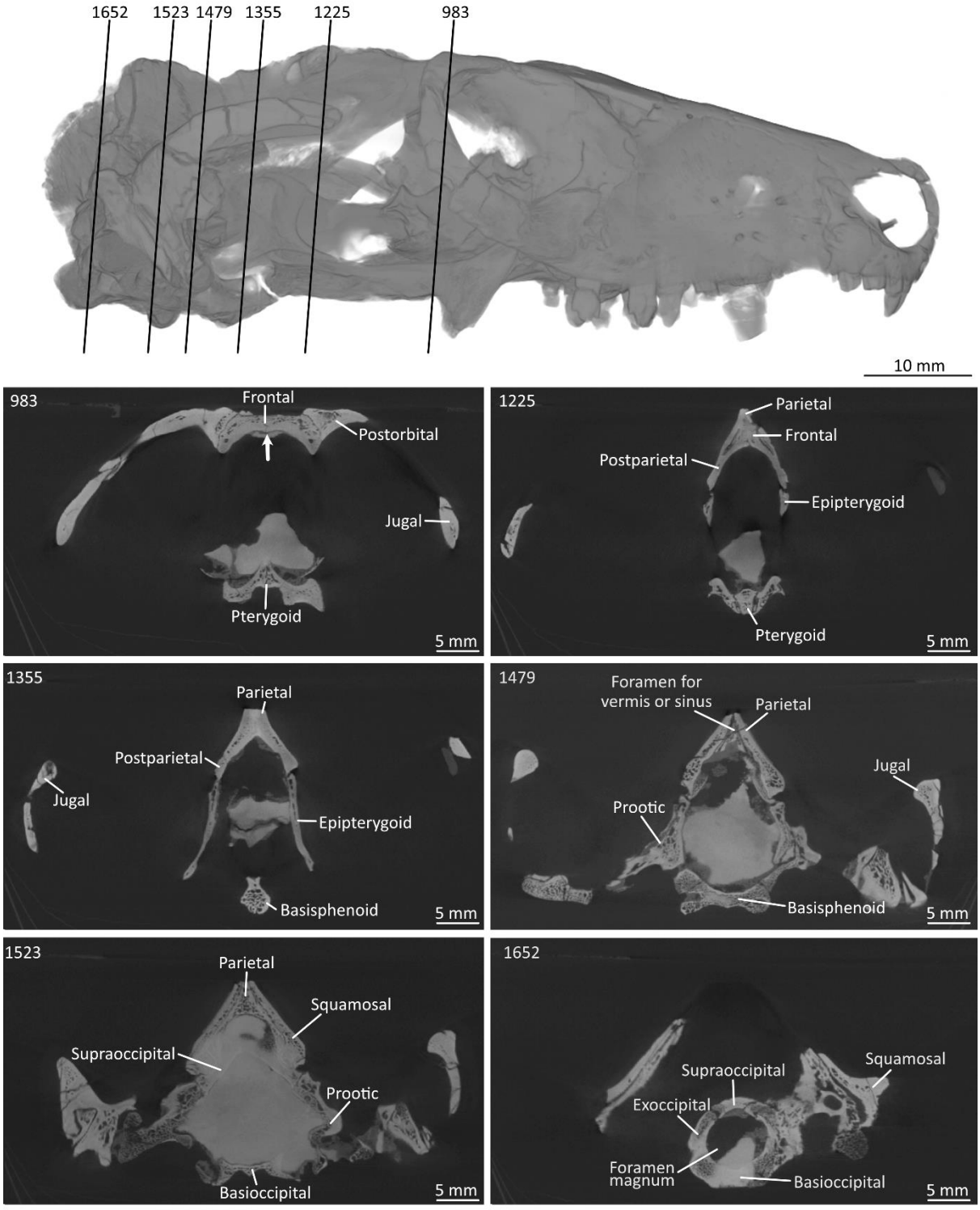


**Figure 3.2.** Digital rendering of *Thrinaxodon liorhinus* (NHMUK PV R511) in lateral view, with five coronal slices displaying labelled braincase bones. Slice 983 marks the anterior region of the olfactory bulb cast, with the bold white arrow marking the depression in the frontal bone used as the anterior limit of the olfactory bulbs during the segmentation process. Slices 1225, 1355, 1429 and 1523 show intermediate skull positions and associated cranial morphology.

Slice 1652 marks the posterior region of the brain cavity, with the foramen magnum used as the termination of the endocast. The specimen shows minimal deformation and contrast between sediment fill and cranial bones is good enough to not hamper reconstruction.

To characterise the morphology of *Thrinaxodon*'s brain, measurements of endocast length and volume were gathered, alongside dimensions of individual brain regions, using the 2D measurement tool and surface area volume function in Avizo. The Avizo measurements were converted to millimetres using a scaling factor associated with the basal skull length as measured on the specimen and 3D rendering of the skull in Avizo (BSL; equation 3.1). All basal skull lengths of the fossils were taken from Jasinoski *et al*. (2015).

**Equation 3.1.** $$\text{Scaling factor} = \frac{BSL_{AVIZO}}{BSL_{SPECIMEN}}$$

The encephalisation quotient (EQ) is the most widely used method for comparing brain size between cynodonts, mammaliaforms and mammals (Quiroga 1979; Macrini *et al*., 2007b; Hoffman *et al*., 2019; Pavanatto *et al*., 2019; Rodrigues *et al*., 2019). From comparing relative proportions between brain regions, estimates of cognitive capabilities can be elucidated using knowledge of extant mammal brains. Two comparable equations are available to calculate the EQ value based on the endocast volume (EV, $cm^3$) and estimated body mass (BM, g). The EQ can be calculated using equations proposed by Jerison (1973; equation 3.2) and Manger (2006; equation 3.3.)). The equation generated by Jerison (1973) was designed to remove the effects of changing body size on brain size estimates, while the equation by Manger (2006) is a recalculation of Eisenberg (1981)'s work and is based on a larger number of taxa. Using both equations provides an upper and lower bracket for *Thrinaxodon*'s EQ value. Both equations

compare the endocranial volume with the body mass of each specimen. However, for fossils (especially those with limited or no postcranial skeletons), estimations of body mass can be challenging and rely on calculations derived from other body parts, such as the humerus and femur (Filippini *et al*., 2022). Here, skull length was used to estimate body mass using equation 3.4, as used in previous cynodont and mammaliaform studies (Luo *et al*., 2001; Rodrigues *et al*., 2014; Rodrigues *et al*., 2019).

**Equation 3.2.** $$EQ_{Jerison} = \frac{EV}{0.12 \text{ X } (BM^{0.66})}$$

**Equation 3.3.** $$EQ_{Manger} = \frac{EV}{0.0535 \text{ X } (BM^{0.7294})}$$

**Equation 3.4.** $$BM = 1.6 \text{ x } BSL^{3}$$

However, due to the uncertainties in endocast volumes and body mass estimations, Rodrigues *et al*. (2019) proposed an alternative method to compare relative sizes of endocasts using the dorsal length of the endocast, as well as the length of the olfactory bulbs, cerebral hemispheres and cerebellum. This method assesses proportional changes in two dimensions, eliminating the problem of challenging ventral interpretations, and associated volumetric errors, for specimens that do not possess ossified basicranial regions. Comparison of relative proportions of individual brain regions then provides insights into potential sensory acuity of extinct taxa, based on similar characteristics in extant mammals. Here, comparisons of olfactory bulb length against overall endocast length were calculated for all seven models to quantify *Thrinaxodon*'s olfactory acuity compared to other species in the mammalian evolutionary lineage.

## 3.3. Results

### 3.3.1. Description of *Thrinaxodon*'s endocranial anatomy

The cranial endocasts generated for *Thrinaxodon liorhinus* (figure 3.3) are largely similar in their morphology. The brain models are bounded anteroposteriorly between the foramen magnum at the back of the skull and a groove within the frontal bone, which indicates the likely termination of the olfactory bulbs. On each CT scan, the endocast follows the anteroposteriorly transverse curve of the skull roof, with a slight horizontal depression in the skull towards the front of the braincase, which marks the start of the olfactory bulb cavity. Based on the endocasts produced within this study, *Thrinaxodon*'s brain appears to have been elongate, with a narrow form retained from the olfactory bulbs through the cerebral hemispheres to the cerebellum. Here, lateral expansion of the cerebellum is enhanced by parafloccular lobes, before the endocast narrows posteriorly to the cast of the foramen magnum. There is a lack of surface crenulations on all seven endocasts. While the overall endocast morphology is somewhat consistent across the models, some variation is apparent in the size and proportion of individual brain regions (further details are provided below). Additionally, the endocasts for specimens NHMUK R5480, BP/1/5905 and BP/1/7199 display a slight longitudinal, S-curve deviation. This deformation was measured between the dorsal midpoint of the foramen magnum of each endocast and the widest point of the olfactory bulbs at their anterior boundary, following the left margin of the brain model. Angles of deviation were measured as –4.9° (NHMUK R5480), 4.2° (BP/1/5905) and 3.6° (BP/1/7199).

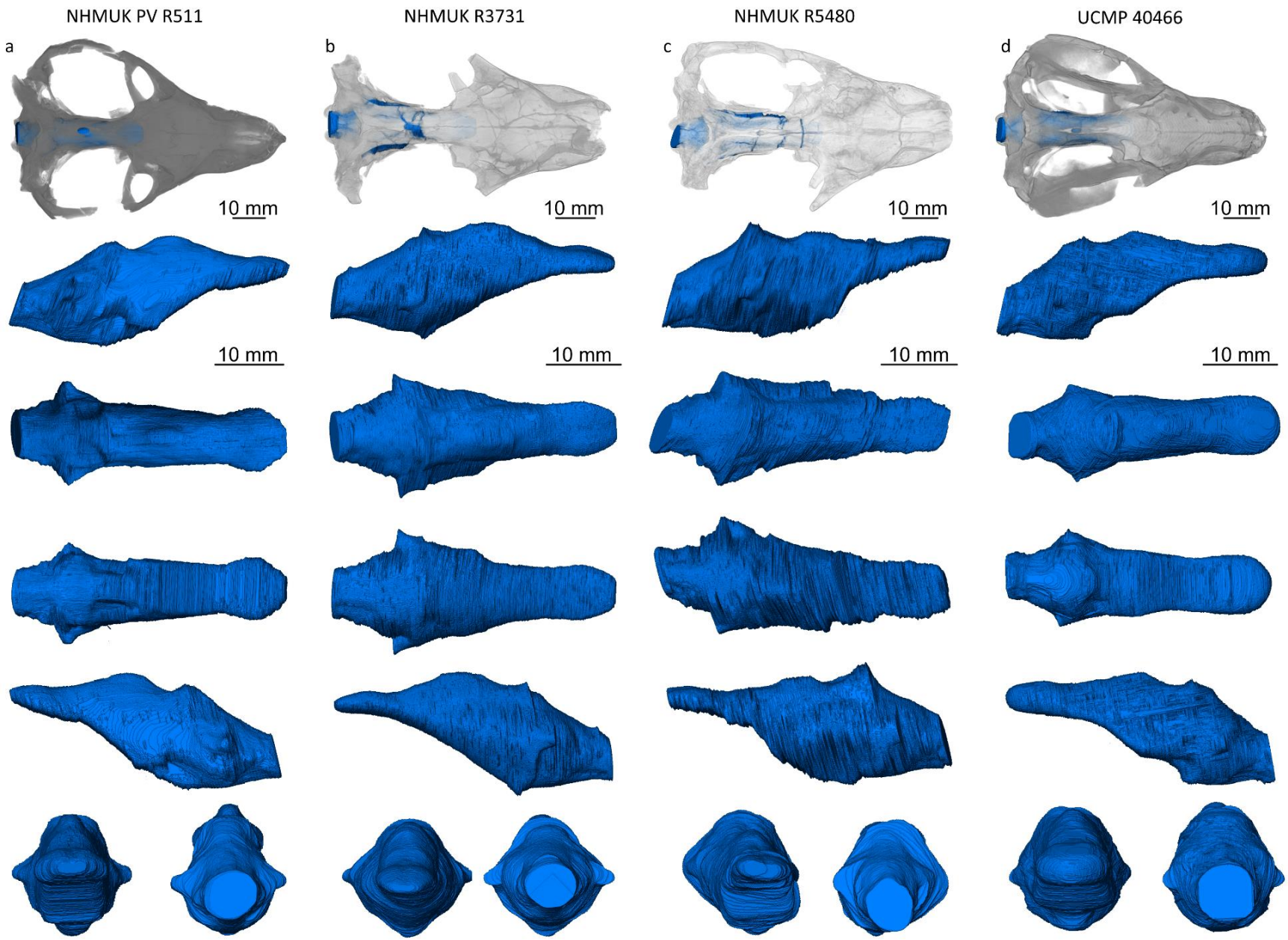
NHMUK PV R511
NHMUK R3731
NHMUK R5480
UCMP 40466
a
b
c
d
10 mm
10 mm
10 mm
10 mm
10 mm
10 mm
10 mm
10 mm

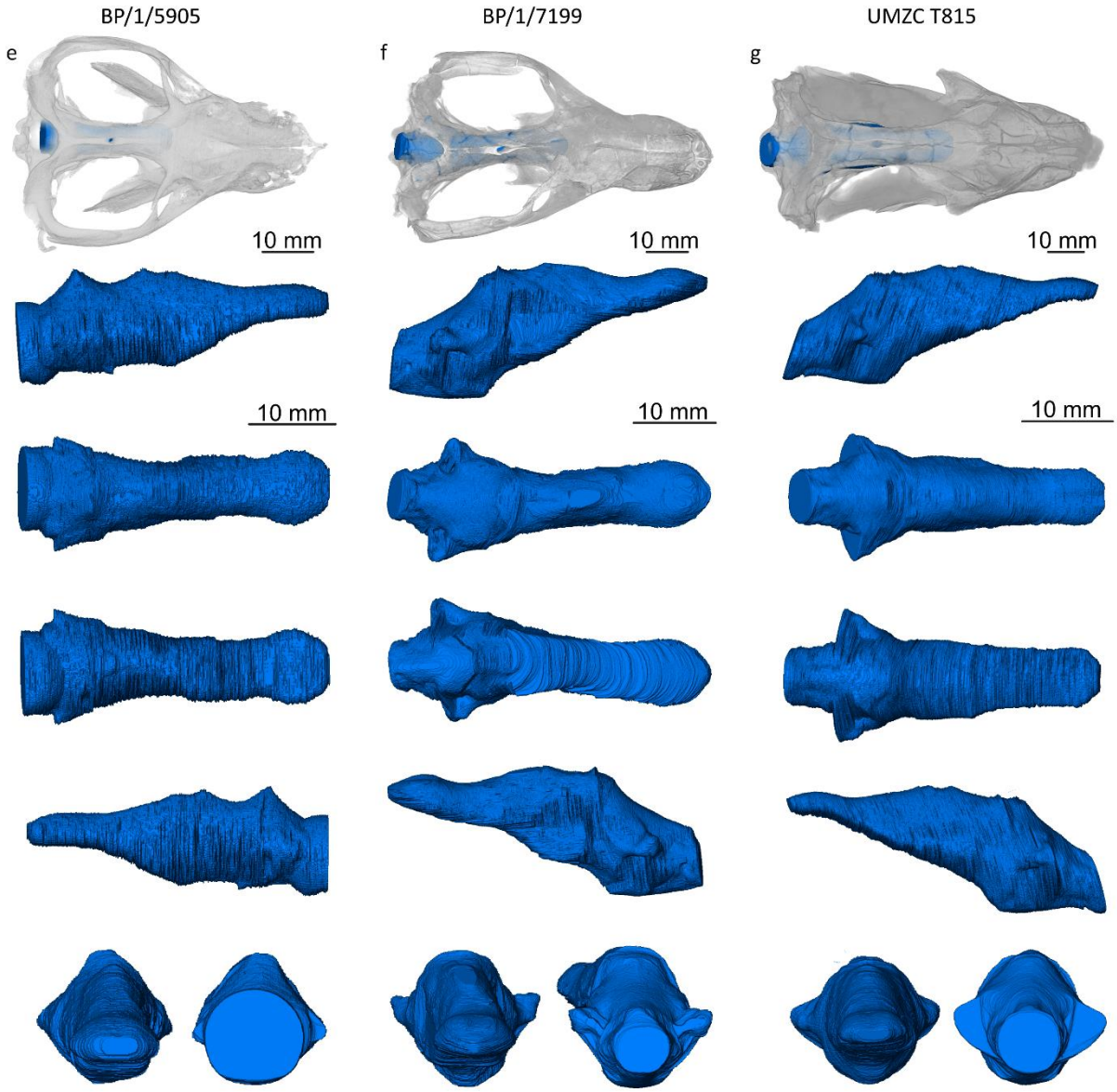


**Figure 3.3. (also previous page).** Endocranial reconstructions for seven adult specimens of *Thrinaxodon liorhinus,* with the digital brain reconstructions shown in life position. Endocasts are shown in the following orientations, from top to bottom: right lateral, dorsal, ventral, left lateral, anterior (left) and posterior (right). **(a)** NHMUK PV R511 (BSL 84 mm). **(b)** NHMUK R3731 (BSL 71 mm). **(c)** NHMUK R5480 (BSL 78 mm). **(d)** UCMP 40466 (BSL 74 mm). **(e)** BP/1/5905 (BSL 87 mm). **(f)** BP/1/7199 (BSL 75 mm). **(g)** UMZC T815 (BSL 69 mm). It should be noted that specimens NHMUK R5480, BP/1/5905 and BP/1/7199 display twisting of the endocast. Specimen BP/1/5905 exhibits an unusually large foramen magnum cast as an

artefact developed during the processing of the CT scan data before endocranial reconstruction.

NHMUK PV R511 was chosen to be the adult representative of *Thrinaxodon liorhinus* as this skull has the most completely preserved braincase, with minimal deformation and sediment infill. This is also the type specimen of *Thrinaxodon*. The subsequent endocast (figure 3.3) is assumed to be the most typical shape of the original brain given current knowledge and specimen availability. The anteroposteriorly elongated endocast of NHMUK PV R511 has a width to length ratio of 0.39 (table 3.1), with a maximum dorsal length of 41.23 mm. The endocast length corresponds to 49% of the basal skull length (84 mm), which is consistent with the other endocasts, where the brain model comprises approximately half of the skull length. The widest part of the endocast (16.09 mm) occurs where the parafloccular lobes protrude by approximately 3 mm each from the cerebellum. By taking a horizontal plane from the dorsal surface of the endocast, the brain model slopes steeply from the cerebellum towards the cast of the foramen magnum by 30.7°. Further details of each brain region are provided in figure 3.4 and table 3.1.

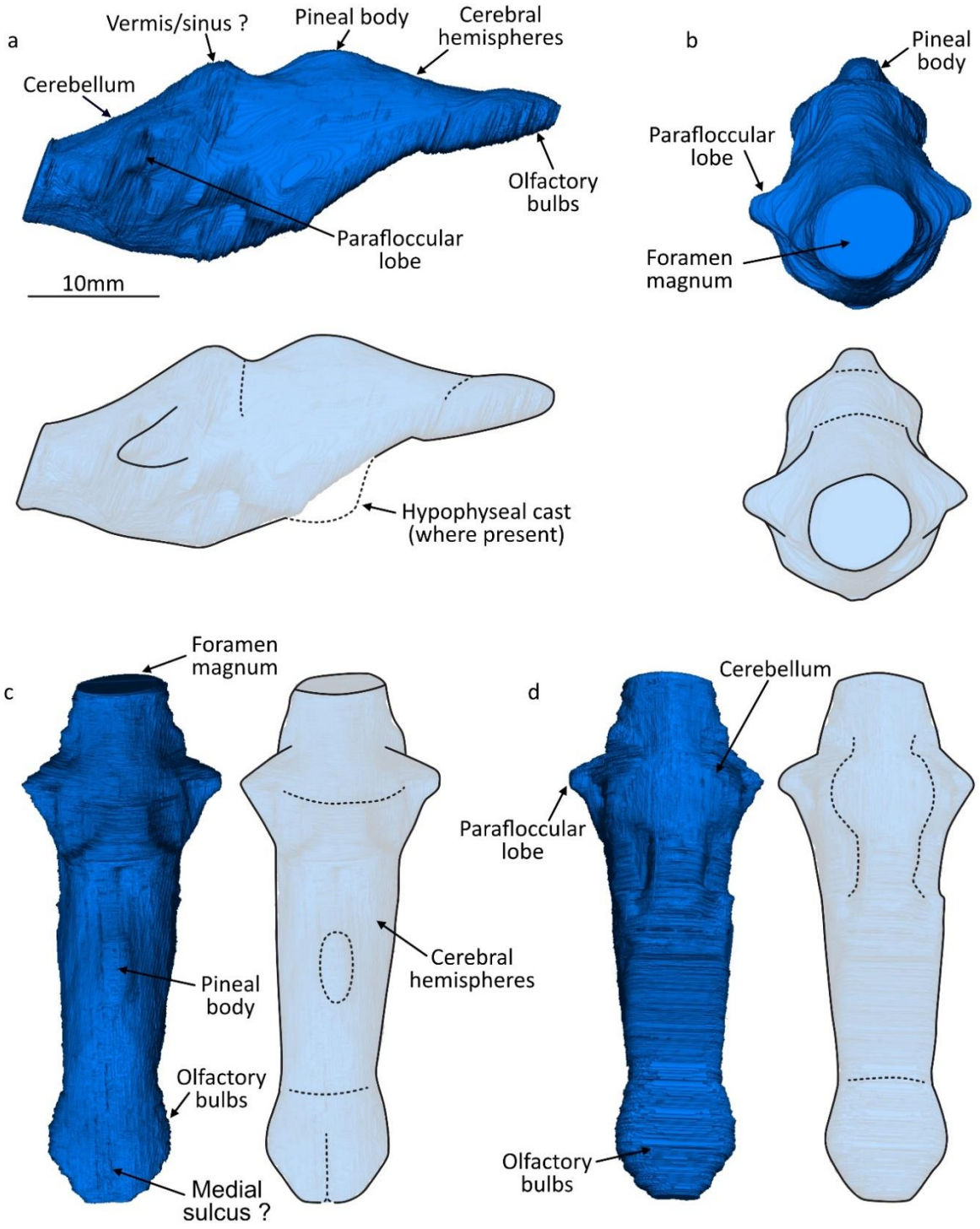


**Figure 3.4.** Reconstructed endocranial morphology of specimen NHMUK PV R511 in **(a)** right lateral, **(b)** posterior, **(c)** dorsal and **(d)** ventral orientations. Schematic representations are provided to highlight key regions of the brain including the olfactory bulbs, cerebral hemispheres, cerebellum, parafloccular lobes and foramen magnum. Possible boundaries between brain regions are denoted by a dashed line.

**Table 3.1.** Linear and volumetric measurements for the endocranial reconstructions of the seven adult *Thrinaxodon liorhinus* specimens studied.

The measurements were calculated after correction using the scaling factor outlined in the methods.

| | **NHMUK PV R511** | **NHMUK R3731** | **NHMUK R5480** | **UCMP 40466** | **BP/1/5905** | **BP/1/7199** | **UMZC T815** |
|---|---|---|---|---|---|---|---|
| **Basal skull length[1] (mm)** | 84 | 71 | 78 | 74 | 87 | 75 | 69 |
| Foramen magnum diameter (skull, mm) | 7.48 | 7.06 | 6.65 | 6.93 | 9.46 | 6.67 | 10.78 |
| Foramen magnum diameter (endocast, mm) | 7.31 | 6.52 | 6.47 | 6.41 | 9.64 | 6.12 | 6.22 |
| Endocast length[2] (mm) | 41.23 | 38.36 | 38.24 | 36.86 | 35.67 | 38.69 | 34.81 |
| Maximum endocast width[3] (mm) | 16.09 | 17.23 | 16.05 | 14.22 | 13.21 | 15.64 | 15.43 |
| Minimum endocast width (mm) | 7.70 | 6.93 | 7.07 | 7.77 | 6.40 | 7.09 | 6.30 |
| Maximum endocast depth[4] (mm) | 16.18 | 16.73 | 16.43 | 15.01 | 13.21 | 15.46 | 14.03 |
| Maximum width:length ratio of endocast | 0.39 | 0.45 | 0.42 | 0.39 | 0.37 | 0.40 | 0.44 |
| Endocast:BSL ratio (%) | 49.08 | 54.03 | 49.02 | 49.81 | 41.00 | 51.59 | 50.45 |
| Volume of the whole endocast ($mm^3$) | 2942.27 | 1907.62 | 2558.92 | 2313.97 | 1890.61 | 1920.57 | 1779.31 |
| Length of olfactory bulb cast[5] (mm) | 9.60 | 8.48 | 9.19 | 9.26 | 7.42 | 10.14 | 6.30 |
| Olfactory bulb:endocast length ratio (%) | 23.29 | 22.11 | 24.04 | 25.12 | 20.79 | 26.21 | 18.09 |
| Maximum width of both olfactory bulbs (mm) | 9.85 | 7.54 | 7.63 | 8.31 | 8.77 | 8.37 | 6.99 |
| Maximum depth of the olfactory bulb casts[6] (mm) | 4.70 | 3.03 | 3.40 | 4.73 | 4.05 | 4.31 | 2.72 |
| Endocast width at the transition between the olfactory bulbs and cerebral hemispheres (mm) | 7.61 | 6.90 | 7.05 | 7.53 | 6.79 | 7.16 | 6.48 |

| | | | | | | | |
|---|---|---|---|---|---|---|---|
| Maximum width:length ratio of olfactory bulbs | 1.03 | 0.89 | 0.83 | 0.90 | 1.18 | 0.83 | 1.11 |
| Length of cerebral hemisphere casts[7] (mm) | 17.76 | 17.99 | 19.56 | 16.14 | 20.61 | 16.85 | 18.00 |
| Cerebral hemisphere:endocast length ratio (%) | 43.08 | 46.89 | 51.15 | 43.80 | 57.78 | 43.53 | 51.70 |
| Maximum width of both cerebral hemispheres[8] (mm) | 9.86 | 12.23 | 12.33 | 9.68 | 9.52 | 8.74 | 9.10 |
| Maximum width:length ratio of cerebral hemispheres | 0.56 | 0.68 | 0.63 | 0.60 | 0.46 | 0.52 | 0.51 |
| Anteroposterior length of the slope of the cerebellum[9] (mm) | 15.41 | 13.73 | 12.48 | 12.69 | 7.94 | 11.86 | 10.46 |
| Angle of the cerebellum slope[10] (°) | 30.7 | 33.0 | 24.6 | 38.6 | 34.2 | 26.3 | 41.1 |
| Maximum depth of the cerebellum[11] (mm) | 15.84 | 15.51 | 14.79 | 13.92 | 10.62 | 14.21 | 13.34 |
| Cerebellum width between the paraflocculars lobes (mm) | 9.38 | 10.88 | 10.09 | 8.92 | 9.61 | 8.66 | 8.44 |
| Maximum width:length ratio of cerebellum (with the paraflocculllar lobes) | 0.61 | 0.79 | 0.81 | 0.70 | 1.21 | 0.73 | 0.81 |
| Length of the left paraflocculars lobe cast (mm) | 3.50 | 3.26 | 3.17 | 2.60 | 1.80 | 3.86 | 3.32 |
| Length of the right paraflocculars lobe cast (mm) | 3.03 | 3.16 | 2.35 | 2.82 | 2.04 | 3.12 | 3.77 |
| Scaling factor[12] | 19.67 | 0.88 | 0.94 | 14.51 | 1.01 | 0.97 | 0.99 |

**Table 3.1. (continued)**

[1] Taken from Jasinoski *et al*. (2015); [2] Measured from the anterior limit of the olfactory bulbs to the foramen magnum in dorsal view; [3] Including the cerebellum and parafloccular lobes; [4] Measured from a horizontal line taken at the dorsal and ventral boundaries of the endocast; [5] Measured in dorsal view; [6] Measured in lateral view; [7-9] Measured in dorsal view; [10] Measured in lateral view from a horizontal line on the dorsal surface of the endocast; [11] Measured from the ventral limit of the cerebellum to the dorsal surface directly above it; [12] Calculated based on the basal skull length of each specimen.

## 3.3.2. Forebrain

The most anterior section of the brain model contains casts of the olfactory bulbs. The bulbs have a convex dorsal surface in lateral view, although a flatter ventral surface has been reconstructed for all of the models. In dorsal view, the olfactory bulb casts are round with a very shallow depression between the bulbs in some of the endocasts, although the depression is difficult to discern in NHMUK R3731, UCMP 40466, BP/1/5905 and BP/1/7199. The curvature at the anterior end of the olfactory bulbs varies noticeably between the models (figure 3.3). Some models retain the straight and narrowing shape of the cerebral hemispheres, with only a slight curve at the anterior-most point (NHMUK R3731, NHMUK R5480 and UMZC T815), while the rest are noticeably more rounded (NHMUK PV R511, UCMP 40466, BP/1/5905 and BP/1/7199). In NHMUK PV R511, the maximum width of the olfactory bulbs is 9.85 mm, length is 9.60 mm and the width to length ratio of the bulb casts is 1.03. However, for the rest of the endocasts, the olfactory bulbs range in length between 6.30 mm (UMZC T815) and 10.14 mm (BP/1/7199), comprising between 18 and 26% of the endocast length, respectively. As with the entire endocast, it is not possible to reconstruct the ventral boundary of the olfactory bulbs (or any transition into olfactory tracts) with certainty due to

the absence of the orbitosphenoids. Therefore, a relatively flat ventral surface has been reconstructed for the olfactory bulbs in the seven *Thrinaxodon* specimens studied.

In NHMUK PV R511, the cerebral hemispheres extend for 17.76 mm from the posterior limit of the olfactory bulbs to the dorsal ridge in the hindbrain which is taken to be the posterior boundary for the cerebral hemispheres. The dorsal surface is prominently convex and does not appear to be separated into two hemispheres by a medial sulcus. There is a slight longitudinal depression running the length of the cerebral hemispheres in specimen NHMUK R5480 which could be an artefact of deformation as the feature is not observed in the other endocasts. In dorsal view, the cerebral hemispheres are narrowest at the boundary with the olfactory bulbs (7.61 mm) and widest at the posterior boundary with the cerebellum (9.86 mm). The cerebral hemispheres comprise 43% of the endocast length for NHMUK PV R511 and up to 58% of the endocast length in BP/1/5905. All models show a distinctive, somewhat oval ridge on the dorsal surface of the cerebral hemispheres, corresponding to the pineal body, which filled the parietal foramen observed on each of the CT scans. However, in ventral view, no definitive feature of the forebrain can be observed due to the absence of ossified elements to delimit the lower boundary of the brain here. The cerebral hemispheres do not display any complex convolutions (such as the gyri and sulci of mammals) across their surface and there is no rhinal sulcus marking the presence of the rhinencephalon (part of the olfactory system) as *Thrinaxodon*'s brain did not have a neocortex where this feature is found in extant mammals.

The ventral depth of the forebrain is challenging to reconstruct due to the brain not being fully enclosed in bone. Forebrain depth also varies due to the range in skull sizes between 69 mm and 87 mm long, with the specimens therefore being at different growth stages of adulthood.

There is also a noticeable lack of ossification between the frontals and pterygoids, hence the endocast here has been estimated and may be an underrepresentation of endocast morphology. Overall, the forebrain is relatively consistent in shape, with the morphology reconstructed in NHMUK PV R511 being similar to the endocranial interpretations generated for specimens NHMUK R3731, BP/1/7199 and UMZC T815. However, specimens UCMP 40466, BP/1/5905 and (to a lesser extent) BP/1/7199 do not retain a straight morphology along the base of the cerebral hemispheres but instead possess a bulge which may correspond to the hypophyseal cast where the pituitary gland would have been housed. The hypophyseal cast may also be present in NHMUK R5480, although it is not as clearly separated from the cerebellum as in the other specimens.

### 3.3.3. Hindbrain

*Thrinaxodon liorhinus*' hindbrain has numerous distinctive features that are present in all of the endocasts: the cerebellum with laterally expanding parafloccular lobes, a dorsal projection which may be the vermis or a sinus, and a posterior narrowing into the foramen magnum cast. First considering the cerebellum, this structure is quite consistently reconstructed throughout the endocasts, with a rounded ventral surface and a posteriorly sloping dorsal margin, which varies between 25° (NHMUK R5480) and 39° (UCMP 40466). Specimen BP/1/5905 has an anomalous morphology here, with a widening of the foramen magnum cast being an artefact of CT scan preparation (figure 3.3). For type specimen NHMUK PV R511, the widest part of the hindbrain (16.09 mm) occurs where the pyramidal parafloccular lobe casts protrude laterally from the cerebellum by 3.50 mm (left) and 3.03 mm (right). This morphology is similarly reflected in the other six endocasts. There is also some consistency in the width of the reconstructed hindbrains, with the cerebellum ranging between 8.44 mm (UMZC T815) and

10.88 mm (NHMUK R3731) wide. The cerebellum depth is more variable, between 10.62 mm (BP/1/5905) and 15.84 mm (NHMUK PV R511) but may be accounted for by variable skull sizes.

On the dorsal surface behind the parafloccular lobe casts is a slightly raised area that could represent the vermis which connects two lateral hemispheres of the cerebellum in extant mammals (Sillitoe *et al*., 2012). However, as there is no obvious division of the cerebellum in the reconstructions of *Thrinaxodon*'s brain, this protrusion may also be a sinus. The larger dorsal features in specimens NHMUK R5480 and BP/1/5905 could be more reflective of a sinus than the vermis, but as these specimens both have some deformation in the hindbrain, drawing a conclusion either way is tentative. When observing the ventral surface of the hindbrain, a wide, longitudinal band runs medially along the cerebellum of specimens NHMUK PV R511, NHMUK R5480, UCMP 40466, BP/1/7199 and UMZC T815, although it is not clear if this structure had a functional purpose. Furthermore, it is not possible to identify if parts of the hindbrain correspond to the medulla oblongata (the connection between the brainstem and spinal cord) or the pons (part of the brain stem linked to the spinal cord), if indeed such structures were present at all in *Thrinaxodon*, as the brain would have also been surrounded by meninges, nerves and blood vessels (Macrini *et al.,* 2007a). As such, some soft tissues may not have a corresponding skeletal impression or cavity on which to base the brain reconstruction.

All endocasts terminate with a somewhat cylindrical cast of the foramen magnum, through which the spinal cord and associated neurovascular structures would have passed. In NHMUK PV R511, the foramen magnum has a diameter of 7.31 mm, which is largely consistent with the other adult specimens apart from BP/1/5905 where the wide foramen magnum diameter (9.64 mm) is an artefact of the CT scan preparation. Bounded between the foramen magnum

and olfactory bulbs, the endocasts average approximately 50% of the skull length across all of the adult specimens. However, as the basal skull lengths vary between 69 mm (UMZC T815) and 87 mm (BP/1/5905), the endocast size accordingly varies in length and volume. The shortest endocast length is 34.81 mm (UMZC T815) and the longest endocast is 41.23 mm (NHMUK PV R511), although this is not the specimen with the largest basal skull length. Additionally, endocast volumes vary between 1779.31 $mm^3$ (UMZC T815) and 2942.27 $mm^3$ (NHMUK PV R511), with the largest volumetric variation being apparent in the reconstructions of the olfactory bulbs and cerebellum (figure 3.3).

### 3.3.4. Investigating *Thrinaxodon*'s cognitive and sensory capabilities

Based on the skull lengths of the studied specimens and the reconstructed endocranial volumes, the encephalisation quotient for an adult *Thrinaxodon liorhinus* ranges from 0.16 (BP/1/5905) to 0.27 (NHMUK PV R511, NHMUK R5480 and UCMP 40466) for $EQ_{Jerison}$ and 0.22 (BP/1/5905) to 0.38 (NHMUK R5480 and UCMP 40466) for $EQ_{Manger,}$ with the average EQ values being 0.24 ($EQ_{Jerison}$) and 0.34 ($EQ_{Manger}$; table 3.2). With an EQ of 0.27 being the most frequently calculated value (and the EQ derived for type specimen NHMUK PV R511), this is taken to be the representative value for an adult *Thrinaxodon liorhinus*. This EQ value can be considered in the context of other cynodonts and extant mammals to make inferences about the cognitive capability of *Thrinaxodon* (see section 3.4.2).

**Table 3.2.** Calculated body mass and encephalisation quotients for the seven studied adult *Thrinaxodon liorhinus* specimens.

| | NHMUK PV R511 | NHMUK R3731 | NHMUK R5480 | UCMP 40466 | BP/1/5905 | BP/1/7199 | UMZC T815 |
|---|---|---|---|---|---|---|---|
| Body mass (g) | 948.33 | 572.66 | 759.28 | 648.36 | 1053.60 | 675.00 | 525.61 |
| $EQ_{Jerison}$ | 0.27 | 0.24 | 0.27 | 0.27 | 0.16 | 0.22 | 0.24 |
| $EQ_{Manger}$ | 0.37 | 0.35 | 0.38 | 0.38 | 0.22 | 0.31 | 0.34 |

However, the olfactory bulbs are one of the most prominent regions of the endocast that can be identified and considered for their sensory processing capabilities. Given the uncertainty in the ventral boundary of the olfactory bulb casts (and therefore their volume), the ratio between the olfactory bulb and endocast lengths provides a useful comparison between mammalian and non-mammalian species about how much of the brain may have been dedicated to detecting odours. In the studied specimens, the olfactory bulbs comprise between 18% (UMZC T815) and 26% (BP/1/7199) of the endocast length, although discrepancies in the anterior boundary of the olfactory bulbs should be considered when comparing how much of *Thrinaxodon*'s brain was comprised of the olfactory bulbs compared to in other species. The olfactory bulb:endocast ratio was also calculated for a variety of other cynodonts to contextualise the proportion of the early cynodont brain that was dedicated to olfactory processing compared to increasingly mammalian species (figure 3.5). *Thrinaxodon*'s olfactory bulbs were found to be proportionally similar in length to other late Permian and Early Triassic taxa, as well as some Late Triassic cynodonts, although there is a greater variation in the olfactory bulb to endocast ratio among Late Triassic taxa.

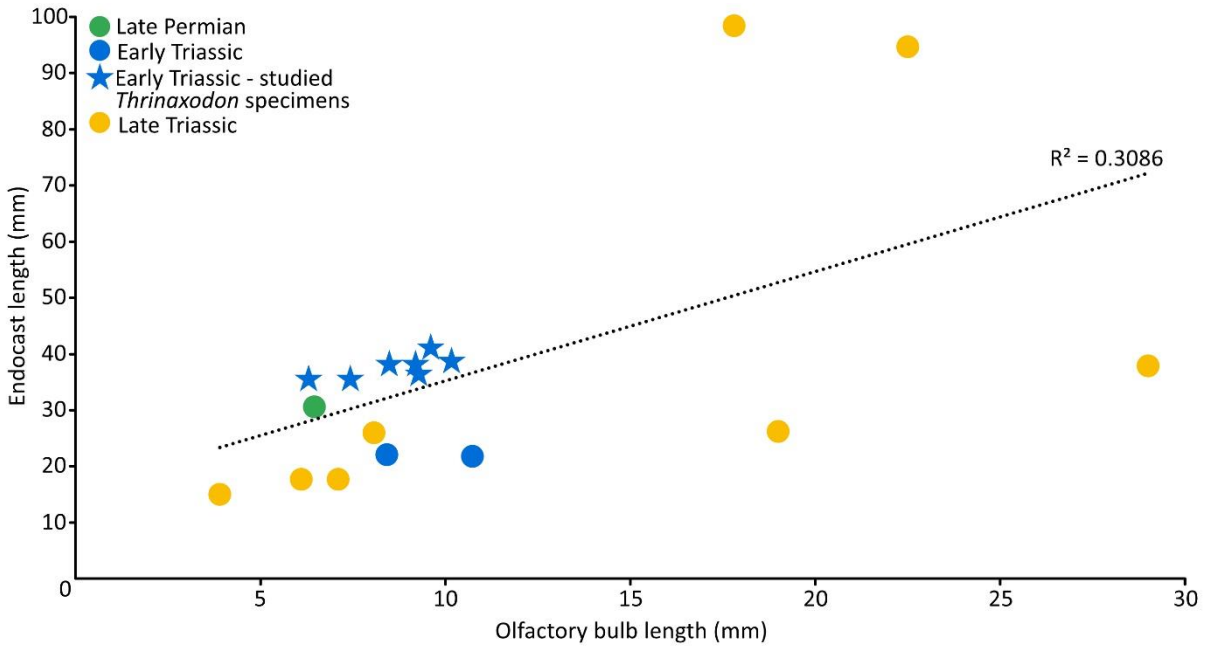


**Figure 3.5.** The olfactory bulb to endocast ratio plotted for late Permian to Late Triassic cynodonts (late Permian species - *Nshimbodon muchingaensis*; Early Triassic taxa - *Thrinaxodon liorhinus, Galesaurus planiceps* and *Diademodon sp.;* Late Triassic taxa - *Riograndia guaibensis*, *Brasilitherium riograndensis*, *Siriusgnathus niemeyerorum*, *Exaeretodon riograndensis*, *Probelesodon kitchingi*, *Massetognathus ochagaviae*, *Prozostrodon brasiliensis* and *Therioherpeton cargnini*). The seven studied *Thrinaxodon* specimens are denoted by stars and these specimens all cluster together, showing similarities in their reconstructed proportions. There is greater variation in the amount of Late Triassic cynodont brains that were comprised of the olfactory bulbs.

## 3.4. Discussion

### 3.4.1. Updating knowledge of *Thrinaxodon*'s brain morphology

The first known digital brain reconstructions for an adult specimen of *Thrinaxodon liorhinus* have been presented here. Harnessing the power of CT scans and digitally peering inside of the skull, it has been possible to gain a new insight into *Thrinaxodon*'s brain morphology since

the hypothesised endocranial anatomy proposed by Kielan-Jaworowska *et al.* (2004; figure 3.1). In Kielan-Jaworowska *et al.* (2004)'s reconstruction, the illustrations show a slender, elongate brain with pronounced olfactory bulbs which narrow into tubular cerebral hemispheres. There is a noticeable dorsal protrusion of the pineal body from the cerebral hemispheres and an ambiguous ventral surface due to the lack of ossified basicranial bones within *Thrinaxodon*'s braincase (Benoit *et al*., 2017). The hypothesised hindbrain has a small, raised area on the dorsal surface which Kielan-Jaworowska *et al*. (2004) suggests is the vermis at the centre of the cerebellum. Small parafloccular lobes protrude laterally from the cerebellum, before the brain narrows posteriorly to the foramen magnum. Overall, Kielan-Jaworowska *et al*. (2004) present a brain which is simple and narrow in morphology with no surface ornamentation and no noticeably expanded brain regions, contrasting with the enlarged olfactory bulbs and cerebral hemispheres seen in many mammaliaforms and extant mammals (Macrini *et al*., 2007b; Huttenlocker *et al*., 2018; Benoit *et al*., 2023).

As one of the largest adult specimens studied, and with minimal deformation or sediment infill, NHMUK PV R511 provides the best insight into what the brain of a fully grown *Thrinaxodon* may have looked like. Broadly, the brain morphology of NHMUK PV R511 presented here corresponds well with that of Kielan-Jaworowska *et al.* (2004), with a narrow, elongated brain that is widest where the parafloccular lobes extend laterally from the cerebellum. Prominent parafloccular lobes are suggested to be the plesiomorphic condition for *Thrinaxodon* and other eucynodonts (Rowe 1996; Rodrigues *et al*., 2019). The parafloccular lobes and cerebellum are reconstructed with broadly similar morphologies across the seven adult specimens studied. This similarity in hindbrain shape is due to the greater constraint of segmentation mask application because of more complete ossification of the braincase by the

basisphenoid, prootic, supraoccipital, basioccipital and exoccipital in the posterior part of the skull.

Additionally, even with new digital segmentation techniques used to reconstruct *Thrinaxodon*'s brain, there remains uncertainty in the dorsoventral depth of the endocast, both for the olfactory bulbs and whether the hypophyseal cast was present or not. The hypophyseal cast was not reconstructed for all adult specimens, so segmentation of more adult specimens may help to definitively conclude if the hypophyseal cast was present or not. The hypophyseal cast has, however, been identified in other cynodonts from the Triassic, including *Riograndia guaibensis* (Rodrigues *et al*., 2019) and *Nythosaurus larvatus* (Pusch *et al*., 2022). *Nythosaurus larvatus* has often been described as synonymous with *Thrinaxodon liorhinus* (see below) and therefore it may be inferred that the hypophyseal cast could have been present on the ventral surface of *Thrinaxodon*'s brain.

Regarding *Nythosaurus larvatus,* it is now considered a distinct species from *Thrinaxodon*, although its brain morphology (Pusch *et al*., 2022) is strikingly similar to the endocasts generated in this study and presented by Kielan-Jaworowska *et al.* (2004). The endocasts of NHMUK PV R511, *Nythosaurus larvartus* (Pusch *et al*., 2022) and the illustrated *Thrinaxodon* brain by Kielan-Jaworowska *et al.* (2004) all have long, narrow cerebral hemispheres. However, no comments have yet been made on whether the hemispheres functioned separately or together in *Thrinaxodon*. Interestingly, divided cerebral hemispheres have been reconstructed for Late Triassic cynodonts such as *Probainognathus* (Quiroga 1980c) and *Brasilitherium* (Rodrigues *et al*., 2014), but Pusch *et al*. (2022) note that a natural endocast of *Nythosaurus larvatus* displays undifferentiated cerebral hemispheres, consistent with the endocranial anatomy interpreted for *Chiniquodon* (Kemp 2009), *Exaeretodon* (Bonaparte

1966) and *Massetognathus* (Quiroga 1979). As such, it is concluded that *Thrinaxodon*'s cerebral hemispheres were similarly undivided.

Kielan-Jaworowska *et al.* (2004) proposed a pineal body was present on the dorsal surface of *Thrinaxodon*'s brain. The location of the pineal body can be identified as a raised, oval feature in the centre of the cerebral hemispheres reconstructed for the specimens in this study and is confirmed by examination of each of the skulls, which have a parietal foramen in the centre of the skull roof, consistent with Benoit *et al*. (2016a) who state that *Thrinaxodon* specimens always have a parietal foramen. Similarly, *Nythosaurus larvatus* also has a parietal foramen with pineal body reconstructed, and the presence of this structure is confirmed by a cast of the pineal body observed on a natural endocast of the species (Pusch *et al*., 2022). However, the presence of the pineal body in *Thrinaxodon* was proposed by Kielan-Jaworowska *et al.* (2004) to be the exception to the rule, with most eucynodonts (those cynodonts more derived than *Thrinaxodon*; Kemp 1982) not having a parietal foramen at all.

Elsewhere, the vermis remains questionably reconstructed in the seven adult skulls studied and in Kielan-Jaworowska *et al.* (2004)'s brain reconstruction but has been identified in other cynodonts such as *Riograndia* (Rodrigues *et al*., 2019) and *Brasilitherium* (Rodrigues *et al*., 2014). The vermis is not thought to have functioned separately to the cerebellum in cynodonts (Rodrigues *et al*., 2019), which contrasts with the mammalian crown group, where the vermis joins the two sides of the cerebellum (Ho Cho *et al*., 2011) and conveys sensory inputs between them to coordinate spinal movements (Coffman *et al*., 2011). It should be noted, however, that when viewing coronal slices through *Thrinaxodon* skulls at the point of the vermis, there is a foramen with some loosely articulated skeletal elements running fully

through the parietal bone (figure 3.2, slice 1479), suggesting that this feature could also be a sinus, or a sinus overlying the vermis.

The main area of difference between Kielan-Jaworowska *et al.* (2004)'s brain reconstruction and those presented here are that the olfactory bulbs do not appear to have been divided in *Thrinaxodon*. This contrasts with the divided morphology depicted by Kielan-Jaworowska *et al.* (2004), although a shallow sulcus may be present in some of the reconstructions (figure 3.3). A depression between the olfactory bulbs is seen more prominently in other cynodonts such as *Brasilitherium* (Rodrigues *et al*., 2014), *Massetognathus* (Kielan-Jaworowska *et al*., 2004) and *Nythosaurus larvatus* (Pusch *et al*., 2022), with the olfactory bulbs becoming increasingly separated in mammaliaforms (such as *Cifelliodon*) and extant mammals, including *Monodelphis domestica* (Huttenlocker *et al*., 2018). The increasing separation of the olfactory bulbs along the mammalian evolutionary lineage corresponds with overall brain enlargement (Rowe *et al*., 2011), fine-tuning of the olfactory epithelium with an associated increase in sensory neurons (Klingler 2017; Tufo *et al*., 2022), and development of a rigid support for the olfactory epithelium which activated olfactory receptor genes to assist with processing olfactory cues (Rowe *et al*., 2005).

The uncertainty in the reconstruction of *Thrinaxodon*'s olfactory apparatus is largely due to the lack of an ossified boundary between the brain and nasal cavities, which contrasts with the cribriform plate defining the olfactory region in mammal brains, through which olfactory nerves pass (Bird *et al*., 2014; Rodrigues *et al*., 2019; Franco *et al*., 2021). Some very well preserved *Thrinaxodon* specimens have been found with the orbitosphenoids in place (Benoit *et al*., 2017) which could help to define the ventral boundary of the olfactory bulbs, but the orbitosphenoids were not preserved in position within the skulls studied. It is also not possible

to identify any olfactory tracts in *Thrinaxodon*'s brain, which would have joined the olfactory bulbs to the cerebral hemispheres (Pavanatto *et al*., 2019). Macrini *et al.* (2007a) further suggested that it would not be possible to reconstruct the olfactory tracts in cynodonts as these structures would have been concealed within the meninges surrounding the brain as in extant mammals, thus leaving no skeletal impression. Without soft tissue preservation or evidence from braincase anatomy, it is not possible to confirm the morphology of olfactory tracts in *Thrinaxodon*, if they were present. Similarly, the absence of fossilised brains or impressions of brain morphology in Triassic cynodonts means that there is no record of brain patterning, such as gyri and sulci, in these mammalian ancestors. Given that the brain was likely surrounded by the protective meningeal tissues and intracranial fluids (Rodrigues *et al.,* 2019), it would be unlikely for such impressions to be made on the internal braincase surface (Laaß et al., 2017a). The lissencephalic (smooth) brain constructed here for *Thrinaxodon liorhinus* is, therefore, likely to be true to life as a lissencephalic brain has previously been suggested to be the ancestral condition for the mammalian crown group (Kielan-Jaworowska *et al*., 2004).

In all of the specimens, including the well preserved NHMUK PV R511, there is no clear midbrain exposure. However, it has been debated whether the pineal body resides within the midbrain or forebrain of mammalian ancestors (Quiroga, 1980a; Pusch *et al*., 2019; Rodrigues *et al*., 2019) due to its dorsal exposure in the endocasts. Here, the pineal body is taken to be part of the forebrain, as in the cynodont *Galesaurus planiceps* (Pusch *et al*., 2019). As such, non-exposure of the midbrain is assumed to be the case for *Thrinaxodon*, consistent with a concealed midbrain being the plesiomorphic condition for the mammalian crown group (Macrini *et* al., 2007a).

### 3.4.2. Estimating *Thrinaxodon*'s cognitive, olfactory and behavioural characteristics

From comparison with other cynodonts and extant mammals, it is possible to make inferences about *Thrinaxodon*'s cognitive and olfactory capabilities to better understand how these characteristics influenced its mode of life. Based on the endocast volumes generated in this study, an encephalisation quotient of 0.27 was determined to be the most representative value for an adult *Thrinaxodon liorhinus*. This EQ value is noticeably larger than the 0.1 calculated for *Thrinaxodon* by Jerison (1973) and falls between the EQ values calculated for Triassic cynodonts *Massetognathus* (0.22; Quiroga 1980b) and *Riograndia* (0.22; Rodrigues *et al*., 2019), and the Jurassic mammaliaforms *Morganucodon* (0.32; Rowe *et al*., 2011) and *Hadrocodium* (0.47; Rowe *et al*., 2011). It may be considered that based on these values, *Thrinaxodon* was less cognitively advanced that Jurassic mammaliaforms, but conversely, *Thrinaxodon* could have possessed more pronounced cognitive capabilities than, for example, *Riograndia* which evolved later in the Triassic. However, it should be noted that this difference in EQ value could also be attributed to size differences between *Thrinaxodon* (BSL of 84 mm for NHMUK PV R511) and *Riograndia* (BSL of 35 mm; Rodrigues *et al*., 2019) which have a consequent impact on the reconstructed endocranial volume (2942 $mm^3$ and 445 $mm^3$, respectively) used within the EQ calculation.

Furthermore, the calculated EQ values for the *Thrinaxodon* endocasts generated here range between 0.16 and 0.27 ($EQ_{Jerison}$) and 0.22 and 0.38 ($EQ_{Manger}$). If these *Thrinaxodon* endocasts and specimens were considered in isolation, then the calculated EQ values could change the evolutionary trajectory of *Thrinaxodon* in the context of brain development. For example, an EQ of 0.16 corresponds with the values calculated using equation 3.2 for Late Triassic

cynodonts such as *Massetognathus* (0.15; Quiroga 1979; EQ number derived from one specimen (n = 1)), *Exaeretodon* (0.10 or 0.15; Quiroga 1980d; n = 2), *Probelesodon* (0.13; Quiroga 1979; n = 1) and *Probainognathus* (0.17; Quiroga 1980d; n = 2). However, an EQ of 0.38 would mean that *Thrinaxodon*'s cognitive capabilities seemingly surpasses that of Jurassic mammaliaform, *Morganucodon* (0.32; Rowe *et al*., 2011; n = 1) and even that of Cretaceous mammal *Vincelestes neuquenianus* (0.37; Macrini *et al*., 2007a; n = 1). Therefore, the variation in EQ could shift *Thrinaxodon* backwards or forwards in an evolutionary trajectory compared to other species and provide a misleading insight into cognitive capabilities. As such, the EQ value should be used with caution and the variables (including the accuracy of endocranial volumes or body mass estimates) should be taken into account when drawing conclusions about *Thrinaxodon* and other extinct species where there is no brain preservation.

More telling is when endocast size is scaled to the EQ value (Rowe *et al*., 2011; figure 3.6), which highlights that all cynodont brains are dwarfed by mammal brains and are also generally smaller than mammaliaform brains (such as *Morganucodon* and *Hadrocodium*). However, while some mammals, including the genus *Felis* (which includes the domestic cat) has an EQ of 1, *Thrinaxodon*'s contemporary analogue, *Monodelphis*, only has an EQ value of 0.44. Despite the adult brains reconstructed for *Thrinaxodon* in this study providing EQ values ranging between 0.16 and 0.38, these values largely place the basal cynodont's cognitive capabilities as being less developed than in extant mammals.

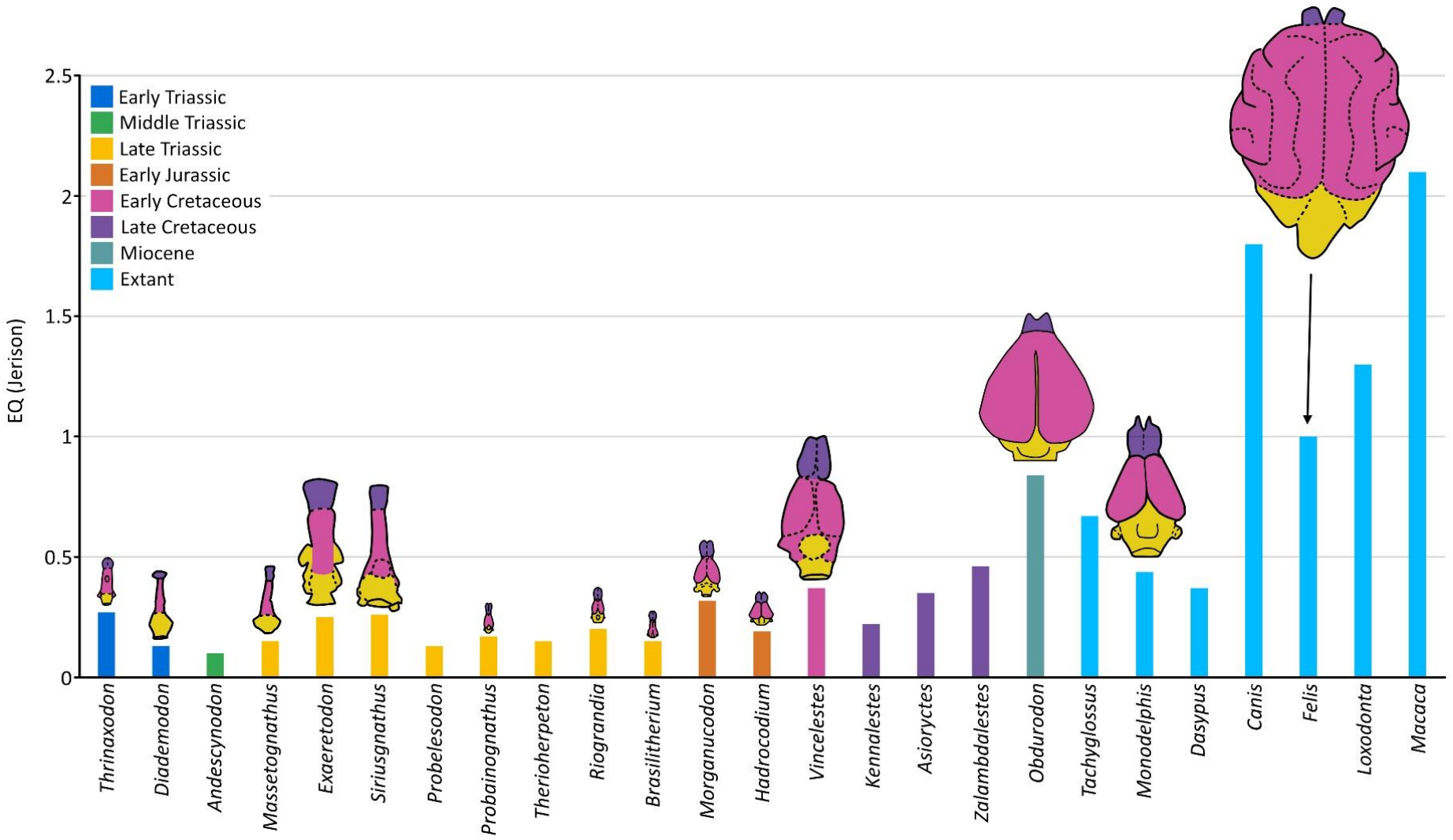
Early Triassic
Middle Triassic
Late Triassic
Early Jurassic
Early Cretaceous
Late Cretaceous
Miocene
Extant
EQ (Jerison)
2.5
2
1.5
1
0.5
0
Thrinaxodon
Diademodon
Andescynodon
Massetognathus
Exaeretodon
Siriusgnathus
Probelesodon
Probainognathus
Therioherpeton
Riograndia
Brasilitherium
Morganucodon
Hadrocodium
Vincelestes
Kennalestes
Asioryctes
Zalambdalestes
Obdurodon
Tachyglossus
Monodelphis
Dasypus
Canis
Felis
Loxodonta
Macaca

**Figure 3.6. (previous page).** Calculated EQ values for cynodont, mammaliaform and mammalian taxa through time. Endocasts are shown scaled to EQ value but are not life size. Brain anatomy is denoted by purple for the olfactory bulbs, pink for the cerebral hemispheres and yellow for the cerebellum. Species studied: *Thrinaxodon* (this study), *Diademodon* (Macrini 2006), *Andescynodon* (Quiroga 1980d), *Massetognathus* (Quiroga 1979), *Exaeretodon* (Pavanatto *et al*., 2019), *Siriusgnathus* (Pavanatto *et al*., 2019), *Probelesodon* (Quiroga 1979), *Probainognathus* (Quiroga 1980d), *Therioherpeton* (Quiroga 1984), *Riograndia* (Rodrigues *et al*., 2019), *Brasilitherium* (Rodrigues *et al*., 2014), *Morganucodon* (Rowe *et al*., 2011), *Hadrocodium* (Macrini 2006), *Vincelestes* (Macrini *et al*., 2007a), *Kennalestes* (Kielan-Jaworowska 1984), *Asioryctes* (Kielan-Jaworowska 1984), *Zalambdalestes* (Kielan-Jaworowska 1984), *Obdurodon* (Macrini *et al*., 2006), *Tachyglossus* (Macrini 2006), *Monodelphis* (this study), *Dasypus* (Macrini 2006), *Canis* (Saganuwan 2021), *Felis* (Ruiz-Núñez *et al*., 2013), *Loxodonta* (Ruiz-Núñez *et al*., 2013) and *Macaca* (Ruiz-Núñez *et al*., 2013).

However, while EQ values provide a somewhat useful evolutionary comparison, it should be noted that the relationship between brain volume and cognitive capabilities is more complex than simply the volume of the different processing regions; the density and interconnectedness of neurons would have greatly influenced signal transmission times within the brain and subsequently processing ability (Rodrigues *et al*., 2019). Additionally, the equations for the EQ value rely on the assumption that 1 $cm^3$ is equal to 1 g (Rodrigues *et al*., 2014), but this may not correspond to the actual brain volume depending on neuron density and the presence of surface convolutions which act to increase the surface area for the transmission of signals within the brain and influence behavioural outputs (Lin *et al*., 2021). Furthermore, it is not ideal to use an estimate of body mass based on skull length, or indeed any other parameter (such as limb bone length, postcanine tooth size or cross-sectional area

of vertebrae; Rodrigues *et al*., 2014) to calculate EQ value. However, with the rarity of cranial and postcranial remains being found together in the fossil record, these alternative methods of estimating body mass at least allow an approximation of cognitive capabilities to be gleaned from the EQ value.

An alternative approach (proposed by Rodrigues *et al*., 2019) which overcomes the error generated through body mass estimation is to compare species based on the proportion of the endocast occupied by the olfactory bulbs. In adult specimens of *Thrinaxodon liorhinus*, the olfactory bulbs were found to comprise approximately 23% of the endocast length, averaged across the brain models produced in this study. Comparing this to other cynodonts, the olfactory bulbs account for 40% of *Riograndia guaibensis*' brain length (Rodrigues *et al*., 2019), 35% in *Brasilitherium riograndensis* (Rodrigues *et al*., 2014), 26% in *Prozostrodon brasiliensis* (Kerber *et al*., 2023), 26% in *Probelesodon kitchingi* (Hoffman *et al*., 2019) and 38% in *Massetognathus ochagaviae* (Hoffman *et al*., 2019). Among mammaliaforms, the olfactory bulbs comprised 43% of the brain length in *Morganucodon oehleri* (Rowe *et al.*, 2011) and 28% in *Hadrocodium wui* (Rowe *et al.*, 2011). When considering extant mammals, the olfactory bulb:endocast ratio of an adult specimen of *Thrinaxodon*'s contemporary analogue, *Monodelphis domestica,* is 25% (Macrini *et al*., 2007b), surprisingly comparable to the adult specimens of *Thrinaxodon* studied here, where the olfactory bulb:endocast ratio ranges between 18% and 26%. It appears that the proportion of the endocast dedicated to the olfactory bulbs is somewhat consistent between *Thrinaxodon*, some Middle and Late Triassic cynodonts as well as the extant opossum (although this finding cannot be extrapolated across all living mammals). The species considered here suggest that the proportion of the brain dedicated to detecting and processing olfactory cues was not significantly larger in basal

cynodonts such as *Thrinaxodon*, but there was a proportional increase in the olfactory bulbs during the Triassic.

However, this method is still problematic for *Thrinaxodon* as the lack of an ossified boundary prohibits reconstruction of a definitive anterior boundary for the olfactory bulbs, meaning that direct comparison of olfactory bulb to endocast length (and therefore olfactory capabilities) between cynodonts, mammaliaforms and mammals remains challenging. Additionally, the linear method does not account for changes in density of neurons or development of nasal epithelium over time which improved olfactory acuity along the mammalian lineage (Rowe *et al*., 2011). If the linear measurements are considered alongside volumetric data, then the measurements are more revealing. In this instance, *Thrinaxodon'*s olfactory bulbs volumetrically comprised a greater proportion of the brain than they do in mammaliaforms and mammals, who instead have much wider cerebral hemispheres than the tubular structures reconstructed for *Thrinaxodon* (Rowe *et al*., 2011; figure 3.6) as more of the brain's volume is dedicated to the expansion of the cerebral cortex during mammalian evolution (Northcutt 2011; Kaas 2013). Therefore, despite linear measurements suggesting *Thrinaxodon*'s olfactory bulbs were of comparable proportions to its descendants, consideration of the endocast as a whole may indicate that olfactory processing was a more important influence on brain size and shape in *Thrinaxodon* than it is in mammalian descendants.

It has been suggested that *Thrinaxodon* exhibited a fossorial lifestyle (Damiani *et al*., 2003; Fernandez *et al*., 2013), perhaps in response to the changing environmental conditions above ground following the Permian-Triassic mass extinction. To better understand whether olfactory acuity facilitated this mode of life, it is helpful to compare *Thrinaxodon* to a modern

burrowing group – leporids, which include rabbits and hares. In leporids, burrowing species were found to have larger olfactory bulbs than non-burrowing species and those species with larger olfactory bulbs were better at avoiding predation and the impacts of seasons (Todorov *et al*., 2022). Given that there is some evidence that *Thrinaxodon* may have inhabited burrows (Damiani *et al*., 2003; Fernandez *et al*., 2013), larger olfactory bulbs could have helped orientation within the burrow and the search for prey. Additionally, Jerison (1973) suggested that an enhanced sense of smell was correlated with enlarged olfactory bulbs in small, nocturnal mammaliaforms. As such, the parts of *Thrinaxodon*'s brain dedicated to processing odours (olfactory bulbs) may have been more enhanced than the regions dedicated to processing visual cues (such as the occipital lobe), although a separate study into the orbital region would be needed to investigate this further.

## 3.5. Chapter summary

The first digital brain reconstructions of *Thrinaxodon liorhinus* have been presented since the illustrations created by Kielan-Jaworowska *et al*. (2004), shedding light on the form and function of soft tissues lost to the fossil record. Alike many mammaliaforms and mammals, *Thrinaxodon*'s brain had the basic functional components before evolutionary expansion – olfactory bulbs connected to tubular cerebral hemispheres which merged into the cerebellum. The hindbrain was laterally expanded into parafloccular lobes before narrowing into the brain stem.

The lack of ossified basicranial elements makes reconstructing *Thrinaxodon*'s brain morphology challenging, and this may account for why no previous attempt has been made to define the different brain regions it may have had during life. It is also important to note that the endocasts offer a reconstruction of the entire endocranial cavity, but the brain may

have been surrounded by other protective tissues and vascular structures meaning that endocranial volumes may be an overestimation. Nevertheless, digital segmentation of the seven adult skulls provides the best insight yet into *Thrinaxodon*'s brain morphology, which can reveal new insights about the development of the mammalian brain.

In the broader evolutionary context of mammals, *Thrinaxodon* reveals the beginnings of the brain before a series of evolutionary advancements transformed it into the complex organ it is today. The initial improvement in cognitive capabilities associated with enlargement of the olfactory bulbs, cerebral hemispheres and cerebellum was followed by a more substantial change to the nasal cavity around the time that the mammalian crown group originated. The ossification of nasal turbinals, development of a cribriform plate and a rigid support for the olfactory epithelium activated olfactory receptor genes which improved olfactory capabilities in mammals compared to non-mammalian forebears, such as *Thrinaxodon liorhinus*.

Future work would attempt to identify *Thrinaxodon* specimens that have the orbitosphenoids preserved in life position (or as close as possible) to better constrain reconstructions of the olfactory region. This would provide a more accurate estimate of the volume of the olfactory bulbs, permitting more reliable comparisons with mammaliaforms and mammals to understand how brain morphology fuelled the pulses in mammalian brain enhancement. Finally, depending on the specimen studied, the encephalisation quotient places *Thrinaxodon*'s brain between early Triassic cynodonts and Cretaceous mammals. Therefore, it is recommended that EQ values are used cautiously as a proxy for cognitive capabilities and instead direct comparisons of size and shape changes to individual brain regions may be more telling about the development of the mammalian brain.

# CHAPTER FOUR

# Ontogenetic changes to the endocranial anatomy of *Thrinaxodon liorhinus*

## 4.1. Introducing variation during the lifetime of animals

Ontogenetic variation refers to developmental changes that occur during an organism's life cycle from fertilisation to adulthood. Variability arising from ontogeny is commonly seen across different vertebrate groups, from mammals (Leigh 1992; Miller *et al*., 2008; Werneburg and Geiger, 2017) and birds (Heers 2016; Navalón *et al*., 2021), to reptiles (Gray *et al*., 2019; Griffin *et al*., 2021) and amphibians (Lutz 1948, Smirnov and Vassilieva, 2022). Such variation reflects developmental changes associated with size and shape modifications to the body, onset of reproductive activity, refining feeding strategies and developing behavioural characteristics including social interactions and learning (Herrel *et al*., 2016; Franks and Thorogood, 2018; Sakai 2018). Some of the developmental changes between juveniles and adults are obvious, such as the metamorphosis of tadpoles into frogs (Lutz 1948) and the onset of sexual maturity in humans (Abreu and Kaiser, 2016). However, some organisms, such as the axolotl, retain their juvenile form throughout their life (a condition known as neoteny), which can make the identification of adult specimens more challenging (Rosenkilde and Ussing, 1996).

In mammals, juvenile forms of most species are much smaller and less developed than adult forms (Ellstrand 1983). Besides the general trend of juvenile mammals getting larger as they grow into adulthood, numerous other ontogenetic changes have been observed across the mammalian lineage including full cranial ossification (Wilson 2018), dental growth (Rodrigues

*et al*., 2017), colour change (Booth 1990), circadian rhythm development (Weinert 2005) and modifications to the ear (Sánchez-Villagra *et al*., 2002), among others. Macrini *et al.* (2007b) also identified ontogenetic changes in the brain morphology of the opossum *Monodelphis domestica.* Through examining digitally rendered cranial endocasts, Macrini *et al*. (2007b) observed an increase in endocast length, width and volume with specimen age. The authors also discovered enlargement of the olfactory bulbs towards adulthood, although the paraflocculars lobes became smaller with age. As *Monodelphis domestica* is taken to be a modern analogue for cynodonts (Luo 2007; Rodrigues *et al*., 2014; Jasinoski *et al*., 2015; Rodrigues *et al*., 2019), it is important to consider whether ontogenetic variation can also be identified in endocasts of extinct pre-mammalian taxa (such as *Thrinaxodon liorhinus*) to make inferences about changing brain development, cognition and sensory capabilities during an individual's life.

Endocranial studies have been conducted for several cynodonts (but only for a single specimen) including *Brasilitherium riograndensis* (Rodrigues *et al*., 2014), *Chiniquodon theotenicus* (Kemp 2009), *Exaeretodon riograndensis* (Pavanatto *et al.,* 2019), *Galesaurus planiceps* (Pusch *et al.,* 2019), *Massetognathus ochagaviae* (Hoffman *et al*., 2021), *Prozostrodon brasiliensis* (Kerber *et al.,* 2023), *Riograndia guaibensis* (Rodrigues *et al*., 2019) and *Therioherpeton cargnini* (Kerber *et al.,* 2023). There have also been several studies reporting ontogenetic variation in the size and morphology of cynodont skulls, including *Galesaurus planiceps* (Jasinoski and Abdala, 2017) and *Thrinaxodon liorhinus* (Jasinoski *et al*., 2015). However, no studies have yet investigated whether variation exists in cynodont brain morphology associated with a particular ontogenetic stage of a single cynodont species. This is primarily due to the lack of well-preserved braincases for cynodonts at the same developmental stage, but there is the added problem of juvenile specimens often lacking

ossification and being more prone to taphonomic deformation than adult specimens, thus making studies of juvenile fossils, and as such ontogenetic changes, challenging (Wynd *et al*., 2021).

Understanding more about ontogenetic variation in cynodonts is important for constraining the timing of mammalian characteristics' origination as well as identifying how developed cynodont brains were at different growth stages compared to mammalian analogues. For *Thrinaxodon liorhinus*, ontogenetic variation was investigated by Jasinoski *et al.* (2015) who analysed 68 *Thrinaxodon* skulls and found that numerous cranial features separated juveniles from adults (figure 4.1). Juveniles were defined by a lack of sagittal and occipital crests, an inverted V-shaped nasal-frontal suture, the supraoccipital projecting beyond the occipital condyle and both bicuspid and tricuspid teeth were present, among other features. Conversely, adult specimens were found to have anterior sagittal and external occipital crests, a transverse nasal-frontal suture, occipital condyles which protruded posteriorly past the supraoccipital, and dentition predominantly comprised of tricuspids. Postcranial ontogenetic differences were also found in *Thrinaxodon* through histological analysis. Botha and Chinsamy (2005) analysed ten *Thrinaxodon* limb bones (humeri, radii, ulnae and femora), finding that bone deposition was highest in juveniles, indicating rapid growth during early ontogeny with a slower growth rate as *Thrinaxodon* individuals aged.

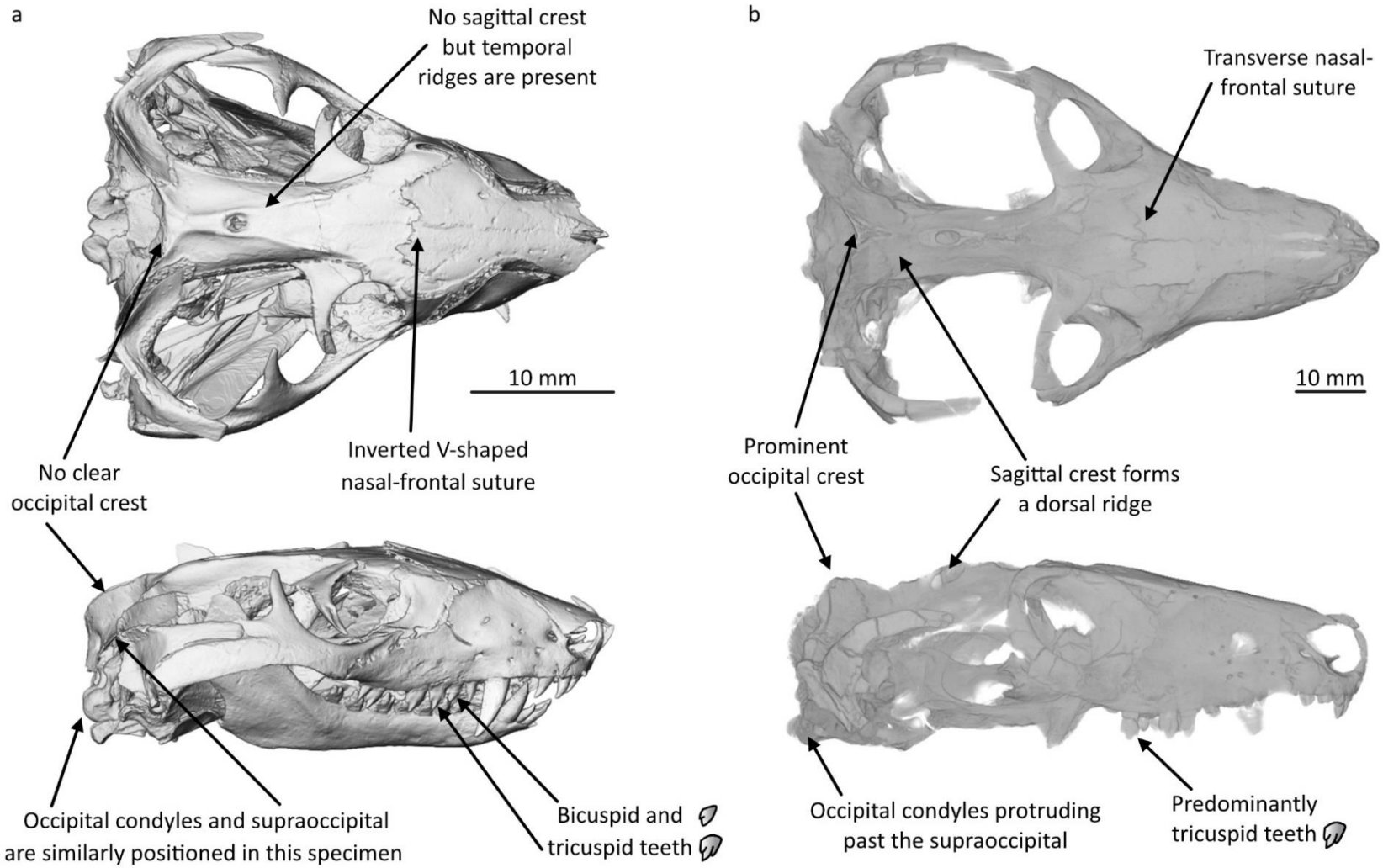


**Figure 4.1.** Cranial anatomy of digitally rendered **(a)** juvenile (BP/1/5372) and **(b)** adult (NHMUK PV R511) specimens of *Thrinaxodon liorhinus* in dorsal (top) and right lateral (bottom) views, highlighting cranial morphological variation which can be used as a proxy for developmental stage.

Given that there is size and shape variation in *Thrinaxodon*'s cranial and postcranial anatomy associated with growth stage, it is possible that internal soft tissue structures, such as the brain, would also show variation. Yet the lack of cynodont endocranial studies focussing on growth stages means that attention should be turned to modern mammals to see whether changes to brain shape and size can be observed between juvenile and adult forms. Macrini *et al*. (2007b) investigated ontogenetic disparity in opossum brains, finding that juvenile specimens of *Monodelphis domestica* displayed rounded olfactory bulbs, which grew larger into adulthood, while the cerebral hemispheres became more elongated and widened with age. With ontogenetic variability observed in extant mammals, it is thus hypothesised that *Thrinaxodon* brains would also show some morphological changes associated with age.

However, no known attempt has been made to investigate whether variation within *Thrinaxodon*'s cranial anatomy during growth translates into ontogenetic changes to the structure of the brain itself. Indeed, ontogenetic changes in the endocranial anatomy of cynodonts more broadly remains elusive. This lack of study in *Thrinaxodon* is likely due to the challenges posed in obtaining multiple, well-preserved braincases, at the same developmental stage, for study. The issue is compounded by the frequency of unossified or cartilaginous areas within *Thrinaxodon*'s braincase which promote disarticulation and deformation (and is particularly prevalent in delicate juvenile specimens; Jasinoski *et al*., 2015). This study therefore aims to identify whether ontogenetic changes can be observed within the brain of *Thrinaxodon liorhinus* through the comparison of endocasts generated for one adult and one juvenile specimen. If ontogenetic variation is found, the changes to brain morphology will be considered in their functional and evolutionary contexts, with reference to *Thrinaxodon*'s modern analogue, *Monodelphis domestica*, who's biology is well known due to the frequency with which *Monodelphis* has been studied as a laboratory specimen.

## 4.2. Methods

### 4.2.1. Specimen selection: adult and juvenile *Thrinaxodon liorhinus*

The studied specimens comprise an adult *Thrinaxodon liorhinus* (NHMUK PV R511) and a juvenile specimen (BP/1/5372), with this classification derived from Jasinoski *et al*. (2015; figure 4.1; see chapter two for further details). NHMUK PV R511 (BSL 84 mm) has a well-preserved braincase, with very minimal brittle or plastic deformation, meaning that the brain cavity is preserved in close to its original morphology (as far as is known). Being a juvenile, BP/1/5372 (BSL 37 mm) lacks the more complete ossification of the braincase seen in adult fossils and shows displacement of cranial bones. Additionally, there is some dorsoventral compression of the skull, leading to overlapping skeletal elements within the braincase. However, juvenile *Thrinaxodon* specimens are very rare, therefore, this specimen still provides a valuable insight into the brain cavity of a young *Thrinaxodon liorhinus* and highlights the challenge of studying fossils of juveniles.

These two specimens provide an approximation of cranial (and subsequently endocranial) anatomy near to the beginning and end stages of *Thrinaxodon*'s known life span, given the *Thrinaxodon* fossils studied by Jasinoski *et al*. (2015) had basal skull lengths ranging between 30 mm and 96 mm. The *Thrinaxodon* fossils were chosen based on the limited availability of juvenile skulls discovered to date and NHMUK PV R511 being one of the larger adult specimens available to study (Jasinoski *et al*., 2015).

For comparison, a growth series of 14 *Monodelphis domestica* endocasts was provided by Thomas Macrini (Macrini *et al*., 2007b) encompassing individuals between the ages of 27 days old (TMM M-7595) and a fully grown adult (TMM M-7599; taken to be over 183 days old when

opossums reach sexual maturity; see chapter two and Macrini *et al*. (2007b) for further specimen and segmentation details). While the endocasts generated in Macrini *et al.* (2007b)'s study were derived from animals, no new data was collected from living specimens for the research presented here. For this study, juvenile *Monodelphis* specimen TMM M-7595 was compared with *Thrinaxodon* specimen BP/1/5372 and adult *Monodelphis* TMM M-7599 was equated to *Thrinaxodon* NHMUK PV R511 (figures 4.1 and 4.2). *Monodelphis* specimens TMM M-7536 (day 48), TMM M-7539 (day 57), TMM M-7542 (day 75) and TMM M-7545 (day 90) were also considered as part of the growth series, as increasingly older opossums bracketed by the two main opossum specimens analysed.

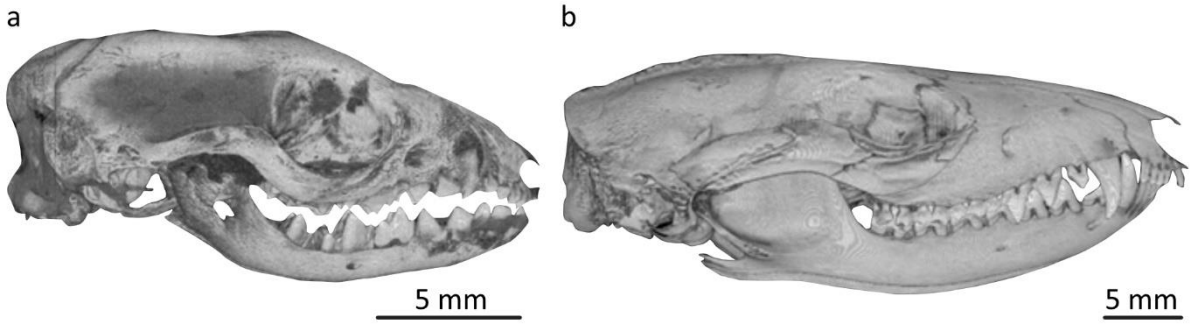


**Figure 4.2.** Digitally rendered skulls of the **(a)** juvenile (TMM M-7595) and **(b)** adult (TMM M-7599) opossum specimens studied and for which endocranial reconstructions were provided by Macrini *et al*. (2007b). Skulls shown in right lateral view.

## 4.2.2. Digitally extracting fossil brains: segmentation techniques

To study ontogenetic variation in *Thrinaxodon liorhinus,* the CT scans of BP/1/5372 and NHMUK PV R511 were imported into Avizo 9.3.0 for digital segmentation of the braincase (see chapters 2.2 and 3.2 for segmentation techniques). The mask was delimited by the inner surface of bone boundaries including the frontal, parietal, postparietal, epipterygoid, pterygoid, basisphenoid, prootic, supraoccipital, basioccipital and exoccipital. Only the brain

was reconstructed in this study and other endocranial features that can be identified in the CT scans (such as the inner ear), were not included because there are only a few studies with reconstructions of cynodont inner ear anatomy (Rodrigues *et al*., 2013; Laaß 2016) and no inner ear growth series are available for comparison. Furthermore, the plastic and brittle deformation observed within the CT scan of the juvenile specimen (figure 4.3) meant that some parts of the endocast had to be inferred between parts of the braincase that appeared to be in near to life position (based on comparisons made with the adult cranial anatomy). As such, an attempt was made to retain an organic shape, which would not have been possible if solely reconstructing to displaced bone boundaries.

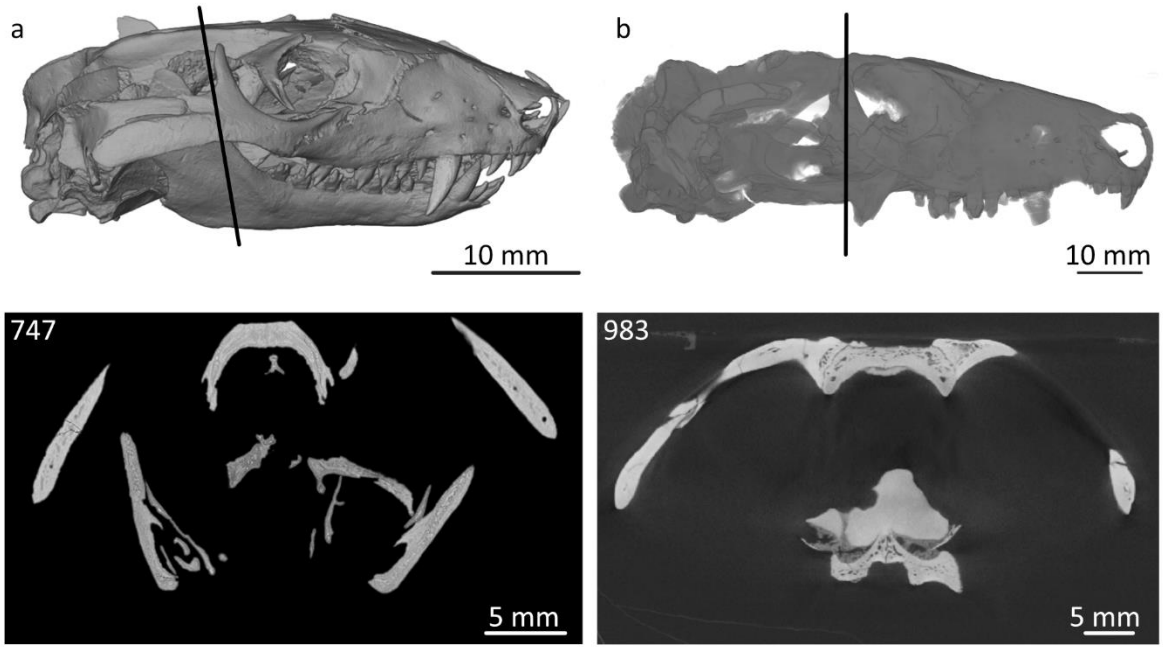


**Figure 4.3.** CT scan orthoslices taken at comparable positions within the juvenile **(a)** and adult **(b)** skulls of *Thrinaxodon liorhinus* (shown in right lateral view). The slices highlight the disarticulated bones within the brain cavity of BP/1/5372 compared to NHMUK PV R511, while the bones that are in life position within the juvenile specimen can be correlated with the associated bones in the adult skull to delimit the endocranial cast.

### 4.2.3. Quantifying ontogenetic variation

To assess morphological variation in the endocasts of *Thrinaxodon liorhinus* and *Monodelphis domestica*, linear and volumetric measurements were collected for each brain model (as outlined in figure 4.4) in Avizo using the 2D measurement and surface area volume tools, respectively. The Avizo measurements were converted into physical measurements using a scaling factor derived from the corresponding endocast lengths provided in Macrini *et al*. (2007b), as digitally rendered basal skull lengths could not be collected for the opossum craniums. The size difference between different brain regions of the juvenile and adult specimens were then calculated as a relative increase (%) so that comparisons could be made between the different developmental stages of *Thrinaxodon* and *Monodelphis*. Relative increase values overcome the physical size differences the endocast measurements would highlight based on the opossums having smaller basal skull lengths than the cynodont (Macrini *et al*., 2007b).

As the encephalisation quotient (EQ) provides a method of assessing relative brain size between organisms along the mammalian evolutionary lineage, it can be tentatively used to make inferences about cognitive capabilities through comparison with extant taxa. To provide upper and lower values for the encephalisation quotients of *Thrinaxodon* and *Monodelphis*, the equations of Jerison (1973; equation 3.2) and Manger (2006; equation 3.3) were used (see chapter 3.2 for the method of calculating EQ values). For the opossum specimens, the body mass is known: 3.53g for TMM M-7595 and 80.4g for TMM M-7599 (Macrini *et al*., 2007b). For *Thrinaxodon*, the body mass was calculated from the basal skull length (BSL) of each specimen in centimetres using equation 3.4.

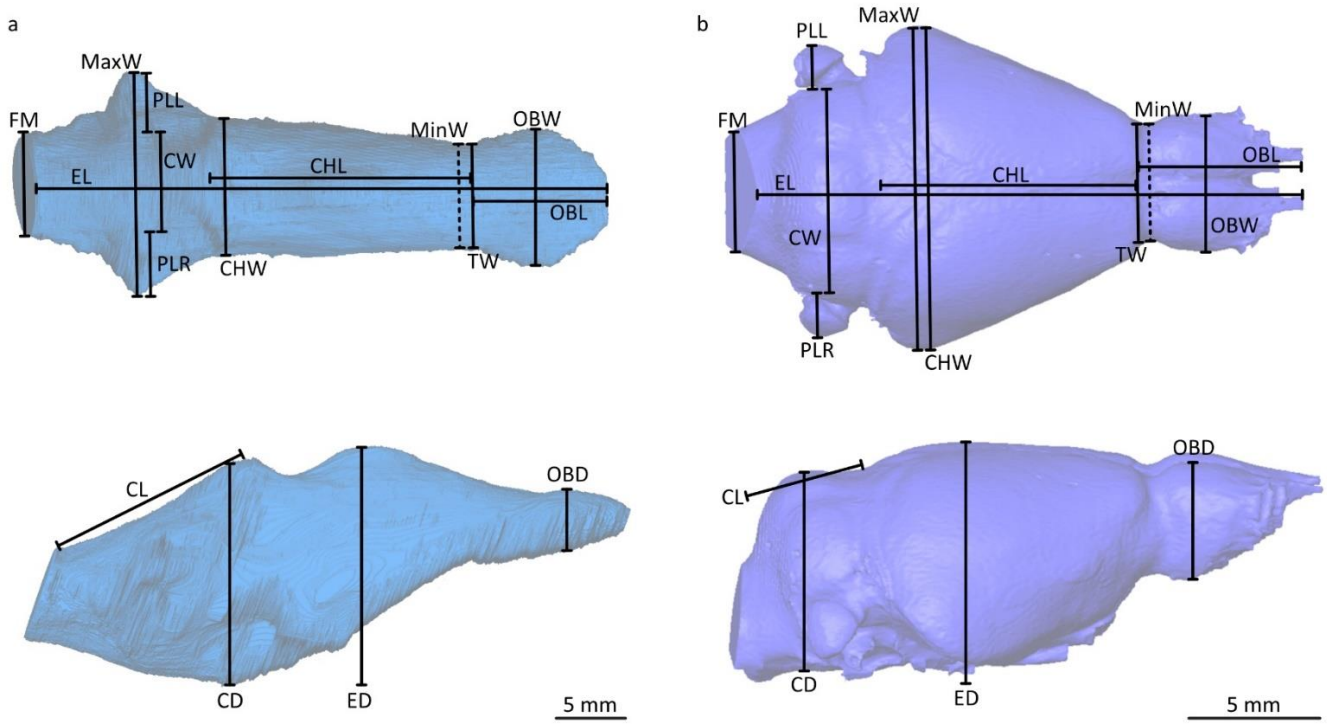


**Figure 4.4.** Ontogenetic variation in the reconstructed endocasts of **(a)** *Thrinaxodon liorhinus* (NHMUK PV R511) and **(b)** *Monodelphis domestica* (TMM M-7599) was assessed through linear measurements (as outlined above) to identify size changes between juvenile and adult brains for each species. Measurement abbreviations are: endocast length (EL), foramen magnum width (FM), maximum endocast width (MaxW), cerebellum width (CW), left parafloccular lobe (PLL), right parafloccular lobe (PLR), cerebral hemisphere width (CHW), cerebral hemisphere length (CHL), minimum endocast width (MinW), transition width (TW), olfactory bulb width (OBW), olfactory bulb length (OBL), cerebellum length (CL), cerebellum depth (CD), endocast depth (ED) and olfactory bulb depth (OBD). Endocasts shown in dorsal (top) and right lateral (bottom) views.

## 4.3. Results

### 4.3.1. Simple beginnings: *Thrinaxodon*'s juvenile brain morphology

The adult and juvenile cranial endocasts (figure 4.5) of *Thrinaxodon liorhinus* are somewhat similar in their overall morphology but vary based on the shape and proportion of different features (see chapter three for a detailed description of an adult *Thrinaxodon* brain). The endocast reconstructed for juvenile specimen BP/1/5372 has a dorsal length of 21.03 mm and a width to length ratio of 0.48. The brain comprises 57% of the skull length and the widest part of the endocast (10.13 mm) occurs in the hindbrain where the parafloccular lobes extend from the cerebellum. From the dorsal transition between the cerebral hemispheres and cerebellum towards the foramen magnum, the cerebellum slopes by 40.9°.

Alike the adult specimen, the forebrain and hindbrain of the reconstructed juvenile endocast can be distinguished. The most prominent feature of the forebrain is the olfactory bulbs, which are gently rounded with a convex dorsal surface and a flatter ventral surface. The lack of ventral curvature to the olfactory bulbs is due to braincase ossification not being present for the lower portion of the anterior brain cavity, meaning it is difficult to reconstruct the olfactory bulbs with certainty here. When viewed dorsally, the olfactory bulbs comprise almost 20% of the endocast length and can be seen to have a very shallow depression between them. The olfactory bulbs have a maximum width of 4.99 mm, length of 4.11 mm and width to length ratio of 1.21.

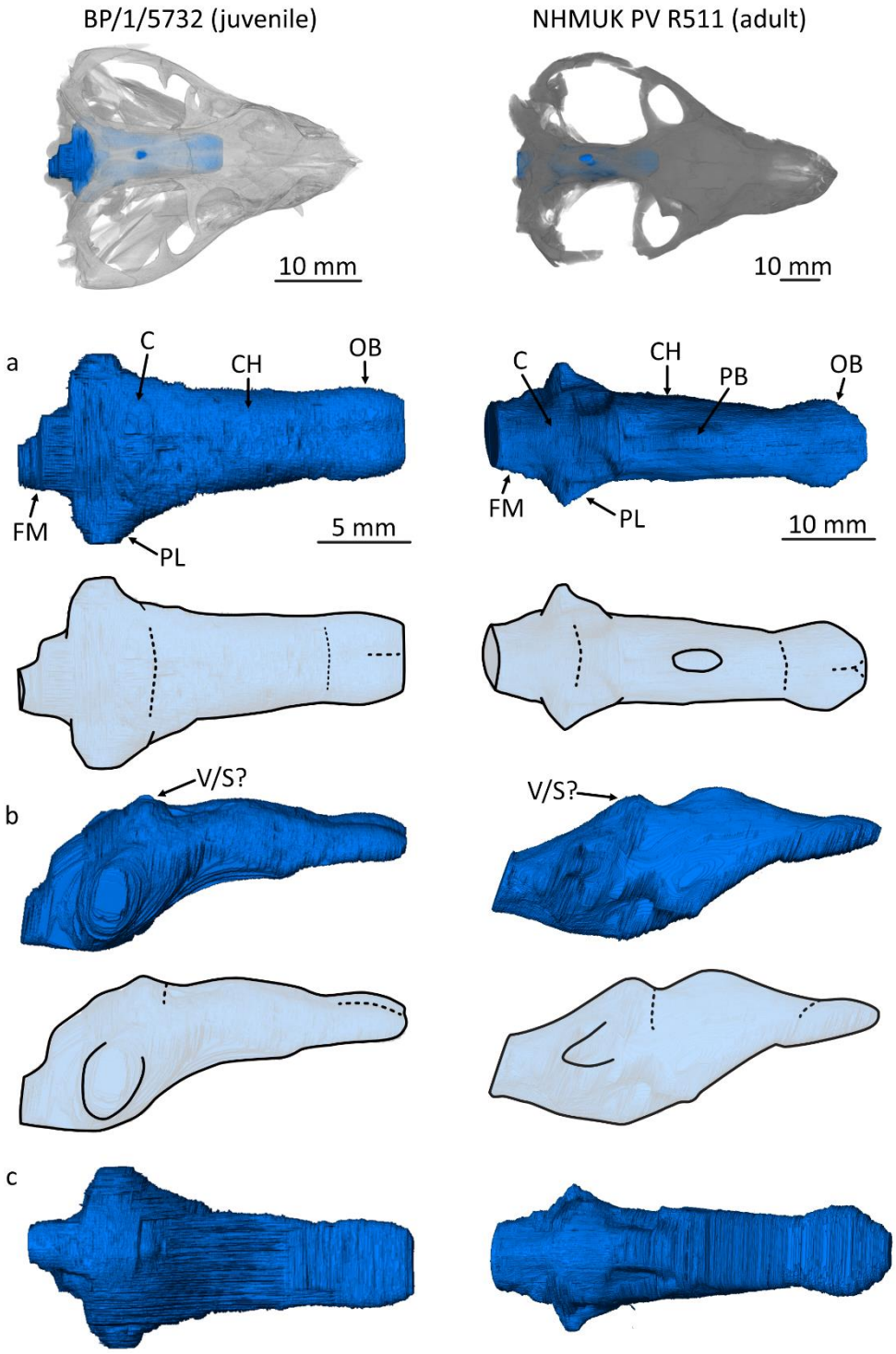


**Figure 4.5.** Digitally reconstructed endocasts of juvenile (BP/1/5732) and adult (NHMUK PV R511) specimens of *Thrinaxodon liorhinus* in dorsal **(a)**, right lateral **(b)** and ventral **(c)** orientations accompanied by schematic illustrations of brain anatomy. Anatomical abbreviations are as follows: foramen magnum (FM), cerebellum (C), parafloccular lobe (PL), cerebral hemispheres (CH), pineal body (PB), olfactory bulbs (OB) and vermis/sinus (V/S).

In the juvenile specimen, the cerebral hemispheres extend for 9.45 mm from the posterior boundary of the olfactory bulbs (where a clear depression in the endocast marks this transition in lateral view), to a ridge on the dorsal surface of the hindbrain, which acts as the posterior limit of the cerebral hemispheres. The hemispheres comprise 45% of the endocast length, following an anteroposteriorly transverse curve, and display no surface features, such as a medical sulcus, to divide the cerebral hemispheres. This section of the endocast is narrowest at the transition with the olfactory bulbs (4.55 mm) and widest just before the cerebellum begins (6.54 mm). There is no reconstruction of the pineal body as the opening for this structure is not resolved in the CT scan, although a small, circular parietal foramen can be discerned in the skull roof.

Due to the absence of basicranial bones in the anterior portion of the braincase, and a lack of ossification between the frontals and pterygoids, the ventral depth of the forebrain is challenging to reconstruct with certainty. Therefore, the endocast reconstructed here may be an underestimation of brain morphology in this region. However, the hindbrain of the juvenile *Thrinaxodon* specimen has more cranial ossification than the forebrain but suffers from dislocation of bones within the brain cavity. Nevertheless, the hindbrain can still be divided into several features, including the cerebellum, parafloccular lobes and cast of the foramen magnum. The cerebellum is similar in morphology in both the juvenile and adult specimens, widening from the cerebral hemispheres out to the parafloccular lobes, which protrude laterally by 2.46 mm (left lobe) and 2.87 mm (right lobe). The pyramidal structures make this the widest part of the juvenile endocast, when viewed dorsally. In lateral view, there is a raised area on the dorsal surface of the cerebellum (figure 4.5), possibly consistent with the vermis or sinus structure seen in the adult brain, although it is not fully resolved in the endocast of

BP/1/5372. Posterior to the cerebellum is a somewhat conical cast of the foramen magnum, which has a diameter of 2.45 mm.

Between the juvenile and adult *Thrinaxodon* specimens studied here, there is a 127% increase in basal skull length and a 96% increase in the length of the reconstructed endocast (table 4.1). The brain model widens by 59% between the two growth stages and the cerebellum becomes substantially deeper (by 114%). Although *Thrinaxodon*'s brain is not as compartmentalised as the extant opossum, there are size changes in the different brain regions (figure 4.6), most noticeably an enlargement of 134% in the length and 98% in the width of the olfactory bulbs. Figure 4.5 also highlights a shape change in *Thrinaxodon*'s olfactory bulbs during development, becoming more prominently rounded in the adult compared to the juvenile form. The cerebellum also enlarges noticeably, with the cerebellum length increasing by 111% and widening by 96%. However, although the cerebral hemispheres show enlargement between the juvenile and adult endocasts, the change is not quite as dramatic, lengthening by 88% and widening by 51%. In lateral view, the ventral boundary of the cerebral hemispheres and hindbrain is deeper in the adult (figure 4.5). This may be a true ontogenetic change, but the poorer preservation and disarticulation of the juvenile braincase should be considered when drawing conclusions. As a proportion of the endocast length, the olfactory bulbs account for 19% more of the adult endocast than in the juvenile. However, the cerebral hemispheres, while lengthening during ontogeny, hardly change at all proportionally and indeed show a negative allometry, accounting for 4% less of the endocast length in the adult than in the juvenile. As expected, the endocast volume increases noticeably between BP/1/5372 and NHMUK PV R511, by 607%. However, the two endocasts generated here show a negative endocast to basal skull length ratio, with the adult brain model comprising 14% less of the skull length than in the juvenile specimen.

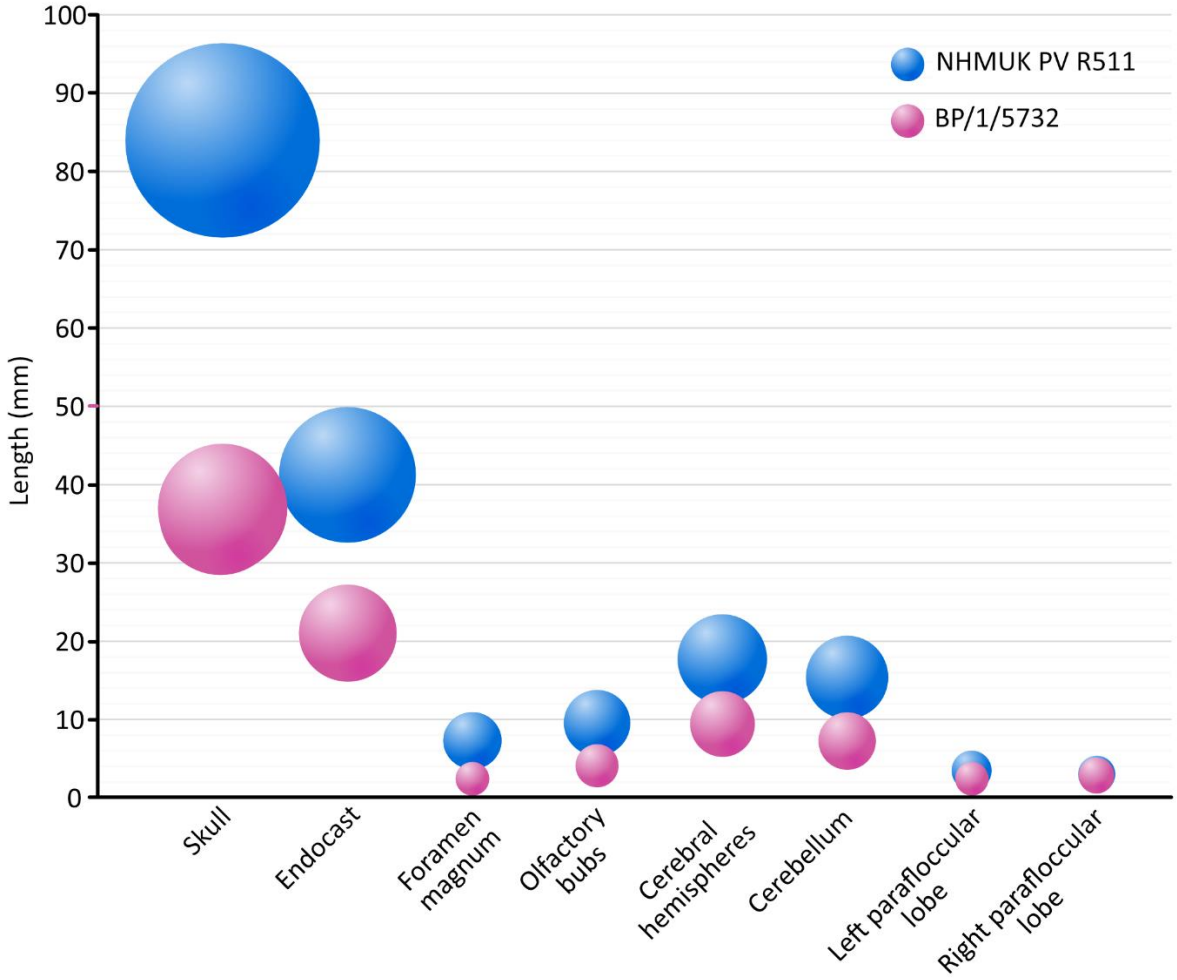


**Figure 4.6**. Bubble plot displaying the size of each skull and brain region studied in the juvenile (pink) and adult (blue) *Thrinaxodon* fossils. Bubble size reflects the increase in the linear measurement gathered for a particular morphological feature. The noticeable enlargement of all regions (except the parafloccular lobes) is clearly shown between the juvenile and adult growth stages.

**Table 4.1.** Linear and volumetric measurements for the endocranial reconstructions of BP/1/5372, NHMUK PV R511, TMM M-7595 and TMM M-7599, accompanied by the relative increase in measurements between the juveniles and adults of each species. The measurements were calculated after correction using the scaling factor outlined in the methods.

| | ***Thrinaxodon liorhinus*** | | | ***Monodelphis domestica*** | | |
|---|---|---|---|---|---|---|
| | **BP/1/5372** | **NHMUK PV R511** | **Relative increase for *Thrinaxodon* (%)** | **TMM M-7595** | **TMM M-7599** | **Relative increase for *Monodelphis* (%)** |
| Basal skull length[1] (mm) | 37 | 84 | 127.0 | 18.50 | 40.00 | 116.22 |
| Foramen magnum diameter[2] (skull, mm) | 3.85 | 7.48 | 94.2 | - | - | - |
| Foramen magnum diameter (endocast, mm) | 2.45 | 7.31 | 198.2 | 2.97 | 4.73 | 59.26 |
| Endocast length[3] (mm) | 21.03 | 41.23 | 96.02 | 12.02 | 20.79 | 72.96 |
| Maximum endocast width[4] (mm) | 10.13 | 16.09 | 58.8 | 8.07 | 12.30 | 52.37 |
| Minimum endocast width (mm) | 4.55 | 7.70 | 69.1 | 4.25 | 4.43 | 4.19 |
| Maximum endocast depth[5] (mm) | 8.57 | 16.18 | 88.9 | 5.53 | 7.54 | 36.44 |
| Maximum width:length ratio of endocast | 0.48 | 0.39 | - | 0.67 | 0.59 | - |
| Endocast:BSL ratio (%) | 56.84 | 49.08 | –13.7 | 64.97 | 51.98 | –20.01 |
| Volume of the whole endocast ($mm^3$) | 416.10 | 2942.27 | 607.1 | 248.52 | 954.78 | 284.19 |
| Length of olfactory bulb cast[6] (mm) | 4.11 | 9.60 | 133.6 | 2.70 | 6.04 | 123.56 |

| | | | | | | |
|---|---|---|---|---|---|---|
| Olfactory bulb:endocast length ratio (%) | 19.54 | 23.29 | 19.2 | 22.49 | 29.07 | 29.25 |
| Maximum width of both olfactory bulbs (mm) | 4.99 | 9.85 | 97.5 | 4.35 | 5.21 | 19.64 |
| Maximum depth of the olfactory bulb casts[7] (mm) | 2.36 | 4.70 | 99.0 | 2.75 | 4.32 | 56.75 |
| Endocast width at the transition between the olfactory bulbs and cerebral hemispheres (mm) | 4.55 | 7.61 | 67.2 | 4.25 | 4.43 | 4.19 |
| Maximum width:length ratio of olfactory bulbs | 1.21 | 1.03 | - | 1.61 | 0.86 | - |
| Length of cerebral hemisphere casts[8] (mm) | 9.45 | 17.76 | 88.1 | 5.75 | 8.21 | 42.70 |
| Cerebral hemisphere:endocast length ratio (%) | 44.91 | 43.08 | –4.1 | 47.85 | 39.48 | –17.50 |
| Maximum width of both cerebral hemispheres[9] (mm) | 6.54 | 9.86 | 50.7 | 8.07 | 12.30 | 52.37 |
| Maximum width:length ratio of cerebral hemispheres | 0.69 | 0.56 | - | 1.40 | 1.50 | - |
| Anteroposterior length of the cerebellum slope[10] (mm) | 7.29 | 15.41 | 111.3 | 3.62 | 6.51 | 80.06 |
| Angle of the cerebellum slope[11] (°) | 40.9 | 30.7 | - | 17.3 | 15.5 | - |
| Maximum depth of the cerebellum[12] (mm) | 7.42 | 15.84 | 113.5 | 5.34 | 6.68 | 25.18 |
| Cerebellum width between the parafloccular lobes (mm) | 4.80 | 9.38 | 95.7 | 6.30 | 8.07 | 28.05 |
| Maximum width:length ratio of cerebellum with the paraflocculllar lobes | 0.66 | 0.61 | - | 1.74 | 1.24 | - |
| Length of the left parafloccular lobe cast (mm) | 2.46 | 3.50 | 42.4 | 0.57 | 1.53 | 169.40 |
| Length of the right parafloccular lobe cast (mm) | 2.87 | 3.03 | 5.9 | 0.88 | 1.81 | 105.72 |
| Scaling factor[13] | 1.04 | 19.67 | - | 0.99 | 1.05 | - |

**Table 4.1. (continued)**

[1] Taken from Jasinoski *et al*. (2015) for *Thrinaxodon* and Macrini *et al*. (2007b) for *Monodelphis*; [2] The foramen magnum diameter was not available for the physical specimens of *Monodelphis*; [3] Measured from the anterior limit of the olfactory bulbs to the foramen magnum in dorsal view; [4] Including the cerebellum and parafloccular lobes; [5] Measured from a horizontal line taken at the dorsal and ventral boundaries of the endocast; [6] Measured in dorsal view; [7] Measured in lateral view; [8-10] Measured in dorsal view; [11] Measured in lateral view between a horizontal line on the dorsal surface of the endocast and the dorsal point of the foramen magnum; [12] Measured from the ventral limit of the cerebellum to the dorsal surface directly above it; [13] Calculated based on the basal skull length for *Thrinaxodon* and the endocast length provided by Macrini *et al.* (2007b) for *Monodelphis*.

### 4.3.2. Ontogenetic changes in opossum brain morphology

When considering the anatomy of the juvenile and adult opossum brains, the endocasts of *Monodelphis domestica* show a differing morphology to *Thrinaxodon liorhinus*, with a wider, more compartmentalised brain shape (figure 4.7) than in the extinct cynodont. The endocast produced by Macrini *et al*. (2007b) for the juvenile specimen TMM M-7595 has a dorsal length of 12.02 mm, with a width to length ratio of 0.67 (table 4.1). The brain model accounts for 65% of the skull length and is widest (8.07 mm) at the posterior boundary of the cerebral hemispheres. Unlike *Thrinaxodon*, there is no prominent posterior slope to the cerebellum (14.8°) and there is a poorly resolved transition into the foramen magnum, which has a diameter of 2.97 mm. Similar to *Thrinaxodon*, all of the opossum endocasts considered in this study have a forebrain and hindbrain that can be identified within the endocasts. However, the midbrain is obscured by meninges and transverse sinuses (Macrini *et al*., 2007b), thus the midbrain has no surface exposure within the *Monodelphis* endocasts presented here.

Additionally, the endocasts of *Monodephis* specimens are all lissencephalic brains, that is, displaying no surface convolutions such as gyri and sulci.

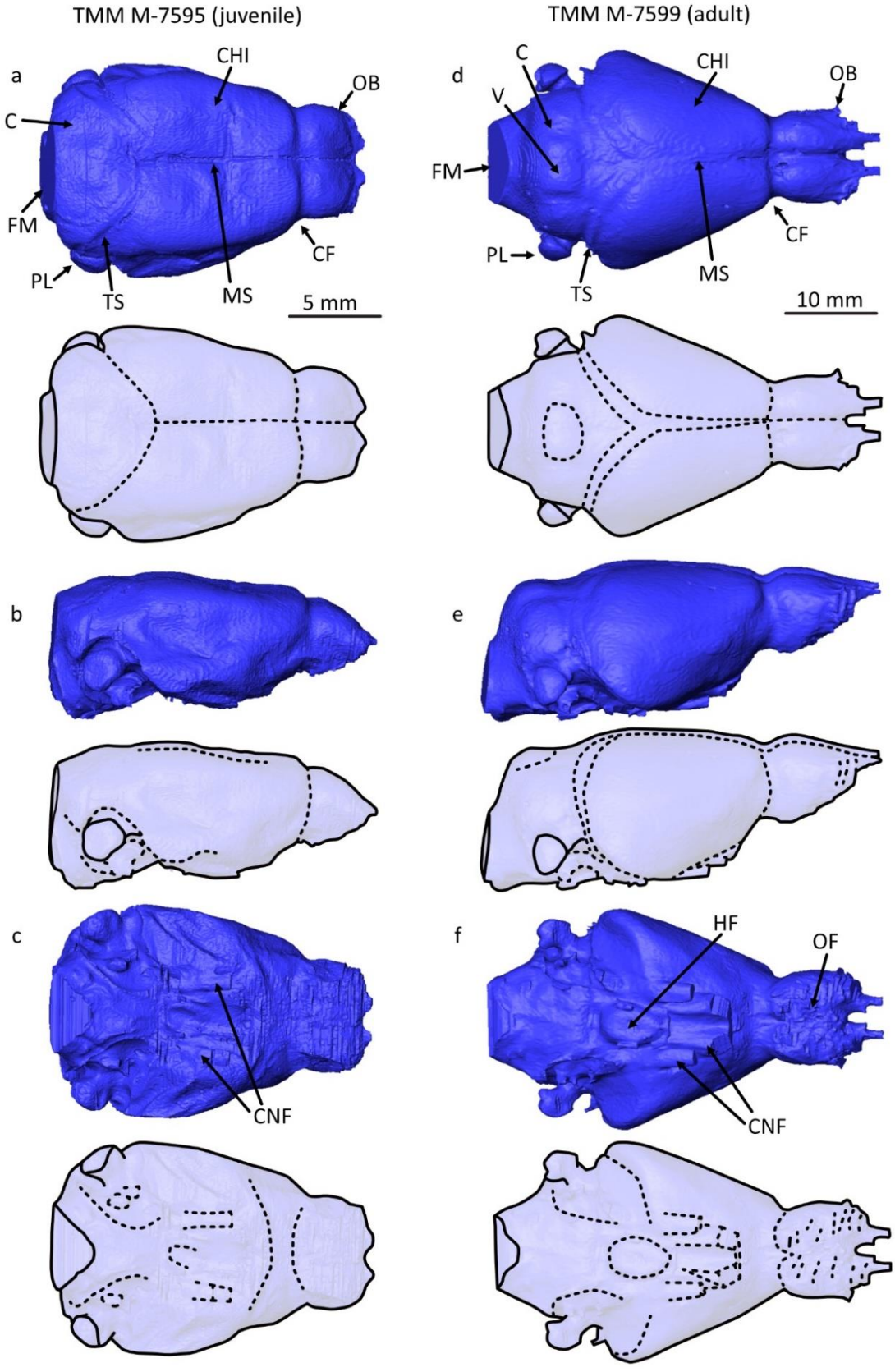

**Figure 4.7. (previous page).** Digitally reconstructed endocasts of juvenile (TMM M-7595) and adult (TMM M-7599) specimens of *Monodelphis domestica* in **(a, d)** dorsal, **(b, e)** right lateral and **(c, f)** ventral orientations accompanied by schematic illustrations of brain anatomy. Anatomical abbreviations are as follows: foramen magnum (FM), cerebellum (C), transverse sinus (TS), parafloccular lobe (PL), cerebral hemispheres - isocortex (CHI), medial sulcus (MS), olfactory bulbs (OB), olfactory nerve foramens (OF), circular fissure (CF), vermis (V), cranial nerve foramens (CNF) and hypophyseal fossa (HF). As CT data was not available for the opossum skulls, the endocasts cannot be viewed in position within the skull (as for *Thrinaxodon* in figure 4.5).

The forebrain is primarily comprised of the olfactory bulbs and cerebral hemispheres. In the juvenile opossum, the olfactory bulbs are short and well-rounded in dorsal view, with a clear medial sulcus dividing the bulbs (figure 4.7). Very short anterior projections can be seen in lateral view, with the olfactory bulbs appearing to be somewhat wedge shaped and symmetrical, as the bulbs are constrained between the nasal bone dorsally and nasal turbinates ventrally. As such, the ventral surface of the olfactory bulbs is not smooth and depicts impressions of cranial nerves and olfactory foramina through which nerves and vascular structures would have passed. The olfactory bulbs have a maximum width of 4.35 mm, length of 2.70 mm and width to length ratio of 1.61. In specimen TMM M-7595, the olfactory bulbs account for 23% of the endocast length.

The cerebral hemispheres are laterally expanded and 5.75 mm long between the transition from the olfactory bulbs (circular fissure), along the dorsal surface to the transverse sinus marking the beginning of the cerebellum (figure 4.7). The hemispheres comprise 48% of the endocast length and are clearly divided by a medial sulcus. Dorsally, the surface is relatively

flat, but the ventral brain reconstruction is much more rounded and incorporates casts of vascular canals (figure 4.7c). There is no reconstruction of a pineal body as the parietal eye is not present in extant mammals and the pineal gland now resides deeper within the brain (Benoit *et al*., 2016).

Alike the forebrain, the hindbrain is encased by a fully ossified braincase, allowing for a clear reconstruction boundary to be used. As such, the main reconstructed feature of the hindbrain is the cerebellum, which is 3.62 mm long and 6.30 mm wide. Located towards the base of the endocast are reconstructions of the parafloccular lobes, which appear as rounded structures protruding by 0.57 mm (left lobe) and 0.88 mm (right lobe) from the main brain body. No reconstruction of the vermis is apparent on the dorsal surface of the cerebellum in the juvenile. Additionally, there is no obvious narrowing of the cerebellum into the foramen magnum dorsally, but the foramen magnum can be identified by an oblique surface on the ventral side of the endocast. The ventral surface of the hindbrain also shows small, longitudinal casts of foramens through which cranial nerves would have passed (figure 4.7c). When observing a physical opossum brain extracted from the skull, Macrini *et al*. (2007b) noted that the cerebellum of *Monodelphis domestica* (irrespective of age) is gyrencephalic, meaning that there are visible convolutions on the brain's surface. However, in the endocast of the juvenile, the hindbrain is largely smooth, which indicates that the brain's surface convolutions do not produce impressions on the interior of the braincase, hence such surface ornamentation is not depicted in the brain reconstructions presented.

The adult *Monodelphis* specimen, TMM M-7599*,* has a more clearly defined brain morphology (figure 4.7), appearing almost diamond-shaped in dorsal view compared to the sub-oval shape of the juvenile brain. The adult endocast has a dorsal length of 20.79 mm, width of 12.30 mm

and fills 52% of the skull length. There is a slight slope to the dorsal surface of the cerebellum (12.4°), which transitions posteroventrally into the foramen magnum. The hindbrain is more elongated than in the juvenile specimen, meaning that cranial foramens are more spatially dispersed on the ventral surface (figure 4.7f). Laterally, the parafloccular lobes protrude with a mushroom-like appearance by 1.53 mm and 1.81 mm for the left and right lobes, respectively. The dorsal length of the cerebellum is 6.51 mm and it has a width of 8.07 mm. Unlike the juvenile, a raised oval cast of the vermis is present on the dorsal surface of the cerebellum (figure 4.7d).

Transitioning into the forebrain, the cerebral hemispheres are 12.30 mm wide and 8.21 mm long, with a prominent medial division and an impression of what may be layering of cerebral tissues when viewed dorsally (figure 4.7d). The cerebral hemispheres comprise 40% of the endocast length. The upper surface of the cerebral hemispheres follows a gentle, transverse curve while the lower surface is rounded with prominent casts of the housing for cranial nerves. Among these nerve foramens is a tear-drop shaped cast of the hypophyseal fossa. At the anterior boundary of the cerebral hemispheres is the circular fissure, which marks the start of the olfactory bulbs. The olfactory bulbs are dorsally rounded, with prominent, narrow projections at the anterior margin and a deep groove bisecting them. The bulbs are 5.21 mm wide, 6.04 mm long and account for 29% of the endocast length. The ventral surface of the bulbs shows crenulations indicative of impressions made by the olfactory bulbs meeting the surface of the cribriform plate.

When considering the full ontogenetic series of *Monodelphis* endocasts generated by Macrini *et al*. (2007b; figure 4.8), there is almost a 73% increase in the endocast length between the juvenile and adult, and a 284% increase in the endocast volume between the two end stages

presented here (table 4.1). In profile, the six endocasts are broadly similar, with lobe shaped cerebral hemispheres, rounded parafloccular lobes protruding from the main brain body, a flat posterior surface (with the exception of specimen TMM M-7599 which has a more prominent foramen magnum) and conical olfactory bulbs with increasingly larger projections from the anterior tip. When viewed dorsally, the changing endocast shape is more pronounced, with the juvenile exhibiting a sub-oval outline. Through the numerous growth stages, the opossum brain becomes increasingly laterally expanded (particularly regarding the cerebral hemispheres) and more angular, culminating in a diamond-shaped morphology in the adult (TMM M-7599). Broadly speaking, the day 48, 57, 75 and 90 brains are all very similar in morphology, and it is only the adult brain that shows a clear morphological change. Ventrally, the cast of cranial nerve canals become more numerous and pronounced from the day 48 brain onwards. Additionally, the day 27 brain does not possess a reconstruction of the hypophyseal fossa, but all other *Monodelphis* endocasts do (figures 4.7 and 4.8).

The size increases between different brain components are variable throughout the ontogenetic series of opossum endocasts (table 4.2; figure 4.9), with a larger increase in skull and endocast length between the day 27 and 48, and day 90 and adult individuals, than for the specimens in between. Throughout development, the endocast occupies a progressively smaller proportion of the skull length, encompassing 64.97% of the juvenile skull but 51.98% of the adult skull. Generally, the olfactory bulbs, cerebral hemispheres and cerebellum all increase in size during development (table 4.2; figure 4.9). However, there are some unexpected negative trends, such as the cerebral hemisphere length decreasing between day 57 and 75 opossums, which could be accounted for by the fact that the measurements are taken from endocasts derived from six individuals, rather than following the growth trajectory of a single opossum over time.

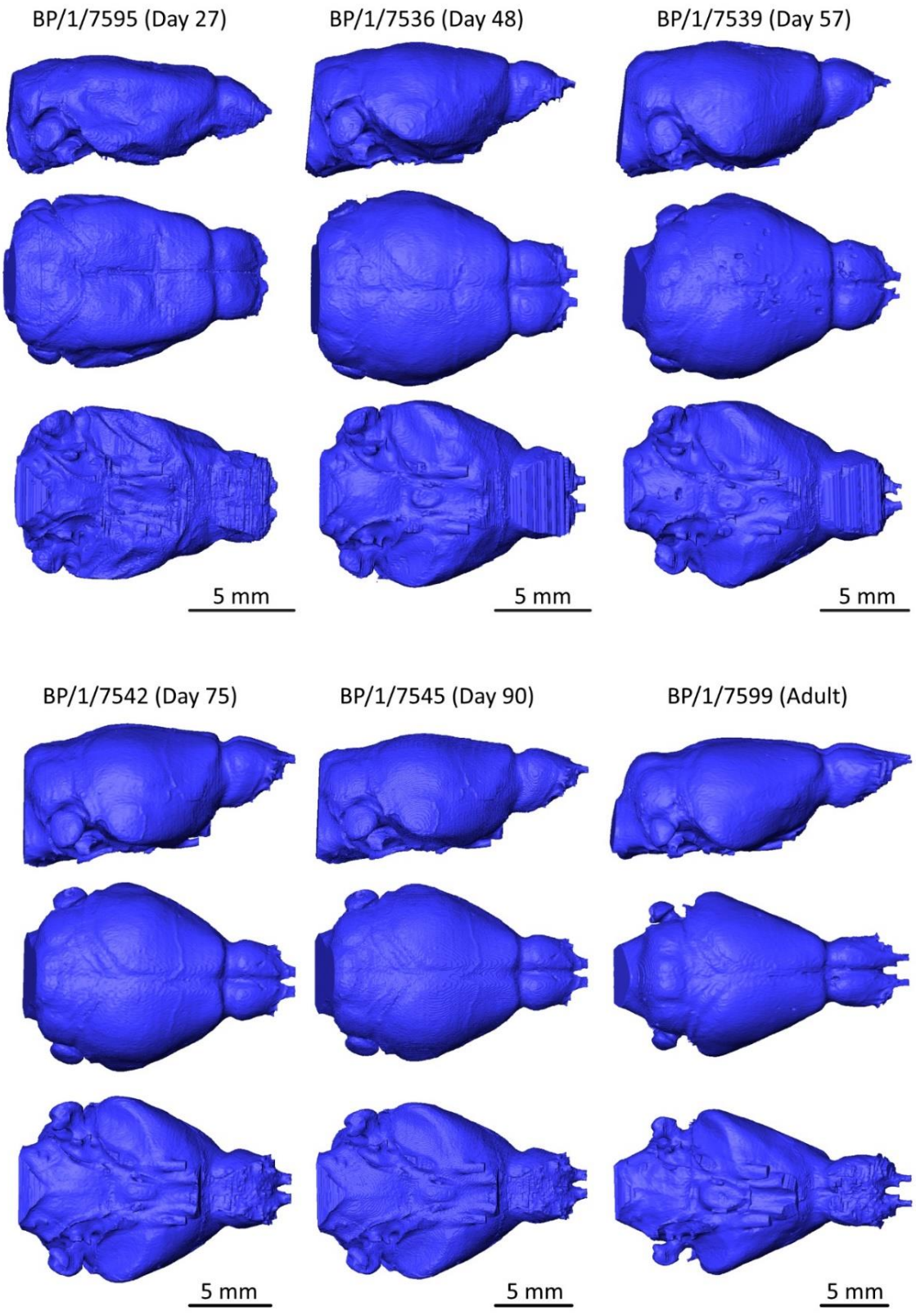


**Figure 4.8**. Digitally rendered endocasts of six *Monodelphis domestica* specimens comprising a growth series, highlighting size increases and gradual morphological changes during development. Endocasts generated by Macrini *et al*. (2007b).

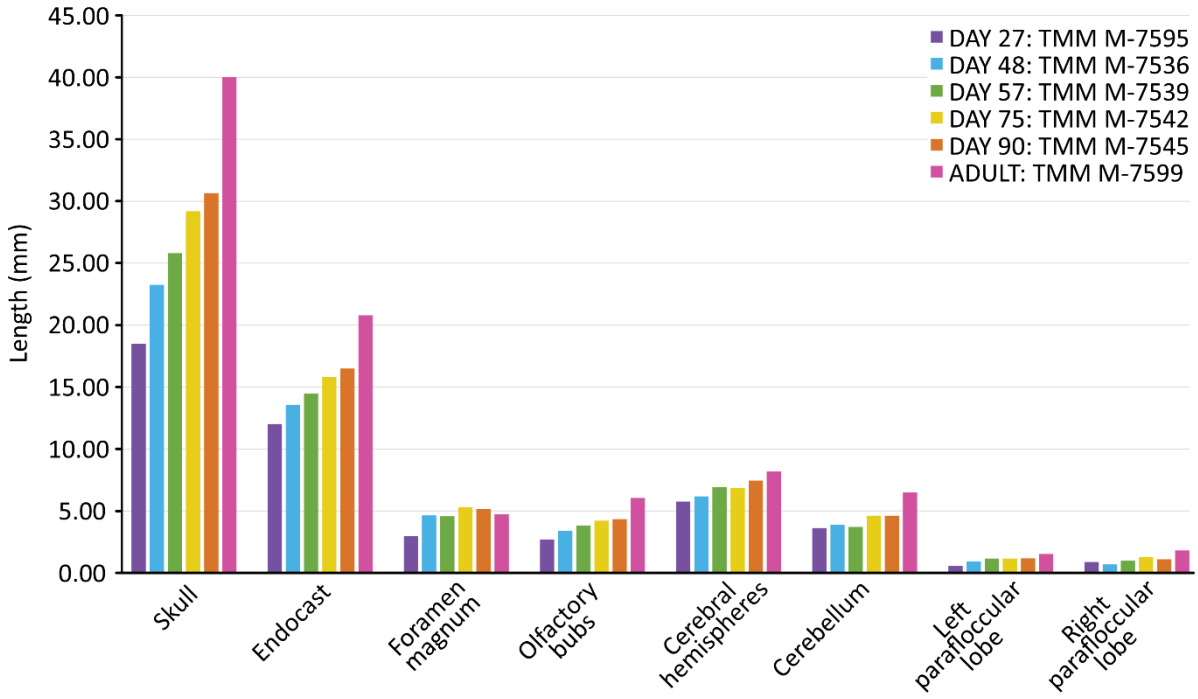


**Figure 4.9.** Bar chart displaying the size of each brain region studied in the ontogenetic growth series of *Monodelphis domestica*. There is a general trend of enlargement of all regions from the juvenile to adult form, with some differences in the amount of growth seen between each age group (such as disruption to a continuous growth pattern suggested by the measurements for the foramen magnum diameter and cerebellum length).

**Table 4.2.** Linear and volumetric measurements for all *Monodelphis domestica* specimens studied, including the relative increase in the measurements between each specimen (with arrows indicating the specimens being compared), and therefore, different development stages. The measurements were calculated after correction using the scaling factor outlined in the methods.

| | **TMM M-7595 Day 27** | **Relative increase <- (%) ->** | **TMM M-7536 Day 48** | **Relative increase <- (%) ->** | **TMM M-7539 Day 57** | **Relative increase <- (%) ->** | **TMM M-7542 Day 75** | **Relative increase <- (%) ->** | **TMM M-7545 Day 90** | **Relative increase <- (%) ->** | **TMM M-7599 Adult** |
|---|---|---|---|---|---|---|---|---|---|---|---|
| Basal skull length[1] (mm) | 18.50 | 25.68 | 23.25 | 10.97 | 25.80 | 13.18 | 29.20 | 4.97 | 30.65 | 30.51 | 40.00 |
| Foramen magnum diameter (endocast, mm) | 2.97 | 56.72 | 4.65 | – 1.50 | 4.58 | 15.96 | 5.31 | – 2.87 | 5.16 | – 8.40 | 4.73 |
| Endocast length[2] (mm) | 12.02 | 12.81 | 13.56 | 6.71 | 14.47 | 9.26 | 15.81 | 4.36 | 16.50 | 26.00 | 20.79 |
| Maximum endocast width[3] (mm) | 8.07 | 29.60 | 10.46 | 0.93 | 10.56 | 11.32 | 11.75 | – 2.53 | 11.46 | 7.35 | 12.30 |
| Minimum endocast width (mm) | 4.25 | 14.64 | 4.88 | – 0.16 | 4.87 | – 6.72 | 4.54 | – 1.22 | 4.49 | – 1.21 | 4.43 |
| Maximum endocast depth[4] (mm) | 5.53 | 28.47 | 7.10 | 2.65 | 7.29 | 11.58 | 8.14 | – 0.82 | 8.07 | – 6.52 | 7.54 |
| Maximum width:length ratio of endocast | 0.67 | - | 0.77 | - | 0.73 | - | 0.74 | - | 0.69 | - | 0.59 |
| Endocast:BSL ratio (%) | 64.97 | – 10.24 | 58.32 | – 3.84 | 56.09 | – 3.46 | 54.14 | – 0.57 | 53.83 | – 3.45 | 51.98 |

| | | | | | | | | | | | |
|---|---|---|---|---|---|---|---|---|---|---|---|
| Volume of the whole endocast ($mm^3$) | 248.52 | 75.99 | 437.38 | 11.32 | 486.90 | 25.79 | 612.47 | 5.28 | 644.83 | 48.07 | 954.78 |
| Length of olfactory bulb cast (mm) | 2.70 | 25.67 | 3.40 | 12.44 | 3.82 | 10.52 | 4.22 | 2.86 | 4.34 | 39.17 | 6.04 |
| Olfactory bulb:endocast length ratio (%) | 22.49 | 11.39 | 25.06 | 5.37 | 26.40 | 1.15 | 26.71 | – 1.44 | 26.32 | 10.45 | 29.07 |
| Maximum width of both olfactory bulbs (mm) | 4.35 | 18.34 | 5.15 | 0.84 | 5.20 | – 3.33 | 5.02 | – 1.46 | 4.95 | 5.24 | 5.21 |
| Maximum depth of the olfactory bulb casts (mm) | 2.75 | 16.28 | 3.20 | 20.57 | 3.86 | 12.80 | 4.36 | – 5.51 | 4.12 | 4.91 | 4.32 |
| Endocast width at the transition between the olfactory bulbs and cerebral hemispheres (mm) | 4.25 | 14.64 | 4.88 | – 0.16 | 4.87 | – 6.72 | 4.54 | – 1.22 | 4.49 | – 1.21 | 4.43 |
| Maximum width:length ratio of olfactory bulbs | 1.61 | - | 1.52 | - | 1.36 | - | 1.19 | - | 1.14 | - | 0.86 |
| Length of cerebral hemisphere casts (mm) | 5.75 | 7.26 | 6.17 | 12.03 | 6.91 | – 0.86 | 6.85 | 8.78 | 7.45 | 10.12 | 8.21 |
| Cerebral hemisphere: | 47.85 | – 4.92 | 45.50 | 4.99 | 47.76 | – 9.26 | 43.34 | 4.23 | 45.17 | – 12.60 | 39.48 |

| | | | | | | | | | | | |
|---|---|---|---|---|---|---|---|---|---|---|---|
| endocast length ratio (%) | | | | | | | | | | | |
| Maximum width of both cerebral hemispheres (mm) | 8.07 | 29.60 | 10.46 | 0.93 | 10.56 | 11.32 | 11.75 | – 2.53 | 11.46 | 7.35 | 12.30 |
| Maximum width:length ratio of cerebral hemispheres | 1.40 | - | 1.70 | - | 1.53 | - | 1.72 | - | 1.54 | - | 1.50 |
| Anteroposterior length of the cerebellum slope (mm) | 3.62 | 7.90 | 3.90 | -4.96 | 3.71 | 24.42 | 4.61 | 41.24 | 4.61 | 41.24 | 6.51 |
| Angle of the cerebellum slope[5] (°) | 14.8 | – 23.65 | 11.3 | – 17.70 | 9.30 | 82.80 | 17.0 | – 27.06 | 12.4 | 0 | 12.4 |
| Maximum depth of the cerebellum[6] (mm) | 5.34 | 20.80 | 6.45 | 7.22 | 6.91 | 6.27 | 7.35 | – 1.49 | 7.24 | – 7.67 | 6.68 |
| Width of cerebellum between the parafloccular lobes (mm) | 6.30 | 27.28 | 8.02 | – 6.61 | 7.49 | 14.44 | 8.57 | – 1.27 | 8.46 | – 4.65 | 8.07 |
| Maximum width:length ratio of cerebellum with the paraflocculars lobes | 1.74 | - | 2.06 | - | 2.02 | - | 1.86 | - | 1.84 | - | 1.24 |

| | | | | | | | | | | | |
|---|---|---|---|---|---|---|---|---|---|---|---|
| Length of the left paraflocculare lobe cast (mm) | 0.57 | 61.10 | 0.91 | 27.02 | 1.16 | 0.03 | 1.16 | 1.29 | 1.18 | 29.92 | 1.53 |
| Length of the right paraflocculare lobe cast (mm) | 0.88 | – 20.77 | 0.70 | 42.71 | 1.00 | 26.84 | 1.26 | – 12.94 | 1.10 | 64.76 | 1.81 |
| Scaling factor[7] | 0.99 | - | 0.97 | - | 0.97 | - | 0.97 | - | 1.05 | - | 1.05 |

[1] Taken from Macrini *et al*. (2007b); [2] Measured from the anterior limit of the olfactory bulbs to the foramen magnum in dorsal view; [3] Including the cerebellum and paraflocculare lobes; [4] Measured from a horizontal line taken at the dorsal and ventral boundaries of the endocast; [5] Measured in lateral view between a horizontal line on the dorsal surface of the endocast to the dorsal point of the foramen magnum; [6] Measured from the ventral limit of the cerebellum to the dorsal surface directly above it; [7] Calculated based on the endocast length of each specimen provided by Macrini *et al*. (2007b).

### 4.3.3. Understanding olfactory and cognitive processing during development

In both *Thrinaxodon* and *Monodelphis*, the olfactory bulbs appear as pronounced structures within the forebrain. For the cynodont, the olfactory bulbs comprise 20% of the endocast length in the juvenile and 23% in the adult. In the extant opossum, the olfactory bulb to endocast ratio is 23% in the juvenile and 29% in the adult. When plotting the olfactory bulb to endocast ratios of *Thrinaxodon* against all of the opossums in the studied growth series (figure 4.10), a parallel linear relationship is expressed whereby the juvenile *Thrinaxodon* fossil (BP/1/5272) plots with all of the juvenile and sub-adult opossum specimens. Both of the studied adult fossils (TMM M-7599 and NHMUK PV R511) form outliers to the rest of the data, indicating that the olfactory bulbs comprise a larger proportion of the adult brain than the juvenile brain in both species.

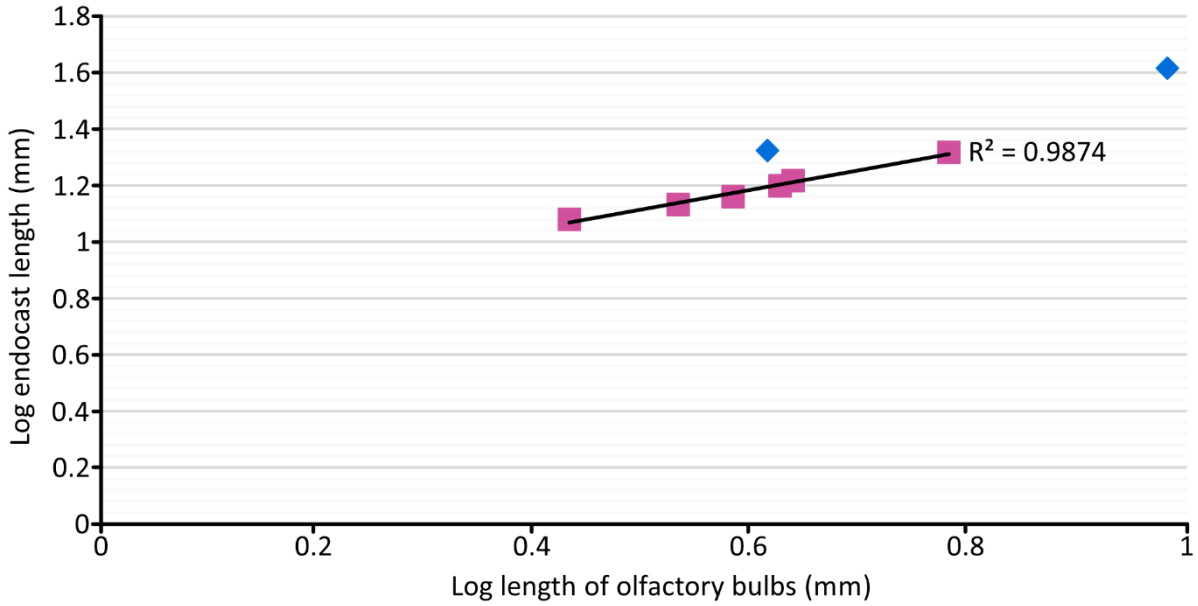


**Figure 4.10.** Plot of olfactory bulb length compared to endocast length of the *Thrinaxodon* (blue) and *Monodelphis* (pink) specimens studied. Axes have been log-transformed to remove the effects of juvenile versus adult size on the proportional relationships of the olfactory bulbs within the brain.

To approximate cognitive capabilities based on relative brain proportions, the encephalisation quotient was calculated for all eight *Thrinaxodon* and *Monodelphis* fossils studied (table 4.3), with the equation from Jerison (1973) providing a lower limit for the EQ value while Manger (2006) generates an upper boundary. All EQ values for *Thrinaxodon* are lower than those calculated for *Monodelphis*. The juvenile cynodont has an EQ value ranging between 0.19 ($EQ_{Jerison}$) and 0.32 ($EQ_{Manger}$). The EQ for the adult cynodont overlaps with much of this range, calculated as 0.27 ($EQ_{Jerison}$) and 0.37 ($EQ_{Manger}$). However, the opossum growth series shows an overall decrease in the calculated EQ value between the juvenile (day 27) and more mature specimens (up to day 90), decreasing from 0.90 to 0.41 ($EQ_{Jerison}$) and 1.85 to 0.70 ($EQ_{Manger}$), respectively. However, the EQ value for the adult opossum is larger than for both the day 75 and 90 specimens, calculated as 0.44 ($EQ_{Jerison}$) and 0.73 ($EQ_{Manger}$).

**Table 4.3**. EQ values calculated for the studied juvenile and adult *Thrinaxodon* and *Monodelphis* specimens.

| | **Specimen** | **EQ value** (Jerison 1973) | **EQ value** (Manger 2006) |
|---|---|---|---|
| ***Thrinaxodon liorhinus*** | BP-1-5372 | 0.19 | 0.32 |
| | NHMUK PV R511 | 0.27 | 0.37 |
| ***Monodelphis domestica*** | Day 27 | 0.90 | 1.85 |
| | Day 48 | 0.68 | 1.28 |
| | Day 56 | 0.52 | 0.94 |
| | Day 75 | 0.40 | 0.69 |
| | Day 90 | 0.41 | 0.70 |
| | Adult | 0.44 | 0.73 |

## 4.4. Discussion

### 4.4.1. Juveniles growing up: changing brain morphology

Examination of cranial fossils of *Thrinaxodon liorhinus* reveals that the skull grew at different rates, with slower growth rates for the orbit and posterior palate, but faster growth for the snout, anterior palate and temporal region (Jasinoski *et al*., 2015). The skull also continued to grow into adulthood, with the largest *Thrinaxodon* cranial fossils achieving a basal skull length of 96 mm and showing tooth replacement into maturity (Abdala *et al*., 2013; Jasinoski *et al*., 2015). Given continued osteological growth, it is possible that *Thrinaxodon*'s brain also continued to grow into adulthood. This suggestion is supported by the endocasts produced here for BP-1-5372 (juvenile) and NHMUK PV R511 (adult), where the endocast length increased by 96% (from 21.03 mm in the juvenile to 41.23 mm in the adult). Similarly, the reconstructed endocranial volume increased by 607% (from 416.10 $mm^3$ to 2942.27 $mm^3$ in the juvenile and adult, respectively). When considering the smallest and largest opossum specimens studied, there is again a large increase in endocast length (73%, from 12.02 mm to 20.79 mm) and endocranial volume (284%, from 248.52 $mm^3$ to 954.78 $mm^3$). Therefore, the endocranial reconstructions for *Thrinaxodon* confirm that there was an enlargement of the brain cavity between the juvenile and adult fossils studied, and consequently, a subsequent enlargement of the brain has been reconstructed (figure 4.5). It should, however, be noted that the brain cavity only provides an approximation of brain shape as, alike extant mammals, *Thrinaxodon* may have possessed meninges and intracranial fluids that also filled the endocranial space (Macrini *et al*., 2007b) and would account for a proportion of the reconstructed brain volume. Furthermore, in humans, the volume of cerebrospinal fluids within the brain cavity increases into adulthood (Wanifuchi *et* al., 2002; Watanabe *et al*.,

2019), thus there may have been additional constraints on brain volume beyond skull size and neuron growth.

Irrespective of any additional soft tissues that may have surrounded the cynodont brain, it is clear that cynodont and mammal brains both display ontogenetic growth. Weickenmeier *et al*. (2017) proposed that the mammalian brain grows and remodels itself in parallel with the skull, with the accretion of bone at sutures accounting for this increase in endocranial volume. *Thrinaxodon*'s skull also grew as a whole during ontogeny (Botha and Chinsamy, 2005; Jasinoski *et al*., 2015), but its brain did not appear to grow at the same rate. In BP/1/5732, the endocast comprises 57% of the skull length, but in NHMUK PV R511, the brain model only accounts for 49%. Therefore, other parts of the skull, particularly the snout (Abdala *et al*., 2013; Jasinoski *et al*., 2015) likely grew more rapidly during development than the brain cavity.

Negative allometry (when an organ grows at a slower rate than the body) is even more pronounced in the cranial growth of *Monodelphis*, where an overall decrease in endocast:skull length of 20% is seen across the studied growth series (table 4.2). Additionally, the greatest amount of skull growth occurred between the day 27 and 48 opossums, resulting in the endocast comprising 10% less of the basal skull length by 48 days after birth. It is thus suggested that *Thrinaxodon* may have experienced similarly rapid early growth of the brain and skull (and body as a whole; Botha and Chinsamy, 2005), with cranial growth outpacing endocranial enlargement as the individual aged.

Early cranial growth is also supported by Koyabu *et al*. (2014), who modelled the ossification history of Jurassic mammaliaform *Morganucodon*. The study again revealed early growth of the snout (maxilla and premaxilla) and dentaries, with later ossification of the braincase

(orbitosphenoid, petrosal, supraoccipital, exoccipital and basisphenoid). This trend was found from the study of 32 non-mammalian taxa and is the reverse of the condition seen in modern mammals, where there is accelerated early ossification of the braincase (Koyabu *et al*., 2014). This developmental trait is important because the transition towards ossification of the braincase during early ontogenetic development marks the timing of the first pulse in morphological transformation of the brain from the simplified, pre-mammalian state seen in *Thrinaxodon* towards the modern mammalian anatomy seen in mammaliaforms and extant mammals, such as *Monodelphis* (Rowe *et al*., 2011; Koyabu *et al*., 2014).

### 4.4.2. Ontogenetic variation between brain regions

While the brains of *Thrinaxodon* and *Monodelphis* show overall ontogenetic variation, it is interesting to consider whether any individual brain region experiences more change than others and whether the timing of developmental changes can be determined for *Thrinaxodon* based on the changes observed in extant opossum analogues. Macrini *et al*. (2007b) noted morphological disparity in the opossum ontogenetic brain series (figure 4.8), with juvenile specimens of *Monodelphis domestica* (27 days old) displaying rounded olfactory bulbs and reaching adult-like proportions at 30 days old. By day 48, olfactory nerve foramens can be observed protruding from the anteroventral surface of the olfactory bulbs. From 56 days old, the cerebral hemisphere casts are elongated, and differentiation of cortical layers is thought to be completed by 75 days after birth (Macrini *et al*., 2007b). Adult opossums are fully formed after 90 days and sexual maturity is seen after four to six months (Stonerook and Harder, 1992).

Despite the lack of intermediate specimens for *Thrinaxodon*, quantitative analysis of the *Monodelphis* endocasts may shed some light on when similar developmental changes could

have occurred within *Thrinaxodon*'s brain (figure 4.11). For example, *Monodelphis*' olfactory bulbs show an enlargement between the day 27 and 48 individuals, and again between the day 90 and adult specimens. Indeed, the olfactory bulbs comprise a larger proportion of the endocast, accounting for 19% more of the endocast's length in the adult than in the juvenile. It, therefore, appears that there may have been an initial early pulse in *Monodelphis*' olfactory development, and a potentially later pulse into adulthood too. Tufo *et al* (2022) supports this hypothesis, finding that the mammalian olfactory bulb forms early during a mammal's growth and is a functioning sensory organ from birth. The olfactory system does not stabilise at the juvenile stage but instead continues to mature during the mammal's life, accounting for the continued growth seen across the *Monodelphis* endocasts (figure 4.8, table 4.2).

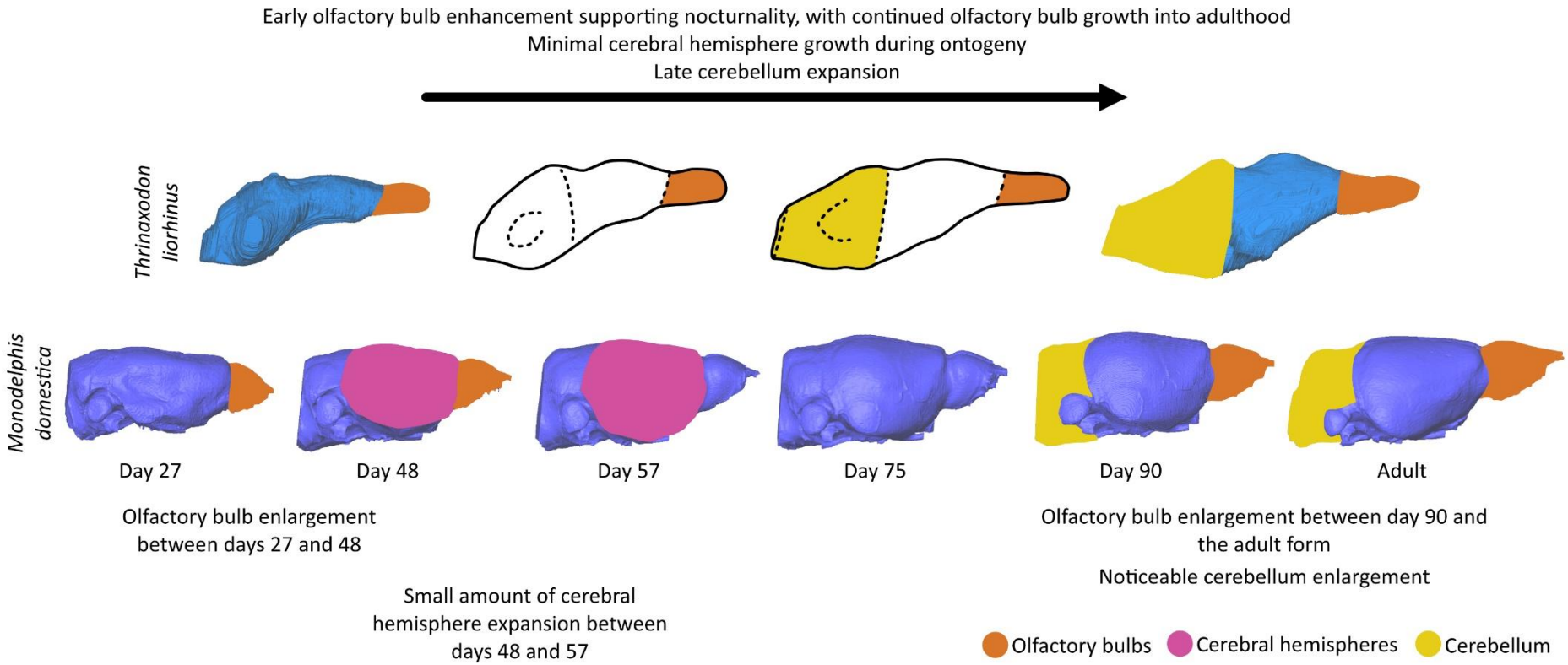


**Figure 4.11.** Hypothesised endocranial growth series for *Thrinaxodon liorhinus* (top) based on the endocasts generated for *Monodelphis domestica* during ontogeny (bottom). Key endocranial developments are noted for *Monodelphis*, with subsequent suggestions proposed for *Thrinaxodon*'s brain development. As there are no intermediate *Thrinaxodon* endocasts presented within this study, brain shape is inferred for two intermediate growth stages. Colours represent a notable change to the size and shape of an individual brain region during development. Endocasts are not to scale.

Given juvenile olfactory enlargement is seen in mammals, it is proposed that pre-mammalian cynodonts, such as *Thrinaxodon*, may also have displayed similar morphological transitions during their early development. Changes to the size and shape of *Thrinaxodon*'s olfactory bulbs are evident between the juvenile and adult specimens studied here (table 4.1; figure 4.5), and despite it not being possible to determine the timing of the enlargement without analysing more *Thrinaxodon* specimens, there is a clear trend of the olfactory bulbs expanding during ontogeny (comprising 23% of the adult's brain endocast compared to almost 20% in the juvenile). A focus on early olfactory development during *Thrinaxodon*'s ontogenetic growth could have been driven by the requirement for a keen sense of smell to detect olfactory cues critical for numerous behavioural characteristics (Rowe and Shepherd, 2016), such as finding prey, avoiding predators and (possibly) identifying nutritious substances produced by mothers (Oftedal 2002; Crompton *et al*., 2018). It has also been suggested that some cynodonts, such as the Early Jurassic *Tritylodon*, were nocturnal, and this is considered to be the ancestral state for mammals (given many extant taxa are also nocturnal; Angielczyk and Schmidt, 2014; Bennie *et al*., 2014). If *Thrinaxodon* was active at night, then improved olfactory acuity from an early age (through olfactory bulb enlargement; Aboitiz and Montiel, 2015) could have benefitted survivability, not only for predator-prey behaviours, but also identifying other species, as seen in the chemo-sensory signalling behaviour of mouse lemurs (Kollikowski *et al*., 2019). However, ascertaining whether chemical signals were part of olfactory interactions in cynodonts would merely be speculation given the lack of fossil evidence for soft tissues and body fluids in which pheromones would be distributed.

Unlike the olfactory bulbs, the cerebral hemispheres remain largely consistent between the different opossum age classes represented, with the largest length increase (12%) between the day 48 and 57 opossums. Yet there is a slight shortening (0.9%) of the cerebral

hemispheres between the day 57 and 75 specimens. It is very unlikely that the cerebral hemispheres physically shortened throughout development (although age related shrinkage of the brain as a whole has been observed in primates, including humans; Peters 2006). Instead, it is more likely to be a trend caused by the opossum growth series being from six individuals, rather than following the developmental changes of a single opossum from birth through to adulthood (a problem echoed in the study of fossils too). However, there is a genuine ontogenetic trend that the cerebral hemispheres comprised less of the endocast length in both adult specimens of *Thrinaxodon* and *Monodelphis* compared to their juvenile counterparts (figure 4.11), accounting for 4% and 18% less of the endocast length, respectively. As yet, there is no published reason for why cerebral hemispheres would shrink during development in mammals, beyond overall aging of the brain (Peters 2006; Sherwood *et al*., 2011; Tepper *et al*., 2019) and this pattern is more likely to be reflecting the proportional decrease in the cerebral hemispheres due to olfactory bulb enlargement.

In the evolutionary lineage towards mammals, the cerebral hemispheres became increasingly complex and expanded (Rowe *et al*., 2011; Molnár *et al*., 2014; Benoit *et al*., 2023). The expansion of the cerebral hemispheres (and development of cortical layers) meant that the brain of early mammals became more functionally compartmentalised than in pre-mammalian cynodonts (Molnár *et al*., 2014), as reflected in the enlargement and restructuring of the *Thrinaxodon* and *Monodelphis* endocasts (figures 4.5 and 4.7). However, Wong and Kass (2009) state that histochemical analysis of *Monodelphis domestica* brains reveals that its brain has fewer cortical areas than many mammals, making it a good analogue for *Thrinaxodon*. Given the opossum's cerebral hemispheres respond to sensory and motor stimuli (Bianki 1983), a small amount of expansion of the cerebral hemispheres between juvenile and adult cynodonts would likely have facilitated more precise sensory and cognitive processing through

increased neuronal connections, which has also, over time, facilitated mammals to occupy a wide range of ecological niches (Cooper *et al*., 2011; Norton *et al*., 2023).

In the hindbrain, a negative growth trend is seen in the length of the cerebellum, which appears to shorten by 5% between the day 48 and 57 opossums studied, and again by 0.1% between the 75- and 90-day old opossums (table 4.2). Conversely, there is a noticeable enlargement (80.06%) of the cerebellum between 90 days old and the adult stage. This dramatic size change is partly accounted for by the age of the adult specimen being at least 183 days or more (the point when opossums reach sexual maturity; Macrini *et al.,* 2007b), meaning that there may have been a large age difference between the two specimens, allowing for additional growth.

However, there does also appear to be an overall ontogenetic trend expressed by both *Thrinaxodon* and *Monodelphis*, with cerebellum expansion into adulthood (tables 4.1 and 4.2). Enlargement of the cerebellum accounts for the greatest proportional change to any individual brain region, comprising 111% and 80% more of the endocast length in the adult of the cynodont and opossum, respectively. Such a profound morphological development to the cerebellum must have a significant functional benefit as the cerebellum is responsible for motor coordination (Reeber *et al*., 2013). What could have caused the cerebellum to grow so much during an individual's life?

Sepp *et al*. (2024) investigated whether ontogenetic and evolutionary changes to the cerebellum can be seen in humans, mice and opossums. From sequencing the RNA of 400,000 cells from the aforementioned taxa, the authors found that foetal Purkinje cells (neurons in the cerebellum) regulate the generation of other cells and neurons within the cerebellum (and

wider brain), contributing to a volumetric increase of the hindbrain throughout a mammal's life. A general expansion of the cerebellum during a mammal or cynodont's development (figure 4.11) would, therefore, be consistent with the cerebellum housing more than half of the mammal brain's neurons, thus facilitating sensory-motor controls in opossums (Sepp *et al*., 2024), and likely expressing a similar function in *Thrinaxodon*.

It is also important to consider the possibility of intraspecific variation among cynodont and mammal brain reconstructions which may have an impact on seemingly ontogenetic variation identified so far. Intraspecific variation distinguishes differences seen between individuals of the same age within a single species (Weisbecker *et al*., 2021). The growing mammal brain is influenced by a variety of factors including the shape of the braincase and contact with cranial bones (Macrini *et al*., 2007b; Budday *et al*., 2015), neuronal connectivity and cortical folding which generates internal constraints on the brain shape (Atkinson *et al*., 2015; Mota and Herculano-Houzel, 2015), genetic controls on both brain and skull development (Hanken and Thorogood, 1993; Koyabu *et al*., 2014), and seasonal impacts on the endocranial morphology (Dechmann *et al*., 2017; Weisbecker *et al*., 2021). Dechmann et al. (2017) reported that some small mammals, such as red-toothed shrews and least weasels, have been discovered to exhibit a juvenile growth overshoot with a subsequent shrinkage of the brain until the mammals have passed their first winter. Perhaps the energy conserved through winter brain shrinkage is an evolutionary advantage to improve survival chances when resource availability is low, with brain enlargement in spring once environmental resources become more abundant for highly metabolically active mammals. Whether *Thrinaxodon*'s brain could have exhibited similar changes to brain volume during its lifetime is impossible to know for certain, but it is an interesting hypothesis to consider when observing changing endocranial volumes in extant mammals.

### 4.4.3. Relative brain size and changing cognition during a lifetime

The encephalisation quotients provide a proxy for cognitive capabilities by comparing relative brain sizes along an evolutionary lineage. *Monodelphis*' growth series expresses an overall decrease in EQ value between the juvenile and more mature specimens. A continuously decreasing trend in ontogenetic cognitive capabilities is very unlikely. It does not make sense for a mature individual to seemingly have a less cognitively capable brain than a young animal. Instead, the data presented highlights the problem of the EQ equations relying on a relationship between brain volume and body mass which may not be applicable to modern mammals and also does not reflect the increasing complexity of neuronal connections that improve mammalian cognitive capabilities in a more morphologically compact space (Radulescu *et al*., 2021; Brito *et al*., 2023). Mammal brains do, however, experience cognitive decline with age (Tierney and Nelson, 2009; Pujol *et al*., 2021), but such a complex process is unlikely to be reflected in a simple relationship between brain volume and body size.

Nevertheless, to understand more about the evolutionary positioning of *Thrinaxodon*'s cognitive capabilities, the calculated EQ values reveal an increase in relative brain size between the juvenile and adult specimens studied, from 0.19 to 0.27 ($EQ_{Jerison}$) and 0.32 to 0.37 ($EQ_{Manger}$). As shown in this study, *Thrinaxodon*'s brain size increased with age and as such, an assumption is made that the adult brain was capable of more complex cognitive processing than the juvenile (Ming and Song, 2011; Paredes *et al*., 2016). This assumption is based on the Principle of Proper Mass (Jerison 1973) which associates the mass of neural tissue with the amount of information processing it completes. Using this principle, the larger volumes of the adult *Thrinaxodon* brain would, therefore, suggest that a greater density of neurons are present within the brain (occupying a greater brain volume; Striedter 2005) to enhance cognitive and sensory acuity. However, in mammals, larger brains result in greater

connection distances between neurons, particularly as the brain is more compartmentalised than in pre-mammalian ancestors (Deacon 1990; Macrini *et al*., 2007b), and as such, brain functions are now frequently shared between several brain regions, which may not have been the case for *Thrinaxodon*'s more simply structured brain.

Interestingly, the changing EQ value calculated during *Thrinaxodon*'s development would place the juvenile specimen at a different evolutionary point to the adult, when comparing with the published EQ values of other non-mammalian cynodonts and mammaliaforms. For example, a juvenile EQ of 0.19 ($EQ_{Jerison}$) for *Thrinaxodon* is consistent with Late Triassic adult specimens of *Massetognathus* (0.15; Quiroga 1979) and *Riograndia* (0.22; Rodrigues *et al*., 2019). On the other hand, calculated EQ values for the studied adult *Thrinaxodon* (0.27 ($EQ_{Jerison}$) and 0.37 ($EQ_{Manger}$)) place the cynodont closer to Jurassic mammaliaform *Morganucodon* (0.32; Rowe *et al*., 2011), which, if true, would suggest that despite the lack of compartmentalisation of *Thrinaxodon*'s brain, the basal cynodont had somewhat comparable cognitive capabilities to descendants millions of years along the mammalian evolutionary lineage. The true processing power of *Thrinaxodon*'s endocranial anatomy is likely to remain elusive and while EQ values may provide a proxy for potentially assessing intelligence, the inferences made from such calculations should be made cautiously as it is unwise to assume that a relatively smaller brain cannot perform as well as a larger brain in mammals. Ultimately, the nature of soft tissue preservation and taphonomic processes mean that there is a limit to how much a CT scan can reveal about the complexity of the brain it once housed (Balanoff and Bever, 2020).

## 4.5. Chapter summary

Understanding more about ontogenetic variation in cynodonts is important for constraining the timing of mammalian characteristics' origination as well as identifying how developed cynodont brains were at different growth stages compared to mammalian analogues. The two reconstructed ontogenetic stages show that *Thrinaxodon*'s endocranial anatomy changed as a result of growth (size) and developmental (shape) factors. Without more intermediate *Thrinaxodon* specimens, which are rare, it is not possible to definitively pinpoint when during development the various size and shape changes seen in the *Thrinaxodon* endocasts may have occurred, and as such correlate these morphological enhancements with the ontogenetic changes seen in *Monodelphis*' brain. However, from studying the reconstructed *Thrinaxodon* brains, it is possible that there was an early developmental growth of the olfactory bulbs, which continued into adulthood, with a slightly later onset of cerebellum growth. The cerebral hemispheres also enlarged in *Thrinaxodon*, but at a rate which was outpaced by the other main brain regions. It would be valuable to reconstruct the brains of more specimens at intermediate skull lengths, reflecting more growth stages of *Thrinaxodon* to further investigate whether there are pulses in growth of certain brain regions, or if there is an overall linear expansion during ontogeny. Furthermore, if the inner ear was also reconstructed from CT scans, then inferences about the onset and acuity of hearing could also be made for *Thrinaxodon*.

It should be noted that ontogenetic variation forms just one part of the variation that may occur between fossils belonging to a specific taxon. Intraspecific variation can also reflect variation among individuals of the same age and sexual dimorphism (Laaß *et al.,* 2017b). Identifying any of these characteristics in fossil taxa can be challenging due to taphonomic processes and a lack of available data to determine the sex of extinct species. Whilst brain

reconstructions for extinct organisms may be crude compared to modern mammal species and lacking any information about neuron connectivity and density, the study of cynodont brains is still valuable for determining the evolutionary and developmental timing of sensory capabilities and behavioural patterns within mammals and their ancestors.

# CHAPTER FIVE

# Quantifying digital endocranial variation in the Triassic cynodont *Thrinaxodon liorhinus*

## 5.1. Understanding reconstruction reliability

Soft tissues offer invaluable insights into the form and function of extinct organisms but are principally lost to the fossil record in all but rare sites of exceptional preservation (lagerstätten; Clements and Gabbott, 2022), meaning that knowledge of past organisms and ecosystems relies predominantly on the preservation of mineralised tissues, such as bone. Rarely, natural internal casts of the cranial cavity are found; for example, for Neanderthals (Eisová *et al*., 2019), lynx (Iurino *et al*., 2015), rhinoceros (Iurino *et al*., 2020), birds (Kuochkin *et al*., 2007), snakes (Triviño *et al*., 2018) and cynodonts (Pusch *et al*., 2022). The natural endocasts are formed via the lithification of tissues or sediment infilling the cavity or deposition of minerals within the skeletal mould, producing a replica of internal morphology to varying degrees of clarity (Hopson 1979; Brasier *et al.*, 2016). However, the paucity of soft tissues and natural endocranial casts within the fossil record make digital endocasts a valuable, alternative source of information about the form and function of extinct organisms (Witmer *et al*., 2008; Rowe *et al*., 2011). Yet the widespread use of digital reconstruction techniques within palaeontology raises questions about the reliability of virtual outputs (Watanabe *et al*., 2019). If there is no fossilised brain tissue from cynodonts, how accurate are the digital brain reconstructions produced from CT-scanned skull data? Do all researchers produce similar brain models for the same specimen, and are these, therefore, reliable interpretations of the original brain morphology?

Two previous studies have investigated the same *Tyrannosaurus rex* specimen (FMNH PR2081) and independently reconstructed the brain using digital techniques (Brochu 2000; Witmer and Ridgely, 2009). The endocasts are somewhat similar, being narrow and elongated with many vascular structures protruding from the brain reconstruction, but Brochu (2000)'s interpretation is not as clearly resolved. However, the olfactory region is very different between the two studies. Much of what Brochu (2000) interpreted to be enormous olfactory bulbs has now been defined as the sensory epithelium of the nasal cavity instead (Witmer and Ridgely, 2009). This finding highlights the subjectivity of modeller interpretations of CT data, given that the oversized olfactory bulbs would have suggested that *Tyrannosaurus rex* had remarkable olfactory acuity compared to other dinosaurs during the Cretaceous. Moreover, advancements in reconstruction technology allowed Witmer and Ridgely (2009) to fully extract the semicircular canals of the inner ear, whereas Brochu (2000) only reconstructed fragments of the bony labyrinth of the inner ear. This reanalysis of the brain reconstruction for a single *Tyrannosaurus rex* specimen raises the question of whether modeller and software subjectivity could be imparted during the reconstruction of brain models for other taxa, such as cynodonts, and thus these sources of variation require further investigation.

When generating endocasts for cynodonts, the reconstructions may vary among modellers for a variety of reasons including the modeller's prior experience with segmentation software, familiarity with interpreting CT data, and knowledge of mammal-like brain morphology. These factors have the potential to influence a modeller's ability to correctly identify and reconstruct anatomical structures of the cynodont brain, meaning that endocranial reconstructions are prone to subjectivity (Broyde *et al*, 2021). Additional reconstruction steps implemented prior to segmentation, such as retrodeformation of specimens sheared or fragmented by taphonomic processes (plastic and brittle deformation, respectively), add an additional layer

of complexity to the reconstruction process and may influence the reliability of the subsequent endocast (Lautenschlager 2016).

However, no known attempt has been made to assess the potential variation introduced by modellers of cranial endocasts, despite digital reconstruction techniques having been used extensively in palaeontology (for example, with dinosaurs (Brochu 2000; Lautenschlager and Hübner, 2013; Ballell *et al*., 2020), birds (Witmer *et al*., 2008; Zelenitsky *et al*., 2011), fish and early tetrapods (Henderson and Challands, 2018; Clement *et al*., 2021), turtles (Lautenschlager *et al*., 2018), non-dinosaur archosauromorphs (Witmer *et al*., 2003; Lautenschlager and Butler, 2016) and cynodonts (Rowe *et al*., 2011), alongside other disciplines). Consequently, this study aims to visualise and quantify the amount of variability in endocranial reconstructions produced by 19 modellers for a single adult specimen of *Thrinaxodon liorhinus*. Modellers are grouped according to their level of knowledge of segmentation software and experience with palaeontological specimens to attempt to identify where any variability may most likely arise from. This study also aims to answer the following questions: (1) does prior experience with segmentation software influence the accuracy of the brain model and produce a more organic morphology? (2) Does having knowledge of brain anatomy, be that for mammals or other species, improve brain reconstruction attempts or do models still show noticeable variability? Endocast analysis aims to resolve these questions and better understand the implications of any variability present on interpretations of cognitive and sensory capabilities. Best practices for the digital segmentation of cynodont brains are also suggested to improve consistency between models made.

## 5.2. Materials and methods

### 5.2.1. Investigating reconstruction variability: selection of modellers

To investigate the amount of variation imparted by the model maker during endocast construction, 19 modellers independently generated a brain model for a single specimen of *Thrinaxodon liorhinus* (specimen UCMP 40466, see section 5.2.2) in Spiers 3.0.1 (www.spiers-software.org; Sutton *et al*., 2012). The modellers were chosen based on their education level in palaeontology, knowledge of brain anatomy and amount of previous experience with digital segmentation software, as outlined in table 5.1. Eleven of the models were generated as part of a first-year undergraduate course of a geology and palaeontology degree program, where modellers were in their first semester and had no formal palaeontological education, no previous knowledge of brain anatomy and no experience with segmentation software. These 11 modellers are viewed as a baseline for the segmentation process, with no preconceptions of what the model should look like based on prior experience. The remaining eight modellers had either completed an undergraduate palaeontology degree (2), completed or were in the final year of a palaeontology PhD (4), completed an earth science PhD without specialising in palaeontology (1) or were a palaeobiology lecturer (1). Of these eight modellers, five had some familiarity with digital reconstruction software and six had an understanding of how to interpret paleontological specimens (although only two modellers were knowledgeable about fossil brain anatomy). The modellers with greater experience of brain morphology or segmentation techniques provided a useful test for whether experience with either of these factors increases the reliability of the endocast produced.

Ideally, more modellers with advanced segmentation skills or specific knowledge of mammalian brain anatomy would have participated in the study. With more time and

modellers, numerous iterations of the study could have been run using different functionalities of the segmentation software (such as manual masking with the paintbrush tool versus using interpolation between slices in more advanced software) and all modellers could have also generated an endocast for an opossum to compare endocast variation in a cynodont and mammal. However, due to time constraints and modeller availability, the study was run as outlined here.

**Table 5.1**. Description of modellers chosen to investigate variation in endocast reconstruction outcomes. Modellers were selected based on their palaeontological education level, knowledge of fossil brain anatomy and previous experience with segmentation software.

| Modeller | Palaeontological education | Brain anatomy knowledge | Digital reconstruction experience |
|---|---|---|---|
| **1** | Completing PhD in palaeontology | Extensive for mammals | Experienced |
| **2** | Associate Professor in Palaeobiology | Extensive for mammals and non-mammalian taxa | Experienced |
| **3** | PhD completed in palaeontology | Some for non-mammalian taxa | Experienced |
| **4** | PhD completed in palaeontology | Minimal | Moderate |
| **5** | Completing PhD in palaeontology | None | None |
| **6** | Master's degree completed in palaeontology | Minimal | Some |

| | | | |
|---|---|---|---|
| **7** | Undergraduate degree completed in palaeontology | Some | None |
| **8** | PhD completed in geology | None | None |
| **9** | First year undergraduate | None | None |
| **10** | First year undergraduate | None | None |
| **11** | First year undergraduate | None | None |
| **12** | First year undergraduate | None | None |
| **13** | First year undergraduate | None | None |
| **14** | First year undergraduate | None | None |
| **15** | First year undergraduate | None | None |
| **16** | First year undergraduate | None | None |
| **17** | First year undergraduate | None | None |
| **18** | First year undergraduate | None | None |
| **19** | First year undergraduate | None | None |

### 5.2.2. *Thrinaxodon liorhinus*: specimen selection and digital reconstruction

As non-mammalian cynodonts are an important group for understanding the evolution of mammals, the basal cynodont, *Thrinaxodon liorhinus*, provides an early window into the development of mammalian characteristics. Additionally, the large number of available specimens (Botha and Chinsamy, 2005; Abdala *et al*., 2013; Jasinoski *et al*., 2015; Gaetano and Abdala, 2020) and small skull size facilitates the gathering of CT scans to investigate variation in models of *Thrinaxodon*'s endocranial anatomy.

Specimen UCMP 40466 was selected for digital endocranial reconstruction and is an adult with a basal skull length of 74 mm, as defined by Jasinoski *et al*. (2015). The dataset is somewhat coarse compared to the results achieved through more modern µCT scanning, but the scan of UCMP 40466 benefits this study by being a smaller dataset which reduces the time burden of

the modelling process on each of the modellers. The smaller dataset also facilitated segmentation on non-specialist computers, which may not have had the memory and appropriate graphics card to support segmentation of a higher resolution, µCT scan (although such a dataset is often preferable to view finer endocranial details). The original CT scan was comprised of 153 slices, however, to generate a smoother brain model, the dataset was resampled in Avizo 9.3.0, increasing the number of slices to 1200 slices. This resampling did not alter the resolution; instead, the original scan was subdivided into more slices.

The image stack was imported into Spiers for digital segmentation of endocranial structures. Good internal contrast was enhanced using thresholding between colour values of 80 (grey) and 255 (white), which increased the contrast between cranial bones and the brain cavity, non-target cranial cavities (such as the inner ear) and the scan background. Manual segmentation of the endocranial cavity was conducted using the paintbrush tool to create a mask. Modellers used a circular brush, varying the size of the brush to fit smaller sections of the endocranial cavity and capture finer details. Unlike other segmentation software, such as Avizo or Slicer, Spiers does not possess a 'magic wand' tool to auto-populate a mask based on greyscale values, hence the use of the brush tool to create the brain mask.

Modellers worked through the CT dataset slice by slice, manually drawing the mask and did not use interpolation. The inner edge of the endocranial cavity was used as the edge of the mask. This provided a clear boundary for the dorsal surface, but the lack of basicranial bones in some areas of *Thrinaxodon*'s braincase meant that some ventral parts of the brain were open to interpretation by the modeller. Modellers were instructed to join these areas with slightly curved lines between the bone boundaries that were visible. The brain mask was constrained posteriorly by the opening of the foramen magnum and anteriorly by the

disappearance of a depression within the frontal bone which divides the olfactory bulbs (figure 5.1).

Bone boundaries of the braincase were chosen as the outer limit of the brain reconstructions because it is assumed that *Thrinaxodon*'s brain largely filled the endocranial cavity (as it does in mammals), although the brain would have also likely been surrounded by meninges, blood vessels, nerves and intracranial fluids during life (Macrini *et al*., 2007b; Balanoff and Bever, 2020). This assumption is based on the fact that cynodonts are often compared to modern opossums (*Monodelphis domestica* and *Didelphis virginiana*; Kaas 2013; Rodrigues *et al*., 2014; Lautenschlager *et al*., 2017; Guignard *et al*., 2018) because of the similarities in jaw and middle ear anatomy during the embryonic stage (although adult opossums transition to a mammalian jaw and middle ear and there is, of course, a significant temporal distance between extant mammals and non-mammalian ancestors; Kaas, 2013; Rodrigues *et al*., 2014; Lautenschlager *et al*., 2017; Rodrigues *et al*., 2019). Nevertheless, given that endocasts from modern mammal skulls are known to have a high fidelity for the original brain shape, the entire endocranial cavity of cynodont skulls is used as an approximation of brain shape and volume during digital reconstruction of cynodont brains (Balanoff *et* al., 2016).

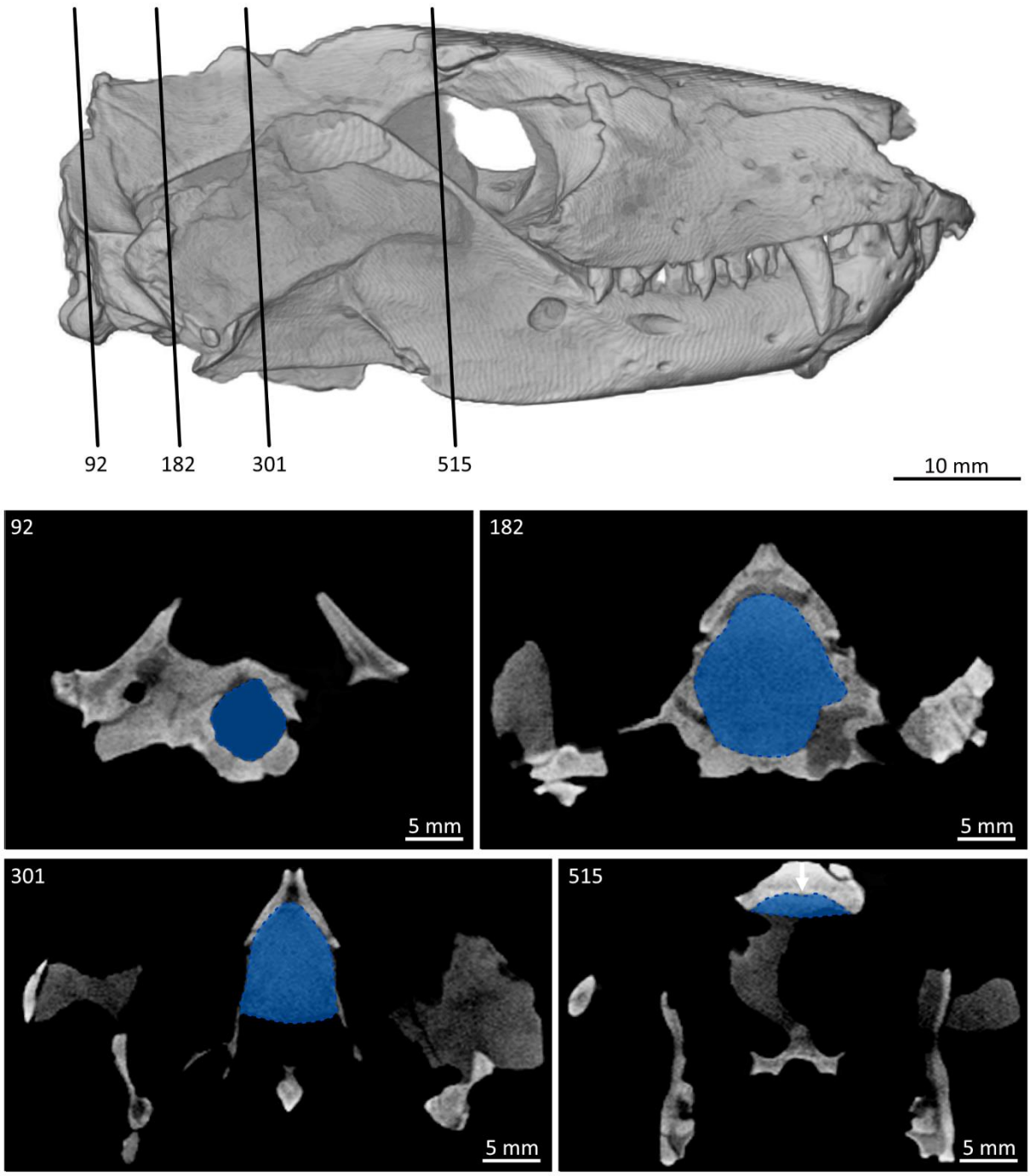


**Figure 5.1.** Lateral view of specimen UCMP 40466. Vertical lines mark the positions of the associated CT scan slices 92, 182, 301 and 515. Slice 92 depicts the foramen magnum which was used as the posterior limit of the endocast. Slice 515 shows the region used as the anterior limit of the endocast, where the depression in the frontal bone disappears (white arrow). While guidance on the features present was given to modellers, the modellers were not told at which slice they should stop applying the mask. Slices 182 and 301 represent intermediate

brain regions with various degrees of brain cavity closure. The blue mask indicates an interpretation of brain anatomy at each point of the skull, with slice 301 showing an example of the curved line modellers were instructed to use to join ossified elements where there were no basicranial bones present.

To ensure all modellers had at least the same basic knowledge of brain anatomy and software functionality, all modellers were provided with training in how to generate a mask in Spiers and export the model as a volume. Modellers were also provided with a basic overview of brain anatomy, where to identify the brain on a CT scan and were provided with a schematic reference image of Middle Triassic cynodont, *Chiniquodon theotenicus*, to assist with interpreting endocranial anatomy from a CT scan (figure 5.2; Kemp 2009). While a hypothesised brain endocast was shown in the reference images, modellers were reminded that this was a different species to *Thrinaxodon* and that, therefore, the modellers should not attempt to recreate the brain shown in figure 5.2. During modelling, only reconstructions of the brain were requested, and additional soft tissues and cranial features (such as neurovascular structures (including sinuses), cranial nerves and the endosseous labyrinth (bony housing of the inner ear)) were not intentionally included within the reconstructions. However, if modellers interpreted these structures to be part of the brain, then these models were still accepted as interpretations of brain anatomy. Once modellers were satisfied that the brain reconstruction was completed, masks were visualised as objects in SpiersView and exported as 3D surface volumes (STL files). Smoothing was not applied to modellers' reconstructions to retain all of the morphological details generated.

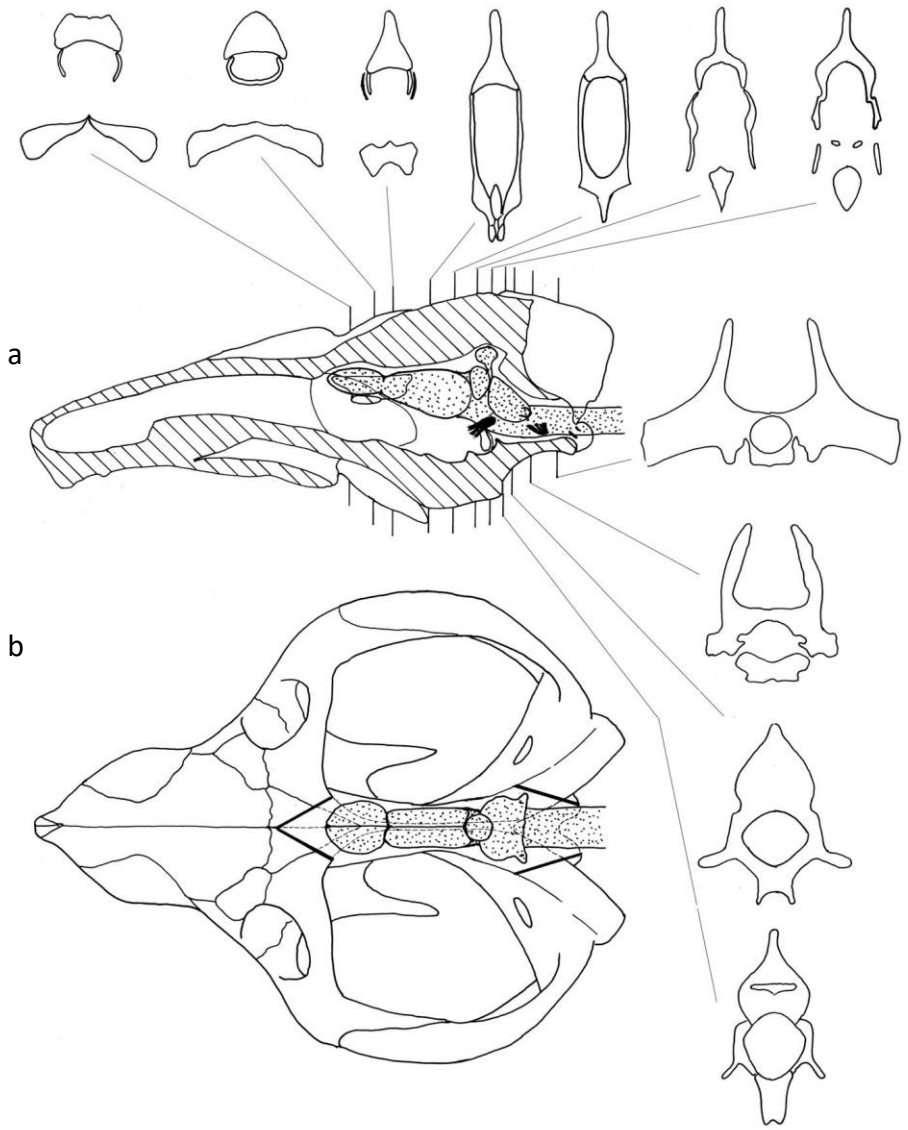


**Figure 5.2.** Schematic illustration of the endocranial anatomy of cynodont, *Chiniquodon theotenicus* (Kemp 2009). The skull is seen in lateral **(a)** and dorsal **(b)** orientations with a hypothesised brain endocast shown in life position (stippled shading). In **(b)**, striped shading denotes the cranial bones, with the endocranial cavity unshaded. Illustrations of the brain cavity as it would be seen in a CT scan are shown at their respective positions in the skull, assisting modellers in interpreting the CT scan for UCMP 40466.

### 5.2.3. Quantifying modeller variation

To quantify any variation between the endocasts generated by the 19 modellers, the brain models were imported into Avizo by the study author (modeller one) to collect linear and volumetric measurements (as Spiers only offers a scale grid for measuring 3D models rather than a specific measurement tool). However, the STL files exported from Spiers were found to produce incorrect values in Avizo due to the inward-facing surface normals (vectors perpendicular to the model's surface) being positioned on the outside of each brain model. To correct for this, all models were individually imported into MeshLab 2021.07 (www.meshlab.net), where the normals were flipped by selecting all of the faces and vertices within the mesh and applying the following settings: Filters → Normals, Curvatures and Orientation → Invert Faces Orientation. This process flipped the normals so that the vectors were positioned on the inside of the brain model, allowing the data contained within the models to be read by Avizo. Models were exported as STLs from MeshLab and imported into Avizo for quantitative analysis.

Length and volume measurements were gathered for all of the models as outlined in figure 5.3, using the 2D measurement and surface area volume tools in Avizo. All measurements were collected by the study author (modeller one) and not the individual endocast makers. However, several scaling steps were needed to ensure the measurements collected from Avizo were life size. The basal skull length was measured for the CT scanned skull in Spiers (1070 mm) and Avizo (1074.02 units) to compare with the specimen skull length (74 mm). The models first needed to be converted between Spiers and Avizo (equation 5.1), before being scaled from Avizo measurements to physical measurements of the fossil (equation 5.2). This produced a scaling factor of 0.996 for Spiers and 14.514 for Avizo. It was then found that models were half of life size due to the scale used by the modellers when exporting their final

brain endocasts. Therefore, the full scaling calculation is provided in equation 5.3. However, model 16 was found to have been erroneously exported at a one-eight scale, so all measurements for this model were multiplied by the Spiers and Avizo scaling factors, and then by eight rather than two.

**Equation 5.1** $$\text{Spiers scaling factor} = \frac{\text{Spiers BSL}}{\text{Avizo BSL}}$$

**Equation 5.2.** $$\text{Avizo scaling factor} = \frac{\text{Avizo BSL}}{\text{Skull BSL}}$$

**Equation 5.3.** Endocast scaling = Spiers scaling factor x Avizo scaling factor x2

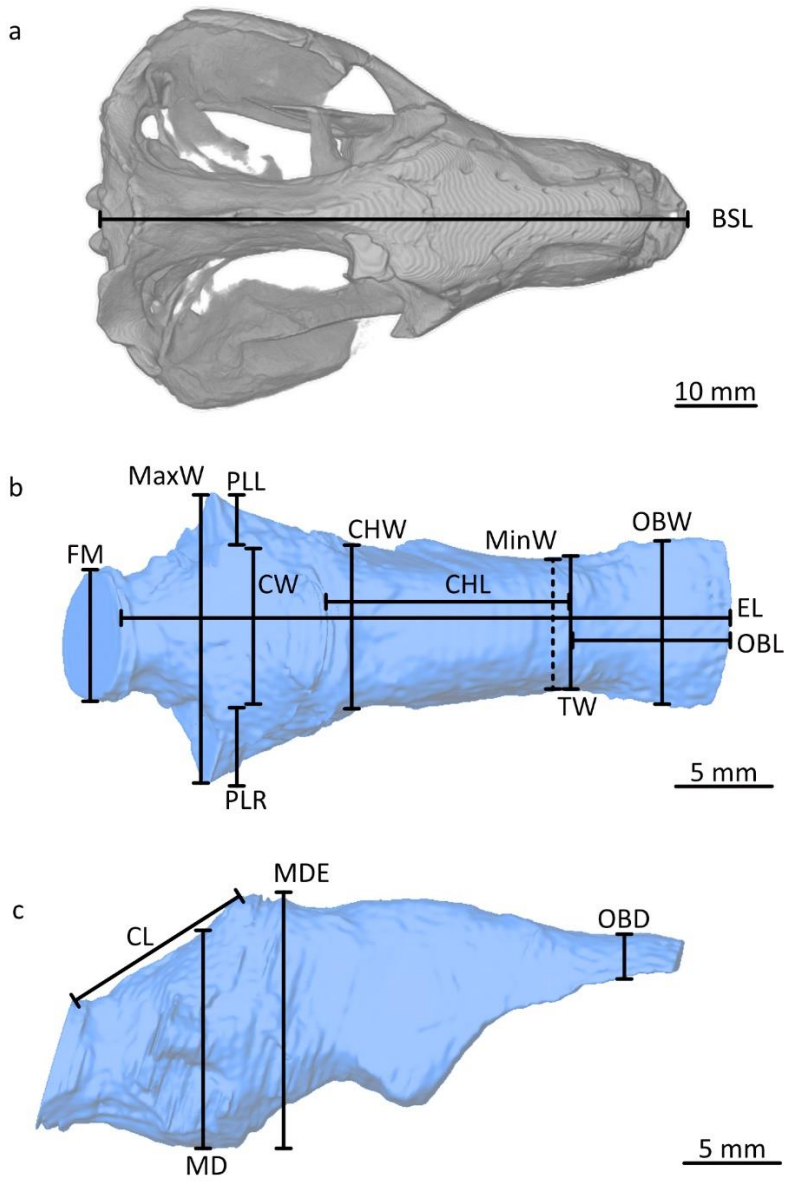


**Figure 5.3.** Specimen UCMP 40466 **(a)** with the associated endocast generated by modeller one and illustration of the main measurements collected. **(b)** Endocast in dorsal view with measurement abbreviations as follows: EL = endocast length; MaxW = maximum width; MinW = minimum width (dashed as usually located near to anterior boundary of cerebral hemispheres); OBL = olfactory bulb length; OBW = olfactory bulb width; TW = width at olfactory bulb - cerebral hemisphere transition; CHL = cerebral hemisphere length; CHW = maximum cerebral hemisphere width; PLL = length of left paraflocculer lobe; PLR = length of right paraflocculer lobe; CW = cerebellum width; FM = foramen magnum diameter. **(c)**

Endocast in right lateral view with measurement abbreviations as follows: MD = maximum depth of cerebellum; MDE = maximum depth of whole endocast from horizontal lines; OBD = olfactory bulb depth; CL = cerebellum length.

To further identify variation between the endocasts, unscaled models were manually landmarked by the study author in Avizo using the 'Landmark (Recents, Points and Lines)' tool. Landmarking uses the positioning of coordinate points placed across a model's surface to map the endocast's shape, permitting morphological comparisons between models. A total of 30 landmarks were placed on each endocast in the same order, covering biologically and spatially homologous points, as detailed in figure 5.4. Thirty landmarks were selected due to the limited number of distinct biological regions within *Thrinaxodon*'s endocast (compared to, for example, an opossum brain) on which homologous landmarks could be placed (see chapter three for the main biological regions of *Thrinaxodon*'s brain). Therefore, spatially homologous landmarks were also added between any biologically homologous landmarks to capture a better representation of endocast surface morphology.

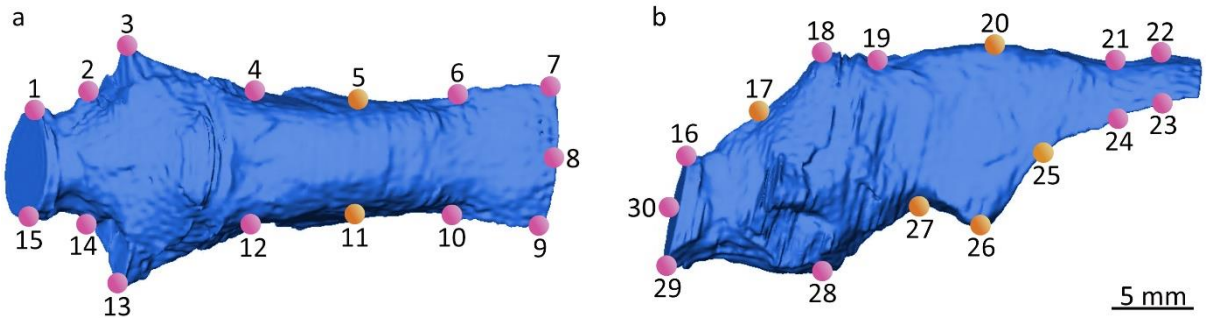


**Figure 5.4.** The reconstructed digital endocast of *Thrinaxodon liorhinus* (UCMP 40466) in **(a)** dorsal and **(b)** lateral view. Thirty landmarks were placed on each endocast, in the order shown above. Pink landmarks are biologically homologous points, whereas orange landmarks

denote spatially homologous points, and these landmarks are generally halfway marks between biological landmarks (to increase surface coverage of endocasts in the landmark data). **1 and 15** – Widest part of the foramen magnum at the most posterior position of the endocast. **2 and 14** – Cerebellum begins to widen into the parafloccular lobes. **3 and 13** – Lateral-most point of the parafloccular lobes. **4 and 12** – Cerebellum and parafloccular lobes narrow into the cerebral hemispheres. **5 and 11** – Halfway between cerebellum-cerebral hemisphere transition and cerebral hemisphere-olfactory bulbs transition. **6 and 10** – Transition between the cerebral hemispheres and olfactory bulbs. **7 and 9** – Widest and anterior-most points of the olfactory bulbs. **8** – Anterior boundary of the olfactory bulbs and endocast as a whole. **16 and 29** – Dorsal and ventral-most points of the foramen magnum. **17** – Halfway between the dorsal point of the foramen magnum and cast of the cerebellum (or position where it would be in cases where it has not been reconstructed). **18** – Located on dorsal-most point of the cerebellum. **19** – Transition between the cerebellum and cerebral hemispheres. **20** – Halfway between cerebellum-cerebral hemisphere transition and cerebral hemisphere-olfactory bulb transition. **21 and 24** – Dorsal and ventral transitions between the cerebral hemispheres and olfactory bulbs. **22 and 23** – Widest dorsal and ventral extent of the olfactory bulbs. **25** – Transition between cerebral hemispheres and hypophyseal cast. **26** – Ventral-most point of the hypophyseal cast (where reconstructed), otherwise it is the ventral boundary of the middle region of the endocast. **27** – transition between hypophyseal cast (where reconstructed) and cerebellum, otherwise this landmark marks halfway between landmark 26 and the ventral-most point of the cerebellum. **28** – Ventral boundary of the cerebellum. **30** – Middle of the foramen magnum.

The landmarks are displayed as a coordinate text file which was then imported into PAST 4.05 (Hammer *et al*., 2001; https://www.nhm.uio.no/english/research/resources/past/). The 3D

coordinates were spatially aligned using a Procrustes superimposition (select data → Transform → Landmarks → Procrustes (2D+3D) and select 3D coordinates). Subsequently, a Principal Component Analysis (PCA) was then applied to the standardised landmark data using the following settings: Select data → Multivariate → Ordination → Principal components (PCA). Principal Component Analysis permits the identification of trends within the morphology of the reconstructed endocasts by mapping models according to the shapes captured by landmark coordinates. The distribution of the models following PCA provides information about which morphological components contribute most to any variation observed. The contributions can be further explored using loading plots generated from the raw measurement data imported into PAST. This data is not subjected to Procrustes superimposition but PCA is applied to the original data, producing a loading plot which shows the contribution of each measurement to a particular principal component.

While PCA quantifiably maps shape variation between models, it is helpful to visualise shape variation between the endocasts to ascertain whether any regions are more consistently reconstructed than others. All endocasts (with flipped normals) were imported into CloudCompare (version 2.12; www.danielgm.net/cc/release) and individually converted into a mesh (Select model → Edit → Mesh → Sample points). Each endocast was then compared to the reference endocast produced by modeller one (the study author). To map the shape comparison, each endocast was spatially aligned with the reference model using manual transformation (Translate/rotate tool). Once rough manual alignment was achieved, both models were selected and aligned computationally using the 'Finely registers already (roughly) aligned entities (clouds or meshes)' tool. This function also scales the endocasts to match as many vertices and faces as possible between the reference endocast and each model so that shape variation can be assessed without size changes significantly contributing to the results.

Shape variation is mapped by selecting both models and applying the 'Compute cloud/cloud distance' function with octree level seven. This process computes the distances between homologous points within the models and identifies where points are closest and furthest from each other using red-green-blue (RGB) colour maps. Cooler colours highlight areas of similarity while warmer tones denote areas where the shape differs between the endocasts. By visualising shape variation among the reconstructed endocasts, it is possible to identify regions that are consistently reconstructed which may, therefore, be more reliable interpretations of *Thrinaxodon*'s brain morphology.

### 5.2.4. Quantifying variability in estimates of cognitive capability

Following the reconstruction of endocranial anatomy, cognitive acuity was investigated to ascertain how much model variation influences the conclusions drawn about the relative intelligence of *Thrinaxodon liorhinus* compared to other cynodonts. To estimate cognitive capabilities based on the relative proportions of brain regions, the encephalisation quotient was calculated using equations 3.2 (which removes the effects of body size on brain size estimates; Jerison 1973) and 3.3 (based on a larger number of taxa; Manger, 2006; Hoffman *et al*., 2021). Endocranial volumes (EV) were collected in Avizo and were converted from cubic millimetres to cubic centimetres for the calculation of encephalisation quotients, consistent with the methodology used by Hoffman *et al*. (2021). Body mass (BM) was estimated using equation 3.4, which is based on the body mass calculated for gracile cynodonts (those with a small and slender skeleton like *Thrinaxodon*; Quiroga, 1979; Quiroga, 1980a; Hoffman *et al.,* 2021). By calculating the encephalisation quotient for each model, it is possible to ascertain whether conclusions about *Thrinaxodon*'s cognitive capabilities would differ if each endocast was considered in isolation.

## 5.3. Results

### 5.3.1. Morphological variation in endocranial reconstructions

The 19 cranial endocasts produced for specimen UCMP 40466 are presented in figures 5.5 and 5.6, where an initial visual inspection highlights some striking morphological variation. The models can be broadly separated into three groups. First, the majority of endocasts exhibit a rectangular overall morphology, with an anterior projection of the olfactory bulbs (models 2, 5, 9, 10, 11, 15, 16, 18 and 19). A second group of endocasts have a smaller, rectangular posterior region with a noticeable protrusion in the middle of the ventral surface (models 4, 6, 12, 13 and 14). Finally, a third, smaller group contains endocasts exhibiting a slender shape, with an overall tapering from the foramen magnum through to the olfactory bulbs (models 1, 3, 7, 8 and 17).

For the first group of endocasts, the rectangular reconstruction is concentrated in the ventral portion, with a relatively flat basal surface of the cerebellum leading to a steep transition into the olfactory bulbs. All of the endocasts in this group have dorsoventrally narrow olfactory bulbs, tapering anteriorly (with the exception of model 9 which retains a rectangular shape across the length of the olfactory bulbs in lateral view). This group of models all have anteroposteriorly convex curvature on the dorsal surface of the cerebellum and cerebral hemispheres. However, some modellers have reconstructed protrusions on the dorsal surface, possibly corresponding with the vermis or a sinus (posterior feature) and pineal body (anterior protrusion), to varying degrees of clarity. Models 2, 5, 15 and 18 exhibit only slight deviations from a smoothly curving dorsal surface. Model 10 only reconstructs the vermis/sinus, models 9 and 16 only reconstruct the pineal body, while models 16 and 18 show both the vermis/sinus and pineal body.

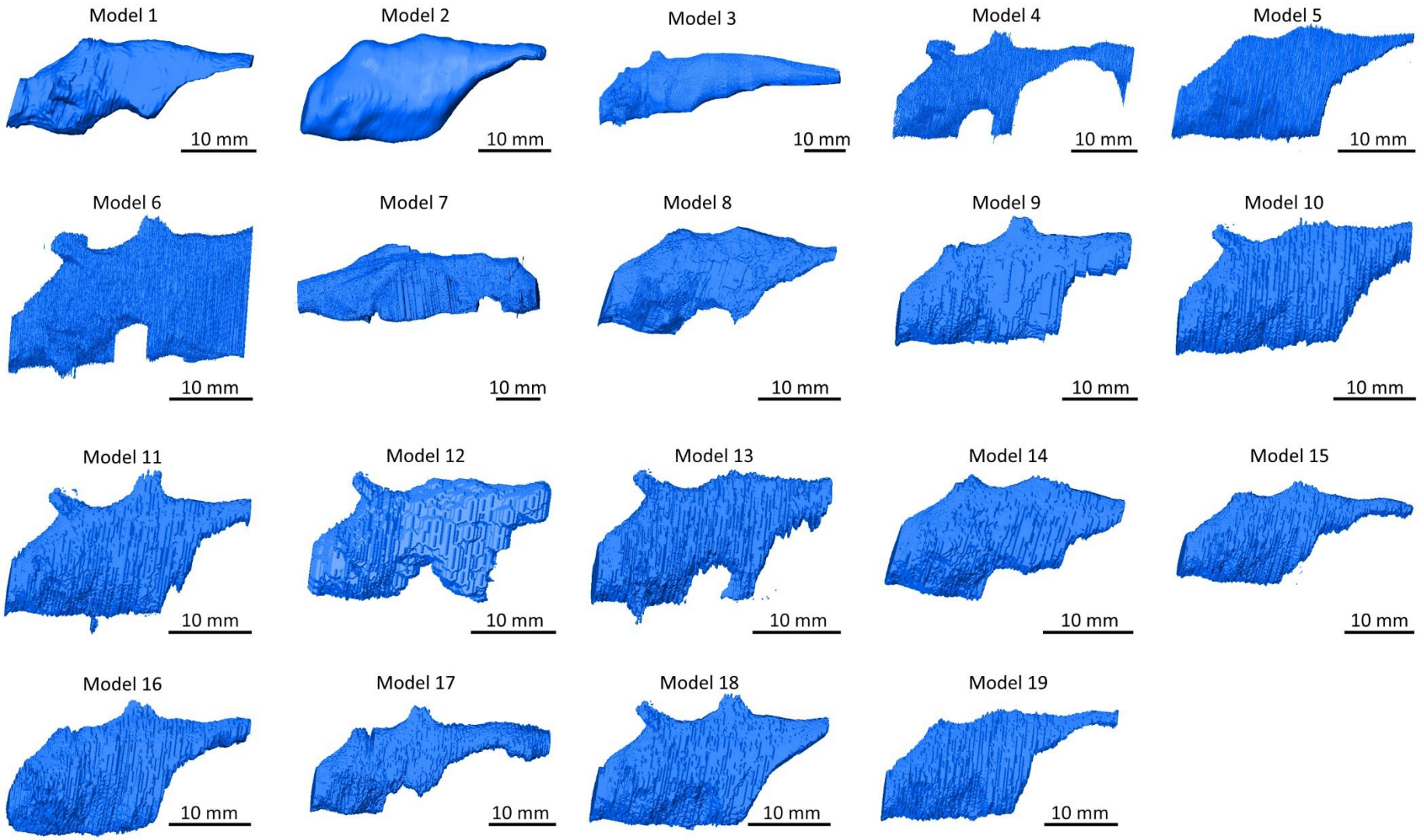


**Figure 5.5.** Endocranial reconstructions of *Thrinaxodon liorhinus* (UCMP 40466) produced by 19 modellers and observed in right lateral view.

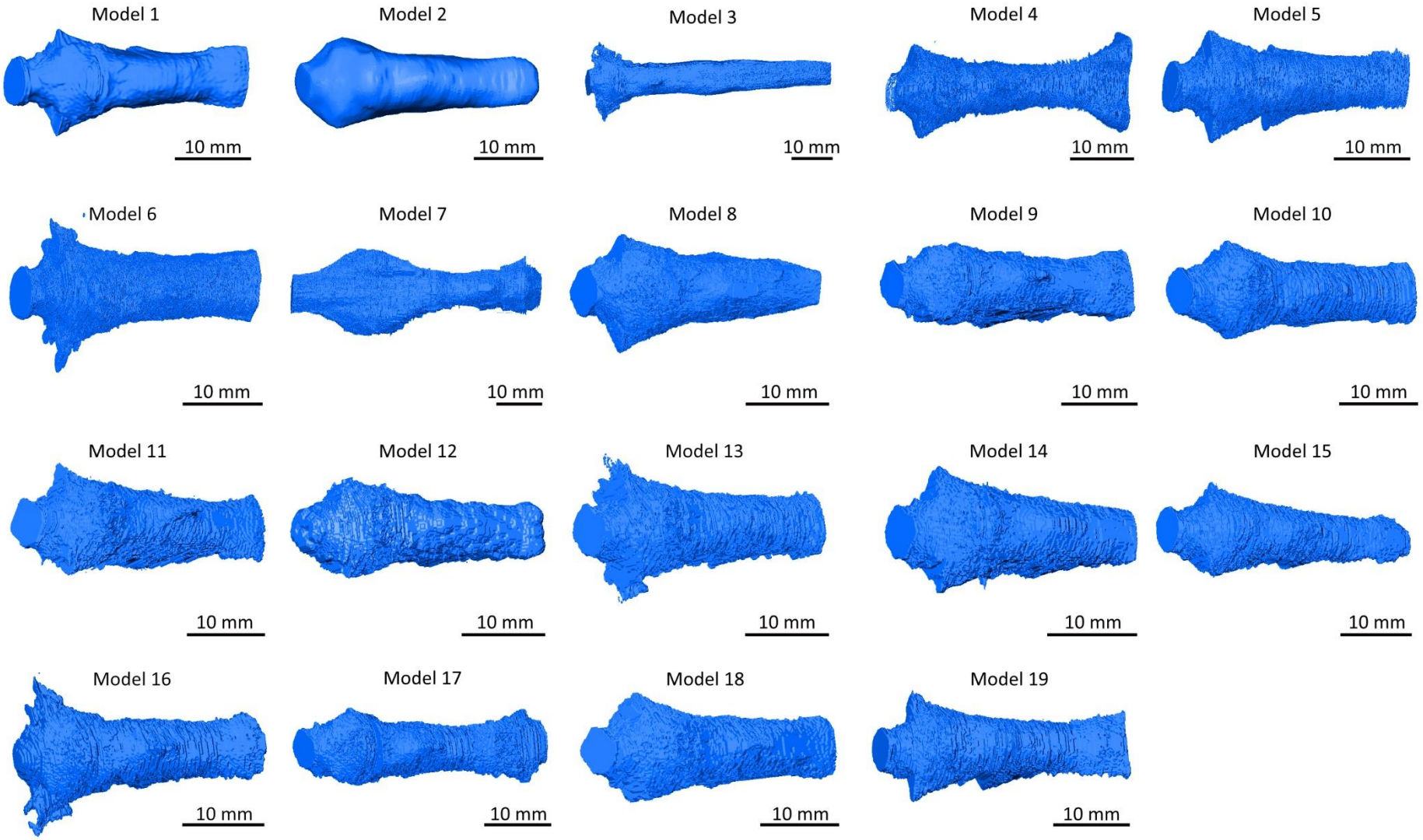


**Figure 5.6**. Endocranial reconstructions of *Thrinaxodon liorhinus* (UCMP 40466) produced by 19 modellers and observed in dorsal view.

The second group of models have a much shorter ventral surface of the cerebellum, which has a concave transition into a prominent ventrally orientated protrusion on the basal surface, which may correspond to the hypophyseal cast, where the pituitary gland would have been in life (Rodrigues *et al*., 2014). There is significant variation in how this structure has been reconstructed, with model 14 being very shallow, models 4 and 13 showing narrow protrusions, while model 12 has a pyramidal structure. Model 6 varies further by displaying a rectangular block for the anterior-most portion of the endocast and as such, the olfactory bulbs of this model are concealed within this extra volume within the reconstruction (figure 5.5). However, models 12, 13 and 14 show similar, tapering morphologies for the olfactory bulbs, while model 4 is noticeably wider and tapers ventrally after the transition from the cerebral hemispheres into the olfactory region. On the dorsal surface, models 4 and 6 show reconstructions of the vermis/sinus and pineal body, whereas models 12, 13 and 14 only show a protrusion for the vermis or sinus.

The third group of models display distinctively different morphologies compared to the other two groups, but the endocasts in this third group share an overall brain shape which tapers anteroposteriorly from the foramen magnum towards the olfactory bulbs. Models 1 and 8 are the most similar with a shallowly dipping cerebellum which transitions concavely into the hypophyseal cast on the ventral surface, before narrowing into the olfactory bulbs. Models 3 and 17 are both elongated, though the latter has a shallow ventral reconstruction of the hypophyseal cast and distinctively rounded olfactory bulbs compared to the other endocasts. Model 7 is an anomalous shape, with a somewhat continuous, cylindrical morphology (with the exception of a concave transition between the cerebral hemispheres and olfactory bulbs). Reconstructed dorsal features are much smaller in this group, with models 1, 3, 7 and 8

showing a small reconstruction of the vermis/sinus, and only model 17 also has a reconstruction of the pineal body.

It should be noted, however, that in dorsal view, models from different groups share some features in common. Notably, the pyramidal paraflocculars lobes are prominent in all of the endocasts, but are largest for models 1, 3, 4, 5, 6, 8, 10, 13, 14, 16, 18 and 19. Models 2 and 7 both display noticeably rounded paraflocculars lobes that encompass a greater volume of the endocast. Models 6, 13 and 16 deviate the most from the cerebellum as these models also contain partial reconstructions of the inner ear as part of the endocast.

For the majority of the brain reconstructions, the olfactory bulbs terminate as a straight line, however, models 2, 7, 15, 16 and 17 display a more organic shape with rounded olfactory bulbs, and model 4 flares anteriorly into a significantly wider structure than in all of the other endocasts. In dorsal view, it is also possible to identify models 3 and 7 as being anomalously elongated compared to the other reconstructions of *Thrinaxodon*'s brain. Furthermore, all of the models display a rough surface texture with dorsoventral lines consistent with the masking method conducted in coronal view, with the exception of model 2, which has been smoothed, and model 12 which is covered in small circles reflective of the paintbrush tool.

The morphological differences between the endocranial reconstructions of *Thrinaxodon liorhinus* are even more apparent after point cloud analysis (figures 5.7, 5.8, 5.9 and 5.10). In this analysis, cool tones show points of greatest similarity between the reference endocast (model 1) and each of the other reconstructions, while warmer tones indicate areas of greatest differences. The most prominent differences are seen in the depth of the cerebellum and the shape of the olfactory bulbs. Regarding the morphology of the cerebellum, the

warmer colour maps clearly show where the rectangular endocasts differ from model 1 by not distinguishing between the cerebellum and hypophyseal cast, which has been reconstructed in the reference model (figure 5.7). This morphological difference is most clearly visible for models 2, 5, 6, 9, 10, 11, 18 and 19. When observing the ventral surface (figure 5.8), the warmer tones are particularly prominent for the olfactory bulbs, reflecting variations in the dorsoventral depth of the olfactory bulb reconstructions. The deeper reconstructions of the olfactory bulbs compared to model 1 are seen for models 4, 6, 7 and 16. Model 3 displays significant variation from the reference endocast on the basal surface of the cerebellum and transition into the olfactory bulbs. This difference is likely due to model 3 being significantly more elongated and dorsoventrally larger than model 1.

When viewed dorsally (figure 5.9), the endocasts are largely similar in morphology, widening from the foramen magnum to the parafloccular lobes, then narrowing through the cerebral hemispheres to the olfactory bulbs. Slight variation is visible in the width of the parafloccular lobes, particularly for models 3, 6, 13 and 16 which erroneously incorporate parts of the inner ear into the reconstruction (figure 5.9). Additionally, dorsal features are highlighted in warmer tones to varying degrees of clarity depending on the amount of divergence from the surface of the cerebellum and cerebral hemispheres. The pineal body is most prominent in models 9, 11, 15, 17 and 18. Conversely, the vermis/sinus is most pronounced in models 3, 10, 11, 12, 13 and 18. Finally, the foramen magnum varies in width between the models (figure 5.10), particularly in the width of the termination of the foramen magnum, with model 7 being wider than in the reference endocast and models 12 and 16 being noticeably smaller.

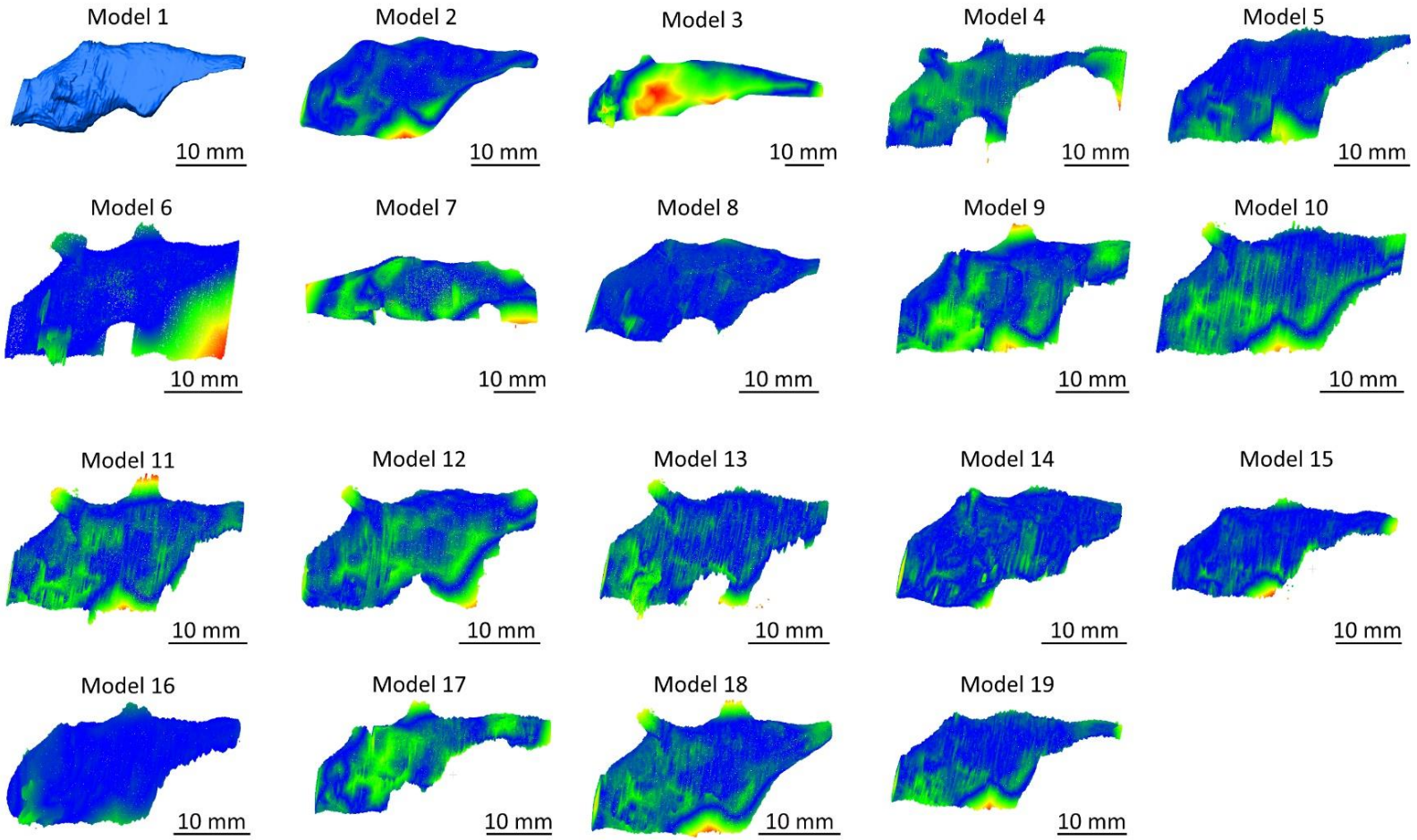


**Figure 5.7.** Point cloud analysis of the 19 endocranial reconstructions produced for *Thrinaxodon liorhinus* (UCMP 40466) in right lateral view. Colour maps are reflective of the differences between each reconstruction and model one, with cooler colours showing areas of similarity and warmer tones highlighting areas of difference. The most prominent regions of variation are consistently found within the ventral reconstruction of the cerebellum and hypophyseal cast, and dorsal reconstructions of the vermis/sinus and pineal body.

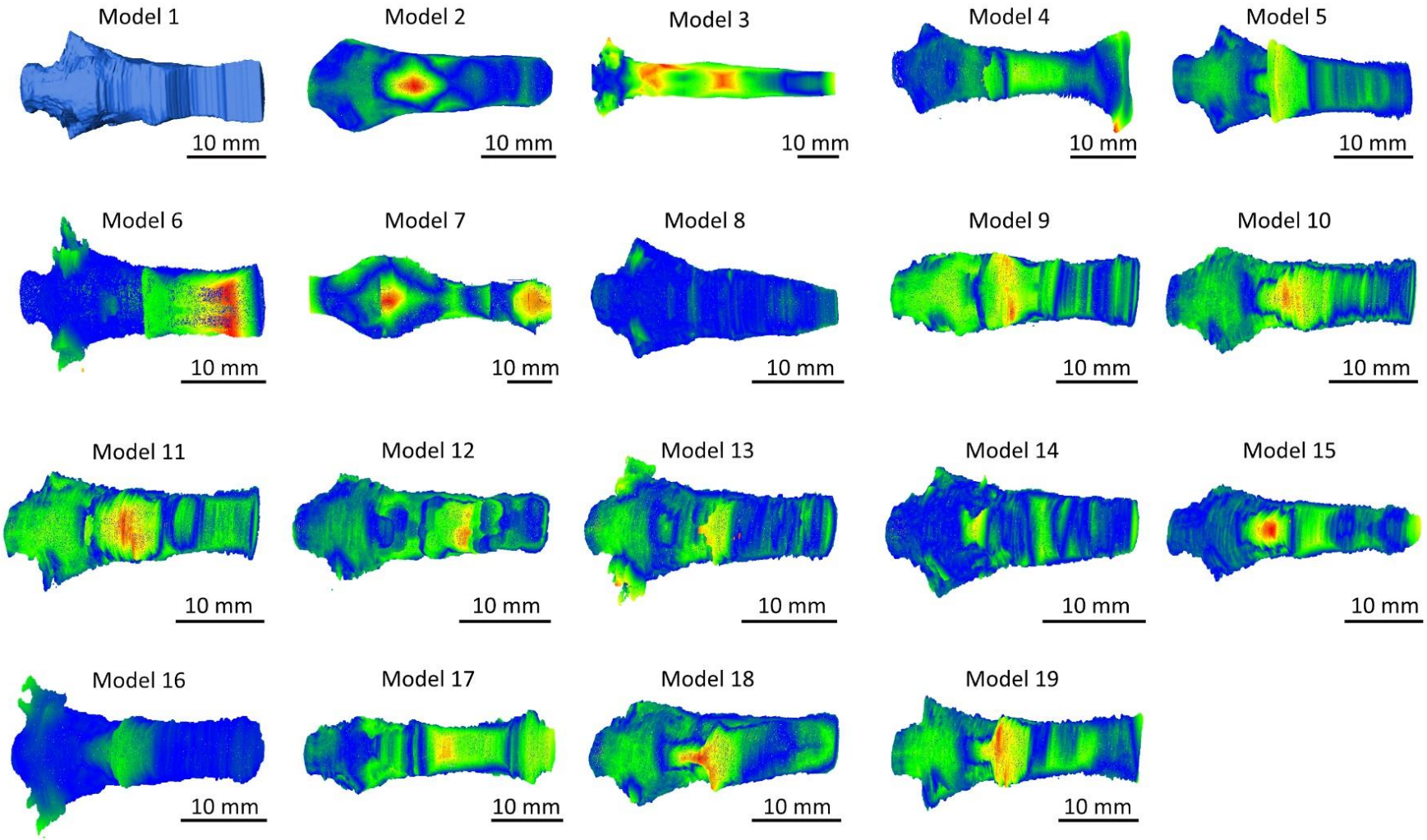


**Figure 5.8.** Point cloud analysis of the 19 endocranial reconstructions produced for *Thrinaxodon liorhinus* (UCMP 40466) in ventral view, comparing each endocast to model one. Cooler colours show areas of similarity and warmer tones areas of difference. The most prominent regions of variation are in the ventral reconstruction of the olfactory bulbs and depth of the hypophyseal cast, where reconstructed.

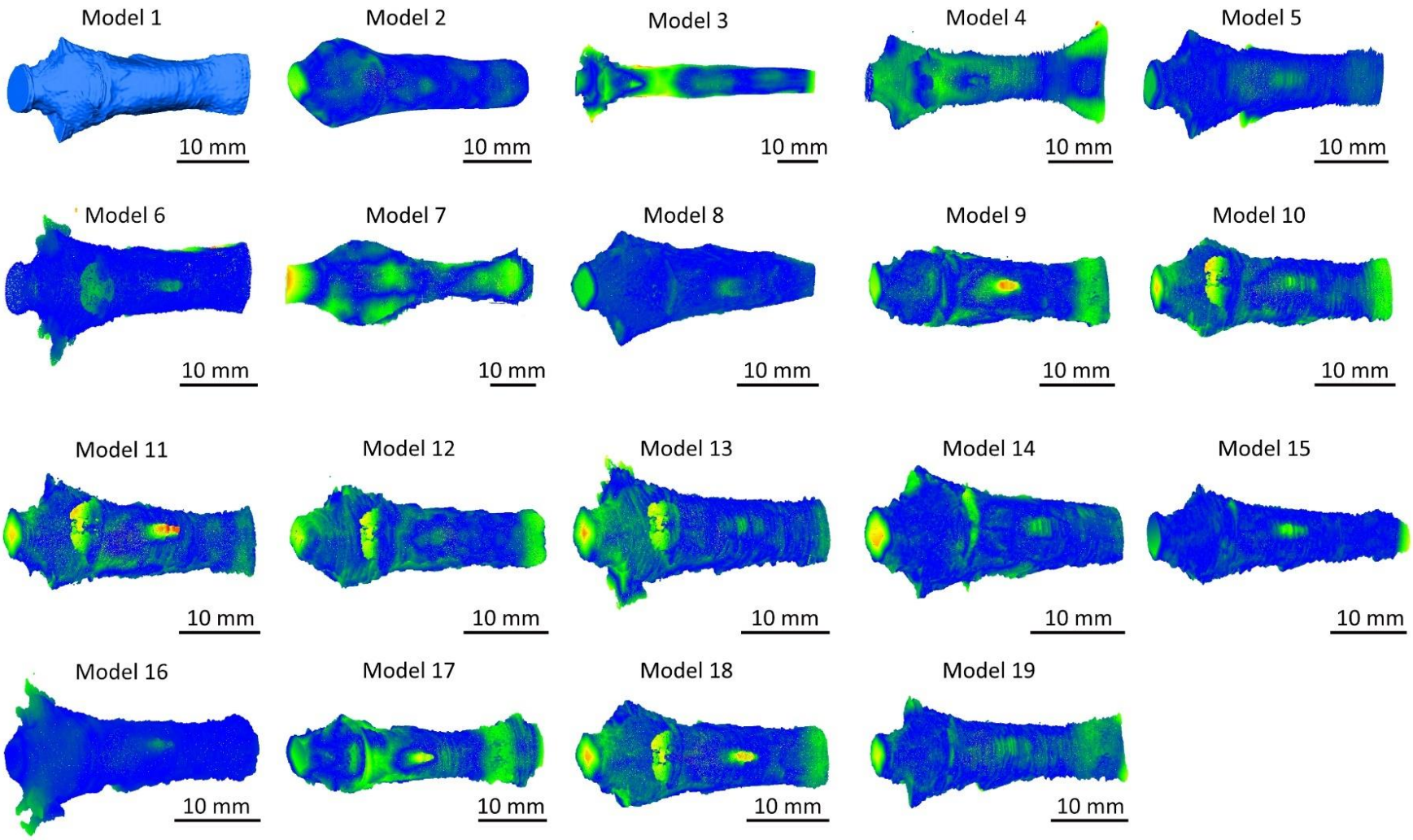


**Figure 5.9.** Point cloud analysis of 19 endocranial reconstructions of *Thrinaxodon liorhinus* (UCMP 40466) in dorsal view, comparing each endocast to model one. Cooler colours indicate areas of similarity while warmer tones show areas of difference. The most notable variation occurs within the shape of the olfactory bulbs, width of the paraflocculars lobes and whether the vermis/sinus and pineal body are reconstructed or not.

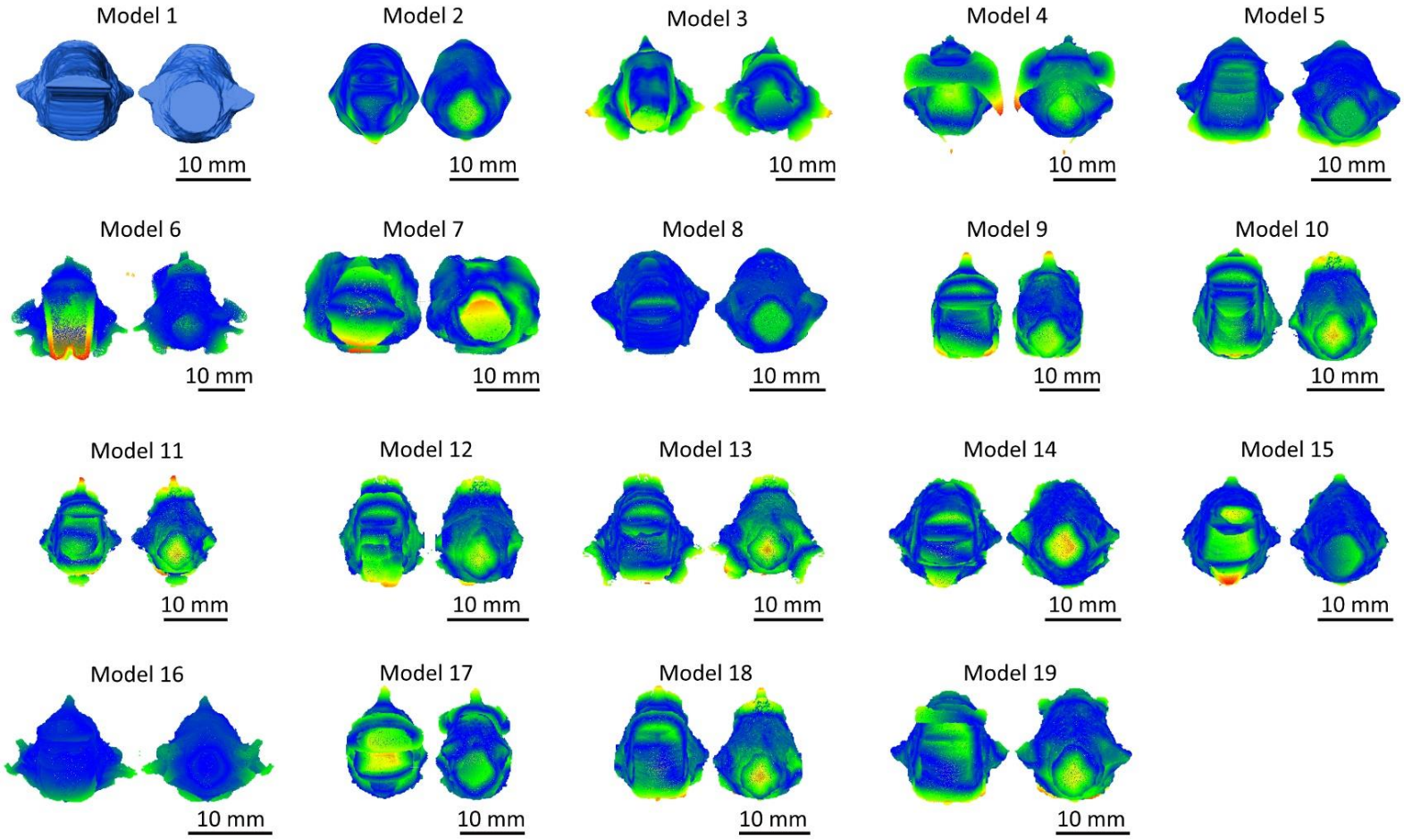


**Figure 5.10.** Point cloud analysis of 19 endocranial reconstructions produced for *Thrinaxodon liorhinus* (UCMP 40466) in anterior (left) and posterior (right) view, comparing each endocast to model one. Cooler colours highlight similarities and warmer tones show differences in reconstructed morphology. Variation is prominent within the shape of the olfactory bulbs, occurrence of a hypophyseal cast (or not), width of the parafloccular lobes and height of the vermis/sinus and pineal body (where present).

### 5.3.2. Quantifying morphological variation in endocranial reconstructions

Linear and volumetric measurements collected for each model (table 5.2; figure 5.11) reveal that reconstructed brain lengths range between 25.35 mm (model 14) and 62.64 mm (model 3). However, endocast lengths for models 3 and 7 (57.69 mm) are anomalously long, therefore, removing these two outliers generates an average endocast length of 30.95 mm (or 34.03 mm including the outliers). When positioned within the skull, the brain reconstructions occupy between 34% (model 14) and 85% (model 3) of the skull length, with an average endocast:BSL ratio of 42% once the outlier models 3 and 7 are removed. Consideration of the reconstructed dorsoventral depths of the endocasts confirms that the elongated models are reconstructed with additional masks at the anterior or posterior of the CT scan, rather than the longer endocast length being an artefact of scaling. Endocast depth (measured from a horizontal line taken at the dorsal and ventral boundaries of the endocast) varies between 13.40 mm (model 8) and 19.52 mm (models 3 and 11). Overall, endocast volumes vary considerably between 1590.54 $mm^3$ and 7050.32 $mm^3$, with the extra volume predominantly contained within the dorsoventral depth of the olfactory bulbs and cerebral hemispheres.

**Table 5.2.** Linear and volumetric measurements of all *Thrinaxodon* endocasts generated by the 19 modellers. The measurements were calculated after correction using the scaling factor outlined in the methods. These measurements detail overall reconstructed brain size, as well as measurements of individual brain regions.

| | **Model 1** | **Model 2** | **Model 3** | **Model 4** | **Model 5** | **Model 6** | **Model 7** | **Model 8** | **Model 9** | **Model 10** |
|---|---|---|---|---|---|---|---|---|---|---|
| Foramen magnum diameter (mm) | 6.70 | 5.83 | 6.41 | 5.83 | 6.12 | 6.70 | 8.74 | 6.12 | 6.41 | 5.54 |
| Endocast length[1] (mm) | 32.05 | 34.09 | 62.64 | 37.59 | 31.18 | 29.72 | 57.69 | 27.68 | 31.47 | 29.14 |
| Maximum endocast width[2] (mm) | 15.44 | 13.69 | 20.69 | 15.44 | 15.44 | 19.81 | 20.10 | 15.15 | 11.65 | 12.53 |
| Minimum endocast width (mm) | 6.70 | 7.28 | 6.99 | 6.99 | 6.99 | 7.87 | 8.16 | 6.99 | 7.28 | 6.99 |
| Maximum endocast depth[3] (mm) | 13.69 | 16.03 | 19.52 | 17.19 | 15.15 | 18.06 | 16.90 | 13.40 | 17.48 | 16.32 |
| Maximum width:length ratio of endocast | 0.48 | 0.40 | 0.33 | 0.41 | 0.50 | 0.67 | 0.35 | 0.55 | 0.37 | 0.43 |
| Endocast:BSL ratio (%) | 43.31 | 46.07 | 84.65 | 50.79 | 42.13 | 40.16 | 77.96 | 37.41 | 42.52 | 39.37 |
| Volume of the whole endocast ($mm^3$) | 1773.13 | 2293.80 | 4427.12 | 1922.47 | 1876.38 | 2462.71 | 7050.32 | 1590.54 | 2288.99 | 1916.19 |
| Length of olfactory bulb casts[4] (mm) | 7.28 | 7.87 | 19.52 | 8.16 | 6.12 | 6.70 | 9.91 | 5.83 | 8.16 | 5.24 |
| Maximum width of both olfactory bulbs (mm) | 9.03 | 7.58 | 7.28 | 15.73 | 8.16 | 9.62 | 12.82 | 6.99 | 9.62 | 7.87 |
| Maximum olfactory bulb depth[5] (mm) | 3.50 | 2.33 | 7.58 | 6.12 | 2.33 | 14.86 | 13.40 | 2.33 | 5.83 | 4.95 |
| Endocast width at the transition between the olfactory bulbs and cerebral hemispheres (mm) | 6.99 | 7.28 | 6.99 | 7.87 | 7.28 | 7.87 | 9.03 | 6.99 | 7.58 | 7.28 |

| | | | | | | | | | | |
|---|---|---|---|---|---|---|---|---|---|---|
| Maximum width:length ratio of the olfactory bulbs | 1.24 | 0.96 | 0.37 | 1.93 | 1.33 | 1.43 | 1.29 | 1.20 | 1.18 | 1.50 |
| Length of cerebral hemisphere casts[6] (mm) | 13.69 | 16.61 | 34.38 | 22.44 | 16.61 | 15.73 | 27.68 | 11.36 | 14.28 | 14.86 |
| Maximum width of both cerebral hemispheres[7] (mm) | 9.03 | 9.32 | 8.45 | 8.45 | 11.95 | 8.74 | 11.07 | 8.45 | 9.91 | 7.87 |
| Maximum width:length ratio of the cerebral hemispheres | 0.66 | 0.56 | 0.25 | 0.38 | 0.72 | 0.56 | 0.40 | 0.74 | 0.69 | 0.53 |
| Anteroposterior length of the slope of the cerebellum[8] (mm) | 15.44 | 9.32 | 9.03 | 7.28 | 8.45 | 7.28 | 20.10 | 10.20 | 9.03 | 9.32 |
| Angle of the cerebellum slope[9] (°) | 28.6 | 38.3 | 46.8 | 43.4 | 38.8 | 47.3 | 21.8 | 32.2 | 39.4 | 45.5 |
| Maximum cerebellum depth[10] (mm) | 11.65 | 12.24 | 13.69 | 12.24 | 11.95 | 11.07 | 14.28 | 11.36 | 11.95 | 11.07 |
| Width of the cerebellum between the paraflocculars lobes (mm) | 8.16 | 7.58 | 7.87 | 8.16 | 8.74 | 8.45 | 10.49 | 7.28 | 7.58 | 8.16 |
| Maximum width:length ratio of cerebellum and paraflocculllar lobes | 0.53 | 0.81 | 0.87 | 1.12 | 1.03 | 1.16 | 0.52 | 0.71 | 0.84 | 0.88 |
| Length of left paraflocculars lobe (mm) | 2.91 | 2.91 | 5.24 | 3.50 | 2.62 | 4.95 | 4.37 | 3.21 | 1.75 | 2.04 |
| Length of right paraflocculars lobe (mm) | 4.08 | 3.50 | 7.28 | 3.79 | 4.08 | 6.41 | 4.95 | 4.37 | 2.04 | 2.33 |

**Table 5.2. (continued)**

| | Model 11 | Model 12 | Model 13 | Model 14 | Model 15 | Model 16 | Model 17 | Model 18 | Model 19 |
|---|---|---|---|---|---|---|---|---|---|
| Endocast length[1] (mm) | 29.72 | 28.85 | 27.39 | 25.35 | 33.80 | 30.30 | 36.42 | 28.85 | 32.63 |
| Foramen magnum diameter (mm) | 6.12 | 4.66 | 6.12 | 6.12 | 6.41 | 4.66 | 6.12 | 5.83 | 5.83 |
| Maximum endocast width[2] (mm) | 14.86 | 12.82 | 17.48 | 14.57 | 13.69 | 19.81 | 11.95 | 13.99 | 15.15 |
| Minimum endocast width (mm) | 6.70 | 6.70 | 6.99 | 6.70 | 5.54 | 6.99 | 6.70 | 6.70 | 6.70 |
| Maximum endocast depth[3] (mm) | 19.52 | 16.32 | 16.61 | 14.28 | 15.44 | 16.32 | 16.61 | 16.61 | 14.28 |
| Maximum width:length ratio of endocast | 0.50 | 0.44 | 0.64 | 0.57 | 0.41 | 0.65 | 0.33 | 0.48 | 0.46 |
| Endocast:BSL ratio (%) | 40.16 | 38.98 | 37.01 | 34.26 | 45.67 | 40.95 | 49.22 | 38.98 | 44.10 |
| Volume of the whole endocast ($mm^3$) | 2002.44 | 1840.49 | 1720.80 | 1594.78 | 1690.14 | 1845.02 | 1825.78 | 1908.87 | 1826.12 |
| Length of olfactory bulb casts[4] (mm) | 6.41 | 4.95 | 5.24 | 4.08 | 7.28 | 6.99 | 9.32 | 5.54 | 6.99 |
| Maximum width of both olfactory bulbs (mm) | 8.74 | 7.28 | 8.16 | 6.70 | 6.99 | 8.16 | 11.07 | 7.87 | 8.96 |
| Maximum olfactory bulb depth[5] (mm) | 3.21 | 4.95 | 5.54 | 5.24 | 2.91 | 3.50 | 4.66 | 2.91 | 2.33 |
| Endocast width at the transition between the olfactory bulbs and cerebral hemispheres (mm) | 6.70 | 6.70 | 6.99 | 6.70 | 5.54 | 6.99 | 7.87 | 6.70 | 7.28 |
| Maximum width:length ratio of the olfactory bulbs | 1.36 | 1.47 | 1.56 | 1.64 | 0.96 | 1.17 | 1.19 | 1.42 | 1.28 |
| Length of cerebral hemisphere casts[6] (mm) | 16.03 | 16.61 | 14.28 | 13.40 | 16.90 | 13.99 | 18.06 | 13.99 | 16.61 |
| Maximum width of both cerebral hemispheres[7] (mm) | 9.62 | 8.45 | 9.03 | 9.62 | 8.74 | 8.16 | 8.74 | 8.74 | 8.16 |

| | | | | | | | | | |
|---|---|---|---|---|---|---|---|---|---|
| Maximum width:length ratio of the cerebral hemispheres | 0.60 | 0.51 | 0.63 | 0.72 | 0.52 | 0.58 | 0.48 | 0.63 | 0.49 |
| Anteroposterior length of the slope of the cerebellum[8] (mm) | 7.28 | 7.28 | 8.16 | 7.87 | 9.62 | 9.32 | 9.32 | 9.62 | 9.03 |
| Angle of the cerebellum slope[9] (°) | 42.9 | 37.4 | 39.8 | 26.6 | 36.9 | 39.9 | 39.9 | 36.4 | 44.0 |
| Maximum depth of the cerebellum[10] (mm) | 11.36 | 11.07 | 12.24 | 11.95 | 11.36 | 12.82 | 10.78 | 10.78 | 10.70 |
| Width of the cerebellum between the paraflocculars lobes (mm) | 9.03 | 7.28 | 7.58 | 8.45 | 8.16 | 8.16 | 7.87 | 8.16 | 8.16 |
| Maximum width:length ratio of cerebellum and paraflocculllar lobes | 1.24 | 1.00 | 0.93 | 1.07 | 0.85 | 0.88 | 0.84 | 0.85 | 0.90 |
| Length of left paraflocculars lobe (mm) | 3.50 | 2.62 | 5.24 | 3.21 | 2.91 | 5.83 | 2.04 | 2.91 | 3.50 |
| Length of right paraflocculars lobe (mm) | 2.62 | 2.91 | 4.95 | 2.91 | 2.62 | 5.83 | 2.04 | 2.91 | 3.50 |

[1] Measured from the anterior limit of olfactory bulbs to the foramen magnum in dorsal view; [2] Including the cerebellum and paraflocculars lobes; [3] Measured from a horizontal line taken at the dorsal and ventral boundaries of the endocast; [4] Measured in dorsal view; [5] Measured in lateral view; [6-8] Measured in dorsal view; [9] Measured in lateral view from a horizontal line on the dorsal surface of the endocast; [10] Measured from the ventral limit of the cerebellum to the dorsal surface directly above it.

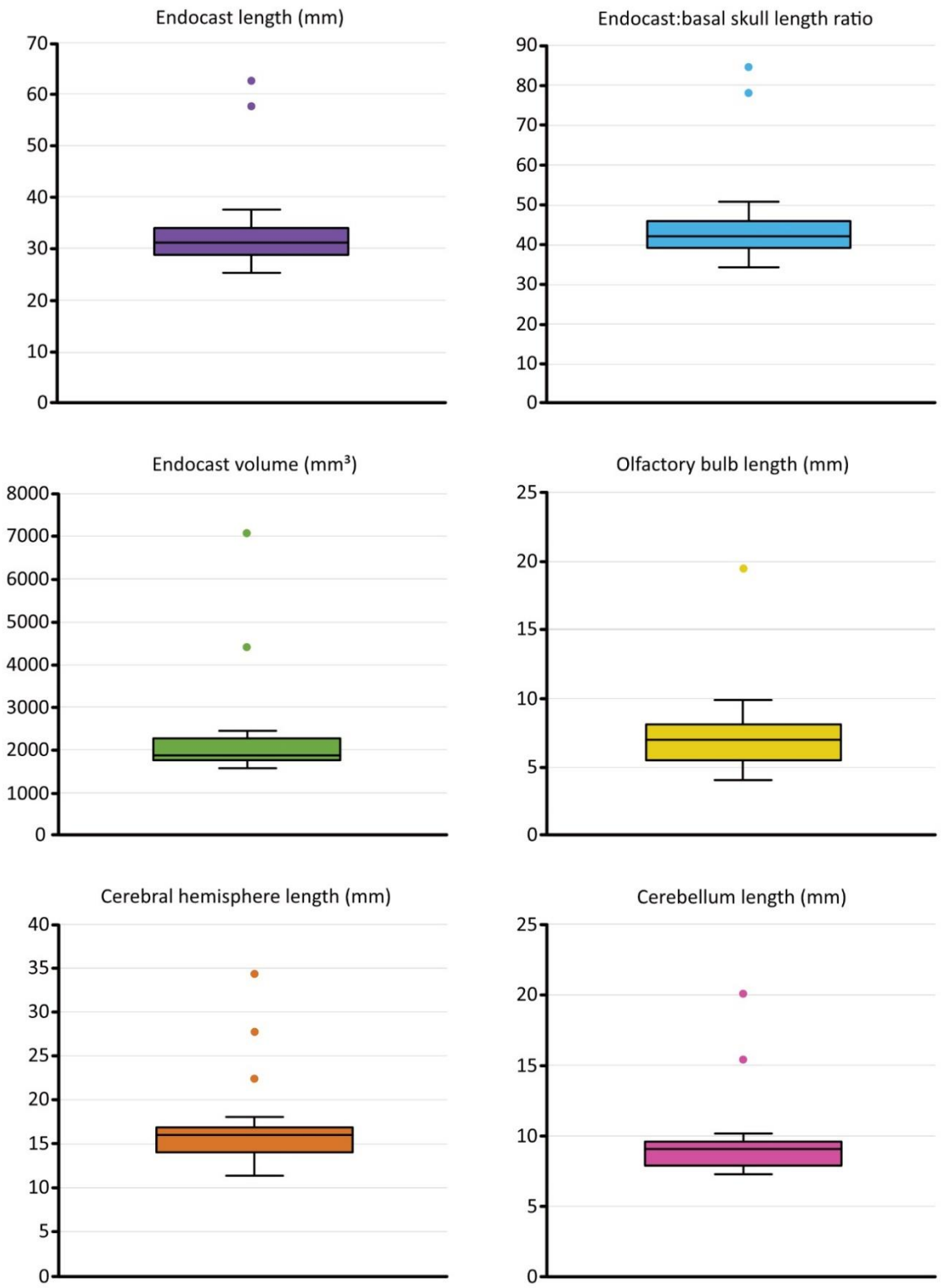


**Figure 5.11.** Box plots showing the range in collected measurements for the main reconstructed brain regions of the 19 endocasts. While many of the models have somewhat similar dimensions, there are some outlier endocasts that highlight the modeller variability in the size of each brain region measured.

When quantifying the size of individual morphological components, the olfactory bulbs range in length from 4.08 mm (model 14) to 9.32 mm (model 17), if excluding the anomalously long model 3, which has 19.52 mm long olfactory bulbs. The average olfactory bulb width is 8.42 mm, excluding model 4 which has anomalously wide olfactory bulb casts, as shown in figures 5.6 and 5.8. The area of greatest variation is in the dorsoventral depth of the olfactory bulbs, which range between 2.33 (models 2, 5, 8 and 19) and 14.86 mm (model 6), with the olfactory bulbs of this latter model concealed within the additional reconstruction of parts of the olfactory tracts. Model 7 has similarly deep reconstructions of the olfactory bulb casts (13.40 mm), contrasting with an average olfactory bulb depth of 5.18 mm and average olfactory bulb width:length ratio of 1.29.

The reconstructed length of *Thrinaxodon*'s cerebral hemispheres varies between 11.36 mm (model 8) and 34.38 mm (model 3), with an average length of 17.24 mm (or 16.28 mm when removing the anomalously long reconstructions of model 3). The width of the cerebral hemispheres is more consistent, ranging between 7.87 mm (model 10) and 11.95 mm (model 5). The cerebral hemispheres have an average width:length ratio of 0.56. After the cerebral hemispheres transition into the cerebellum, the length of the cerebellum ranges between 7.28 mm (models 4, 6, 11 and 12) and 20.10 mm (model 7). However, model 7 has an anomalously long reconstruction of the foramen magnum cast, hence removing this model gives an average cerebellum length of 9.05 mm. The dorsal surface of the cerebellum slopes posteriorly towards the foramen magnum by an average of 38.2° (minimum 21.8° and maximum 47.3°). The width of the cerebellum is quite consistent, ranging between 7.28 mm (models 8 and 12) and 10.49 mm (model 7). However, extending laterally from the cerebellum, the parafloccular lobes show significant variation which can be observed in figures 5.6 and 5.9. The minimum and maximum lengths of the left parafloccular lobe casts are 1.75 mm (model 9) and 5.83 mm

(model 16), respectively. The minimum and maximum lengths of the right paraflocculer lobe casts are 2.04 mm (models 9 and 17) and 7.28 mm (model 3), respectively.

Principal component analysis (figure 5.12) identified variation in the reconstructed morphology of *Thrinaxodon liorhinus'* brain based on landmarking data. The first four principal components (PC; or variables) account for 69.4% of the variation (PC1: 29.7%, PC2: 16.6%, PC3: 15.3%, PC4: 7.8%, PC5 – 18: 30.6%) in endocast outline morphology. When comparing PC1/PC2, PC1/PC3 and PC2/PC3, all PCA plots show an overall clustering of the reconstructed endocasts, suggesting there is a large amount of similarity in overall reconstructed brain morphology, with some outliers (models 3, 4, 6, 7 and 17). With the exception of model 17, all of these outliers are within the group of modellers who have completed undergraduate or postgraduate studies in palaeontology (shown in pink in figure 5.12). From analysing figure 5.12, it is possible to tentatively identify that PC1 likely corresponds to endocast length, with more elongated models plotting with positive PC1 values, consistent with the positioning of model 3 as an outlier. However, the potential morphological components influencing the distribution of the endocasts along PC2 and PC3 are not clearly identifiable from these plots alone. The most prominent, and surprising, trend is that many of the outlier models are those generated by modellers who have completed formal palaeontological education.

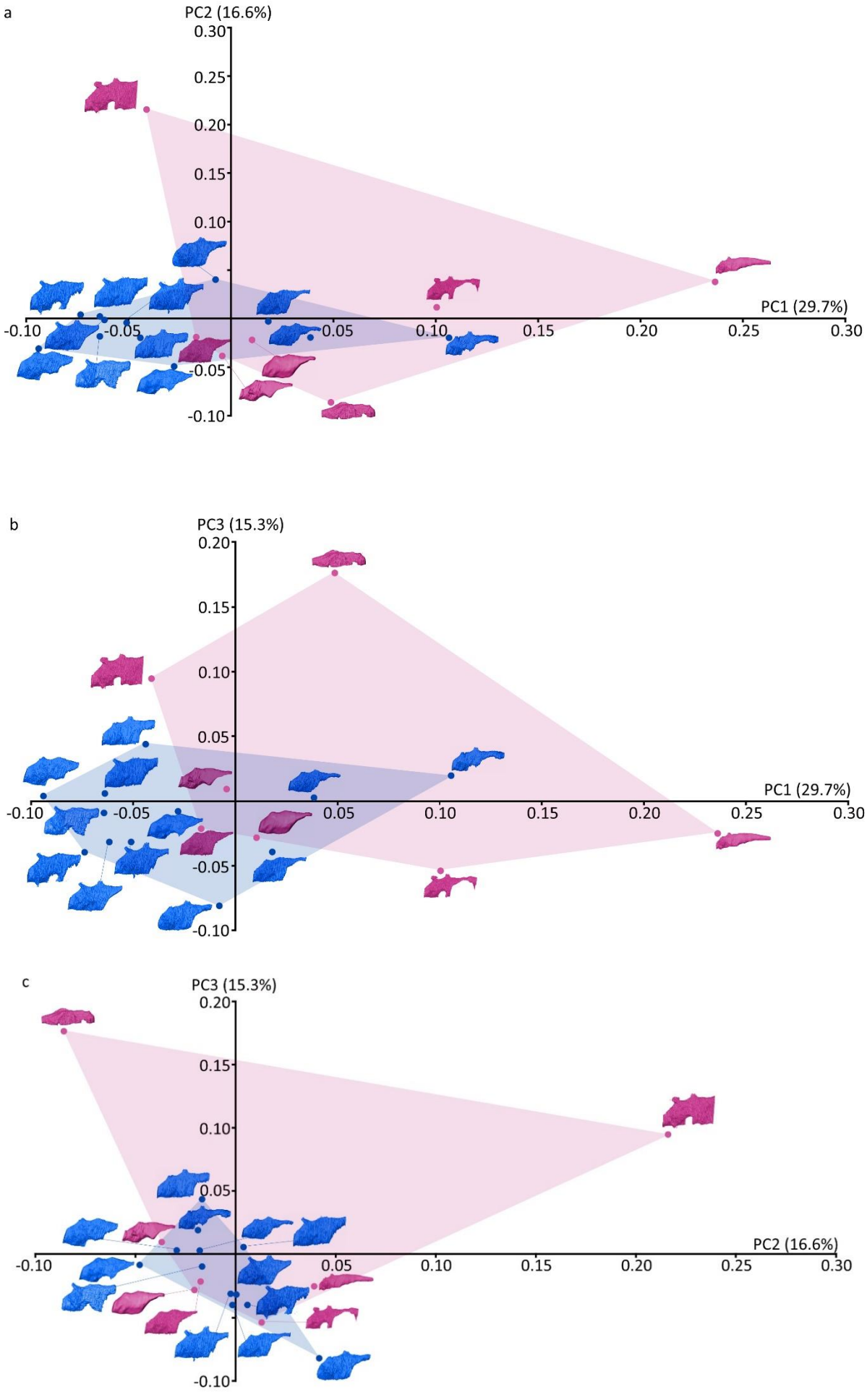
a
PC2 (16.6%)
0.30
0.25
0.20
0.15
0.10
PC1 (29.7%)
-0.10
-0.05
0.05
0.10
0.15
0.20
0.25
0.30
-0.05
-0.10
b
PC3 (15.3%)
0.20
0.15
0.10
0.05
PC1 (29.7%)
-0.10
-0.05
0.05
0.10
0.15
0.20
0.25
0.30
-0.05
-0.10
c
PC3 (15.3%)
0.20
0.15
0.10
0.05
PC2 (16.6%)
-0.10
0.05
0.10
0.15
0.20
0.25
0.30
-0.10

**Figure 5.12. (previous page).** Principal component analysis plots generated from variations in surface morphology of the 19 reconstructed endocasts, as identified through 3D landmarks. **(a)** PC1/PC2, **(b)** PC1/PC3, **(c)** PC2/PC3. In all plots, blue endocasts are those created by modellers 8 to 19, who have not completed a formal palaeontological education (although modeller 8 has a postgraduate degree in geology). Pink models denote those model makers who have completed undergraduate or postgraduate studies in palaeontology**.** The majority of the endocasts cluster together indicating similar overall morphology (irrespective of size differences), but the outlier models are consistently among modellers who have a palaeontological education.

One way to disentangle which features are contributing to the variation in principal components is by consulting loading plots for the data (figure 5.13). The plots reveal that the length of the cerebral hemispheres and whole endocast are represented by principal component one (figure 5.13a). The angle of the cerebellum (measured from a horizontal line on the dorsal surface) is the most significant contributor to the distribution of endocasts along PC2 (figure 5.13b), while PC3 is predominantly impacted by the width of the endocast and depth of the olfactory bulbs (figure 5.13c). These trends cannot be easily discerned from the endocast models in figure 5.12 alone, but when combined with the loading plots, the trends highlight some of the areas of greatest subjectivity when modelling *Thrinaxodon*'s brain, that is, the lack of ventral and anterior boundaries of the braincase by which the brain reconstruction can be constrained.

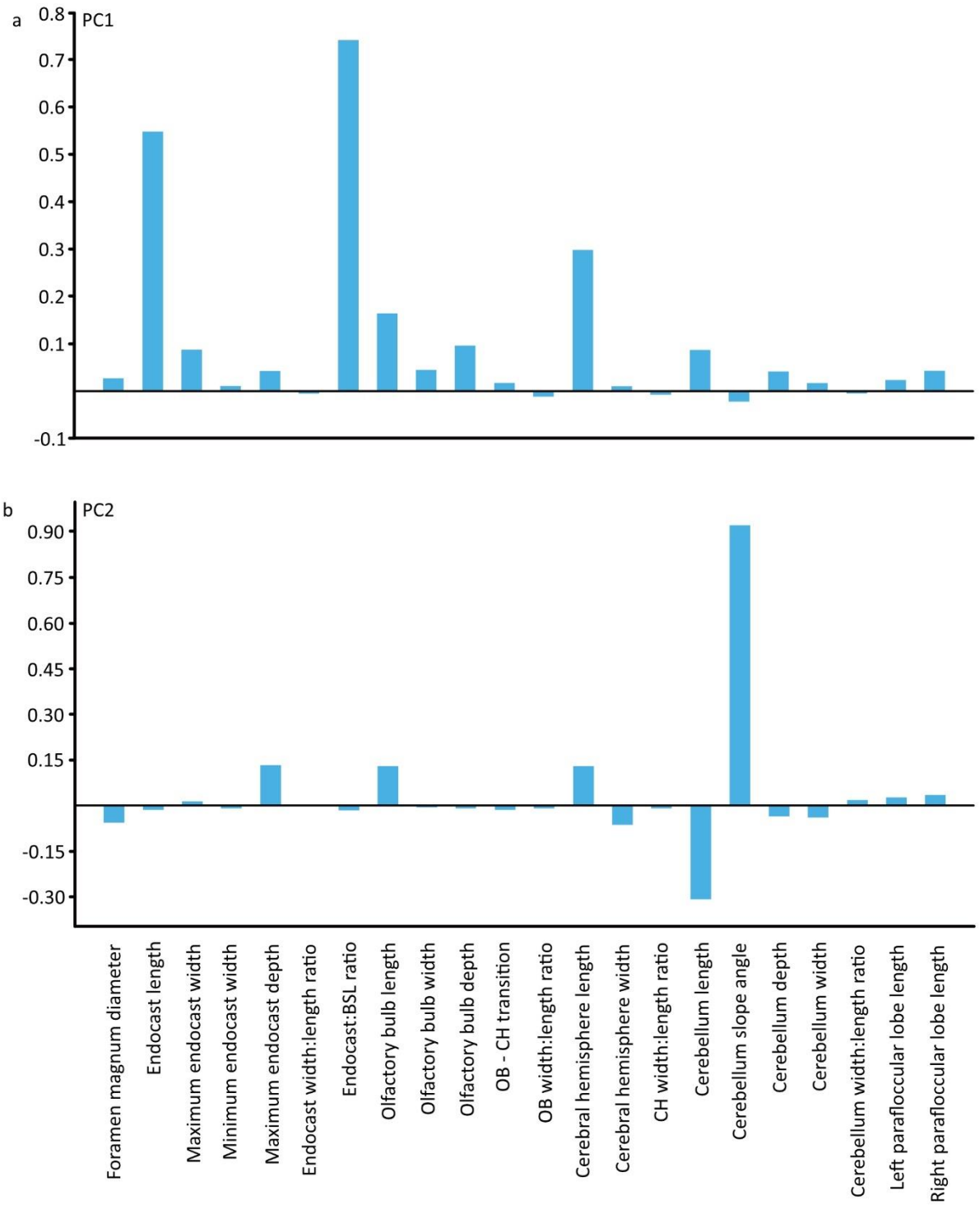
a
PC1
0.8
0.7
0.6
0.5
0.4
0.3
0.2
0.1
-0.1
b
PC2
0.90
0.75
0.60
0.45
0.30
0.15
-0.15
-0.30
Foramen magnum diameter
Endocast length
Maximum endocast width
Minimum endocast width
Maximum endocast depth
Endocast width:length ratio
Endocast:BSL ratio
Olfactory bulb length
Olfactory bulb width
Olfactory bulb depth
OB - CH transition
OB width:length ratio
Cerebral hemisphere length
Cerebral hemisphere width
CH width:length ratio
Cerebellum length
Cerebellum slope angle
Cerebellum depth
Cerebellum width
Cerebellum width:length ratio
Left paraflocculus lobe length
Right paraflocculus lobe length

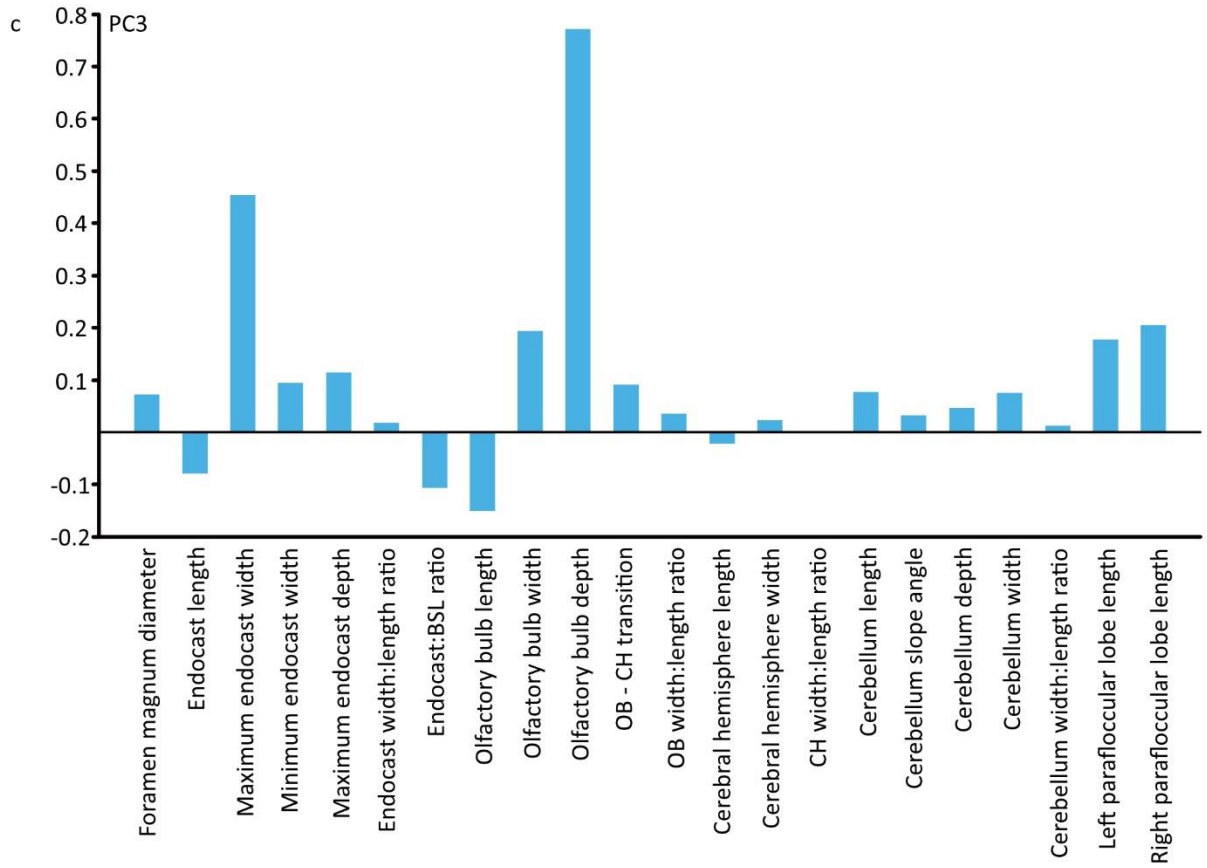


**Figure 5.13. (also previous page).** Loading plots associated with **(a)** PC1, **(b)** PC2 and **(c)** PC3 revealing the endocast region contributing most to variation. Strongly positive and negative loading values correspond to the endocast measurements that have the greatest influence on the principal component distribution of the 19 endocasts (and as such the variability incorporated in the endocasts).

### 5.3.3. Endocranial morphology and estimating cognitive capabilities

The endocranial morphology of *Thrinaxodon liorhinus* can provide insights into the species' potential cognitive capabilities through calculation of the encephalisation quotient (EQ), which is a relative measure of intelligence based on endocast volume. The EQ value is commonly used to evaluate brain evolution between cynodonts, mammaliaforms and mammals (Rowe *et al*., 2011; Rodrigues *et al*., 2019; Hoffman *et al*., 2021; Kerber *et al*., 2023).

To calculate the EQ values of *Thrinaxodon liorhinus*, the estimated body mass was calculated as 648g, using an equation for gracile cynodonts. The EQ values for each endocast are reported in table 5.3 and the variation in calculated EQ values is highlighted in figure 5.14. Encephalisation quotients estimated by the equation from Jerison (1973) are smaller than the EQ values produced by the equation from Manger (2006). For $EQ_{Jerison}$, the values range between 0.18 (model 8) and 0.82 (model 7). However, model 3 also has an anomalously higher EQ value of 0.51 due to the larger reconstructed endocranial volume at the anterior and posterior of the endocast. For $EQ_{Manger}$, the values range between 0.26 (models 2 and 8) and 1.17 (model 7). For *Thrinaxodon liorhinus*, the average $EQ_{Jerison}$ value is 0.26 and for $EQ_{Manger}$ is 0.38. Figure 5.14 shows that while many of the endocasts have EQ values falling within a similar range, there are three models that form outliers (models 3 and 7, plus model 6 to a lesser extent), with higher values than for the rest of the brain models.

**Table 5.3.** Encephalisation quotients calculated for each of the *Thrinaxodon* brain reconstructions.

| Model | Endocast volume (EV) in $cm^3$ | EQ value (Jerison) | EQ value (Manger) |
|---|---|---|---|
| **1** | 1.77313 | 0.21 | 0.29 |
| **2** | 2.2938 | 0.19 | 0.26 |
| **3** | 4.42712 | 0.51 | 0.74 |
| **4** | 1.92247 | 0.22 | 0.32 |
| **5** | 1.87638 | 0.22 | 0.31 |
| **6** | 2.46271 | 0.29 | 0.41 |
| **7** | 7.05032 | 0.82 | 1.17 |
| **8** | 1.59054 | 0.18 | 0.26 |
| **9** | 2.28899 | 0.27 | 0.38 |
| **10** | 1.91619 | 0.22 | 0.32 |
| **11** | 2.00244 | 0.23 | 0.33 |

| | | | |
|---|---|---|---|
| **12** | 1.84049 | 0.21 | 0.31 |
| **13** | 1.72080 | 0.20 | 0.29 |
| **14** | 1.59478 | 0.19 | 0.27 |
| **15** | 1.69014 | 0.20 | 0.28 |
| **16** | 1.84502 | 0.21 | 0.31 |
| **17** | 1.82578 | 0.21 | 0.30 |
| **18** | 1.90887 | 0.22 | 0.32 |
| **19** | 1.82612 | 0.21 | 0.30 |

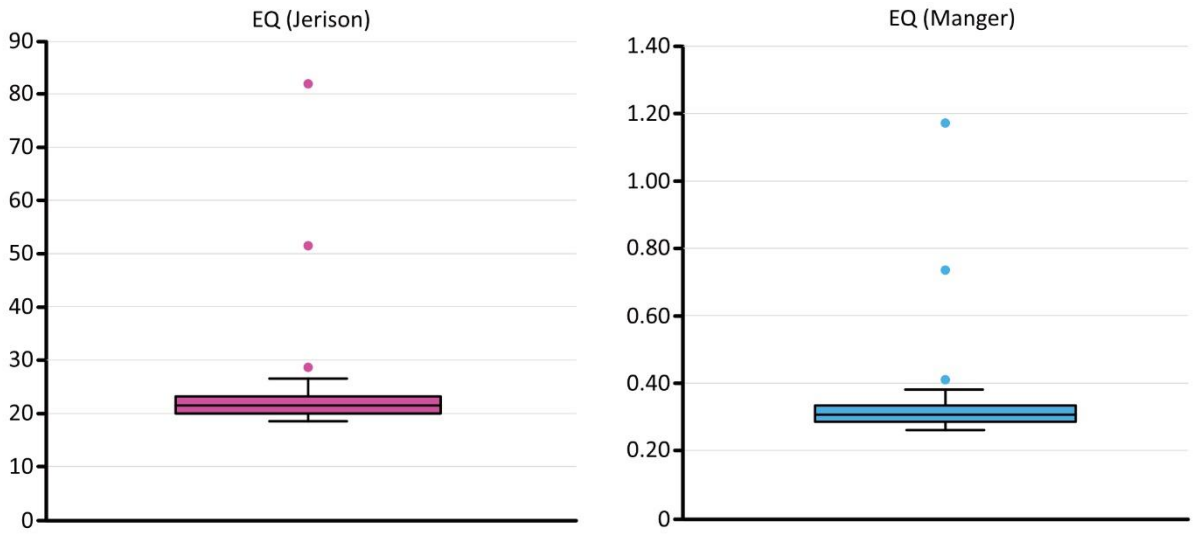


**Figure 5.14.** Box plots showing the range of EQ values calculated for the 19 brain models based on the equations of Jerison (1973) and Manger (2006). Many of the endocast EQ values fall within a similar range, but the anomalously longer models (3 and 7) form outliers and highlight the modeller induced variability for a single *Thrinaxodon* specimen.

## 5.4. Discussion

This study aimed to identify and quantify variation among endocranial reconstructions of a single specimen of *Thrinaxodon liorhinus.* Almost 90% of the models are generally similar in endocranial morphology, with models 3 and 7 being consistently different in size and morphology. For the majority of models, the endocast lengths are similar, the cerebellum has

a recurring shape and the parafloccular lobes are reconstructed in the same location (although to varying lengths). However, some modellers did include parts of the inner ear erroneously. The most inconsistently reconstructed brain regions are the olfactory bulbs (varying in size and shape), whether the hypophyseal cast is defined or not, and whether dorsal projections of the vermis or sinus and pineal body were included as part of the endocast or not. On average, the endocasts comprised 42% of *Thrinaxodon*'s skull length, which corresponds well with the endocast:BSL ratios observed in the Late Triassic cynodonts *Riograndia guaibensis* and *Brasilitherium riograndensis,* with endocast:BSL ratios of 44% (Rodrigues *et al*., 2019) and 46.5% (Rodrigues *et al*., 2014), respectively, and 52.9% in the extant opossum *Monodelphis domestica* (Macrini *et al*., 2007b).

The variation in the reconstructed morphology of the olfactory bulbs is predominantly caused by the ventral surface being unconstrained by basicranial bones, as seen in other early cynodonts (Laaß *et al*., 2017a), although uncommon in therapsids more widely (Balanoff and Bever, 2020). Without full ossification in the nasal region, and with an unknown volume of blood vessels and sinuses also likely occupying the olfactory bulb cavity (Laaß *et al*., 2017a), a definitive interpretation of *Thrinaxodon*'s olfactory bulb morphology cannot be made. Size variations in olfactory bulb reconstructions present a challenge when comparing their size and volumes with extant analogues, such as the opossum, to make conclusions about olfactory acuity and mode of life. However, many of the undergraduate modellers reconstructed olfactory bulbs with similar dorsoventral depths, even if the shapes do not have an organic appearance. By comparing the morphology of *Thrinaxodon*'s reconstructed olfactory bulbs with those of later cynodonts, insights into relative olfactory acuity compared to other species along the mammalian evolutionary lineage can be gained.

A recent study has identified loosely articulated, cancellous bone in the olfactory region of several basal cynodonts (including *Cynosaurus, Galesaurus* and *Thrinaxodon*; Benoit *et al*., 2017). This bone likely corresponds to the orbitosphenoid which forms part of the floor of the olfactory region and, where present, could help to define the olfactory bulbs. However, the orbitosphenoids are not preserved in specimen UCMP 40466, hampering the modeller's ability to accurately reconstruct the nasal region of *Thrinaxodon*'s brain. While a better-preserved specimen would be valuable in this case, UCMP 40466 represents a typical condition where the orbitosphenoids are rarely, or incompletely, preserved. The specimen was also useful as it contains minimal plastic or brittle deformation to affect the reconstruction of the rest of the brain. While the scan quality is somewhat poor, it reflects the limitation of some CT scans; particularly historical scans or those with low internal contrast. A future study would benefit from using a higher resolution µCT scan for a *Thrinaxodon* specimen that has the orbitosphenoids intact. The results from such a study could then be compared with a similar study conducted on mammalian specimens with fully ossified braincases (and where the soft tissue anatomy of the brain is known) to assess if endocranial reconstructions always show variation.

It should be recognised that the endocasts are generated using the inner bone boundary of the braincase as the outer limit of the endocast. This approach allows for consistency within the segmentation process but does not account for any intracranial fluids and tissues that may have surrounded the brain in life (Macrini *et al*., 2007b; Balanoff and Bever, 2020), hence potentially inflating brain volume and inaccurately determining relative intelligence based on calculated encephalisation quotients. However, as using the inner surface of the endocranial cavity as the segmentation boundary is standard practice for endocranial reconstructions (Balanoff *et* al., 2016; Balanoff and Bever, 2020), the calculated values can still be compared

relatively with other cynodonts to draw conclusions about *Thrinaxodon*'s cognitive capabilities.

As such, based on the models produced in this study, encephalisation quotients for *Thrinaxodon* averaged 0.26 ($EQ_{Jerison}$) and 0.38 ($EQ_{Manger}$), but ranged between 0.18 and 1.17. If the endocasts were considered in isolation, then the endocranial volumes, and therefore EQ values, would have considerable implications for relative cognitive capabilities. For example, an EQ of 0.18 corresponds well with some other cynodonts including *Massetognathus* (0.15; Quiroga, 1980a), *Exaeretodon* (0.15; Quiroga, 1980a), *Probelesodon* (0.18; Quiroga, 1979) and *Probainognathus* (0.17; Quiroga, 1980a). However, the upper EQ value of 1.17 better matches more derived species, such as the extinct monotreme *Obdurodon* (1.00; Macrini *et al*., 2006), suggesting great care needs to be taken when using EQ values as a measure of intelligence as the method is limited by the accuracy of the reconstructed endocast volume, the reliability of estimating body mass from skull length where no postcranial skeleton is available and variation resulting from the equation used to calculate the EQ value. It is recommended that instead, studies consider relative brain proportions (both in terms of volume and linear measurements) to relatively compare brain components to make inferences about cognitive and sensory capabilities, as explored by Zelenitsky *et al*. (2009) and Rodrigues *et al*. (2019).

The PCA plots (figure 5.12) offer valuable insights into whether prior experience of palaeontology or digital segmentation techniques influence the brain reconstruction. Surprisingly, all of the outliers (models 3, 4, 6 and 7, with the exception of model 17) are within the group of modellers who have completed undergraduate or postgraduate studies in palaeontology. It was anticipated that prior knowledge of biological structures would make brain reconstructions more consistent, but this did not appear to be the case for this study of

*Thrinaxodon*'s brain. Interestingly, most of the non-experienced modellers produced somewhat similar overall brain reconstructions for *Thrinaxodon* and these broadly shared the same morphology as the endocasts created by the two modellers with knowledge of fossil brain anatomy (models 1 and 2). Conversely, the outlier models (excluding model 17) were generated by modellers with and without prior experience of segmentation software. Similarly, modellers with and without segmentation experience mapped with the undergraduate students who had no palaeontological or segmentation knowledge. Therefore, digital reconstruction experience alone did not necessarily improve the consistency of the endocast produced for *Thrinaxodon*.

Adding more landmarks using automated landmarking techniques (for example, Fischer *et al*., 2022) may capture the morphological differences more accurately by increasing the number of comparable landmark coordinates, providing a better picture of inter-modeller variation. No known attempts have been made to quantify variability in endocranial reconstructions. However, Broyde *et al.* (2021) used a comparable concept to investigate reconstruction variability in a different anatomical structure, asking three modellers to reconstruct rodent jaw muscles. The study found that the modellers reconstructed different muscle proportions, with 70.3%, 12.3% and 94.6% error in the volume of individual muscles (Broyde *et al.*, 2021), which ultimately altered interpretations of bite force and bone stress during finite element analysis.

One way to remove inter-modeller variability would be to auto-generate endocranial masks in segmentation software using, for example, the endomaker algorithm in R proposed by Profico *et al*. (2020). Herbst *et al*. (2022) proposed a different 3D modelling method which uses Python code in Blender to model muscle volumes. Given that variation in soft tissue

reconstruction has been observed both here and in Broyde *et al.* (2021), automated endocast generation using coding scripts could be a valuable tool to create more objective and repeatable models. These techniques would be particularly beneficial for studies that would traditionally require numerous modellers to contribute to a project due to time and resource constraints, eliminating human subjectivity when interpreting the CT scan. Additionally, the generation of digital datasets facilitates the openness and sharing of data to increase international accessibility to digitised fossils (Cunningham *et al*., 2014). However, it also worth considering how realistic it may be to automate endocast generation, particularly for fossils that are prone to deformation, lack full braincase ossification or contain a low-density contrast sediment infill of the brain cavity, which could all interfere with the output of the algorithm or code (Buzi *et al*., 2023). It is beneficial to test new automated methods on specimens where we have either an understanding or physical specimens of a species, for example, the study by Buzi *et al*. (2023) which used the *Icex* tool in R to model the brain of homininds, which are quite similar to modern humans and, therefore, permit verification of the endocasts produced in R. Perhaps in the future, machine or deep learning could advance the field of virtual palaeontology too (Yu *et al*., 2022).

In this study, modeller variation has been shown to exist among the reconstructions of brain anatomy of a single *Thrinaxodon* specimen segmented in Spiers. As there are numerous other digital segmentation software available (such as Amira, Avizo, Mimics, VG Studio, Spiers and Slicer; Lautenschlager, 2016), it would be valuable to investigate whether there is any variation in the endocasts generated in different software based on the diverse functionalities that segmentation software can offer. For example, in Spiers, CT data is segmented in coronal orientation (snout to foramen magnum) using a paintbrush tool, with interpolation available to speed up the segmentation process. However, Avizo and Slicer (among other software)

offer the facility to also generate masks in sagittal (left to right) and horizontal (top to bottom) orientations, which may assist in identifying skeletal elements associated with the braincase compared to, for example, the inner ear. Avizo and Slicer also have magic wand tools, which can auto-populate the brain cavity with a mask that can then be edited with a paintbrush tool. Generating an endocranial reconstruction in Spiers, Avizo and Slicer would allow an evaluation of whether editing masks in numerous orientations, interpolating between slices or auto populating a mask has an influence on the endocast produced. Whether these functions alter the accuracy of the endocast created would be interesting to explore for *Thrinaxodon liorhinus*, but as the braincase is not fully ossified, a comparison would need to be made with the outputs generated for a species that does have a fully ossified braincase and for which the brain anatomy is known, such as the opossums *Didelphis virginiana* or *Monodelphis domestica*. However, investigating variation in endocast morphology arising from segmentation software used is beyond the scope of this study as modellers were not available to repeat the study in different iterations, and software licences for Avizo (or other commercial software) and computers with appropriate processing capabilities were not obtainable. Additionally, over time, objectivity becomes challenging as modellers gain experience with a dataset and familiarity with the segmenting process, making it difficult to disentangle variation arising from the modeller versus the software used.

## 5.5. Chapter summary

Digital endocranial reconstructions offer unparalleled access to specimens and facilitate non-destructive analysis of internal cranial features. This study presents the first attempt to quantify variation in brain reconstructions of *Thrinaxodon liorhinus*. While this is still a relatively small dataset, the inclusion of endocasts from 19 modellers presents the largest assessment of brain anatomy conducted for *Thrinaxodon* to date. Analysis of the endocasts

has shown that overall morphology is broadly similar between modellers with no prior palaeontological education or segmentation experience and modellers with both extensive digital reconstruction knowledge and expertise in fossil brain anatomy. While the endocasts produced by the two modellers with segmentation and mammal brain expertise were somewhat similar, this study did not show that prior knowledge of brain anatomy or segmentation software produced more consistent interpretations of *Thrinaxodon*'s brain morphology. Whether this conclusion would be true for other cynodonts with enclosed braincases would need further investigation to confirm.

The regions of greatest variability were the anterior and ventral boundaries of the olfactory bulbs, reconstruction of the hypophyseal cast and presence of dorsal features – principally, regions where ossification is lacking. As expected, the areas of most consistent size and shape were those constrained by skeletal elements, such as the cerebellum and foramen magnum, although there was still some variation in the reconstruction of these features. The differences in the endocast sizes were likely due to variations in the interpretation of greyscale values (based on the density of scanned material), identification of bone margins (including misinterpreting sediment fill as bone margins) and brain features in the CT scan and smoothing of structures between modellers.

Additional training in brain anatomy and interpreting CT skull data, particularly for cynodonts and mammalian taxa, may prove useful to generate more biologically accurate and consistent endocasts. Specimen UCMP 40466 may not have been an ideal specimen due to low scan resolution and absent cranial bones, but the small dataset was manageable for modellers inexperienced with brain anatomy, CT data and the segmentation process. While a perfectly preserved, fully ossified brain case of, for example, *Didelphis* or *Monodelphis* would have been

ideal for investigating modeller variation, that scenario does not reflect the reality of most palaeontological specimens which show considerable deformation or lack features due to their evolutionary placement. Therefore, this study provides a useful insight into evaluating how the brain morphology of *Thrinaxodon* may be interpreted from CT data. The results of this modeller variation study may be extrapolated for other basal cynodonts and mammalian taxa, possibly even for other vertebrate groups with poorly ossified braincases such as archosaurs, but care should be taken given the differences in brain anatomy and ossification. Consequently, other taxa would require their own investigation into variation within reconstructed brain morphology.

Future research could examine the influence of segmentation software on endocast outputs. Such a study would be valuable for identifying whether any particular software functions (such as generating masks in numerous orientations or using interpolation to auto-populate brain masks with magic wand tools) can improve the endocranial reconstruction produced. Given more time and resources, it would be beneficial to reconstruct the same specimen with and without interpolation, with and without the magic wand tool, and in coronal only versus all three orientations (coronal, sagittal and horizontal) to analyse the output models. However, over time, a single modeller would become very familiar with the endocranial anatomy of a particular specimen, hence testing the influence of segmentation software on brain reconstructions for a species with a fully ossified braincase (such as opossums) would be beneficial to limit the influence of modeller preconceptions on the endocasts generated.

Due to the inherent lack of soft tissues in the fossil record, validation of digital brain reconstructions with fossilised tissues is extremely rare. Natural casts of the brain cavity may prove useful for comparison, but for many extinct species, the endocranial cavity provides the

best approximation of brain shape and volume. There are steps that those conducting digital reconstructions can take to improve the consistency of the endocasts they generate, with suggested improvements to the segmentation process outlined below. Further best practice recommendations for generating endocasts are available in Balanoff *et al*. (2016).

- If possible, choose a specimen with good enclosure of the brain cavity by ossified elements and strong contrast between the bone and endocranial cavities to facilitate segmentation (using the bone boundary as the outer limit of the mask). However, this does not mean that specimens without fully ossified braincases should not be studied. In these instances, it is better to ensure that scan resolution is optimised by using µCT scan data rather than X-ray CT scan data.
- Where tenable, have one experienced individual generate all of the endocasts for a single study to minimise user-induced variation. If multiple modellers are involved in a study, provide a very clear protocol for how the endocast should be generated and, if possible, collect narratives from the modellers to ascertain how they interpreted the CT scan for a species.
- If there is no ossified boundary in part of the cranium, skeletal elements should be joined with straight lines rather than a curved line to prevent additional, potentially erroneous volume being incorporated into the reconstruction. While this shape may look unnatural, it enables greater consistency in the reconstruction method. It must be noted that this approach may lead to an underestimate of endocranial volume.
- Provide modellers with detailed training in cynodont and mammalian brain anatomy (or anatomical education relevant to the study species) to ensure all modellers can confidently interpret biological structures from the CT scan.
- Consider using software with additional segmentation functionalities, such as being able to generate a mask in coronal, sagittal and horizontal planes to better identify

endocranial features. For consistency among modellers (and to reduce segmentation time), use interpolation between every five or ten slices and manually fine tune the masks in between. Similarly, using the lasso tool may help capture smaller details that are only coarsely reconstructed when applied manually with a brush tool.

- However, generating an endocast using an automated technique (such as the endomaker algorithm in R) could eliminate the inter-modeller variation entirely and allow for much more rapid processing of CT data.

# CHAPTER SIX

# Environmental and evolutionary positioning of *Thrinaxodon liorhinus* in the development of the mammalian brain

## 6.1. The Triassic: a time of change

During the Early Triassic, when *Thrinaxodon* roamed Gondwana in what is now South Africa (Jasinoski *et al*., 2015), the Earth was changing. Following the Permian-Triassic mass extinction, the Early Triassic (251 to 247 Ma) was a period of ecosystem adjustment and recovery (Benton 1995) as the world adapted to changing seasonality, ozone depletion and acid rain on land, and anoxia and ocean acidification in the marine realm (Dal Corso *et al*., 2022). The Permian eruptions of the Siberian Traps released vast quantities of volcanogenic gasses and particulates which circulated in the atmosphere and caused a period of rising global temperatures during the Triassic (Gastaldo *et al*., 2021; Smith *et al*., 2022). As such, the Karoo Basin, where the majority of *Thrinaxodon* fossils have been discovered (Botha and Chinsamy, 2005; Abdala *et al*., 2013), experienced a warming climate with intense dry periods (Gastaldo *et al*., 2021; Smith *et al*., 2022). Increased aridity would have promoted large scale ecosystem change as vegetation died and fluvial systems transformed into ephemeral rivers, creating an environment with resource shortages not only for cynodonts but all animals living at that time (Smith 1995; Ward *et al*., 2000).

Environmental stressors forced the cynodonts (and other taxa) to adapt to survive. Huttenlocker (2014) reports a shift towards smaller body sizes in cynodonts living in the Karoo Basin after the Permian-Triassic mass extinction due to the scarcity of resources (Botha-Brink *et al*., 2016). Numerous studies have also identified a tendency towards faster growth rates,

younger breeding ages and reduced life spans as survival strategies employed by therapsids at this time (Botha-Brink and Angielczyk, 2010; Botha-Brink *et al*., 2016; Botha 2020), which may have contributed to the Middle Triassic diversification of cynodonts (Abdala 2004). Furthermore, it has been suggested that some cynodonts, including *Thrinaxodon*, may have taken to living in burrows and becoming dormant during dry periods to cope with limited food, water and shelter (Damiani *et al*., 2003; Fernandez *et al*., 2013). With the need for species to adapt quickly to the changing environment, was there any impact on brain development and behaviours in cynodonts?

Large brains are expensive to maintain (Isler and van Schaik, 2006; Benson-Amram *et al*., 2016). Given the environmental stressors present during the Early Triassic (Botha-Brink *et al*., 2016), smaller brains would seem to be more metabolically and biologically appropriate. *Thrinaxodon*'s brain (and the brains of other Early to Middle Triassic cynodonts) is relatively small in comparison to some later cynodonts (figure 6.1) and has a somewhat simplified morphology when compared to modern mammals (see chapter three for further brain morphology details). These smaller brain sizes are consistent with a period of miniaturisation which occurred following the Permian-Triassic mass extinction (Huttenlocker 2014; Botha-Brink et al., 2016; Lovegrove 2019), driven by the unpredictability of climate change and resource competition arising from the proliferation of archosaurs (including dinosaurs) during the Triassic (Sookias *et al*., 2012; Lovegrove 2019). Another period of miniaturisation occurred in the Early Jurassic following the end Triassic extinction event (Sookias *et al*., 2012), exemplified by the mammaliaforms *Morganucodon* and *Hadrocodium* (figure 6.1). Smaller brains could have facilitated the survival of pre-mammalian species as they explored new, potentially resource-limited ecological niches created by changing environmental and faunal compositions.

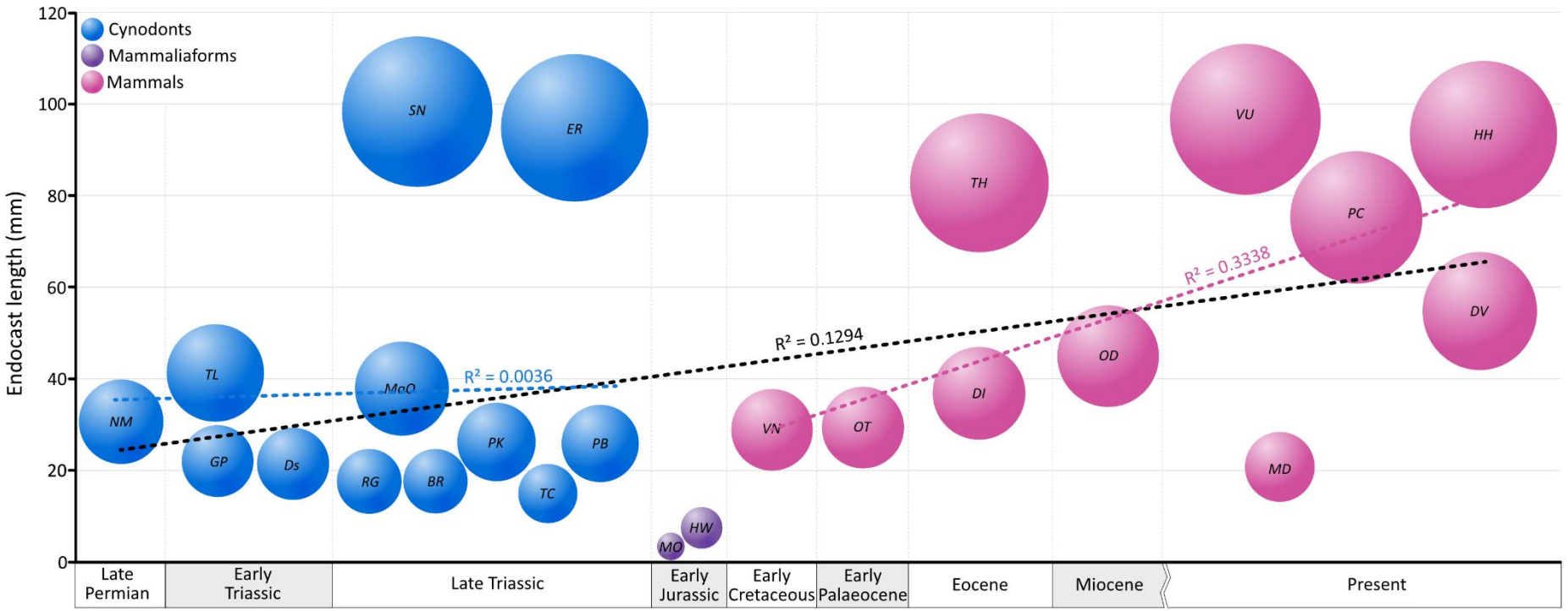


**Figure 6.1.** Reconstructed brain sizes for a sample of cynodonts, mammaliaforms and mammals through time. For the fossils found to date, cynodont brains generally tend to be smaller than mammal brains. The miniaturisation of Early Jurassic mammaliaforms is clearly visible, before brain sizes increase again in mammals (and remain noticeably larger than many of their cynodont ancestors). Endocast sources and species abbreviations overleaf.

**Figure 6.1 continued (previous page).** Endocast sources and species abbreviations: *Nshimbodon muchingaensis* (NM; Huttenlocker and Sidor, 2020), *Thrinaxodon liorhinus* (TL; this study), *Galesaurus planiceps* (GP; Pusch *et al*., 2019), *Diademodon sp.* (Ds; this study, appendix), *Riograndia guaibensis* (RG; Rodrigues *et al.,* 2019), *Brasilitherium riograndensis* (BR; Rodrigues *et al.,* 2014), *Siriusgnathus niemeyerorum* (SN; Pavanatto *et al.,* 2019), *Exaeretodon riograndensis* (ER; Pavanatto *et al.,* 2019), *Probelesodon kitchingi* (PK; Hoffman *et al*., 2021), *Massetognathus ochagaviae* (MaO; Hoffman *et al*., 2021), *Prozostrodon brasiliensis* (PB; Kerber *et al*., 2023), *Therioherpeton cargnini* (TC; Kerber *et al*., 2023), *Morganucodon oehleri* (MO; Rowe *et al*., 2011), *Hadrocodium wui* (HW; Rowe *et al*., 2011), *Vincelestes neuquenianus* (VN; Macrini *et al*., 2007a), *Onychodectes tisonensis* (OT; Napoli *et al*., 2018), *Diacodexis ilicis* (DI; Orliac and Gilissen, 2012), *Trogosus hillsii* (TH; Bertrand *et al*., 2024), *Obdurodon dicksoni* (OD; Macrini *et al*., 2006), *Monodelphis domestica* (Macrini *et al*., 2007b), *Vombatus ursinus* (VU; Sharp 2016), *Phascolarctos cinereus* (PC; Sharp 2016), *Hydrochoerus hydrochaeris* (HH; Ferreira *et al*., 2022) and *Didelphis virginiana* (DV; this study, appendix).

It is worth noting that while *Thrinaxodon* and its contemporaries display a relative decrease in brain size following mass extinctions (exemplified by the Jurassic mammaliaforms), relative brain size compared to skull size actually increases gradually along the mammalian evolutionary lineage (figure 6.2). This trend suggests that the brain remained paramount to survivability in resource-limited environments following mass extinctions (despite the body as a whole shrinking) and that the ancestral mammalian brain continued to expand relative to skull size across the cynodont-mammaliaform and mammaliaform-mammal transitions, enhancing cognitive and sensory capabilities. However, it should be noted that this conclusion is drawn from a small subset of species (principally due to the lack of cynodont and

mammaliaform endocasts) and the trend towards a relatively larger brain compared to skull size is likely to be more pronounced in mammals. The trend also relies on the endocasts being an accurate representation of brain size and morphology in extinct taxa (which comes with its own challenges, as explored in chapters four and five), so the addition of more specimens across the evolutionary lineage would confirm that physical miniaturisation did not cause brain sizes to become relatively small for skull size.

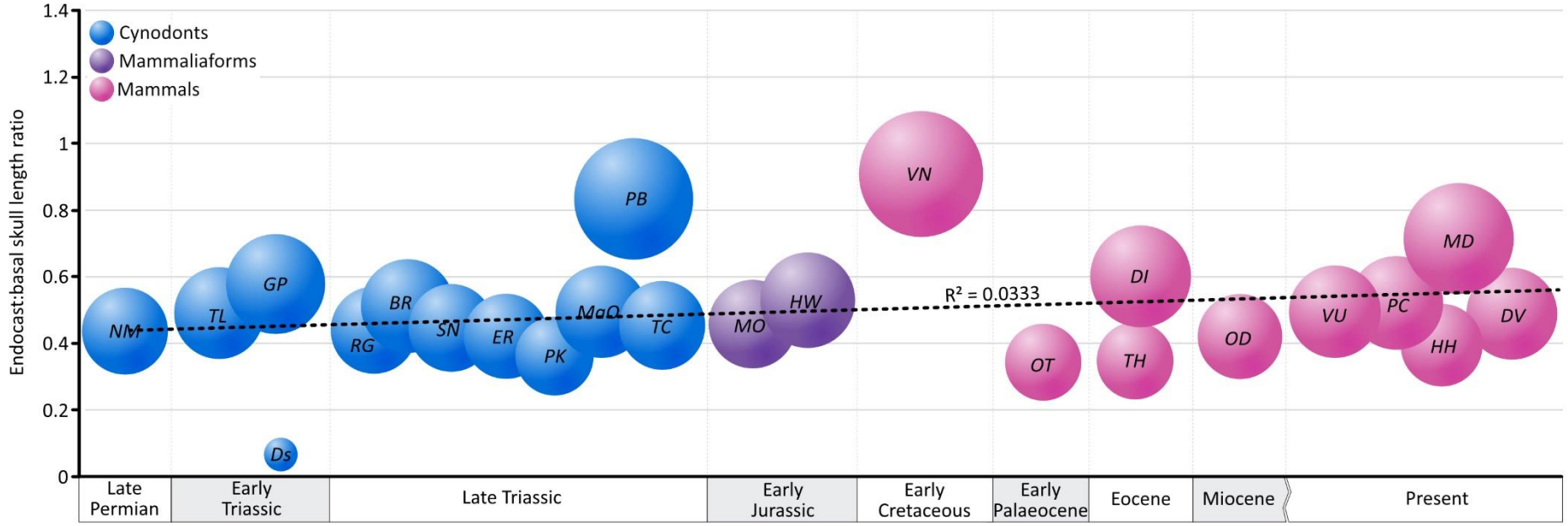


**Figure 6.2.** Relative brain size compared to skull size of cynodonts, mammaliaforms and mammals through time. Unlike when brain size is considered alone, relative brain size shows that the brains were not proportionally smaller during periods of miniaturisation, even though the body shrank overall. Endocast sources and species abbreviations as outlined in figure 6.1.

## 6.2. *Thrinaxodon liorhinus*: the start of mammalian brain development

Over the past 260 million years, a compilation of morphological changes have shaped the cognitive and sensory capabilities of the mammalian lineage. With cynodont fossils known from the late Permian to the Early Cretaceous (Abdala 2021), *Thrinaxodon liorhinus* therefore offers one of the earliest glimpses into the development of the mammalian brain and features that have been lost or gained since the ancestral state (see chapter three for morphological details). Mammalian ancestors have historically been considered to have small, simple brains, with unrefined sensory organs compared to mammals (Kemp 1979; Rowe *et* al., 2011; Benoit *et al*., 2023), including *Thrinaxodon* which was previously reconstructed with a simple endocranial anatomy (chapter three; Kielan-Jaworowska *et al*., 2004). Yet recent studies have shown that mammaliaforms and cynodonts may have been capable of much more than previously thought, with suggestions of nocturnal life habits (Angielczyk and Schmidt, 2014; Bennie *et al*., 2014) and parental care (Jasinoski and Abdala, 2017). So, how did the cynodont brain transform into the complex organ capable of thoughts, emotions, learning, social behaviours and so much more in modern mammals?

Rodrigues *et al*. (2019) noted that the first major change was the loss of the pineal eye in most eucynodonts, which functioned as a thermoreceptor and regulator of the circadian rhythm. The pineal eye is still present in modern reptiles but has been suggested to mark the transition towards endothermy in the mammalian lineage, when light detected by the pineal gland was no longer needed to regulate biological processes such as sleep and body temperature (Benoit *et al*., 2016a; Lovegrove 2019). The timing of the loss of the pineal eye is proposed to have occurred gradually during periods of miniaturisation (Benoit *et al*., 2016a), when therapsids experienced an increase in metabolic rate (evidenced by the closure of the pineal foramen in the skull roof of probainognathian cynodonts; Benoit *et al*., 2016). Therefore, the

reconstructions of *Thrinaxodon*'s adult brain presented in chapter three (and questionably the juvenile brain in chapter four) shows that this cynodont had not yet lost the pineal eye and as such, was unlikely to have been endothermic.

Next came a progressive enlargement of the olfactory bulbs among many Triassic cynodonts (figure 6.3). Rodrigues *et al*. (2019) suggest that the Late Triassic basal probainognathian, *Chiniquodon*, may mark the first point of olfactory bulb enhancement with the presence of a medial division through the olfactory bulbs. Separation of the olfactory bulbs does not appear to be an ancestral mammalian characteristic as it has not been found in earlier cynodonts (Pavanatto *et al*., 2019; Kerber *et al*., 2023), and *Thrinaxodon* only shows a medial depression on the dorsal surface, rather than separation of the olfactory bulbs (see chapters three and four). However, Crompton *et al*. (2017) proposed that Early Triassic cynodonts had more structured olfactory regions than previously thought, with cartilaginous nasal turbinals that increased the surface area for evaporative cooling - an essential biological mechanism during the high Triassic temperatures. The olfactory bulbs appear to have increased in size from the late Permian to Late Triassic but diminished significantly during Early Jurassic miniaturisation before increasing in length towards modern mammals (figure 6.3). The olfactory bulbs also became a proportionally larger part of endocasts towards mammals (figure 6.4), with a noticeable expansion during the late Triassic and again after the Miocene (Kaas 2011). It is likely that there were numerous pulses of olfactory enhancement, as proposed by Rowe *et al*. (2011), with a prominent change seen in mammaliaforms following the development of a cartilaginous cribriform plate to support the nasal turbinals and epithelium, which later became ossified in mammals (Crompton *et al*., 2017). A large nasal epithelium assists mammals in processing olfactory cues related to foraging, predation and finding a mate (Nielsen *et al*., 2015).

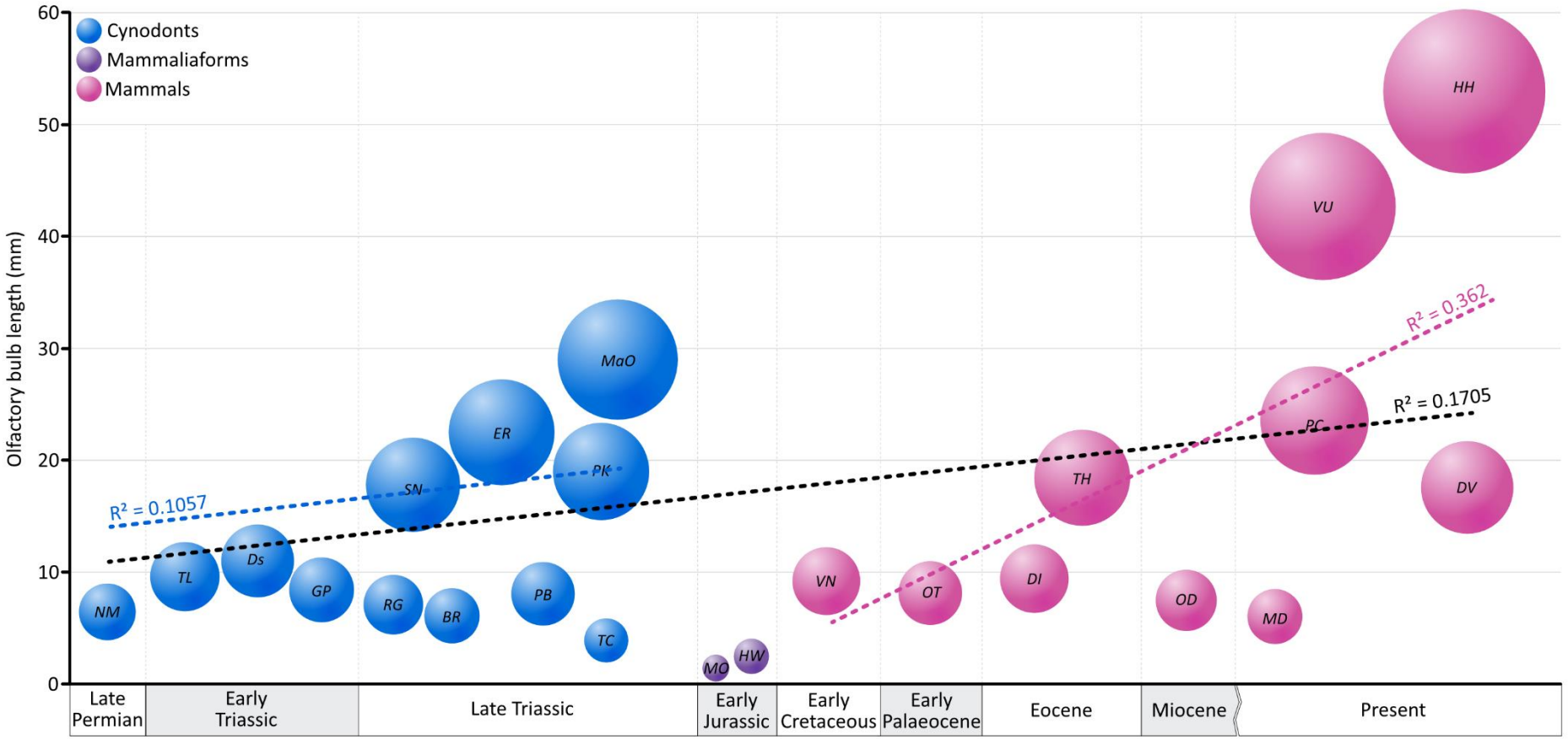


**Figure 6.3.** Olfactory bulb length across the mammalian evolutionary lineage. There appears to be an increase in olfactory bulb size from the late Permian to end Triassic, followed by a period of miniaturisation in the Jurassic before the olfactory bulbs expanded again in mammals. Endocast sources and species abbreviations as outlined in figure 6.1.

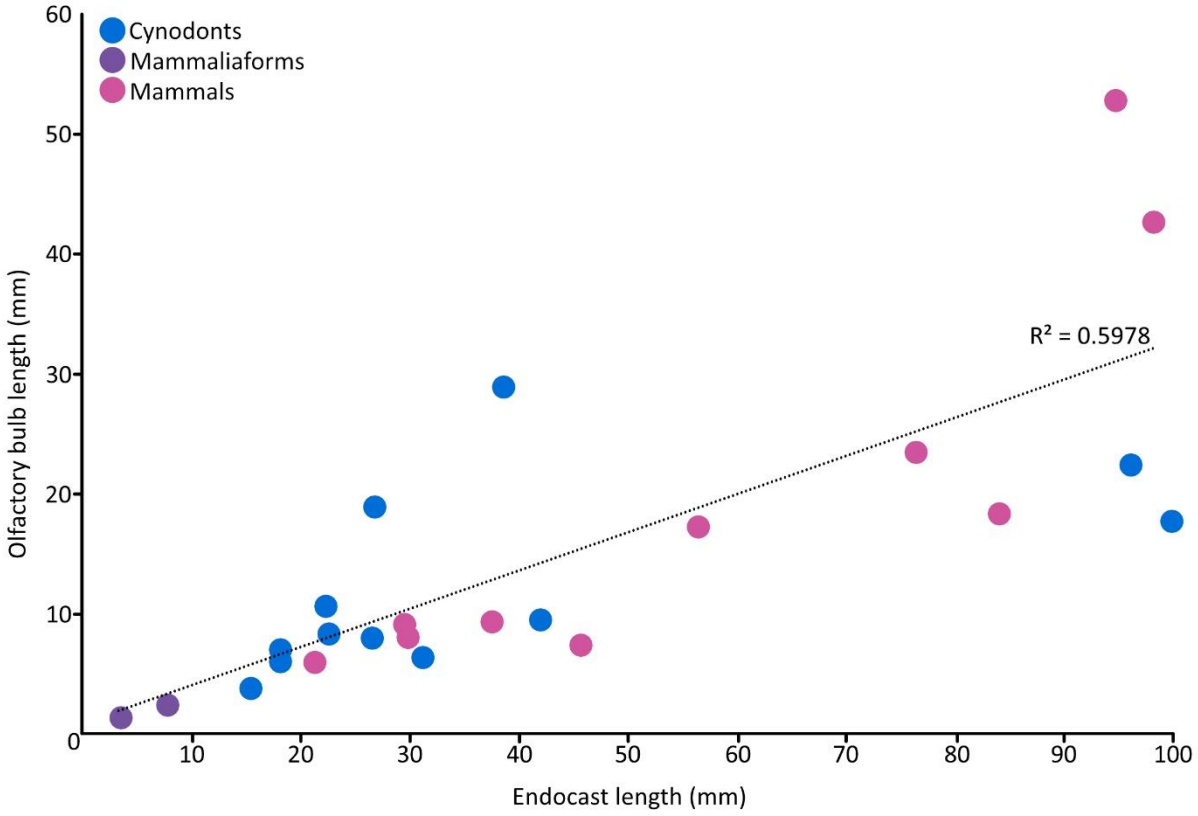


**Figure 6.4.** Olfactory bulb to endocast ratio in cynodonts, mammaliaforms and mammals. There is a clear trend that the olfactory bulbs are more consistently a larger part of the mammal brain than the olfactory bulbs were in cynodonts and mammaliaforms (although there are some cynodont outliers such as *Massetognathus ochagaviae*, *Exaeretodon riograndensis*, *Probelesodon kitchingi* and *Siriusgnathus niemeyerorum* (which have 29 mm, 22.5 mm, 19 mm and 17.81 mm long olfactory bulbs, respectively). Data corresponds to the species outlined in figure 6.1.

Kemp (2009) proposed that enlargement of the cerebellum was also a defining moment of mammalian brain evolution, facilitating more sophisticated and controlled neuromuscular movements. Even in early cynodonts like *Thrinaxodon,* the cerebellum is a prominent feature, being the widest brain region in many cynodonts from the Early Triassic onwards (and particularly later tritheledontid, traversodontid and brasilodontid cynodonts; Rodrigues *et al*., 2019; Pavanatto *et* al., 2019; Hoffman *et al*., 2021; Kerber *et al*., 2023). Mammal brains

highlight that the cerebellum still serves an important function, with prominent folding of the cerebellum increasing the surface area for neuronal connections (Northcutt 2011). Moreover, studies of cynodont and mammaliaform fossils have hinted that a precise bite from jaw muscle reorganisation (Lautenschlager *et al*., 2018b), mobile shoulder girdles and upright hindlimbs are all characteristics of increasingly mammalian bodies that are linked to improved coordination of movements created by a larger cerebellum (Kemp 2005; Rodrigues *et al*., 2019). Therefore, it is concluded that cynodonts probably had equally precise motor coordination to mammaliaforms and mammals.

Fossil craniums of mammaliaforms provide evidence for expansion of the cerebral hemispheres, which likely coincided with improved tactile sensitivity (Rowe *et al*., 2011). It is among mammaliaforms that the first evidence of hair has been found, as soft tissue structures, including whiskers and fur, do not easily preserve in the fossil record. Ji *et al.* (2006) reported the presence of fur in the Middle Jurassic mammaliaform, *Castorocauda lutrasimilis*, which implies that some later cynodonts could have had some sort of hair, but where cynodonts sit between scaly pelycosaurs and furry mammals will only be clarified by finding cynodont fossils with exceptional soft tissue preservation. Furthermore, although pits in *Thrinaxodon*'s snout were previously misidentified as sensory whisker pits (Damiani *et al*., 2003), it is likely that whiskers emerged later in the mammalian lineage, with tentative evidence that sensory whiskers were present in Lower Jurassic cynodonts (Muchlinski *et al*., 2020). A sensory revolution can be seen clearly in the enlargement of the cerebral hemispheres, potentially even as early as the Late Triassic when the cynodont *Probainognathus* displays the first distinctly separated cerebral hemispheres in the posterior region (Rodrigues *et al*., 2019). Towards mammals, the cerebral hemispheres become increasingly separated and expanded (figure 6.5; as evidenced by *Monodelphis domestica* in

chapter four), perhaps because of the developing six-layered neocortex which was one of the most revolutionary moments in forming the mammalian brain, ameliorating sensory perception, problem-solving, movement initiation and cognitive processing in mammals (Aboitiz *et* al., 2003; Kemp 2009; Rowe *et al*., 2011). This theory is supported by the fact that large cerebral hemispheres occur in socially complex mammalian carnivores, where the cerebral hemispheres are proportionally large rather than the brain being large for body size (Benson-Amram *et al*., 2016).

Visual and auditory stimuli are also important parts of behavioural outputs coordinated by the brain. It is thought that because most mammals and their ancestors were nocturnal (Borges *et al*., 2018), the sense of smell was more pronounced than visual acuity (hence the increased development of the olfactory bulbs through time; figure 6.3). However, based on genomic and phylogenetic analysis, numerous studies have stated that the ancestral condition for sight was tetrachromatic vision, where there were four types of cone cells involved in colour vision (Germeka *et al*., 2013; Borges *et al*., 2018; Benoit *et al*., 2023). This contrasts with the dichromatic vision of extant mammals, which only have two types of cone cells meaning they have reduced differentiation between colours. As such, cynodonts may have had better colour perception and could have been active during the day as well as the night (unlike many modern mammals) and the switch to predominantly nocturnal activity occurred in Mesozoic mammaliaforms (a period termed the "nocturnal bottleneck"; Walls 1942; Gerkema *et al*., 2013).

Hearing is also important for many social behaviours in mammals including predation, parental care and finding a mate, yet the poor preservation of delicate ear bones and soft tissue structures makes studying the mammalian auditory system challenging (Rilling and

Young, 2014; Lenschow *et al*., 2022). Mammals have been recorded to hear between infrasonic (15 Hz) and ultrasonic (20 kHz) frequencies (Manley 2018). However, studies of numerous fossils of mammal ancestors suggest that therapsids (including cynodonts and mammaliaforms) could only hear around 5 kHz (Rosowski and Graybeal, 1991; Benoit *et al*., 2017b), meaning that mammalian ancestors do not appear to have had any specialised hearing, and it was not until the late Mesozoic before high-frequency hearing emerged (Benoit *et al*., 2017b). This could explain why olfactory cues were so important to cynodonts and mammaliaforms, reflected in the proportionally large olfactory bulbs in many cynodont endocranial reconstructions (figures 6.4 and 6.5) and highlighted in *Thrinaxodon*, which has here been reconstructed with slightly larger and more rounded olfactory bulbs than some other Permian and Triassic cynodonts studied.

Relative brain sizes are frequently used to estimate behavioural characteristics, based on calculations of the encephalisation quotient (EQ; Rowe *et al*., 2011; Rodrigues *et al*., 2019; Hoffman *et al*., 2021; Kerber *et al*., 2023), yet the EQ value does not always provide a good proxy for intelligence (Benson-Amram *et al*., 2016). Given how complex extant mammal behaviours are, a single number cannot capture the true nature and capabilities of an animal. However, if using the EQ values as a rough comparison for encephalisation, then the EQ values are highly variable among cynodonts (Rowe *et al*., 2011; Rodrigues *et al*., 2019; figure 6.5) and only some mammal species have achieved EQs greater than one, such as canines, which are known to be highly intelligent (Saganuwan 2021). An EQ greater than one indicates that the brain is larger than expected for the body size and that, therefore, there may be an excess of neurons which could be interpreted as increased intelligence.

However, it should be considered where in the brains the neurons are and whether they have equal processing power before a conclusion about intelligence can be made. This is, of course, merely speculation for extinct species as there is, as yet, no fossil record of preserved brain tissue from cynodonts or mammaliaforms. Moreover, as suggested by the enhanced growth of numerous brain regions, there is no evidence to suggest that cynodonts, especially early species like *Thrinaxodon*, were any less cognitively capable than their mammaliaform or mammalian descendants. This conclusion, therefore, makes the EQ values somewhat redundant. It is also important to consider here the reliability of the endocranial models that the conclusions are being based on. In chapter five it was shown how variable brain reconstructions can be for a single specimen, and therefore, reconstructions for fossil taxa (particularly those with poorly preserved braincases) can add to the uncertainty in making conclusions about relative intelligence of animals along the mammalian evolutionary lineage. While the true cognitive capabilities of extinct taxa are likely to remain elusive, fossils do provide a picture of life as a mammalian ancestor, with tentative evidence of complex behaviours such as burrowing (Fernandez *et al*., 2013) and parental care (Jasinoski and Abdala, 2017; Kuznetsov and Panyutina, 2018) showing that cynodonts were not necessarily as primitive as scientists have previously thought.

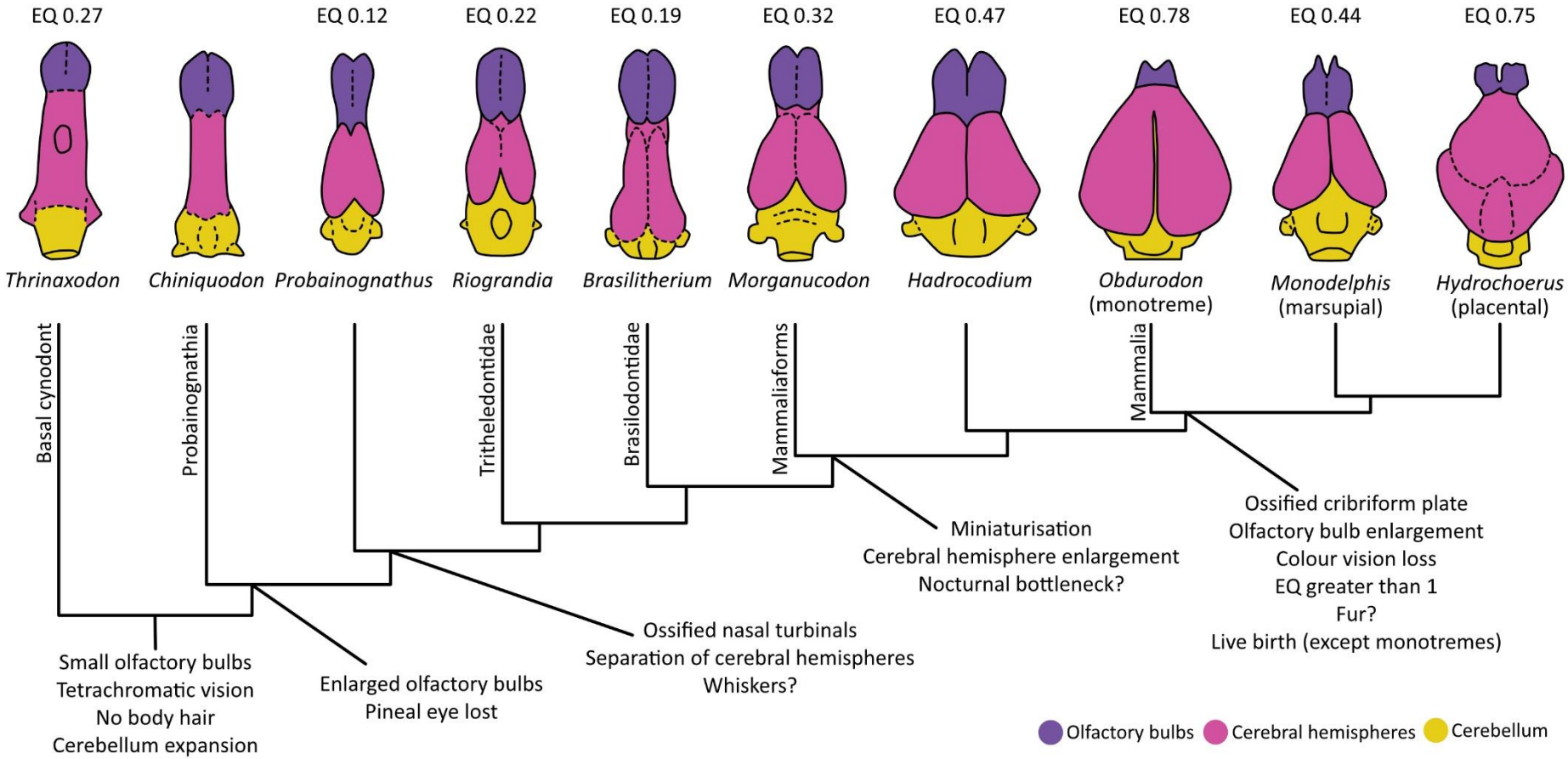


**Figure 6.5.** Evolutionary summary of endocast morphology across the mammalian lineage, including relative changes in the size and shape of the olfactory bulbs, cerebral hemispheres and cerebellum. Key developmental changes are highlighted (based on Benoit *et al*., 2023) and encephalisation quotients presented, showing variability among cynodonts and an increase towards modern mammals. *Brasilitherium* illustration based on the endocast generated in this research (appendix). Endocasts not to scale.

## 6.3. Chapter summary

For the past decade, it has been considered that there were three main pulses of brain development. Rowe *et al*. (2011) suggested three stages of olfactory enhancement, accompanied by enlargement of the cerebellum and development of the neocortex. Yet it seems that this model of mammalian brain evolution may no longer be appropriate, with a continuum of improvements to the brain over the last 260 million years between cynodont ancestors and extant mammals. Fossil evidence now supports Rodrigues *et al*. (2019)'s 'outside-in' model, where changes to the body and environmental pressures helped to shape brain morphology through sensory adaptations over time. The transition to nocturnality for many mammals is a key example of the sensory revolution, where hearing, smell and touch became compensatory characteristics for nocturnality.

Brain endocasts for *Thrinaxodon liorhinus* show how far the mammalian brain has come. The cynodont brain was by no means primitive but was an evolutionary stepping stone towards the more complex mammalian brain seen today, with increased compartmentalisation to allow different regions to have specialised functions. Without preservation of brain tissue, the interpretations made about the ancestral mammalian brain rely on other fields, such as phylogenetics and genomics, to ascertain the timing of when different cognitive advancements occurred. Nevertheless, while endocasts only offer an approximation of brain anatomy, it is clear that cynodonts like *Thrinaxodon* were an integral part of biological experimentation resulting in the distinctive mammal brain and all of its complex functions.

# APPENDIX

Endocasts were generated from CT data for *Brasilitherium riograndensis*, *Diademodon sp.* and *Didelphis virginiana*. These brain models provide evolutionary context to mammalian brain development, plus allow for the calculation of EQ values. However, the endocasts have not been analysed in detail within this thesis and so are presented here for visual reference only.

*Brasilitherium riograndensis* (UFRGS-PV-1043-T)

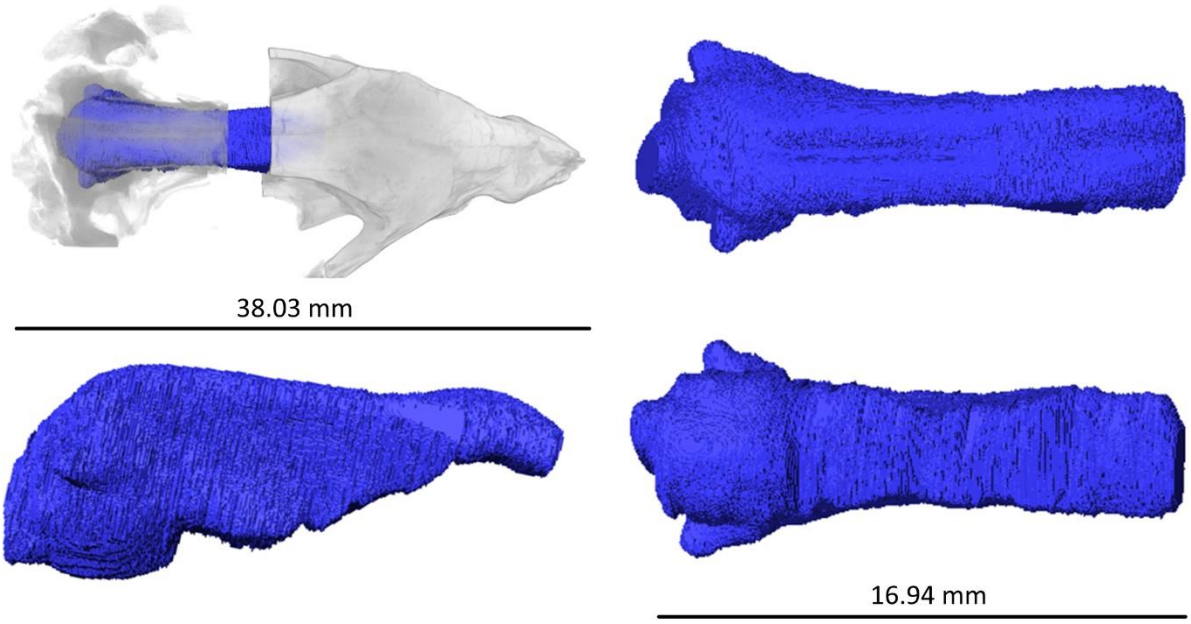


**Figure A.1.** Digital rendering of a *Brasilitherium riograndensis* skull (specimen UFRGS-PV-1043-T), accompanied by the digital endocranial reconstruction produced for this research.

*Diademodon sp.* (UCMP 42446)

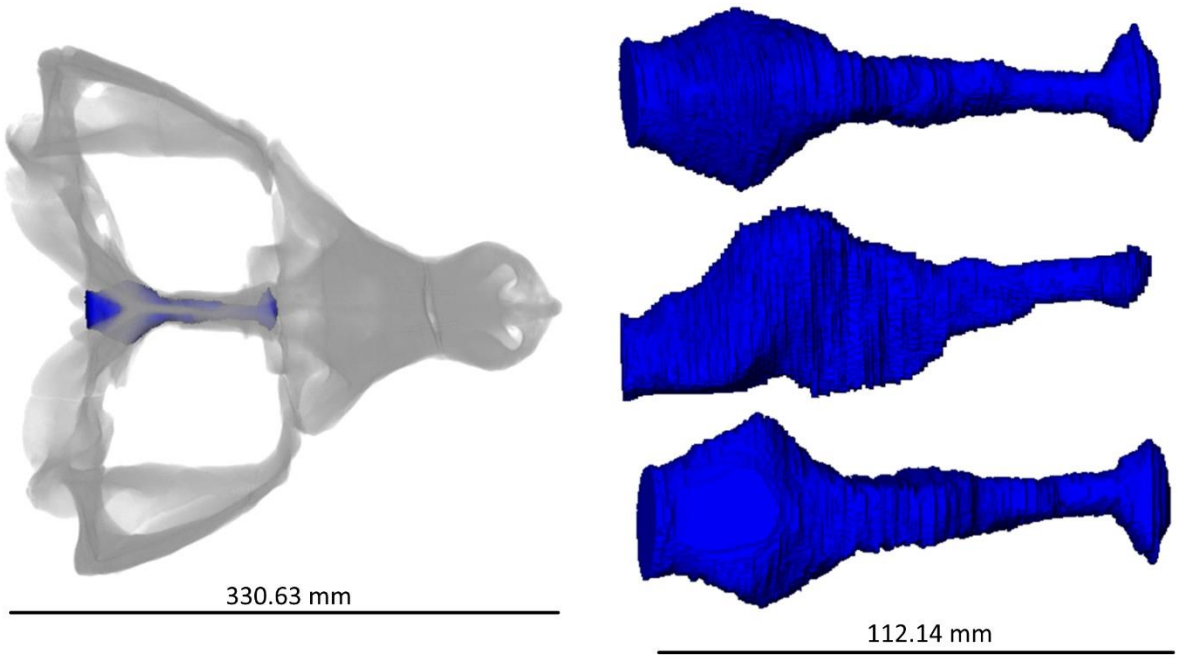


**Figure A.2.** Digital rendering of a *Diademodon sp.* skull (specimen UCMP 42446), accompanied by the digital endocranial reconstruction produced for this research.

*Didelphis virginiana* (TMM M-2517)

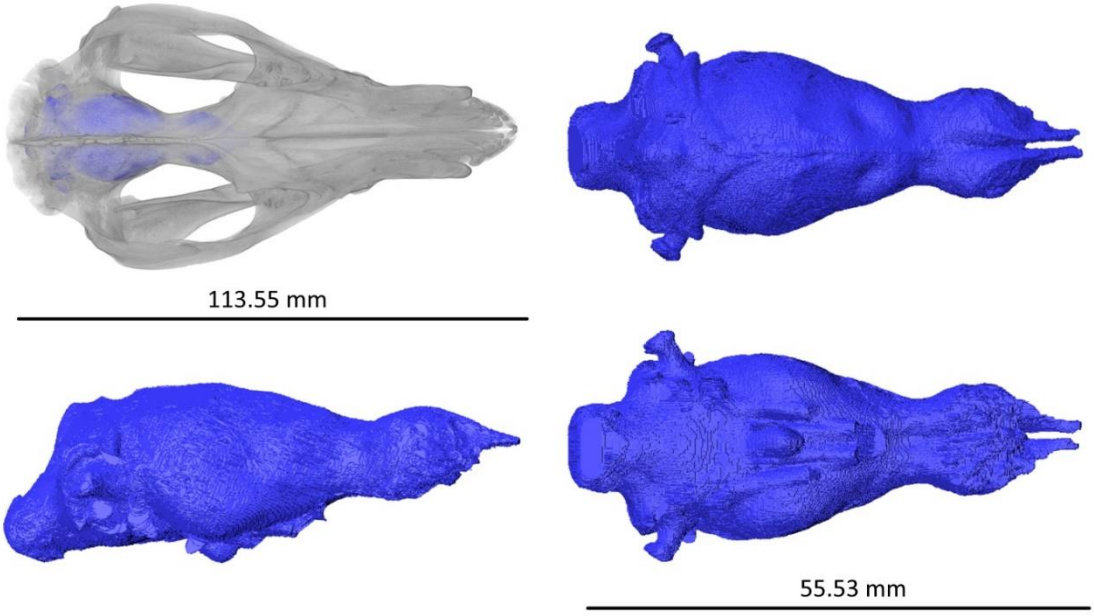


**Figure A.3.** Digital rendering of a *Didelphis virginiana* skull (specimen TMM M-2517), accompanied by the digital endocranial reconstruction produced for this research.

# CHAPTER SEVEN

# Research conclusions

## 7.1. Summary: *Thrinaxodon*'s brain and endocast variability

Fossilisation is an inherently biased process. Not all organisms produce fossils and not all parts of animals are preserved. Soft tissues, such as the brain, are very rarely preserved and even when the brain is fossilised, the internal structures that allow it to function do not remain. The incomplete nature of the fossil record makes palaeontology an imperfect science, but new digital techniques can help to fill the knowledge gap regarding the evolution of mammals as one of the most intelligent groups of animals on the planet. Therefore, digital reconstructions of soft tissues from CT scans provide the best way of non-destructively analysing absent brain morphology. The braincase provides an approximation of brain size and shape for a given specimen, from which inferences can be made about an extinct animal's cognitive, sensory and behavioural characteristics. As such, digital reconstructions are a powerful tool for understanding the brain anatomy of cynodonts, for which there is no known brain tissue preservation (and only one natural braincase cast discovered to date).

Cynodonts offer an important window into the evolution of the mammalian lineage and studying the brain morphology of one of the earliest known cynodonts, *Thrinaxodon liorhinus*, provides an important piece of the puzzle when understanding how the mammalian brain developed through time. Despite *Thrinaxodon* being one of the most prolifically found cynodonts in South Africa, no attempt has been made to digitally reconstruct its brain. Therefore, chapter three presents the first brain reconstruction and description of the species, based on seven adult specimens of *Thrinaxodon*. The brain models show that many of the

characteristics of the mammalian brain were already present in Early Triassic ancestors, including the olfactory bulbs, cerebral hemispheres, cerebellum and parafloccular lobes. Yet the models also highlight the challenge of understanding the brain morphology of basal cynodonts where the ventral part of the braincase was largely unossified, making brain reconstructions somewhat interpretive. Consequently, the lack of basicranial ossification is the greatest limitation during digital reconstruction of *Thrinaxodon*'s brain as it not only affects the size and shape of the 3D models, but also the subsequent calculations of cognitive ability based on estimated brain volumes. The calculations of encephalisation quotients have been shown to be challenging, with the reliance on endocranial volumes and estimates of body mass causing *Thrinaxodon*'s perceived cognitive capabilities to move up and down an evolutionary trajectory purely based on brain size. This is problematic as it does not accurately represent the processing and sensory capabilities suggested by growth of, for example, the olfactory bulbs during life. I conclude that EQ values should be used with care and that it is instead more beneficial to consider the proportional changes of brain regions both during a species' life and throughout an evolutionary trajectory to determine sensory and behavioural characteristics.

However, alongside the first digital insight into *Thrinaxodon*'s adult brain anatomy, this thesis presents the first reconstruction of *Thrinaxodon*'s juvenile brain in chapter four. While juvenile specimens have inherent disadvantages due to the large number of unossified regions making deformation more apparent, the juvenile fossil studied here offers an insight into ontogenetic changes that may have occurred during the lifetime of *Thrinaxodon*. Through comparison with a modern analogue, the grey short-tailed opossum, potential developmental stages in the growth of *Thrinaxodon*'s brain have been proposed. There would likely have been an early growth of the olfactory bulbs which continued throughout *Thrinaxodon*'s life, with the

cerebellum enlarging slightly later (but before adulthood). The cerebral hemispheres also showed later developmental growth, but it was outpaced by the other brain regions. The study of more *Thrinaxodon* specimens (and associated brain endocasts) at intermediate growth stages between the juvenile and adult fossils studied here would help to define the timing of the developmental changes observed across individual brain regions.

Ontogenetic variation forms just one part of the changes that can be observed across cynodont brain reconstructions. Intraspecific variation could play a role too, but it has also been shown in chapter five that the model maker can impart notable variation upon brain reconstructions. This variation can arise from a variety of factors including the modeller's interpretations of greyscale values, bone boundaries and endocranial anatomy within CT scans, plus smoothing of structures in the subsequent 3D model. As such, this research has raised questions about the reliability of brain reconstructions for extinct taxa, particularly those with poorly ossified braincases. There will likely always be an element of subjectivity in the interpretation of brain morphology for extinct species, but steps have been suggested to minimise variation imparted during the segmentation workflow including selecting specimens with good brain enclosure, having a single modeller create brain endocasts for all specimens within a study, joining disconnected skeletal elements with straight lines to avoid overestimations of segmentation masks and consider using reconstruction software with advanced capabilities such as mask placement in three orientations, among other suggestions.

*Thrinaxodon liorhinus* is an important part of the evolutionary lineage of mammals. In chapter six, the developmental changes towards the mammalian brain were considered, with *Thrinaxodon* and its cynodont contemporaries highlighting developmental changes to the brain that coincided with environmental and sensory changes. Since the Early Triassic,

mammal-like brain morphology has changed in response to stressors (such as a warming climate and resource scarcity), with morphological changes to the olfactory bulbs, cerebral hemispheres and cerebellum marking key stages in the evolution of mammals. In time, it would be interesting to explore whether the brains of modern mammals (with relatively quick evolutionary rates) show any endocranial adaptations to current environmental stressors, such as climate change.

## 7.2. Future research

The impact of segmentation software on endocranial reconstructions would be a valuable avenue to explore in the effort to minimise variation during the brain segmentation process. Software that offers additional planes of editing may benefit delimiting transverse features within the skull to improve outputs. Additionally, there are automated endocranial reconstruction techniques (such as the endomaker algorithm in R; Profico *et al*., 2020), which would eliminate inter-modeller variation, although understanding how accurate the subsequent brain model is would need its own investigation. A further potential solution to modeller bias and variation may be to implement machine learning or artificial intelligence techniques to reconstruct the brains of extinct species from CT data. While this technology is still developing (Yu *et al*., 2023), there are examples of palaeontological applications of machine learning and AI, such as CT segmentation of protoceratopsian skulls using deep learning (Yu *et al*., 2022), segmentation of vertebrate microfossils with deep learning (Hou *et al*., 2021) and automatic recognition of fossil and modern pollen grains using neural networks (Bourel *et al*., 2020). Such studies show that advanced technologies could pave the way for a new era in palaeontological reconstructions.

Furthermore, it would be helpful to research whether current reconstruction software have any impact on the reliability of the endocast produced. Different software have different functionalities, such as magic wand tools for delimiting the endocranial cavity in the CT data quickly and segmenting in coronal, sagittal and horizontal planes. Whether these features improve the biological accuracy of brain reconstructions has yet to be tested. It would also be beneficial to run modeller and software variation studies on a later cynodont with a more enclosed braincase, such as *Diademodon*, to provide more data on how much variation is imparted by the model maker and whether any specific software or functionality can reduce this (while removing the poor braincase ossification issue exemplified by *Thrinaxodon*). The studies could also be run with more modellers with a greater range of expertise in either digital reconstructions or mammalian brain anatomy to determine whether either of these factors are beneficial to consider when designing a future study investigating cynodont brain anatomy to improve the reliability of outputs. Additionally, the investigation into ontogenetic variation in *Thrinaxodon*'s brain was limited by specimen availability. A future study could replicate Macrini *et al*. (2007b)'s work on ontogenetic changes to the opossum brain but focussing instead on cynodonts where more specimens of different ages classes are available, or on modern mammals where the reconstructed brain anatomy can be corroborated with physical specimens.

*Thrinaxodon liorhinus* represents the early origins of the recognisably mammalian brain and highlights how development of individual brain regions was impacted by environmental factors (including resource scarcity following mass extinctions) which drove sensory revolutions that can be seen in the brain morphology of the mammalian lineage. Miniaturisation, endothermy and nocturnality are all biological adaptations that can be observed within the changing brain morphology of cynodonts, mammaliaforms and mammals

over the last 260 million years and *Thrinaxodon liorhinus*' brain highlights how far this complex organ has come. Cynodonts should no longer be considered primitive forebears of mammals, but as important evolutionary stepping stones towards the diverse mammalian community we see on Earth today.

# ADDENDUM

Since thesis submission in February 2024, the following paper was published in March 2024. The publication may have had a bearing on the research but has not been included.

Pusch, L.C., Kammerer, C. F. and Fröbisch, J. (2024) The origin and evolution of Cynodontia (Synapsida, Therapsida): Reassessment of the phylogeny and systematics of the earliest members of this clade using 3D-imaging technologies. *The Anatomical Record*, 307(4): 1634–1730.

The publication discusses the origins of cynodonts, including the challenge Permian ghost lineages present in determining the phylogeny of Eutheriodontia (which includes Cynodontia and Therocephalia). The results suggest when different mammalian characteristics evolved within the group, and as such, may have influenced comments made in chapter six about the evolutionary positioning of *Thrinaxodon*.

# REFERENCES

Abdala, F. (2004) 'Abundance and diversity of non-mammaliaform cynodonts in the South African Karoo' in *Geosciences Africa 2004*. Johannesburg: University of the Witwatersrand.

Abdala, F. (2021) Permo-Jurassic cynodonts: the early road to mammalness. *Encyclopaedia of Geology*, 206–226.

Abdala, F., Gaetano, L. C., Martinelli, A. G., Bento Soares, M., Hancox, P. J. and Rubidge, B. S. (2020) Non-mammaliaform cynodonts from western Gondwana and the significance of Argentinean forms in enhancing understanding of the group. *Journal of South American Earth Sciences*, 104: 102884.

Abdala, F., Jasinoski, S. C. and Fernandez, V. (2013) Ontogeny of the Early Triassic cynodont *Thrinaxodon liorhinus* (Therapsida): dental morphology and replacement. *Journal of Vertebrate Palaeontology*. 33(6): 1408–1431.

Abdala, F. and Ribeiro, A. M. (2010) Distribution and diversity patterns of Triassic cynodonts (Therapsida, Cynodontia) in Gondwana. *Palaeogeography, Palaeoclimatology, Palaeoecology*. 286(3): 202–217.

Aboitiz, F. and Montiel, J. F. (2015) Olfaction, navigation and the origin of the isocortex. *Frontiers in Neuroscience*, 9: 402.

Aboitiz, F., Morales, D. and Montiel, J. (2003) The evolutionary origin of the mammalian isocortex: towards an integrated developmental and functional approach. *Behavioral and Brain Sciences*, 26(5): 535–552.

Abreu, A. P. and Kaiser, U. B. (2016) Pubertal development and regulation. *The Lancet Diabetes and Endocrinology*, 4(3): 254–264.

Angielczyk K. D. and Schmitz L. (2014) Nocturnality in synapsids predates the origin of mammals by over 100 million years. *Proceedings of the Royal Society B*, 281(1793): 28120141642.

Araújo, R., David, R., Benoit, J., Lungmus J. K., Stoessel, A., Barrett, P. M., Maisano, J. A., Ekdale, E. *et al*. (2022) Inner ear biomechanics reveals a Late Triassic origin for mammalian endothermy. *Nature*, 607: 726–731.

Atkinson E. G., Rogers, J., Mahaney, M. C., Cox, L. A. and Cheverud, J. M. (2015) Cortical folding of the primate brain: an interdisciplinary examination of the genetic architecture, modularity, and evolvability of a significant neurological trait in pedigreed baboons (genus *Papio*). *Genetics*, 200(2): 651–665.

Bajdek, P., Qvarnström, M., Owocki, K., Sulej, T., Sennikov, A. G., Golubev, V. K. and Niedźwiedzki, G. (2015) Microbiota and food residues including possible evidence of pre-mammalian hair in Upper Permian coprolites from Russia. *Lethaia*, 49(4): 455–477.

Balanoff, A. M. and Bever, G. S. (2020) 'The role of endocasts in the study of brain evolution', in Kaas, J. H. (ed) *Evolutionary Neuroscience*. 2nd edition. Academic Press, pp. 29–49.

Balanoff, A. M., Bever, G. S., Colbert, M. W., Clarke, J. A., Field, D.J., Gignac, P. M., Ksepka D. T et al. (2016). Best practices for digitally constructing endocranial casts: examples from birds and their dinosaurian relatives. *Journal of Anatomy*, 229 (2): 173–190.

Ballell, A., King, J. L., Neenan, J. M., Rayfield, E. J., and Benton, M. J. (2020). The braincase, brain and palaeobiology of the basal sauropodomorph dinosaur *Thecodontosaurus antiquus. Zoological Journal of the Linnean Society*, 1–22.

Banich, M. T. (1998) Integration of information between the cerebral hemispheres. *Current Directions in Psychological Science,* 7(1): 32–37.

Bates, K. T., Falkingham, P. I., Rarity, F., Hodgetts, D., Purslow, A. and Manning, P. L. (2010) Application of high-resolution laser scanning and photogrammetric techniques to data acquisition, analysis and interpretation in palaeontology. *International Archives of Photogrammetry, Remote Sensing and Spatial Information Sciences*, 38(5): 68–73.

Bennie, J. J., Duffy, J. P. Inger, R. and Caston, K. J. (2014) Biogeography of time partitioning in mammals. *Proceedings of the National Academy of Sciences of the United States of America*, 111(38): 13727–13732.

Benoit, J., Abdala, F. Manger, P. R. and Rubidge, B. S. (2016a) The sixth sense in mammalian forerunners: variability of the parietal foramen and the evolution of the pineal eye in South

African Permo-Triassic eutheriodont therapsids. *Acta Palaeontologica Polonica*, 61(4): 777–789.

Benoit, J., Dollman, K. N., Smith, R. M. H. and Manger, P. R. (2023) At the root of the mammalian mind: the sensory organs, brain and behavior of pre-mammalian synapsids. *Progress in Brain Research*, 275: 25–72.

Benoit, J., Jasinoski, S. C., Fernandez, V. and Abdala, F. (2017) The mystery of a missing bone: revealing the orbitosphenoid in basal Epicynodontia (Cynodontia, Therapsida) through computed tomography. *The Science of Nature,* 104: 66.

Benoit, J., Manger, P., Fernandez, V. and Rubidge, B. S. (2017b) The bony labyrinth of late Permian Biarmosuchia: palaeobiology and diversity in non-mammalian Therapsida. *Palaeontologia Africana*, 52: 58–77.

Benoit, J., Manger, P.R. and Rubidge, B. S. (2016b) Palaeoneurological clues to the evolution of defining mammalian soft tissue traits. *Scientific Reports*, 6: 25604.

Benson-Amram, S., Dantzer, B., Stricker, G., Swanson, E. M. and Holekamp, K. E. (2016) Brain size predicts problem-solving ability in mammalian carnivores. *Proceedings of the National Academy of Sciences of the United States of America*, 113(9): 2532–2537.

Benton, M. J. (1995) Diversification and extinction in the history of life. *Science*, 268(5207): 52–58.

Benton, M. J. (2021) The origin of endothermy in synapsids and archosaurs and arms races in the Triassic. *Gondwana Research*, 100: 261–289.

Bertrand, O. C., Jiménez Lao, M., Shelley, S. L., Wible, J. R., Williamson, T. E., Mend, J. and Brusatte, S. L. (2024) The virtual brain endocast of *Trogosus* (Mammalia, Tillodontia) and its relevance in understanding the extinction of archaic placental mammals. *Journal of Anatomy*, 244(1): 1–21.

Bianki, V. L. (1983) Hemisphere specialization of the animal brain for information processing principles. *International Journal of Neuroscience*, 20(1–2): 75–89.

Bird, D. J., Amirkhanian, A., Pang, B. and Van Valkenburgh, B. (2014) Quantifying the cribriform plate: influences of allometry, function, and phylogeny in carnivora. *The Anatomical Record*, 297(11): 2080–2092.

Boles, D. B. (1992) Factor analysis and the cerebral hemispheres: temporal, occipital and frontal functions. *Neuropsychologia*, 30(11): 963–988.

Bonaparte, J. F. (1966) Sobre las cavidades cerebral, nasal y otras estructuras del craneo de *Exaeretodon sp*. (Cynodontia-Traversodontidae). *Acta Geologica Lilloana*, 8: 5–11.

Bonaparte, J. F., Martinelli, A. G., Schultz, C. L. and Rubert, R. (2003) The sister group of mammals: small cynodonts from the Late Triassic of Southern Brazil. *Revista Brasileira de Paleontologia*, 5: 5–27.

Booth, C. L. (1990) Evolutionary significance of ontogenetic colour change in animals. *Biological Journal of the Linnean Society*, 40(2): 125–163.

Borges, R., Johnson, W. E., O'Brien, S. J., Gomes, C., Heesy, C. P. and Antunes, A. (2018) Adaptive genomic evolution of opsins reveals that early mammals flourished in nocturnal environments. *BMC Genomics,* 19: 121.

Botha, J. (2020) The paleobiology and paleoecology of South African Lystrosaurus. *PeerJ,* 8: e10408.

Botha, J., Abdala, F. and Smith, R. (2007) The oldest cynodont: new clues on the origin and early diversification of the Cynodontia. *Zoological Journal of the Linnean Society*, 149(3): 477–492.

Botha-Brink, J. and Angielcyzk, K. D. (2010) Do extraordinarily high growth rates in Permo-Triassic dicynodonts (Therapsida, Anomodontia) explain their success before and after the end-Permian extinction? *Zoological Journal of the Linnean Society*, 160(2): 341–365.

Botha-Brink, J., Bento Soares, M. and Martinelli, A. G. (2018) Osteohistology of Late Triassic prozostrodontian cynodonts from Brazil. *PeerJ*, 6: e5029.

Botha, J. and Chinsamy, A. (2005) Growth patterns of *Thrinaxodon liorhinus*, a non-mammalian cynodont from the Lower Triassic of South Africa. *Palaeontology*, 48(2): 385–394.

Botha-Brink, J., Codron, D., Huttenlocker, A. K., Angielczyk, K. D. and Ruta, M. (2016) Breeding young as a survival strategy during Earth's greatest mass extinction. *Scientific Reports*, 6: 24053.

Bourel, B., Marchant, R., de Garidel-Thoron, T., Tetard, M., Barboni, D. Gally, Y. and Beaufort, L. (2020) Automated recognition by multiple convolutional neural networks of modern, fossil, intact and damaged pollen grains. *Computers and Geosciences*, 140: 104498.

Brasier, M. D., Norman, D. B., Liu, A. G., Cotton, L. J., Hiscocks, J. E. H., Garwood, R. J., Antcliffe, J. B. and Wacey, D. (2016). Remarkable preservation of brain tissues in an Early Cretaceous iguanodontian dinosaur. *Geological Society London Special Publications,* 448: SP448.3.

Bright, J. (2014). A review of paleontological finite element models and their validity. *Journal of Paleontology*, 88(4): 760–769.

Brito, D. V. C., Esteves, F., Rajado, A.T., Silva, N., ALFA score Consortium, Araújo, I., Bragança, J., Castelo-Branco, P. and Nóbrega, C. (2023) Assessing cognitive decline in the aging brain: lessons from rodent and human studies. *npj Aging*, 9: 23.

Brochu, C. A. (2000). A digitally rendered endocast for Tyrannosaurus rex. *Journal of Vertebrate Paleontology*, 20 (1): 1–6.

Brockelhurst, N., Panciroli, E., Benevento, G. L. and Benson, R. B. J. (2021) Mammaliaform extinctions as a driver of the morphological radiation of Cenozoic mammals. *Current Biology*, 31(13): 2955–2963.

Broom, R. (1938) On the structure of the skull of the Cynodont, *Thrinaxodon liorhinus*, Seeley. *Annals of the Transvaal Museum*, 19: 263–269.

Broyde, S., Dempsey, M., Wang, L., Cox, P. G., Fagan, M. and Bates, K. T. (2021). Evolutionary biomechanics: hard tissues and soft evidence? *Proceedings of the Royal Society B*, 288: 20202809.

Bubadué, J., Meloro, C., Hendges, C., Battistella, T., Carvalho, R. and Cáceres, N. (2021) Clinal and allometric variation in the skull of sexually dimorphic opossums. *Journal of Mammalian Evolution*, 28: 185–198.

Budday, S., Steinmann, P., Goriely, A and Kuhl, E. (2015) Size and curvature regulate pattern selection in the mammalian brain. *Extreme Mechanics Letters*, 4: 193–198.

Butler, E., Abdala, F. and Botha-Brink, J. (2019) Postcranial morphology of the Early Triassic epicynodont *Galesaurus planiceps* (Owen) from the Karoo Basin, South Africa. *Papers in Palaeontology*, 5(1): 1–32.

Butler, A.B. and Hodos, W. (1996) *Comparative vertebrate neuroanatomy: evolution and adaptation.* New York: Wiley.

Buzi, C., Profico, A., Liang, C., Khonsari, R. H., O'Higgins, P., Moazen, M. and Harvati, K. (2023) *Icex*: Advances in the automatic extraction and volume calculation of cranial cavities. *Journal of Anatomy*, 242(6): 1172–1183.

Clements, T. and Gabbott, S. (2022) Exceptional preservation of fossil soft tissues. *Encyclopedia of Life Sciences*, 1–10.

Clement, A. M., Mensforth, C. L., Challands, T. J., Collin, S. P., and Long, J. A. (2021). Brain reconstruction across the fish-tetrapod transition; insights from modern amphibians. *Frontiers in Ecology and Evolution*, 9: 160.

Coffman, K. A., Dum, R. P. and Strick, P. L. (2011) Cerebellar vermis is a target of projections from the motor areas in the cerebral cortex. *Proceedings of the National Academy of Sciences of the United States of America*, 108(38): 16068–16073.

Conroy, G. C. and Vannier, M. W. (1984) Noninvasive three-dimensional computer imaging of matrix-filled fossil skulls by high-resolution computed tomography. *Science*, 226(4673): 456–458.

Cooper, N., Freckleton, R. P. and Jetz, W. (2011) Phylogenetic conservatism of environmental niches in mammals. *Proceedings of the Royal Society B*, 278(1716): 2384–2391.

Crompton, A, Musinsky, C., Bonaparte, J., Bhullar, B-A. and Owerkowicz, T. (2018) Evolution of the mammalian fauces region and the origin of suckling. *Havard Library Faculty of Art and Science Scholarly Articles,* 1–57.

Crompton, A. W., Owerkowicz, T., Bhullar, B-A. S. and Musinsky, C. (2017) Structure of the nasal region of non-mammalian cynodonts and mammaliaforms: speculations on the evolution of mammalian endothermy. *Journal of Vertebrate Paleontology*, 37(1): e1269116.

Cunningham, J. A. (2021) The use of photogrammetric fossil models in palaeontology education. *Evolution: Education and Outreach*, 14: 1.

Cunningham, J. A., Rahman, I. A., Lautenschlager, S., Rayfield, E. J. and Donoghue, P. C. J. (2014) A virtual world of paleontology. *Trends in Ecology and Evolution*, 29(6):347–357.

Curley, J. P. and Keverne, E. B. (2005) Genes, brains and mammalian social bonds. *Trends in Ecology and Evolution,* 20(10): 561–567.

Dal Corso, J., Song, H., Callegaro, S., Chu, D., Sun, D., Hilton, J., *et al.* (2022) Environmental crises at the Permian–Triassic mass extinction. *Nature Reviews Earth and Environment*, 3: 197–214.

Damiani, R., Modesto, S., Yates, A. and Neveling, J. (2003) Earliest evidence of cynodont burrowing. *Proceedings of the Royal Society B: Biological Sciences*, 270(1525): 1747–1751.

Davies, T.G. Rahman, I. A., Lautenschlager, S., Cunningham, J. A., Asher, R. J., Barrett, P. M., Bates, K. T., Bengtson, S. *et al*. (2017) Open data and digital morphology. *Proceedings of the Royal Society B: Biological Sciences*, 284(1852): 20170194.

Deacon, T. W. (1990) Rethinking mammalian brain evolution. *American Zoologist*, 30(3): 629–705.

Dechmann, D. K. N., LaPoint, S., Dullin, C., Hertel, M., Taylor, J. R. E., Zub, K. and Wikelski, M. (2017) Profound seasonal shrinking and regrowth of the ossified braincase in phylogenetically distant mammals with similar life histories. *Scientific Reports*, 7: 42443.

de Sousa, A. A., Beaudet, A., Calvey, T., Bardo, A., Benoit, J., Charvet, C. J., Dehay, C., Gómez-Robles, A. *et al*. (2023) From fossils to mind. *Communications Biology*, 6: 636.

dos Reis, M., Thawornwattana, Y., Angelis, K., Telford, M. J., Donoghue, P. C. and Yang, Z. (2015) Uncertainty in the timing of origin of animals and the limits of precision in molecular timescales. *Current Biology*, 25(22): 2939–2050.

Eisenberg, J. F. (1981) *The mammalian radiations*. Chicago: University of Chicago.

Eisová, S., Velemínský, P. and Bruner, E. (2019) The Neanderthal endocast from Gánovce (Poprad, Slovak Republic). *Journal of Anthropological Sciences*, 97: 1–12.

Ellstrand, N. C. (1983) Why are juveniles smaller than their parents? *Evolution*, 37(5): 1091–1094.

Engbretson, G. A. and Lent, C. M. (1976) Parietal eye of the lizard: neuronal photoresponses and feedback from the pineal gland. *Proceedings of the National Academy of Sciences of the United States of America*, 73(2): 654–657.

Estes, R. (1961) Cranial anatomy of the cynodont reptile *Thrinaxodon liorhinus*. *Bulletin of the Museum of Comparative Zoology at Harvard College,* 125(6): 165–183.

Fernandez, V., Abdala, F., Carlson, K. J., Collins Cook, D., Rubidge, B. S., Yates, A. and Tafforeau, P. (2013) Synchrotron reveals Early Triassic odd couple: injured amphibian and aestivating therapsid share burrow. *PLoS ONE,* 8(6): e64978.

Ferner, K., Schultz, J. A. and Zeller, U. (2017) Comparative anatomy of neonates of the three major mammalian groups (monotremes, marsupials, placentals) and implications for the ancestral mammalian neonate morphotype. *Journal of Anatomy,* 231(6): 798–822.

Ferreira, J. D., Teresa Dozo, M., de Moura Bubadué and Kerber, L. (2022) Morphology and postnatal ontogeny of the cranial endocast and paranasal sinuses of capybara (*Hydrochoerus hydrochaeris*), the largest living rodent. *Journal of Morphology*, 283: 66–90.

Figueroa. R. T., Goodvin, D., Kolmann, M. A., Coates, M. I., Caron, A. M., Friedman, M. and Giles, S. (2023) Exceptional fossil preservation and evolution of the ray-finned fish brain. *Nature*, 614: 486–491.

Filippini, F.S., Abdala, F. and Cassini, G.H. (2022) Body mass estimation in Triassic cynodonts from Argentina based on limb variables. *Acta Palaeontologica Polonica,* 67(2): 543–557.

Fischer, V., Bennion, R. F., Foffa, D., MacLaren, J. A., McCurry, M. R., Melstrom, K. M. and Bardet, N. (2022) Ecological signal in the size and shape of marine amniote teeth. *Proceedings of the Royal Society B*, 289: 20221214.

Ford D. P. and Benson, R. B. J. (2020) The phylogeny of early amniotes and the affinities of Parareptilia and Varanopidae. *Nature Ecology and Evolution*, 4: 57–65.

Franks V. R. and Thorogood, R. (2018) Older and wiser? Age differences in foraging and learning by an endangered passerine. *Behavioural Processes*, 148: 1–9.

Franco, A. S., Müller, R. T, Martinelli, A. G., Hoffman, C. A. and Kerber, L. (2021) The nasal cavity of two traversodontid cynodonts (Eucynodontia, Gomphodontia) from the Upper Triassic of Brazil. *Journal of Paleontology*, 95(4): 845–860.

Funston, G. F., de Polo, P. E., Sliwinski, J. T., Dumont, M., Shelley, S. L., Pichevin, L. E., Cayzer, N. J., Wible, J. R. *et al*. (2022) The origin of placental mammal life histories. *Nature*, 610: 107–111.

Gaetano, L. C. and Abdala, F. (2020). The stapes of *Thrinaxodon* Seeley, 1894 and *Galesaurus* Owen, 1859: a case of study for intraspecific variability in basal cynodonts. *Comptes Rendus Palevol.* 20(5): 57–74.

Gastaldo, R. A., Neveling, J., Geissman, J. W., Kamo, S. L. and Looy, C. V. (2021) A tale of two Tweefonteins: what physical correlation, geochronology, magnetic polarity stratigraphy, and palynology reveal about the end-Permian terrestrial extinction paradigm in South Africa. *GSA Bulletin*, 134(3-4): 691–721.

Gerkema, M. P., Davies, W. I. L., Foster, R. G., Menaker, M. and Hut, R. A. (2013) The nocturnal bottleneck and the evolution of activity patterns in mammals. *Proceedings of the Royal Society B*, 280(1765): 28020130508.

Glickstein, M. (2007) What does the cerebellum really do? *Current Biology*, 17(19): R824–R827.

Gray, J. A., Sherratt, E., Hutchinson, M. N. and Jones, M. E. H. (2019) Changes in ontogenetic patterns facilitate diversification in skull shape of Australian agamid lizards. *BMC Evolutionary Biology*, 19: 7.

Griffin, C. T., Stocker, M. R., Colleary, C., Stefanic, C. .M, Lessner, E. J., Riegler, M., Formoso, K., Koeller, K. and Nesbitt, S.J. (2021) Assessing ontogenetic maturity in extinct saurian reptiles. *Biological Reviews*, 96(2): 470–525.

Guignard, M. L., Martinelli, A. G. and Soares, M. B. (2018) Reassessment of the postcranial anatomy of *Prozostrodon brasiliensis* and implications for postural evolution of non-mammaliaform cynodonts. *Journal of Vertebrate Palaeontology*, 38(5): e1511570.

Hammer, Ø., Harper, D. A., and Ryan, P. D. (2001). PAST: Paleontological statistics software package for education and data analysis. *Palaeontologia electronica,* 4(1): 9.

Hanken, J. and Thorogood, P. (1993) Evolution and development of the vertebrate skull: The role of pattern formation. *Trends in Ecology and Evolution*, 8(1): 9–15.

Heers, A. M. (2016) New perspectives on the ontogeny and evolution of avian locomotion. *Integrative and Comparative Biology*, 56(3): 428–441.

Henderson, S. A. C. and Challands, T. J. (2018) The cranial endocast of the Upper Devonian dipnoan `*Chirodipterus' australis*. *PeerJ*, 6: e5148.

Herbst, E. C., Meade, L. E., Lautenschlager, S., Fioritti, N. and Scheyer, T. M. (2022). A toolbox for the retrodeformation and muscle reconstruction of fossil specimens in Blender. *Royal Society Open Science*, 9(8): 220519.

Herrel, A., Lopez-Darias, M., Vanhooydonck, B., Cornette, R., Kohlsdorf, T. and Brandt, R. (2016) Do adult phenotypes reflect selection on juvenile performance? A comparative study on performance and morphology in lizards. *Integrative and Comparative Biology*, 56(3): 469–478.

Ho Cho, K., Rodríguez-Vázquez, J. F., Kim, J. H., Abe, H., Murakami, G. and Cho, B. H. (2011) Early fetal development of the human cerebellum. *Surgical and Radiologic Anatomy*, 33: 523–530.

Hoffman, E. A. and Rowe, T. B. (2018) Jurassic stem-mammal perinates and the origin of mammalian reproduction and growth. *Nature,* 561: 104–108.

Hoffman, C. A., Rodrigues, P. G., Soares, M. B. and de Andrade, M. B. (2021) Brain endocast of two non-mammaliaform cynodonts from southern Brazil: an ontogenetic and evolutionary approach. *Historical Biology,* 33(8): 1196–1207.

Hopson, J. A. (1979). 'Paleoneurology', in Gans, C., Northcutt, R. G. and Ulinski, P. *Biology of the Reptilia*. New York: Academic Press Inc.

Hou, Y., Canul-Ku, M., Cui, X., Hasimoto-Beltran, R. and Zhu, M. (2021) Semantic segmentation of vertebrate microfossils from computed tomography data using a deep learning approach. *Journal of Micropalaeontology*, 40(2): 163–173.

Huttenlocker, A. K. (2014) Body size reductions in nonmammalian eutheriodont therapsids (Synapsida) during the End-Permian mass extinction. *PLOS ONE*, 9(2): e87553.

Huttenlocker, A.K., Grossnickle, D. M., Kirkland, J. I., Schultz J. A. and Luo, Z-X. (2018) Late-surviving stem mammal links the lowermost Cretaceous of North America and Gondwana. *Nature*, 558: 108–112.

Huttenlocker, A. M. and Sidor, C. A. (2020) A basal non-mammaliaform cynodont from the Permian of Zambia and the origins of mammalian endocranial and postcranial anatomy. *Journal of Vertebrate Paleontology*, 40(5): e1827413.

Isler, K. and van Schaik, C. P. (2006) Metabolic costs of brain size evolution. *Biology Letters*, 2(4): 2557–560.

Iurino, D. A., Conti, J, Mecozzi, B. and Sardella, R. (2020) Braincase with natural endocast of a juvenile rhinocerotinae from the Late Middle Pleistocene site of Melpignano (Apulia, Southern Italy). *Frontiers in Earth Science,* 8: 1–14.

Iurino, D. A., Profico, A., Cherin, M., Veneziano, A., Costeur, L., and Sardella, R. (2015). A lynx natural brain endocast from Ingarano (Southern Italy; Late Pleistocene): taphonomic,

morphometric and phylogenetic approaches. *Hystrix, the Italian Journal of Mammalogy*, 26(2): 110–117.

Jasinoski, S. C. and Abdala, F. (2017) Aggregations and parental care in the Early Triassic basal cynodonts *Galesaurus planiceps* and *Thrinaxodon liorhinus*. *PeerJ*, 5: e2875.

Jasinoski, S. C., Abdala, F. and Fernandez, V. (2015) Ontogeny of the Early Triassic cynodont *Thrinaxodon liorhinus* (Therapsida): cranial morphology. *The Anatomical Record*, 298: 1440–1464.

Jerison, H. J. (1973) *Evolution of the Brain and Intelligence*. New York: Academic Press.

Jerison, H. J. (1991) 'Fossil Brains and the evolution of the neocortex', in Finlay, B. L., Innocenti, G. and Scheich, H. (ed.). *The Neocortex: Ontogeny and Phylogeny*. New York: Springer New York, 5–19.

Ji, Q., Luo, Z-X., Yuan, C-X. and Tabrum, A. R. (2006) A swimming mammaliaform from the Middle Jurassic and ecomorphological diversification of early mammals. *Science*, 311(5764): 1123–1127.

Kaas, J. H. (1989) The evolution of complex sensory systems in mammals. *Journal of Experimental Biology,* 146: 165–176.

Kaas, J. H. (2009). 'Evolution of the Brain in Mammals', in Binder, M. D., Hirokawa, N. and Windhorst, U. (eds) *Encyclopedia of Neuroscience*, Berlin; Springer.

Kaas, J. H. (2011) Neocortex in early mammals and its subsequent variations. *Annals of the New York Academy of Sciences*, 1225: 28–36.

Kaas, J. H. (2013) The evolution of brains from early mammals to humans. *WIREs Cognitive Science*, 4(1): 33–45.

Kammerer, C. F. (2016) A new taxon of cynodont from the *Tropidostoma* Assemblage Zone (upper Permian) of South Africa, and the early evolution of Cynodontia. *Papers in Palaeontology*, 2(3): 387–397.

Karten, H. J. (2015) Vertebrate brains and evolutionary connectomics: on the origins of the mammalian 'neocortex'. *Philosophical Transactions B,* 370(1684): 20150060.

Kemp, T. S. (1979) The primitive cynodont *Procynosuchus*: functional anatomy of the skull and relationships. *Philosophical Transactions of the Royal Society of London Series B Biological Sciences*, 285(1005): 73–122.

Kemp, T. S. (1982) *Mammal-like reptiles and the origin of mammals*. London: Academic Press.

Kemp, T. S. (2005) *The origin and evolution of mammals*. New York: Oxford University Press.

Kemp, T. S. (2009) The endocranial cavity of a nonmammalian eucynodont, *Chiniquodon theotenicus*, and its implications for the origin of the mammalian brain. *Journal of Vertebrate Paleontology*, 29(4): 1188–1198.

Kerber, L., Ferreira, J. D., Fonseca, P. H. M., Franco, A., Martinelli, A. G., Soares, M. B. and Ribeiro, A. M. (2021) An additional brain endocast of the ictidosaur *Riograndia guaibensis* (Eucynodontia: Probainognathia): intraspecific variation of endocranial traits. *Annals of the Brazilian Academy of Sciences*, 93(2): e20200084.

Kerber, L., Roese-Miron, L., Bubadué, J. M. and Martinelli, A. G. (2023) Endocranial anatomy of the early prozostrodonts (Eucynodontia: Probainognathia) and the neurosensory evolution in mammal forerunners. *The Anatomical Record*, 1–32.

Kielan-Jaworowska, Z. (1984). Evolution of the therian mammals in the Late Cretaceous of Asia, part VI - endocranial casts of eutherian mammals. *Palaeontologia Polonica*, 46: 157–171.

Kielan-Jaworowska, Z., Cifelli, R. L. and Luo, Z.-X. (2004) *Mammals from the age of dinosaurs: origin, evolution, and structure*. New York: Columbia University Press.

Klinger, E. (2017) Development and organization of the evolutionarily conserved three-layered olfactory cortex. *eNeuro*, 4(1): 1–14.

Kollikowski, A., Zimmermann, E. and Radespiel, U. (2019) First experimental evidence for olfactory species discrimination in two nocturnal primate species (*Microcebus lehilahytsara* and *M. murinus*). *Scientific Reports*, 9: 20386.

Koyabu, D., Werneburg, I., Morimoto, N., Zollikofer, C. P. E., Forasiepi, A. M., Endo, H. *et al*. (2014) Mammalian skull heterochrony reveals modular evolution and a link between cranial development and brain size. *Nature Communications*, 5: 3625.

Kurochkin, E. N., Dyke, G. J., Saveliev, S. V., Pervushov, E. M. and Popov, E. V. (2007) A fossil brain from the Cretaceous of European Russia and avian sensory evolution. *Biology Letters*, 3(3): 309–313.

Kuznetsov, A. N. and Panyutina, A. A. (2018) First paleoichnological evidence for baby-riding in early mammals. *Ameghiniana*, 55(6): 668–676.

Laaß, M. (2016) The origins of the cochlea and impedance matching hearing in synapsids. *Acta Palaeontologica Polonica*, 61(2): 267–280.

Laaß, M., Schillinger, B. and Kaestner, A. (2017a) What did the "unossified zone" of the non-mammalian therapsid braincase house? *Journal of Morphology*, 278(8): 1020–1032.

Laaß, M., Schillinger, B. and Werneburg, I. (2017b) Neutron tomography and x-ray tomography as tools for the morphological investigation of non-mammalian synapsids. *Physics Procedia*, 88: 100–108.

Lautenschlager, S. (2016) Reconstructing the past: methods and techniques for the digital restoration of fossils. *Royal Society Open Science*, 3(10): 160342.

Lautenschlager, S. (2022) Functional and ecomorphological evolution of orbit shape in Mesozoic archosaurs is driven by body size and diet. *Communications Biology,* 5: 754.

Lautenschlager, S., and Butler, R. J. (2016). Neural and endocranial anatomy of Triassic phytosaurian reptiles and convergence with fossil and modern crocodylians. *PeerJ*, 4: e2251.

Lautenschlager, S., Fagan, M. J., Luo, Z-X., Bird, C. M., Gill, P. and Rayfield, E. J. (2023) Functional reorganisation of the cranial skeleton during the cynodont-mammaliaform transition. *Communications Biology,* 6: 367.

Lautenschlager, S., Ferreira, G. S., and Werneburg, I. (2018). Sensory evolution and ecology of early turtles revealed by digital endocranial reconstructions. *Frontiers in Ecology and Evolution,* 6(7): 1–16.

Lautenschlager, S., Gill, P., Luo Z-X., Fagan M. J. and Rayfield, E. J. (2017) Morphological evolution of the mammalian jaw adductor complex. *Biological Reviews*, 92(4): 1910–1940.

Lautenschlager, S., Gill, P. G., Luo, Z-X., Fagan, M. J. and Rayfield, E. J. (2018) The role of miniaturization in the evolution of the mammalian jaw and middle ear. *Nature*, 561: 533–537.

Lautenschlager, S. and Hübner, T. (2013) Ontogenetic trajectories in the ornithischian endocranium. *Journal of Evolutionary Biology*, 26(9): 2044–2050.

Lautenschlager, S. and Rücklin, M. (2014). Beyond the print - virtual paleontology in science publishing, outreach, and education. *Journal of Paleontology*, 88(4): 727–734.

Lefèvre, C. M., Sharp, J. A. and Nicholas, K. R. (2010) Evolution of lactation: ancient origin and extreme adaptations of the lactation system. *Annual Review of Genomics and Human Genetics*, 11: 219–238.

Legendre, L. J. and Davesne, D. (2020) The evolution of mechanisms involved in vertebrate endothermy. *Philosophical Transactions of the Royal Society B,* 375(1793): 20190136.

Leigh, S. (1992) Patterns of variation in the ontogeny of primate body size dimorphism. *Journal of Human Evolution*, 23(1): 27–50.

Lenschow, C., Mendes, A. R. P. and Lima, S. Q. (2022) Hearing, touching, and multisensory integration during mate choice. *Frontiers in Neural Circuits*, 16: 1–37.

Lieberwirth, C. and Wang, Z. (2012) The social environment and neurogenesis in the adult mammalian brain. *Frontiers in Human Neuroscience*, 6: 00118.

Lin, H.-Y., Huang, C.-C., Chou, K.-H., Yang, A. C., Lo, C.-Y. Z., Tsai, S.-J. and Lin, C.P. (2021) Differential patterns of gyral and sulcal morphological changes during normal aging process. *Frontiers in Aging Neuroscience*, 13: 625931.

Lovegrove, B. G. (2019) Obligatory nocturnalism in Triassic archaic mammals: preservation of sperm quality? *Physiological and Biochemical Zoology*, 92(6): 544–553.

Lukic-Walther, M., Brocklehurst, N., Kammerer, C. F. and Frösbisch, J. (2019) Diversity patterns of nonmammalian cynodonts (Synapsida, Therapsida) and the impact of taxonomic practice and research history on diversity estimates. *Paleobiology,* 45(1): 56–69.

Luo, Z.-X. (2007) Transformation and diversification in early mammal evolution. *Nature,* 450: 1011–1019.

Luo, Z.-X., Crompton, A. W. and Sun, A. L. (2001) A new mammaliaform from the early Jurassic and evolution of mammalian characteristics. *Science,* 292(5521): 1535–1540.

Lutz, B. (1948) Ontogenetic evolution in frogs. *Evolution*, 2(1): 29–39.

MacLarnon, A. (1996) The evolution of the spinal cord in primates: evidence from the foramen magnum and the vertebral canal. *Journal of Human Evolution*, 30(2): 121–138.

Macrini, T. E. (2006). *The evolution of endocranial space in mammals and non-mammalian cynodonts*. Texas: The University of Texas at Austin.

Macrini, T. E. (2012) Comparative morphology of the internal nasal skeleton of adult marsupials based on x-ray computed tomography. *Bulletin of the American Museum of Natural History*, 365: 1–91.

Macrini, T. E., Rougier, G. W. and Rowe, T. (2007a) Description of a cranial endocast from the fossil mammal *Vincelestes neuquenianus* (Theriiformes) and its relevance to the evolution of endocranial characters in Therians. *The Antonomical Record*, 290(7): 875–892.

Macrini, T. E., Rowe, T. and Archer, M. (2006). Description of a cranial endocast from a fossil platypus, *Obdurodon dicksoni* (Monotremata, Ornithorhynchidae), and the relevance of endocranial characters to monotreme monophyly. *Journal of Morphology*, 267(8): 1000–1015.

Macrini, T. E., Rowe, T. and VandeBerg, J. L. (2007b) Cranial endocasts from a growth series of *Monodelphis domestica* (Didelphidae, Marsupialia): a study of individual and ontogenetic variation. *Journal of Morphology*, 268(10): 844–865.

Manger, P. R. (2006) An examination of cetacean brain structure with a novel hypothesis correlating thermogenesis to the evolution of a big brain. *Biological Reviews*, 81(2): 293–338.

Manley, G.A. (2018) The foundations of high-frequency hearing in early mammals. Journal of Mammalian Evolution, 25: 155–163.

Martin, T., Marugán-Lobón, J., Vullo, R., Martín-Abad, H., Luo, Z-X. and Buscalioni, A. D. (2015) A Cretaceous eutriconodont and integument evolution in early mammals. *Nature,* 526: 380–384.

Martinelli, A. G., Eltink, E., Da-Rosa, A. A. S. and Langer, M. C. (2017) A new cynodont from the Santa Maria formation, south Brazil, improves Late Triassic probainognathian diversity. *Papers in Palaeontology*, 3(3): 401–423.

Matsuoka, H., Kusuhashi, N. and Corfe, I. J. (2016) A new Early Cretaceous tritylodontid (Synapsida, Cynodontia, Mammaliamorpha) from the Kuwajima Formation (Tetori Group) of central Japan. *Journal of Vertebrate Paleontology*, 36(4): e1112289.

Miller, C. E., Basu, C., Fritsch, G., Hildebrandt, T. and Hutchinson, J. R. (2008) Ontogenetic scaling of foot musculoskeletal anatomy in elephants. *Journal of the Royal Society Interface,* 5(21): 465–475.

Ming, G-I. And Song, H. (2011) Adult neurogenesis in the mammalian brain: significant answers and significant questions. *Neuron*, 70(4): 687–702.

Molnár Z., Kaas, J. H., de Carlos, J. A., Hevner, R. F., Lein, E. and Němec, P. (2014) Evolution and development of the mammalian cerebral cortex. *Brain, Behaviour and Evolution,* 83(2): 126–139.

Mota, B. and Herculano-Houzel, S. (2015) Cortical folding scales universally with surface area and thickness, not number of neurons. *Science*, 349(6243): 74–77.

Mota-Rojas, D., Titto, C. G., Orihuela, A., Martínez-Burnes, J., Gómez-Prado, J., Torres-Bernal, F., Flores-Padilla, K., Carvajal-de la Fuente, V. *et al*. (2021) Physiological and behavioral mechanisms of thermoregulation in mammals. *Animals*, 11(1733): 1–27.

Moustakas, J. E., Smith, K. K. and Hlusko, L. J. (2010) Evolution and development of the mammalian dentition: Insights from the marsupial *Monodelphis domestica*. *Developmental Dynamics*, 240 (1): 232–239.

Muchlinski, M. N., Wible, J. R., Corfe, I., Sullivan, M. and Grant, R. A. (2020) Good vibrations: the evolution of whisking in small mammals. *The Anatomical Record*, 303(1): 89–99.

Napoli, J. G., Williamson, T. E., Shelley, S. L. and Brusatte, S. L. (2018) A digital endocranial cast of the Early Paleocene (Puercan) 'archaic' mammal *Onychodectes tisonensis* (Eutheria: Taeniodonta). *Journal of Mammalian Evolution*, 25: 179–195.

Navalón, G., Nebreda, S. M., Bright, J. A., Fabbri, M., Benson, R. B. J., Bhullar, B-A *et al.* (2021) Craniofacial development illuminates the evolution of nightbirds (Strisores). *Proceedings of the Royal Society B*, 288(1948): 28820210181.

Nicholls, M. E. R. (1996) Temporal processing asymmetries between the cerebral hemispheres: evidence and implications. *Laterality*, 1(2): 97–138.

Nielsen, B. L., Jezierski, T., Bolhuis, J. E., Amo, L., Rosell, F., Oostindjer, M. *et al*. (2015) Olfaction: an overlooked sensory modality in applied ethology and animal welfare. *Frontiers in Veterinary Science*, 2: 1–3.

Northcutt, R. G. (2011) Evolving large and complex brains. *Science*, 332(6032): 926–627.

Norton, L. A., Abdala, F. and Benoit, J. (2023) Craniodental anatomy in Permian–Jurassic Cynodontia and Mammaliaformes (Synapsida, Therapsida) as a gateway to defining mammalian soft tissue and behavioural traits. *Philosophical Transactions of the Royal Society B*, 378(1880): 20220084.

Oftedal, O. T. (2002) The mammary gland and its origin during synapsid evolution. *Journal of Mammary Gland Biology and Neoplasia,* 7(3): 225–252.

Orliac, M. J. and Gilissen, E. (2012) Virtual endocranial cast of earliest Eocene *Diacodexis* (Artiodactyla, Mammalia) and morphological diversity of early artiodactyl brains. *Proceedings of the Royal Society B*, 279(1743): 2793670–3677.

Owen, R. (1887) On the skull and dentition of a Triassic saurian (*Galesaurus planiceps*, Owen). *Quarterly Journal of the Geological Society of London,* 43: 1–6.

Panksepp, J. (2011) The basic emotional circuits of mammalian brains: do animals have affective lives? *Neuroscience and Biobehavioural Reviews*, 35(9): 1791–1804.

Paredes, M. F., Sorrells, S. F., Garcia-Verdugo, J. M. and Alvarez-Buylla, A. (2016) Brain size and limits to adult neurogenesis. *Journal of Comparative Neurology*, 524(3): 646–664.

Parrington, F. R. (1933) II. On the cynodont reptile *Thrinaxodon liorhinus,* Seeley. *Annals and Magazine of Natural History*, 11(61): 16–24.

Parrington, F. R. (1946) On the cranial anatomy of cynodonts. *Proceedings of the Zoological Society of London*, 116(2): 181–197.

Pavanatto, A. E. B., Kerber, L. and Dias-da-Silva, S. (2019) Virtual reconstruction of cranial endocasts of traversodontid cynodonts (Eucynodontia: Gomphodontia) from the upper Triassic of Southern Brazil. *Journal of Morphology,* 280(9): 1267–1281.

Peters, R. (2006) Ageing and the brain. *Postgraduate Medical Journal*, 82(964): 84–88.

Poirier, C., Baumann, S., Dheerendra, P., Joly, O., Hunter, D., Balezeau, F., Sun, Li *et al*., (2017) Auditory motion-specific mechanisms in the primate brain. *PLoS Biology*, 15(5): e2001379.

Poldrack, R. A. and Packard, M. G. (2003) Competition among multiple memory systems: converging evidence from animal and human brain studies. *Neuropsychologia*, 41(3): 245–251.

Power, M. L. and Schulkin, J. (2013) Maternal regulation of offspring development in mammals is an ancient adaptation tied to lactation. *Applied and Translational Genomics*, 2: 55–63.

Profico, A., Buzi, C., Melchionna, M., Veneziano, A. and Raia, P. (2020) *Endomaker*, a new algorithm for fully automatic extraction of cranial endocasts and the calculation of their volumes. *American Journal of Physical Anthropology*, 172(3): 511–515.

Prounis, G. S. and Ophir, A. G. (2020) One cranium, two brains not yet introduced: distinct but complementary views of the social brain. *Neuroscience and Biobehavioural Reviews*, 108: 231–245.

Pujol, J., Blanco-Hinojo, L., Macia, D., Martínez-Vilavella, G., Deus, J., Pérez-Sola, V. *et al*. (2021) Differences between the child and adult brain in the local functional structure of the cerebral cortex. *NeuroImage*, 237: 118150.

Pusch, L. C., Kammerer, C. F., Fernandez, V. and Fröbisch, J. (2022) Cranial anatomy of *Nythosaurus larvatus* Owen, 1876, an Early Triassic cynodont preserving a natural endocast. *Journal of Vertebrate Paleontology*, 42(3): e2174441.

Pusch, L.C., Kammerer, C.F. and Fröbisch, J. (2019) Cranial anatomy of the early cynodont *Galesaurus planiceps* and the origin of mammalian endocranial characters. *Journal of Anatomy*, 234(5): 592–621.

Quiroga, J. C. (1979) The brain of two mammal-like reptiles (Cynodontia-Therapsida). *Journal für Hirnforschung*, 20: 341–350.

Quiroga, J.C. (1980a) The brain of the mammal-like reptile *Probainognathus jenseni* (Therapsida, Cynodontia). A correlative paleo-neoneurological approach to the neocortex at the reptile-mammal transition. *Journal für Hirnforschung*, 21: 299–336.

Quiroga, J.C. (1980b) 'Description of the endocasts of two cynodonts (Reptilia-Therapsida) of Los Chanares-Middle Triassic-of the Province of La Rioja (Argentina)' in *Actas II Congreso Argentino de Paleontologia y Bioestratigrafia y I Congreso Latinoamericano de Paleontologia*. Buenos Aires, pp. 103–122.

Quiroga, J.C. (1980c) On an endocranial cast of the cynodont *Probainognathus jenseni* Romer, 1970 (Reptilia, Therapsida), of the Ischichuca Formation (Middle Triassic), La Rioja, Argentina. *Ameghiniana*, 17: 181–190.

Quiroga, J. C. (1980d) Further studies on cynodont endocasts (Reptilia-Therapsida). *Zeitschrift für Mikroskopisch-Anatomische Forschung*, 94(4): 580–592.

Quiroga, J. C. (1984). The endocranial cast of the advanced mammal-like reptile *Therioherpeton cargnini* (Therapsida-Cynodontia) from the Middle Triassic of Brazil. *Journal Für Hirnforschung*, 25(3): 285–290.

Radinsky, L. B. (1968) A new approach to mammalian cranial analysis, illustrated by examples of prosimian primates. *Journal of Morphology*, 124(2): 167–179.

Radulescu, C. II, Cerar, V., Haslehurst, P., Kopanitsa, M. and Barnes, S. J. (2021) The aging mouse brain: cognition, connectivity and calcium. *Cell Calcium*, 94: 102358.

Rahman, I. A., Adcock, K. and Garwood, R. J. (2012) Virtual fossils: a new resource for science communication in paleontology. *Evolution: Education and Outreach*, 5: 635–641.

Rakic, P. (2009) Evolution of the neocortex: perspective from developmental biology. *Nature Reviews Neuroscience*, 10: 724–735.

Ray, S. (2015) A new Late Triassic traversodontid cynodont (Therapsida, Eucynodontia) from India. *Journal of Vertebrate Paleontology*, 35(3): e930472.

Rayfield, E. J. (2007) Finite element analysis and understanding the biomechanics and evolution of living and fossil organisms. *Annual Review of Earth and Planetary Sciences*, 35: 541–576.

Reeber, S. L., Otis, T. S. and Sillitoe, R. V. (2013) New roles for the cerebellum in health and disease. *Frontiers in Systems Neuroscience*, 7: 1–11.

Rey, K., Amiot, R., Fourel, F., Abdala, F., Fluteau, F., Jalil, N-E., Liu, J., Rubidge, B. S. *et al.* (2017) Oxygen isotopes suggest elevated thermometabolism within multiple Permo-Triassic therapsid clades. *eLife*, 6: e28589.

Rilling, J. K. and Young, L. J. (2014) The biology of mammalian parenting and its effect on offspring social development. *Science*, 345(6198): 771–776.

Rodrigues, H. G., Lefebvre, R., Fernández-Monescillo, M., Mamani Quispe, B. and Billet, G. (2017) Ontogenetic variations and structural adjustments in mammals evolving prolonged to continuous dental growth. *Royal Society Open Science*, 4(7): 4170494.

Rodrigues, P. G., Martinelli, A. G., Schultz, C. L., Corfe, I. J., Gill, P. G., Soares, M. B. and Rayfield, E. J. (2019) Digital cranial endocast of *Riograndia guaibensis* (Late Triassic, Brazil) sheds light on the evolution of the brain in non-mammalian cynodonts. *Historical Biology*, 31(9): 1195–1212.

Rodrigues, P. G., Ruf, I. and Schultz, C. L. (2013) Digital reconstruction of the otic region and inner ear of the non-mammalian cynodont *Brasilitherium riograndensis* (Late Triassic, Brazil) and its relevance to the evolution of the mammalian ear. *Journal of Mammalian Evolution*, 20: 291–307.

Rodrigues, P. G., Ruf, I. and Schultz, C. L. (2014) Study of a digital cranial endocast of the non-mammaliaform cynodont *Brasilitherium riograndensis* (Later Triassic, Brazil) and its relevance to the evolution of the mammalian brain. *Paläontologische Zeitschrift*, 88: 329–352.

Rokszin, A., Márkus, Z., Braunitzer, G., Berényi, A., Benedek, G. and Nagy, A. (2010) Visual pathways serving motion detection in the mammalian brain. *Sensors*, 10: 3218–3242.

Rosenkilde. P. and Ussing, A. P. (1996) What mechanisms control neoteny and regulate induced metamorphosis in urodeles? *International Journal of Developmental Biology*, 40(4): 665–673.

Rosowski, J. J. and Graybeal, A. (1991) What did *Morganucodon* hear? *Zoological Journal of the Linnean Society*, 101(2): 131–168.

Rowe, T. (1996) Coevolution of the mammalian middle ear and neocortex. *Science*, 273(5275): 651–654.

Rowe, T., Carlson, W. and Bottorff, W. (1993) *Thrinaxodon*: Digital Atlas of the Skull (CD-ROM). University of Texas Press.

Rowe, T. B., Eiting T. P., Macrini, T. E. and Ketcham R. A. (2005) Organization of the olfactory and respiratory skeleton in the nose of the grey short-tailed opossum *Monodelphis domestica*. *Journal of Mammalian Evolution*, 12: 303–336.

Rowe, T. B., Macrini, T. E. and Luo, Z-X. (2011) Fossil evidence on origin of the mammalian brain. *Science*, 332(6032): 955–957.

Rowe, T. B. and Shepherd, G. M. (2016) Role of ortho-retronasal olfaction in mammalian cortical evolution. *Journal of Comparative Neurology*, 524 (3): 471–495.

Ruf, I., Maier, W., RodrIgues, P. G. and Schultz, C. L. (2014) Nasal anatomy of the non-mammaliaform cynodont *Brasilitherium riograndensis* (Eucynodontia, Therapsida) reveals new insight into mammalian evolution. *The Anatomical Record*, 297(11): 2018–2030.

Ruiz-Núñez, B., Pruimboom, L., Dijck-Brouwer, D. A. and Muskiet, F. A. J. (2013) Lifestyle and nutritional imbalances associated with western diseases: causes and consequences of chronic systemic low-grade inflammation in an evolutionary context. *The Journal of Nutritional Biochemistry*, 24(7): 1183–1201.

Ruta, M., Botha-Brink, J., Mitchell, S. A. and Benton, M.J. (2013) The radiation of cynodonts and the ground plan of mammalian morphological diversity. *Proceedings of Royal Society B*, 280(1769): 20131865.

Saganuwan, S.A. (2021) Modified formulas for calculation of encephalization: quotient in dogs. *BMC Research Notes*, 14: 223.

Sakai, O. (2018) Comparison of personality between juveniles and adults in clonal gecko species. *Journal of Ethology*, 36: 221–228.

Sánchez-Villagra, M. R., Gemballa, S., Nummela, S., Smith, K. K. and Maier, W. (2002) Ontogenetic and phylogenetic transformations of the ear ossicles in marsupial mammals. *Journal of Morphology*, 251(3): 219–238.

Seebacker, F. and Krause, J. (2017) Physiological mechanisms underlying animal social behaviour. *Philosophical Transactions of the Royal Society B*, 372(1727): 20160231.

Seeley, H.G. (1889) Researches on the structure, organisation, and classification of the fossil reptilia. VI. On the anomodont reptilia and their allies. *Philosophical Transactions of the Royal Society of London B*, 180: 215–296.

Seeley, H.G. (1894) Research on the structure, organisation, and classification of the fossil reptilia. IX. On the cynodontia. *Annals and Magazine of Natural History*. 14(83): 387–390.

Seeley, H. G. (1894b) Research on the structure, organisation, and classification of the fossil reptilia: on *Diademodon*. *Philosophical Transactions of the Royal Society of London*, 185: 1029–1041.

Sepp, M., Leiss, K., Murat, F., Okonechnikov, K., Joshi, P., Leushkin, E. *et al.* (2024) Cellular development and evolution of the mammalian cerebellum. *Nature*, 625: 788–796.

Sharp, A. C., (2016) A quantitative comparative analysis of the size of the frontoparietal sinuses and brain in vombatiform marsupials. *Memoirs of Museum Victoria*, 74: 331–342.

Sherwood, C. C., Gordon, A. D., Allen, J. S., Phillips, K. A., Erwin, J. W., Hof, P. R. and Hopkins, W. D. (2011) Aging of the cerebral cortex differs between humans and chimpanzees. *Proceedings of the National Academy of Sciences of the United States of America*, 108(32): 13029–13034.

Sillitoe, R. V., Fu, Y. and Watson, C. (2012) 'Chapter 11 – Cerebellum' in Watson, C., Paxinos, G. and Puelles, L. (ed) *The Mouse Nervous System*. Academic Press, pp. 360–397.

Smaers, J. B., Rothman, R. S., Hudson, D. R., Balanoff, A. M., Beatty, B., Dechmann, D. K. N., de Vries, D., Dunn, J. C. *et al*. (2021) The evolution of mammalian brain size. *Science Advances*, 7(18): eabe2101.

Smaers, J. B., Turner, A. H., Gómez-Robles, A. and Sherwood, C. C. (2018) A cerebellar substrate for cognition evolved multiple times independently in mammals. *eLife*, 7: e35696.

Smirnov, S. V. and Vassilieva, A. B. (2022) Amphibian ontogeny: major trends, mechanisms, and paradoxes of evolution. *Paleontological Journal*, 56: 1257–1273.

Smith, F. A. (2022) The road to a larger brain. *Science*, 376(6588): 27–28.

Smith, R. M. H. (1995) Changing fluvial environments across the Permian-Triassic boundary in the Karoo Basin, South Africa and possible causes of tetrapod extinctions. *Palaeogeography, Palaeoclimatology, Palaeoecology*, 117(1–2): 81–104.

Smith, K. T., Bhullar, B-A. S., Köhler, G. and Habersetzer, J. (2018) The only known jawed vertebrate with four eyes and the bauplan of the pineal complex. *Current Biology*, 28(7): 1101–1107.

Smith, R. M. H., Botha, J. and Viglietti, P. A. (2022) Taphonomy of drought afflicted tetrapods in the Early Triassic Karoo Basin, South Africa. *Palaeogeography, Palaeoclimatology, Palaeoecology*, 604: 111207.

Sollas, W. J. (1904) A method for the investigation of fossils by serial sections. *Philosophical Transactions of the Royal Society of London Series B (Containing Papers of a Biological Character)*, 196: 259–265.

Song, J. (2019) Pineal gland dysfunction in Alzheimer's disease: relationship with the immune-pineal axis, sleep disturbance, and neurogenesis. *Molecular Neurodegeneration*, 14: 28.

Sookias, R. B., Butler, R. J. and Benson, R. B. J. (2012) Rise of dinosaurs reveals major body-size transitions are driven by passive processes of trait evolution. *Proceedings of the Royal Society B,* 279(1736): 2792180–2187.

Stonerook, M. J. and Harder, J. D. (1992) Sexual maturation in female grey short-tailed opossums, *Monodelphis domestica*, is dependent upon male stimuli. *Biology of Reproduction*, 46(2): 290–294.

Striedter, G. F. (2005) *Principles of Brain Evolution*. Massachusetts: Sinauer Associates.

Suárez, R., Paolino, A., Fenlon, L. R., Morcom, L. R., Kozulin, P., Kurniawan, N.D. and Richards, L. J. (2018) A pan-mammalian map of interhemispheric brain connections predates the evolution of the corpus callosum. *The Proceedings of the National Academy of Sciences*, 115(38): 9622–9627.

Sues, H-D. (2018) Palaeontology: many babies or bigger brains? *Current Biology*, 28(21): 1254–1256.

Sutton, M. D., Garwood, R. J., Siveter, D. J., and Siveter, D. J. (2012). SPIERS and VAXML: a software toolkit for tomographic visualisation and a format for virtual specimen interchange. *Palaeontologia Electronica*, 15(2): 1–14.

Sutton, M. D., Rahman., I. A. and Garwood, R. J. (2014) *Techniques for virtual palaeontology*. John Wiley and Sons Ltd.

Tate, J. R. and Cann, C. E. (1982) High-resolution computed tomography for the comparative study of fossil and extant bone. *American Journal of Biological Anthropology*, 58 (1): 67–73.

Tepper, B., Aniszewska, A., Bartkowska, K., Grochocka, L., Turlejski, K. and Djavadian, R. (2019) Aged opossums show alterations in spatial learning behaviour and reduced neurogenesis in the dentate gyrus. *Frontiers in Neuroscience*, 13: 1–12.

Tierney, A. L. and Nelson, C. A. (2009) Brain development and the role of experience in the early years. *Zero Three*, 30(2): 9–13.

Todorov, O.S., Hird, C., Kraatz, B., Sherratt, E., Hill, N, de Sousa, A. A., Blomberg, S. and Weisbecker, V. (2022) Down a rabbit hole: burrowing behaviour and larger home ranges are related to larger brains in leporids. *Journal of Mammalian Evolution*, 29: 957–967.

Triviño, L. N., Albino, A. M., Dozo, M. T. and Williams, J. D. (2018), First natural endocranial cast of a fossil snake (Cretaceous of Patagonia, Argentina). *The Anatomical Record*, 301(1): 9–20.

Tufo, C., Poopalasundaram, S., Dorrego-Rivas, A., Ford, M.C., Graham, A. and Grubb, M.S. (2022) Development of the mammalian main olfactory bulb. *Development*, 149 (3): dev200210.

Vullo, R., Girard, V., Azar, D. and Néraudeau, D. (2010) Mammalian hairs in Early Cretaceous amber. Naturwissenschaften, 97: 683–687.

Wallace, R. V. S., Martinez, R. and Rowe, T. (2019) First record of a basal mammaliamorph from the early Late Triassic Ischigualasto Formation of Argentina. *PLoS ONE*, 14(8): e0218791.

Walls, G. L. (1942) *The vertebrate eye and its adaptive radiation*. Bloomfield Hills, MI: Cranbrook Institute of Science.

Wanifuchi, H., Shimizu, T. and Maruyama, T. (2002) Age-related changes in the proportion of intracranial cerebrospinal fluid space measured using volumetric computerized tomography scanning. *Journal of Neurosurgery*, 97(3): 607–610.

Ward, P. D., Montgomery, D. R. and Smith, R. (2000) Altered river morphology in South Africa related to the Permian-Triassic extinction. *Science*, 289(5485): 1740–1743.

Watanabe, A., Gignac, P. M., Balanoff, A. M., Green, T. L., Kley, N. J. and Norell, M. A. (2019) Are endocasts good proxies for brain size and shape in archosaurs throughout ontogeny? *Journal of Anatomy*, 234(3): 291–305.

Weichenmeier, J., Fischer, C., Carter, D., Kuhl, E. and Goriely, A. (2017) Dimensional, geometrical, and physical constraints in skull growth. *Physical Review Letters*, 118: 248101.

Weinert, D. (2005) Ontogenetic development of the mammalian circadian system. *Chronobiology International*, 22(2): 179–205.

Weisbecker, V., Rowe, T., Wroe, S., Macrini, T. E., Garland, K. L. S., Travouillon, K. J., *et al.* (2021) Global elongation and high shape flexibility as an evolutionary hypothesis of accommodating mammalian brains into skulls. *Evolution*, 75(3): 625–640.

Werneburg, I. and Geiger, M. (2017) Ontogeny of domestic dogs and the developmental foundations of carnivoran domestication. *Journal of Mammalian Evolution*, 24: 323–343.

Wilson, L. A. B. (2018) The evolution of ontogenetic allometric trajectories in mammalian domestication. *Evolution*, 72(4): 867–877.

Witmer, L. M., Chatterjee, S., Franzosa, J., and Rowe, T. (2003). Neuroanatomy of flying reptiles and implications for flight, posture and behaviour. *Nature*, 425(6961): 950–953.

Witmer, L. M. and Ridgely, R. C. (2009) New insights into the brain, braincase, and ear region of tyrannosaurs (Dinosauria, Theropoda), with implications for sensory organization and behavior. *The Anatomical Record*, 292(9): 1266–1296.

Witmer, L. M., Ridgely, R. C., Dufeau, D. L., and Semones, M. C. (2008). 'Using CT to peer into the past: 3D visualization of the brain and ear regions of birds, crocodiles, and nonavian dinosaurs'. In *Anatomical Imaging.* Tokyo: Springer.

Wong, P. and Kaas, J. H. (2009) An architectonic study of the neocortex of the short-tailed opossum (*Monodelphis domestica*). *Brain, Behaviour and Evolution*, 73(3): 206–228.

Wu, X. and Schepartz, L. A. (2009) Application of computed tomography in paleoanthropological research. *Progress in Natural Science*, 19(8): 913–921.

Wynd, B. M., Peecock, B. R., Whitney, M. R. and Sidor, C. A. (2017) The first occurrence of *Cynognathus crateronotus* (Cynodontia: Cynognathia) in Tanzania and Zambia, with implications for the age and biostratigraphic correlation of Triassic strata in southern Pangea. *Journal of Vertebrate Paleontology*, 37(1): 228–239.

Wynd, B. M., Uyeda, J. C., and Nesbitt, S. J. (2021) Including distorted specimens in allometric studies: linear mixed models account for deformation. *Integrative Organismal Biology*, 3(1): obab017.

Yu, C., Qin, F., Li, Y., Qin, Z. and Norell, M. (2022) CT segmentation of dinosaur fossils by deep learning. *Frontiers in Earth Science*, 9: 1–8.

Yu, C., Qin, F., Watanabe, A., Yao, W., Li, Y., Qin, Z. *et al*. (2023) 'AI in paleontology'. *BioRXiv*, Preprint, viewed 6th February 2024, DOI: https://doi.org/10.1101/2023.08.07.552217.

Zaidel, E. (2001) Brain asymmetry. *International Encyclopedia of the Social and Behavioral Sciences,* 1321–1329.

Zelenitsky, D. K., Therrien, F., and Kobayashi, Y. (2009). Olfactory acuity in theropods: palaeobiological and evolutionary implications. *Proceedings of the Royal Society B: Biological Sciences*, 276(1657): 667–673.

Zelenitsky, D. K., Therrien, F., Ridgely, R. C., McGee, A. R., and Witmer, L. M. (2011). Evolution of olfaction in non-avian theropod dinosaurs and birds. *Proceedings of the Royal Society B: Biological Sciences*, 278 (1725): 3625–3634.

Zhou, Y., Shearwin-Whyatt, L., Li, J., Song, Z., Hayakawa, T., Stevens, D., Fenelon, J. C., Peel, E. *et al*. (2021) Platypus and echidna genomes reveal mammalian biology and evolution. *Nature*, 592: 756–762.

Zhou, C-F., Wu, S., Martin, T. and Luo, Z-X. (2013) A Jurassic mammaliaform and the earliest mammalian evolutionary adaptations. *Nature*, 500: 163–167.